The many facets of stochastic resetting in first-passage and non-equilibrium processes

Report submitted by

Arup Biswas

Enrolment No : PHYS10202104001

The Institute of Mathematical Sciences, Chennai.

Supervisor: Dr. Arnab Pal

The Institute of Mathematical Sciences, Chennai.

A thesis submitted to the
Board of Studies in Physical Science Discipline
In partial fulfilment of requirements
For the degree of
DOCTOR OF PHILOSOPHY

HOMI BHABA NATIONAL INSTITUTE, MUMBAI, May 2026

Homi Bhabha National Institute

Recommendations of the Viva Voce Committee

As members of the Viva Voce Committee, we certify that we have read the dissertation prepared by Arup Biswas entitled "The many facets of stochastic resetting in first-passage and non-equilibrium processes" and recommend that it may be accepted as fulfilling the thesis requirement for the award of Degree of Doctor of Philosophy.

Date: 25/05/2026

Chairman – Prof. Rajesh Ravindran

Date: 25/05/2026

Guide/Convenor – Dr. Arnab Pal

Date: 25/05/2026

Examiner – Prof. Sanjib Sabhapandit

Date: 25/05/2026

Member 1 – Dr. Ajit C Balram

Date: 25/05/2026

Member 2 – Dr. Sayantan Sharma

Date: 25/05/2026

Member 3 – Dr. Anupam Kundu

Final approval and acceptance of this thesis is contingent upon the candidate's submission of the final copies of the thesis to HBNI.

I hereby certify that I have read this thesis prepared under my direction and recommend that it may be accepted as fulfilling the thesis requirement.

Date: 25/05/2026

Place: Chennai

Guide

Statement by author

This dissertation has been submitted in partial fulfillment of requirements for an advanced degree at Homi Bhabha National Institute (HBNI) and is deposited in the Library to be made available to borrowers under rules of the HBNI.

Brief quotations from this dissertation are allowable without special permission, provided that accurate acknowledgement of source is made. Requests for permission for extended quotation from or reproduction of this manuscript in whole or in part may be granted by the Competent Authority of HBNI when in his or her judgement the proposed use of the material is in the interests of scholarship. In all other instances, however, permission must be obtained from the author.

Arup Biswas

Declaration

I, Arup Biswas, hereby declare that the investigation presented in the thesis has been carried out by me. The work is original and has not been submitted earlier as a whole or in part for a degree / diploma at this or any other Institution / University.

Arup Biswas

List of publications

Published (presented in the thesis)

1. **Target search optimization by threshold resetting**
   – A. Biswas, S.N. Majumdar, A. Pal; Physical Review Letters 135, 227101 (2025)

2. **A resetting particle embedded in a viscoelastic bath**
   – A. Biswas, J. L.A. Dubbeldam, T. Sandev, A. Pal; Chaos, 35, 031102 (2025) [published as cover of the special issue]

3. **Drift-diffusive resetting search process with stochastic returns: speed-up beyond optimal instantaneous return**
   – A. Biswas, A. Dubey, A. Kundu, A. Pal; Physical Review E 111, 014142 (2025)

4. **Queues with resetting: a perspective**
   – R. Roy*, A. Biswas*, A. Pal (2024); Journal of Physics: Complexity, 5, 2, 021001 (2024) [*Equal contributions]

5. **Search with stochastic home returns can expedite classical first passage under resetting**
   – A. Biswas, A. Kundu, A. Pal; Physical Review E (*Letters*), 110, L042101 (2024)

6. **Rate enhancement of gated drift-diffusion process by optimal resetting**
   – A. Biswas, A. Pal, D. Mondal, S. Ray; Journal of Chemical Physics, 159, 054111, (2023) [*Featured* article and also highlighted in an article by A. Thompson in *Sci-light*].

Arup Biswas

Published (not presented in the thesis)

1. **Current fluctuations in finite-sized one-dimensional non-interacting passive and active systems**
   – A. Biswas, S. Jose, A. Pal, K. Ramola; J. Phys. A: Math. Theor. 58 035001 (2025)

2. **Statistical basis of the optimal homing time in a foraging robot: learning universal characteristics of homing paths**
   – S. Paramanick, A. Biswas, H. Soni, A. Pal, and N. Kumar; PRX Life 2, 033007, (2024)

Submitted (not presented in the thesis)

1. **Emulating microbial run-and-tumble and tactic motion by stochastically reorienting synthetic active Brownian particles**
   – S. Kundu, D. Mondal, A. Biswas, A. Pal, M. Khan; arXiv:2509.21903 (2025), Submitted to Physical Review Letters

Arup Biswas

List of presentations and participation in conferences

Talks

1. 17 January, 2024, INYAS Saransh, New Delhi - A thesis presentation completion for students all over India **(3rd position)**
   Title: Benefits of starting again: A new paradigm in statistical physics

2. 23 January, 2024, Institute Seminar Day, The Institute of Mathematical Sciences
   Title: A brief revisit to the classical random walk and its potential applications

3. 08 January, 2025, Frontiers in Non-equilibrium Physics, The Institute of Mathematical Sciences
   Title: Target search with First-Passage Resetting

4. 03 February, 2025, In-house Symposium, The Institute of Mathematical Sciences
   Title: Expediting a first-passage process with intermittently switching dynamics

5. 16 April, 2025, Institute Seminar, Indian Statistical Institute, Kolkata
   Title: Expediting a stochastic search process with non-instantaneous resetting

6. 18 April, 2025, KVRSS, Hyderabad - a thesis presentation competition for students all over India **(3rd position)**
   Title: Thermodynamics work of first passage resetting

Posters

1. 04-08 December, 2023, Frontiers in Statistical Physics, Raman Research Institute, Bangalore
   Topic: Rate enhancement of gated drift-diffusion process by optimal resetting

2. 17-20 January, 2023, Frontiers in Non-equilibrium Physics, The Institute of Math-

ematical Sciences, Chennai
Topic: Search with stochastic home returns can expedite classical first passage under resetting

3. 23-24 February, 2024, Chennai Soft Matter Days, The Institute of Mathematical Sciences, Chennai
   Topic: Search with stochastic home returns can expedite classical first passage under resetting
4. 01-03 July, 2023, Discussion Meeting On Statistical Physics and Complex Systems, IIT Kharagpur, Kharagpur, 2023
   Topic: Rate enhancement of gated drift-diffusion process by optimal resetting

Research visits

1. 01 September, 2025 - 30 April, 2026 (*eight months*), Harvard University, USA, Fulbright-Nehru doctoral research fellow, Host: Prof. Lakshminarayanan Mahadevan

To my parents – the fundamental forces of my life

Acknowledgements

Besides the content of my scientific work as presented in this thesis, something perhaps even more valuable has been the journey that led me here—the journey of sleepless nights, rejected papers, uncertainty about the future, and, most importantly, leaving home for the first time to come to Chennai. Throughout this long journey, apart from my family, I found some wonderful people who were always there when I needed them the most. Below, I express my gratitude to each of them, without whom the dream of completing a PhD would not have become a reality.

Needless to say, the first person who comes to my mind is my supervisor, Dr. Arnab Pal. Beyond science, he has been the go-to person for me whenever I was in distress. He was never too busy to talk for hours and always encouraged me to think beyond traditional boundaries. His clarity of vision on any topic influenced me greatly during the last three years. I will forever be grateful for his guidance—not only for shaping this thesis but also for shaping me as a person.

I am also thankful to some of my collaborators—Dr. Anupam Kundu, Dr. Kabir Ramola, Dr. Somrita Ray, and Dr. Nitin Kumar—with whom I had the opportunity to work closely. The way Anupam da approaches the core of a problem has always amazed me. His critical comments not only helped me understand specific problems better but also taught me how to think about other problems. I thank Kabir for finding time to discuss with me on multiple occasions and for helping me understand a relatively new topic, which eventually led to a paper. I am indebted to Somrita di for her help during my early PhD days; she was the first person who taught me how to use Mathematica. With Nitin, I had the chance to experience aspects of experimental research, where his insights helped me appreciate the interplay between theory and experiments.

I would also like to thank USIEF, India, for granting me the Fulbright-Nehru Doctoral Research Fellowship. During this fellowship, I had the excellent opportunity to work under the supervision of L. Mahadevan at Harvard University, USA. Each interaction with him taught me something new. His broad insights, intellectual generosity, and ability to connect ideas across disciplines deeply influenced my approach to research.

I am grateful to my friends from Jadavpur University - Sanjib, Ramkrishna, Kamalakanta, Soumen, Samim, Budhaditya, Sourav, Joydip, Subhranil, Sam da, Indra da for the wonderful time I had with them. I also thank Dr. Kaustuv Das, Dr. Dhruba Banerjee, Dr. Subhankar Roy from whom I had the opportunity to learn Physics. I

would also like to thank my school teachers Muktakamal Sir, Subrata Sir, Amarnath Sir, Kaushik Sir, Debu Sir, Biswajit Sir, Tubla Sir without whom I could not even come this far.

I express my gratitude to the doctoral committee at IMSc—Prof. R. Rajesh, Dr. Sayantan Sharma, and Dr. Ajit Balram—for their continuous monitoring and support. Their constructive comments throughout my time at IMSc strengthened this thesis in many ways. I would also like to thank Sayantan da for the long hours of adda in the canteen; those moments will always remain special. I also thank Debayan da, Dhiraj da for their unconditional support whenever I needed. I am also grateful to the director of our institute, Prof. V. Ravindran, for being approachable and for his care for the students. I also thank Prof. Rahul and Viswanath for their help when my family visited Chennai for a medical urgency.

Despite being away from home, IMSc became nothing less than a second family. The love and support I received from the people here are beyond expressing in words. First and foremost, I thank my batchmates—Vishwajeet, Harshit, Saurav, and Sashikanta. I will forever miss the moments spent with them: hours of gossip, playing cricket, going out for dinners, and the institute trips. I feel fortunate to have been part of a group that complemented each other at every step of our stay at IMSc. I would specially thank Vishwajeet for accompanying me through countless hours of scientific and non-scientific discussions. I would like to thank Sushant, Rohit, Suvam, Velmurugan, Priytotosh, and Nikhil for being close friends. I was also fortunate to receive guidance from many seniors. I express my gratitude to Apurba da, Arindam da, Amit da, Debabrata da, Hitesh, Vinod, Sahil da, Subashri, Roni, Gopal, Abhimanyu, Koyena, Tanmay da, Vaibhav, Biswajit da, Amir, Prem, Chandrani, Samim da, Sitender, Manikandan, Mrityunjay da, Arunabha da, Anupam da, Sourjya da and many others whom I might have missed to mention it over here. I thank I am indebted to Rohitasya da for his invaluable suggestions during my initial days at IMSc. I owe special thanks to Reshmi di, Aashutosh da, and Arghya da who, besides being collaborators, were also tremendous sources of love and support. I also found wonderful juniors to interact with, including Rahul Nayak, Rahul Das, Goutham, Jitin, Sarbartha, Sayak, Swagatam, Subham, Siddhartha, Sheryl, Nayan, Sadeep, Nirmal, Bhabani, Adarsh, Revanth, Tanishk, Rabindranath and Sobyasachi. I would also like to thank my officemates—Sumit da, Pritesh, Ananta, and Saptarshi—with whom I spent most of my days. Finally, I thank Prof. Pinaki for maintaining a high-quality computing facility at IMSc, Vasan for technical support with the computing facilities, as well as Indra Madam, Prema and Johnson for their endless help. I would also like to thank all the administrative staff at IMSc. Beyond being wonderful people, their efficiency in handling administrative matters enabled me to work without worry. I would take this opportunity to thank IMSc library for the resources provided. I would also like to thank our institute's canteen staffs, including Rajkumar and Balaji for preparing delicious food every day. In short, I could happily spend my years at this beautiful

institute only because of people like them.

Finally, I thank my family for their continuous support throughout my life. I am forever grateful to my Maa and Baba. They not only raised me but also supported every decision I made. Having them beside me is truly one of the greatest blessings one can have. I also thank Noa Kaka, Kaki, Meso, Masi, and Mami for supporting me during difficult times. I can never repay the debt I owe them. Lastly, I thank my wife, Anwesha. It was pure luck that our paths crossed, and the last three years with her have been the best of my life. This thesis is a testament to the belief, support, and love they all have given me throughout this journey.

This page intentionally left blank.

Contents

List of Figures xii

1 Stochastic resetting - a new paradigm in statistical physics 1
1.1 Benefits of starting anew . . . 2
1.1.1 Harnessing non-equilibrium features with resetting . . . 3
1.1.2 First-passage optimization with resetting . . . 6
1.2 Goal of this thesis . . . 12
1.2.1 Applications of stochastic resetting in diverse contexts . . . 13
1.2.2 Towards experimental realization of stochastic resetting . . . 15
1.2.3 A novel target search optimization strategy based on threshold resetting . . . 17

2 Stochastic resetting in gated chemical reactions 19
2.1 Introduction . . . 19
2.2 Completion time statistics . . . 21
2.3 The optimal resetting rate and a phase diagram for expedited completion 25
2.3.1 The limit $\alpha \to 0$ . . . 28
2.3.2 The limit $\alpha, \beta \to \infty$ . . . 29
2.4 The maximal speedup for process completion . . . 30
2.5 The complete phase diagram . . . 32
2.6 The case of confined geometry . . . 33
2.7 Details of numerical simulations . . . 36
2.8 Conclusions . . . 37

3 Stochastic resetting in operation research 39
3.1 Introduction . . . 39
3.2 Preliminaries . . . 41
3.3 Service with resetting . . . 42
3.4 M/G/1 Queues with Poissonian service resetting . . . 44
3.5 Service at an optimal resetting rate . . . 45
3.5.1 Resetting with no overhead . . . 46
3.5.2 Overhead time with $CV_{on} < 1$ . . . 46

3.5.3 Overhead time with $CV_{on} = 1$ . . . 47
3.5.4 Overhead time with $CV_{on} > 1$ . . . 47
3.6 Application . . . 48
3.6.1 Case I: $CV_{on} < 1$ . . . 48
3.6.2 Case II: $CV_{on} = 1$ . . . 49
3.6.3 Case III: $CV_{on} > 1$ . . . 50
3.6.4 Mean queue length for different $\langle S_{on} \rangle$ . . . 50
3.7 Discussion and Summary . . . 51

4 Stochastic resetting in a viscoelastic medium 55
4.1 Introduction . . . 55
4.2 Generalized Langevin equation . . . 57
4.3 GLE with stochastic resetting . . . 60
4.3.1 MSD in presence of resetting . . . 61
4.3.2 Correlation function with resetting . . . 62
4.4 Jeffreys fluid as a viscoelastic bath . . . 63
4.4.1 MSD . . . 64
4.4.2 Correlation function . . . 70
4.5 Simulation scheme for GLE with resetting . . . 71
4.6 Discussion and outlook . . . 73

5 Towards experimental realization of stochastic resetting 75
5.1 Introduction . . . 75
5.2 General framework . . . 76
5.3 A universal criterion for the trade-off between instantaneous and stochastic return . . . 78
5.4 Diffusive search with resetting and stochastic return via controlled potential trap. . . . 79
5.4.1 A universal phase diagram for diffusive search . . . 81
5.5 A pragmatic application of the phase diagram . . . 82
5.5.1 Theoretical result for MFPT with return by harmonic trap . . . 83
5.5.2 The phase diagram for search efficiency: identification of realistic range of parameters . . . 84
5.6 Optimal speed-up for the drift-diffusive search process . . . 86
5.6.1 Problem set-up and MFPT . . . 86
5.6.2 Speed up over underlying process - the *CV criterion* . . . 90
5.6.3 Speed up over instantaneous resetting- the *SR criterion* . . . 92
5.6.4 Speed-up beyond optimal instantaneous return . . . 94
5.7 Discussion . . . 96

6 First-passage optimization with collective threshold resetting 98
6.1 Introduction . . . 98
6.2 General formalism . . . 99
6.3 Ballistic search under TR mechanism . . . 102
6.3.1 MFPT . . . 103
6.4 First-passage distribution as optimality . . . 107
6.4.1 FPT distribution of the ballistic searchers without TR ($u \to 0$) . . . 107
6.4.2 FPT distribution of the ballistic searchers under optimal TR . . . 108
6.5 Cost of TR mechanism . . . 110
6.6 Conclusions . . . 110

7 Conclusions 112

References 116

Appendices

A Appendices for Chapter 1 139
A.1 Derivation of $\langle min(T,R)\rangle$ . . . 139

B Appendices for Chapter 2 141
B.1 Calculation of the average MFPT by solving Eq. (2.1) in the Laplace space 141
B.2 The average MFPT for gated drift-diffusion without resetting . . . 145

C Appendices for Chapter 3 147
C.1 Moment generating function of S_R . . . 147
C.2 Moments of the service time for Poissonian resetting . . . 149
C.3 General discussion on the "resetting induced efficiency criterion" for the mean queue length with different variability CV_{on} . . . 151
C.3.1 Case I: $CV_{on} < 1$ . . . 151
C.3.2 Case II: $CV_{on} = 1$ . . . 151
C.3.3 Case III: $CV_{on} > 1$ . . . 152
C.4 Moments for sharp resetting times . . . 152

D Appendices for Chapter 4 155
D.1 Exact expressions for the MSD and correlation function . . . 155

E Appendices for Chapter 5 158
E.1 Exact expression for the MFPT for the drift-diffusive process under stochastic return . . . 158
E.2 Derivation of the CV criterion for resetting with stochastic return . . . 159

F Appendices for Chapter 6 **162**
F.1 Survival probability and probability current of a single ballistic searcher 162
F.2 Derivation of exact form of the scaling function for $N = 2$ 163
F.3 Asymptotic behaviors of scaling funtion for general $N \geq 2$ 166
F.3.1 The limit $u \to 0$ 166
F.3.2 The limit $u \to 1$ 167
F.4 Derivations of $\langle \mathcal{N}_{\rm TR}(u, N) \rangle$, $\langle \overline{\mathbb{T}}_N^{\rm TR}(u) \rangle$ and $\langle \overline{\mathbb{T}}_N^{\rm FP}(u) \rangle$ 169
F.4.1 Derivation of $\langle \mathcal{N}_{\rm TR} \rangle$ 170
F.4.2 Derivation of $\langle \overline{\mathbb{T}}_N^{\rm TR}(u) \rangle$ 170
F.4.3 Derivation of $\langle \overline{\mathbb{T}}_N^{\rm FP}(u) \rangle$ 172

This page intentionally left blank.

List of Figures

1.1 **Brownian motion in one dimension subjected to stochastic resetting** – At random intervals of time $\{\tau_1, \tau_2, ...\}$ the particle is instantaneously brought back (reset) to the initial position $x = 0$. After being reset, the particle goes back to its original dynamics and the entire process renews. 2

1.2 Variation of probability density of a Brownian particle with time without resetting (left panel) and with resetting (right panel) at a resetting rate $r = 0.3$. Note that without resetting the density spreads indefinitely with time, whereas resetting stablilizes the distribution and a NESS is reached at $t \to \infty$ as in Eq. (1.5). 5

1.3 **First-passage of a Brownian particle under stochastic resetting –** The particle starts from the origin $x = 0$ at time $t = 0$. It undergoes free diffusion until at random intervals of time $\{\tau_1, \tau_2, \tau_3...\}$ the particle gets reset to the origin again. This diffusion and reset motion continues until the particle reaches the target at $x = L$. Upon reaching this target the process is terminated and we call it a first-passage event. 7

1.4 **Mean first-passage time (MFPT) for diffusion under resetting –** The MFPT (as obtained from Eq. (1.12) with $L = 1, D = 1$) shows non-monotonic dependence on the resetting rate r. For low resetting rates the MFPT is infinite mimicking that of the reset-free process. On the other hand, too much of resetting also causes the MFPT to diverge. In between, there exist an optimal resetting rate r^* at which the MFPT is the lowest. . . 10

1.5 **ORR for drift-diffusive process under resetting** – Note that the ORR r^* becomes zero when v is sufficiently large. In that case (shown by the shaded region), the reset-free process itself is the most optimised situation and adding any amount of resetting would only prolong the search process. The parameters for the plot are: $L = 1, D = 1$. 12

1.6 Experimental trajectory of a resetting Brownian particle from the study of (a) Tal-Friedman et. al. [14] (b) Besga. et. al. [15]. Unlike the theoretical model as shown in Fig. (1.3) where the particle resets instantaneously to the origin, in experiments, it always costs a finite time penalty. 16

2.1 Scheme for a gated chemical reaction between two reactants R_1 and R_2, catalysed by C. In the first step, the catalyst binds reversibly with R_1 to form a metastable intermediate CR_1: $C + R_1 \rightleftharpoons CR_1$. Next, CR_1 reacts selectively with $R_2^\star$ (the *reactive* or *open-gate* state of R_2) to form the product P and release the catalyst: $CR_1 + R_2^\star \longrightarrow C + P$. This step is modeled as gated drift-diffusion, while unbinding of C from R_1 represents resetting. 21

2.2 Schematic diagram of a gated drift-diffusion process in semi-infinite space with resetting, where the target (placed at the origin) switches stochastically between a reactive state ($\sigma = 1$) and a non-reactive state ($\sigma = 0$). The transition from the non-reactive to the reactive state takes place with a constant rate $\alpha > 0$, and the opposite transition takes place with a constant rate $\beta > 0$. When the particle, starting at x_0, hits the target in its reactive state (dashed line), the process ends. T_r^G marks the random completion time of the gated drift-diffusion process with resetting. 22

2.3 The average MFPT, $\langle T_r^G \rangle$, vs the resetting rate r for different values of the drift velocity λ. The lines represent analytical results following Eq. (2.7) and the symbols represent results from numerical simulations [see section 2.7 for details]. The curves with $\lambda > 0$ denote cases where the drift acts towards the gated target and that with $\lambda < 0$ denote otherwise. The variation of $\langle T_r^G \rangle$ with r is always non-monotonic for $\lambda \leq 0$, however, for $\lambda > 0$ it is non-monotonic for lower values of λ, but monotonic for sufficiently high values of λ. Here we take $x_0 = 2$, $D = 1$, $\alpha = 0.5$, and $\beta = 0.5$ for all cases. 24

2.4 The scaled optimal resetting rate, $r^\star/r_0^\star$, vs λ for different values of p_r. Resetting transition in each case is observed at $\lambda = \lambda_c$, where the scaled ORR becomes zero, marked by dashed lines of the same color as the curve. For $\lambda < \lambda_c$, resetting expedites transport, whereas for $\lambda \geq \lambda_c$ it can not. Here we take $D = 1$, $x_0 = 2$, and $\alpha = 0.5$ [which leads to $p_r = 1/(2\beta + 1)$] for all cases. For ungated drift-diffusion [given by $p_r = 1$, since $\beta \longrightarrow 0$], the resetting transition is observed at $\lambda_c = 1$ (gray curve). For gated drift-diffusion with $p_r < 1$, λ_c decreases below unity. 25

2.5 A phase diagram of p_r vs. λ based on the qualitative effect of resetting on gated drift-diffusion. The black line represents the condition for resetting transition (λ_c), which divides the entire phase space in two parts. For $\lambda < \lambda_c$ resetting expedites transport (white regime), whereas for $\lambda \geq \lambda_c$ resetting fails to expedite transport (gray regime). Here we take $D = 1$, $x_0 = 2$ and $\alpha = 0.5$ [i.e., $p_r = 1/(2\beta + 1)$] for all cases. For the ungated process ($p_r = 1$), $\lambda_c = 1$ and it decreases with p_r. The colored discs on the black line present the cases shown in Fig. (2.4). Following the analysis of $\langle T_r^G \rangle$ in the limit $r \to 0$ [see Eq. (2.10) and Eq. (2.12)], the separatrix (black line) is also obtained by plotting $f = 0$ (as defined by Eq. (2.12)). Resetting is beneficial for $f < 0$ (white regime), but not for $f > 0$ (gray regime). . . . 26

2.6 A phase diagram of p_r vs. λ for different values of α. Each phase boundary (obtained for a certain value of α, shown by the curves) divides the phase space into a "resetting-beneficial" phase (left to the curve) and a "resetting-detrimental" phase (right to the curve). For large values of α, the "resetting-beneficial" phase becomes considerably smaller as the "resetting-detrimental" phase occupies the majority of the phase space. 28

2.7 Monotonic and non-monotonic behaviour of the MFPT in the limit $\alpha \to 0$ (i.e., $\beta/\alpha \gg 1$), as obtained from Eq. (2.14). The non-monotonic behaviour gradually vanishes as λ goes beyond the resetting transition point $\lambda_c = D/x_0 = 0.5$. This can be obtained by setting $r^\star$ in Eq. (2.15) to zero. . 30

2.8 The maximal speedup for the gated process with resetting compared to the gated process without resetting, $\langle T^G \rangle / \langle T_{r^\star}^G \rangle$, vs the drift velocity λ, for different values of the reactive occupancy, p_r. The vertical dashed lines mark the points of resetting transitions for curves of same color, denoted λ_c, such that $\langle T^G \rangle / \langle T_{r^\star}^G \rangle > 1$ for $\lambda < \lambda_c$, and $\langle T^G \rangle / \langle T_{r^\star}^G \rangle = 1$ at $\lambda \geq \lambda_c$. We take $D = 1$, $x_0 = 2$ and $\alpha = 0.5$ [i.e., $p_r = 1/(2\beta + 1)$] for all cases. In the absence of gating ($p_r = 1$, gray curve), the resetting transition is observed at $\lambda_c = 2D/x_0 = 1$, and λ_c decreases when gating is introduced ($p_r < 1$). 31

2.9 The maximal speedup for the gated process with resetting compared to the ungated process without resetting, $\langle T \rangle / \langle T_{r^\star}^G \rangle$, vs λ, for different values of p_r. The vertical dashed lines mark the points of resetting transition (λ_c) for curves of same color, whereas the colored discs mark the values of λ_c^0, such that optimal resetting expedites gated process beyond the original ungated process only when $\lambda < \lambda_c^0$. Here $D = 1$, $x_0 = 2$ and $\alpha = 0.5$ [i.e., $p_r = 1/(2\beta + 1)$] for all cases. In the absence of getting ($p_r = 1$, gray curve), the point of resetting transition ($\lambda_c = 2D/x_0 = 1$) coincides with λ_c^0. 32

2.10 A complete phase diagram of p_r vs. λ showing three distinct phases; (i) phase I: where optimal resetting enhances the rate of gated drift-diffusion beyond the original (without resetting) ungated process, given by $\langle T^G_{r^\star} \rangle < \langle T \rangle < \langle T^G \rangle$, (ii) phase II: when optimal resetting improves the rate of the gated process, but not compared to the original ungated process, given by $\langle T \rangle \leq \langle T^G_{r^\star} \rangle < \langle T^G \rangle$, and (iii) phase III: when resetting can not improve the rate of gated process, given by $\langle T \rangle < \langle T^G \rangle \leq \langle T^G_{r^\star} \rangle$. The horizontal colored lines mark the cases shown in Fig. (2.9). Here we consider $\alpha = 0.5$ [such that $p_r = 1/(2\beta + 1)$], $D = 1$ and $x_0 = 2$. Phases I and II merge together at $\lambda_c = 2D/x_0 = 1$, the point of resetting transition for drift-diffusion in the absence of gating ($p_r = 1$). 33

2.11 The average MFPT $\langle T^G_r \rangle$ as a function of the resetting rate r for different values of λ in the case of bounded domain. Here, the reflecting boundary is placed at $L = 3$, where the resetting/initial location is at $x_0 = 2$. The colored discs mark the optimal resetting rate ($r^\star$) in each case. Notably, resetting may not always be helpful ($r^\star = 0$) even when $\lambda < 0$ (e.g., yellow and brown curves). 34

2.12 Main: Variation of ORR ($r^\star$) as a function of λ for different domain size L. For $\lambda < \lambda_c$, resetting proves itself beneficial, as indicated by the non-zero values of $r^\star$, whereas for $\lambda \geq \lambda_c$, resetting becomes detrimental, as indicated by $r^\star = 0$. The resetting transition is thus marked by λ_c. Inset: Phase diagram with reflecting barrier at L, by plotting λ_c that acts as the separatrix (black line; the colored discs mark the specific cases shown in the main panel) that divides the phase space in two parts; one where resetting is beneficial (white regime) and the other where resetting is detrimental (gray regime). Existence of negative λ_c essentially implies that resetting can be detrimental even when $\lambda < 0$. The dashed horizontal line corresponds to $\lambda_c = 0.78$, obtained for the semi-infinite case (i.e. $L \to \infty$), as displayed in Fig. (2.5) for $p_r = 0.5$. Note that we consider $\alpha = 0.5, \beta = 0.5$ and $D = 1$ for each case in the main panel and in the inset. 35

3.1 Schematic of a queuing system under resetting. Jobs arrive at the queue with a rate λ and they are being served at the service station according to a first-come, first-served policy. The server has two components: a service time S followed by an overhead time S_{on}. It can complete a task in time $S_u = S + S_{on}$ prior to resetting (upper branch). Otherwise, resetting can occur in time R (lower branch), following which the service is renewed. The process repeats by itself until the task is completed which is possible only via the upper branch. 43

3.2 (a) Mean service time $\langle S_r \rangle$ from Eq. (3.8) as a function of resetting rate for different choices of $\langle S_{on} \rangle$. The underlying service time S is sampled from the log-normal distribution (3.27) with $\langle S \rangle = 1$ and $\alpha = 1.5$. Circles mark the optimal resetting rate r^* for each value where $\langle S_r \rangle$ attains its minimum. (b) Mean queue length at optimal resetting, $\langle N_{r^*} \rangle$, versus squared CV_u. Here, $\langle S \rangle$ is fixed at unity and α is varied to tune CV_u in Eqs. (3.31), (3.32), and (3.35). Results are shown for deterministic ($CV_{on} = 0$), exponential ($CV_{on} = 1$), and Weibull ($CV_{on} > 1$) overheads, all with $\langle S_{on} \rangle = 0.5$. Dashed lines indicate the standard Pollaczek–Khinchin result (3.1) at $r^* = 0$. For larger CV_u, optimal resetting becomes nonzero, causing $\langle N_{r^*} \rangle$ to dip below the standard value, and the transition points agree with theoretical predictions. Optimal resetting efficiently reduces queue lengths for any S_{on} and CV_{on}, and all results here use $\lambda = 0.4$. 49

3.3 Mean queue length at optimal Poisson resetting as a function of squared CV_u for multiple choices of $\langle S_{on} \rangle$ and variability, taking deterministic ($CV_{on} = 0$), exponential ($CV_{on} = 1$), and Weibull ($CV_{on} = 1.4624$) overheads. The underlying service distribution is log-normal [Eq. (3.27)] with $\langle S \rangle = 1$ and variable α setting CV_u via Eq. (3.31), Eq. (3.32), Eq. (3.35). Dashed lines show standard PK formula ($r^* = 0$). Left vertical dashed line at $CV_u < 1$ reflects the order $\langle N^I_{r^*=0} \rangle > \langle N^{II}_{r^*=0} \rangle > \langle N^{III}_{r^*=0} \rangle$, tracking $\langle S_{on} \rangle$ from largest to smallest. Resetting has no effect here. When r^* becomes nonzero (right dashed line, $CV_u > 1$), the order reverses: $\langle N^I_{r^*} \rangle < \langle N^{II}_{r^*} \rangle < \langle N^{III}_{r^*} \rangle$ for a fixed CV_u. This means queues with smaller overhead fluctuations (but larger mean overhead) are most impacted by optimal resetting. 50

3.4 Panel (a): The mean service time from Eq. (3.39) as a function of resetting period τ for various overhead S_{on} values, with service S drawn from a log-normal distribution (Eq. (3.27)). In each curve, the global minimum at τ^* (shown by a solid circle) marks the optimal resetting. We use $\langle S \rangle = 1$, $\alpha = 1.5$, and $\lambda = 0.4$. Panel (b): $\langle N_{\tau^*} \rangle$ as a function of CV_u^2 (tuned via α). The dashed line is the classical PK formula, valid when $\tau^* = 0$. Once τ^* becomes positive, the mean queue length falls below the baseline: evidence for the improved performance enabled by sharp resetting. Overhead times S_{on} are sampled from three distributions with differing CV_{on} as indicated. . 53

3.5 The difference in mean queue length between optimal Poisson and sharp resetting as a function of squared CV_u. The service S is log-normal (Eq. (3.27)) with $\langle S \rangle = 1$ and $\langle S_{on} \rangle = 0.5$, and α is varied to tune CV_u. Overhead S_{on} is drawn from deterministic ($CV_{on} = 0$), exponential ($CV_{on} = 1$) and Weibull ($CV_{on} > 1$) distributions. In all scenarios, $\langle N_{r^*} \rangle - \langle N_{\tau^*} \rangle > 0$ for all CV_u, confirming that sharp resetting universally outperforms Poisson resetting. Here, $\lambda = 0.4$. 53

4.1 Schematic representation of a colloidal particle diffusing in a viscoelastic bath under harmonic trapping. The motion of the particle is governed by the generalized Langevin equation (GLE) as in Eq. (4.5). In addition, the particle undergoes stochastic resetting at random time intervals drawn from an exponential distribution with mean $1/r$. 57

4.2 A simple schematic illustrating the contribution to the correlation function from two different scenarios depending on the event of the last resetting (shown by the arrow). In (a) the last resetting happens in $[0, t']$ whereas in (b) the last resetting happens in $[t', t]$. 62

4.3 MSD of the underlying reset-free process for the Jeffreys fluid model as a function of time for different values of γ_s. The circles represent results from the simulation. For $\gamma_s = 0$, the MSD is the same as that of an OU process. The plots indicate the existence of two distinct time scales for a non-zero value of γ_s with the emergence of a plateau. In Fig. 4.4, we discuss the origin of these characteristics and illustrate further. The parameters for this simulation are set at: $\gamma_f = 1, \omega = 1, \tau_s = 1$. 65

4.4 Variation of the MSD of the underlying process (the solid line) as a function of time and emergence of the plateaus for parameters fixed at $\gamma_s = 1000, \gamma_f = 1, \omega = 1, \tau_s = 1$. This is the bottom-most curve for the MSD as borrowed from Fig. 4.3. The vertical dotted lines represents three three different timescales as in Eq. (4.34), Eq. (4.38) and Eq. (4.42). The asymptotic behaviour of the MSD at different timescales is also shown above the curve in each region. The dashed line shows the MSD with $\omega = 0$ as in Eq. (4.33). 66

4.5 Variation of MSD with time for the resetting system for different values of resetting rate r. The parameters are fixed at: $\gamma_f = 1, \gamma_s = 100, \tau_s = 1, \omega = 1$. The circles represent results from the simulation. The dashed curve represents the result for the underlying reset-free process, *i.e.*, $r = 0$. The solid circles represent the results from numerical simulation. The rightmost vertical dashed line represents the longest timescale of the system under resetting while the other two vertical dashed lines are associated with the timescales t_r for different values of r (color-codes represent the values of r respectively). At sufficiently short times $t \ll t_r, t^r_{\text{long}}$, the curves follow the MSD of the underlying reset-free process. 68

4.6 Variation of the correlation function with time under resetting for Jeffreys fluid model. The parameters chosen are: $\gamma_f = 1, \gamma_s = 10, \omega = 1, \tau_s = 1$. As before, the dashed line represents the reset-free process ($r = 0$) and the solid circles represent data points from numerical simulation. Note that the correlation decays exponentially with time as given by Eq. (4.50). 70

5.1 Schematic diagram of an agent (could be a foraging animal, colloid or a bio-molecule) searching for targets (could be resources, sticky surface or a defected site along DNA). The agent can find the target during the *search phase* (violet solid trajectory). Otherwise, after a random resetting time R the agent, currently located at $\vec{x}$, switches to a return phase (facilitated e.g., by a chemical or potential gradient or simply, by choice) when it either returns to its home or relocates to a new location in finite time $T^{O}_{ret}(\vec{x})$ (red dot-dashed trajectory). The agent also has a finite probability to find the target during its return phase (red dotted trajectory) in time $T^{A}_{ret}(\vec{x})$. Target detection marks the completion of the global search regardless of its phase. We ask: Whether search with a finite-time home return can perform better than the instantaneous return process? 76

5.2 Variation of the MFPT $\langle\tau(\overline{r},\overline{\lambda})\rangle$ from (5.15), shown by the solid curves, as a function of $\overline{\lambda}$ for different resetting rate $\overline{r}$. The horizontal dashed lines represent $\langle\tau_{inst}(\overline{r})\rangle$ for respective $\overline{r}$. Evidently, stochastic return can both reduce ($\overline{r}=10$) or prolong ($\overline{r}=5$) the completion time compared to the instantaneous returns. This behavioural transition occurs at $\overline{r}^{*}$ which is strictly a function of $\overline{\lambda}$. Numerical data (depicted by the stars) shows an excellent agreement with the theory. Inset schematic: Possible trajectories of a diffusive searcher under resetting and stochastic return facilitated by a potential trap. Violet (red) trajectory corresponds to search & trap-off (return & trap-on) phase. 80

5.3 Phase diagram for diffusive search with stochastic returns driven by linear- (panel a) and harmonic- (panel b) potentials: The region right to the phase boundary (red dashed curve) is where condition (5.9) is satisfied and stochastic return (SR) supersedes instantaneous return (IR). The red curve is obtained by setting (5.9) to an equality. The side colorbar is an estimation of search efficiency, defined by the ratio $\frac{\langle\tau(\overline{r},\overline{\lambda})\rangle}{\langle\tau_{inst}(\overline{r})\rangle}$; values in log-scale - positive (negative) for slow-down (speed-up) by the stochastic return. In panel (a), the yellow star indicates the critical $\overline{r}^{*}$ which is obtained from the intersection of the separatrix and the horizontal white line spanned by each $\overline{\lambda}$ (here, $\overline{\lambda}=5$, $\overline{r}^{*}\approx 12$). In panel (b), we have superimposed the data points (marked as crosses) from the experimental parameter sets $\left(\overline{\lambda},\overline{r}\right)$ from [15]. 82

5.4 Illustrative representation of drift-diffusive resetting search process under stochastic return. A drift of magnitude v (red arrow) always acts on the particle, biasing its motion towards a fixed target located at A. Once a resetting time is set (drawn randomly from a distribution), a potential $U(x) = \lambda|x|$ with $\lambda > 0$ is turned on at the resetting location which is denoted by O here (shown by the blue strips). This potential causes an additional drift of magnitude λ towards the origin. Overall, an effective potential $U_{\text{eff}}(x)$ as in Eq. (5.30) acts on the particle during the return. After the particle reaches the origin the potential is turned off marking the completion of one resetting event. The search process can end in two ways: either the target is found during the search phase (potential turned off - shown by the violet trajectory) or during the return phase (potential turned on - shown by the yellow trajectory). 87

5.5 Variation of the MFPT $\langle\tau(\overline{r},\overline{\lambda},\overline{v})\rangle$ with potential strength $\overline{\lambda}$ (panel a,c) and resetting rate $\overline{r}$ (panel b,d) for exponentially distributed resetting times. Panel (a,b) are for $\overline{v} = 0.2$ and panel (c,d) are shown for $\overline{v} = 3$. The limit $\overline{\lambda} \to 0$ gives the MFPT of the underlying process *i.e.* $\frac{1}{\overline{v}}$ shown by the dashed horizontal lines. Note the contrasting behaviour for different values of $\overline{v}$. For lower value of $\overline{v}$ each plot shows a non-monotonic behaviour implying the utility of resetting compared to the reset-free process. However, as $\overline{v}$ becomes higher MFPT for a finite value of $\overline{r}$ and $\overline{\lambda}$ is always greater than that of the underlying process. Also in some of the curves in panel (a) and in each of the curves in panel (c), there exists a range of $\overline{\lambda}$ where MFPT becomes lower than the instantaneous return limit ($\overline{\lambda} \to \infty$). 89

5.6 (a) Phase space obtained from the CV criterion (5.44) for the drift-diffusive system with return via $U_{\text{eff}}(x)$. The blue-shaded region is where resetting will help to reduce the MFPT beyond the underlying process. The black dashed line at $\overline{v} = 2$ refers to the phase boundary in the instantaneous limit ($\overline{\lambda} \to \infty$). (b) Variation of the ORR with respect to $\overline{v}$ for several values of $\overline{\lambda}$. 91

5.7 A unified phase diagram for the drift-diffusive search process for exponential resetting with rate $\overline{r} = 2$. Different regions in this parameter space represent the regions where either of the CV criteria in Eq. (5.44) or the SR criteria as in Eq. (5.9) is satisfied. The most important is region IV (the red-shaded region) where both the criteria are satisfied, and stochastic return facilitates the process beyond both the underlying process and also that of resetting with instantaneous return. The behaviour of the MFPT for a sample point (star) in each of these regions is shown in the corners. In these plots, the horizontal solid lines represent the MFPT that with instantaneous return and the dashed horizontal line represents the MFPT of the underlying reset-free process. 93

5.8 (a) MFPT with stochastic return *i.e.* $\langle \tau(\overline{r}, \overline{\lambda}, \overline{v}) \rangle$ (blue and orange curves) and instantaneous return *i.e.* $\langle \tau(\overline{r}, \overline{v}) \rangle_{\text{inst}} = \langle \tau(\overline{r}, \overline{\lambda} \to \infty, \overline{v}) \rangle$ (green curve) are plotted with respect to the resetting rate $\overline{r}$, for a fixed drift velocity $\overline{v} = 1.8$. Remarkably, for $\overline{\lambda} = 1.4$ we find that optimal stochastic return can lower the MFPT (the blue circle) even beyond the optimal instantaneous return (the green circle). (b) Phase space showing regions where stochastic (or instantaneous) return is better at the optimal resetting rate (which is different in general for both the protocols). The blue shaded region (obtained by setting the speed-up parameter γ^* as in Eq. (5.54), to be greater than unity) is where stochastic return performs better than the optimal instantaneous return. 94

6.1 Schematic representation of the TR mechanism with N searchers (here, $N = 3$) starting from x_0 and undergoing generic stochastic dynamics. The process is considered complete when any of the searchers reaches the target located at the origin, and the corresponding first passage time is denoted by $\mathcal{T}_N^{\text{TR}}(L, x_0)$. However, if any searcher reaches the resetting threshold at position L before the target is found, all searchers are collectively returned to their initial positions, and the search process is restarted. 100

6.2 Panel (a): Variation of the scaled MFPT (6.20) with respect to u and N. The plot shows a global minima in the MFPT at $u = 1$ for any $N > 1$. A cross section for $N = 7$ is shown in panel (b). Panel (b) - central figure: Optimization of $\langle \overline{\mathcal{T}}_N^{\text{TR}}(u) \rangle$ as a function of u (shown by the solid blue curve) – superimposed with individual components as given by the RHS of (6.23) namely $\langle \mathcal{N}_{\text{TR}}(u, N) \rangle$ (shown by orange dotted-dashed line), $\langle \overline{\mathbb{T}}_N^{\text{TR}}(u) \rangle$ (shown by green dashed line) and $\langle \overline{\mathbb{T}}_N^{\text{FP}}(u) \rangle$ (shown by red dotted line). Simulation results are shown by the cross markers demonstrating an excellent match. The accompanying subpanels showcase typical stochastic trajectories (with x and t standing for the position and time, respectively) generated for different values of u (marked by the circles) showing disparate behavior (global minima, local maxima & minima, divergence) as explained in the main text. In this analysis, we fix $x_0 = 0.5$ and vary L within the range $[0.5, 333.33]$ to explore the regime corresponding to $u \in (0.0015, 1)$. 101

6.3 (a) The scaled FPT density $f_{T_0}(x_0, t)/\frac{N x_0}{2^N}$ for the ballistic searchers (without TR) exhibits $\sim 1/t^2$ decay for any values of N. The markers represents results from numerical simulation. The solid black line is the asymptotic result as in Eq. (6.28). (b) The FPT density $f_{\mathcal{T}_N^{\text{TR}}}(L = x_0, t)$ under optimal TR. Note that the tail exponent becomes N-dependent in this case as mentioned in the main text – see Eq. (6.35). 108

6.4 Behavior of the cost function with respect to $u = x_0/L$ for $N = 3$ and $\beta = 1$. The cost attains a minimum at an optimal u^* – the variation of which as a function of N is shown in the inset panel. The squares represent data from simulations. 110

F.1 Comparison of the scaling function for $N = 2$ as in Eq. (F.27) with that obtained via numerical integration of Eq. (6.20) 165

F.2 Variation of the splitting probabilities with u for $N = 7$ as found from Eq. (F.50). Note that when $u < 1/2$ we have $\epsilon_0 > \epsilon_L$. 171

F.3 Variation of $\langle \mathcal{N}_{\rm TR}(u, N)$ as in Eq. (F.49), $\langle \overline{\mathbb{T}}_N^{\rm TR}(u)\rangle$ as in Eq. (F.53) and $\langle \overline{\mathbb{T}}_N^{\rm FP}(u)\rangle$ as in Eq. (F.55) with respect to u for distinct values of N. 171

This page intentionally left blank.

1

Stochastic resetting - a new paradigm in statistical physics

"Start again — perhaps this time you will succeed." This familiar refrain echoes in many aspects of daily life: when an origami fold goes wrong, when a web browser stalls and needs refreshing, or when the reset button on a remote restores a frozen screen. Such benefits of resetting and starting anew are not limited to qualitative anecdotes, but have been quantitatively shown to have deep and meaningful consequences in wide ranging applications. For example, in chemical reactions, the unbinding of the enzyme and substrate leads to the decomposition of the complex to its initial constituents. Such rebinding is akin to resetting, where the parent molecules start the reaction afresh. Interestingly, it has been shown that intermittent unbinding or resetting of the reaction can sometimes lead to a faster product formation rate than the unidirectional reaction with no backward reaction [1]. In biology, the mechanism of facilitated diffusion has gained notable attention to explain the ultrashort timescales arising in the protein-DNA search mechanism. In simple terms, the DNA molecules combine one-dimensional (1-d) diffusion and three-dimensional (3-d) jumps to expedite the search for the binding site in the long DNA strand. The 3-d jumps land the protein to a random site in the strand, from which the search is reset [2]. A possibly broader application of the resetting strategy is seen in the optimisation algorithms. To avoid the simulation getting stuck at some local minima, one restarts the simulation from scratch with a new set of parameters and initial conditions [3]. In ecology, dung beetles intermittently stop their motion to rise up the dung ball and course-correct their way of heading by resetting the goal of heading to the intended direction, popularly known as 'dung-beetle dance' [4]. In all such physical processes, 'resetting' plays a pivotal role in determining the system's functioning. Evidently, a complete understanding of the statistical properties of resetting is indispensable. In this section, we will review some of the notable theoretical developments in this field till now and their potential applications, which will also serve as a prerequisite for the remainder of the thesis. Finally, we will elaborate in detail on how this thesis fills

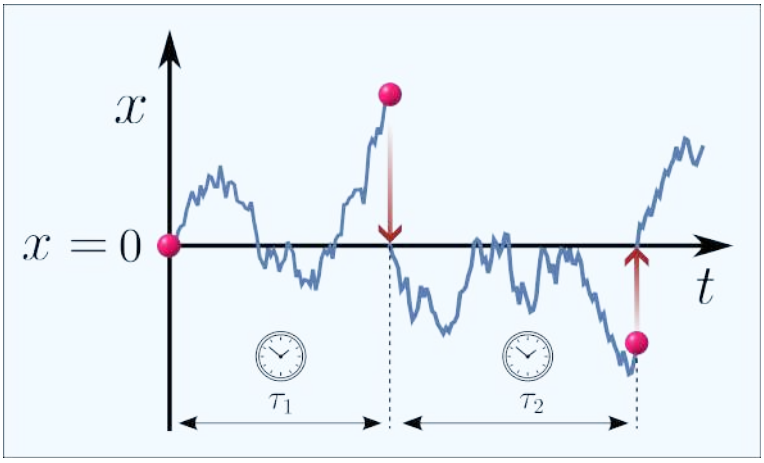

Figure 1.1: ***Brownian motion in one dimension subjected to stochastic resetting*** *– At random intervals of time* $\{\tau_1, \tau_2, ...\}$ *the particle is instantaneously brought back (reset) to the initial position* $x = 0$*. After being reset, the particle goes back to its original dynamics and the entire process renews.*

the gap existing in the current knowledge of the field.

1.1 Benefits of starting anew

The formal mathematical treatment of physical processes under restart originally emanated from the seminal work of Evans and Majumdar, namely "Diffusion with stochastic resetting" in the year 2011 [5]. The term 'stochastic resetting' refers to the strategy where one intermittently halts the dynamic evolution of a physical process at randomly chosen time intervals and restarts (resets) it from the initial configuration. Let us try to understand the strategy in depth by applying it to the paradigmatic Brownian motion (diffusion) in one dimension as shown in Fig. (1.1). Starting from the origin $x = 0$ at time $t = 0$, the particle freely diffuses till time τ_1. At $t = \tau_1$ the particle is instantaneously brought back to the starting position $x = 0$, resetting its position. After that, the particle once again starts diffusing until another resetting epoch occurs after a time interval τ_2 (i.e., at time $t = \tau_1 + \tau_2$) where the particle is again reset back to the origin. The random resetting time intervals i.e., $\{\tau_1, \tau_2, ...\}$ are generally drawn from a distribution $f_R(\tau)$. This seemingly simple method of restarting a process back from scratch gives rise to a variety of rich dynamical features in a broad class of physical systems. Primarily, it has two major cornerstones: first, it is an intuitively simple mechanism to probe statistical properties of a system far-from-equilibrium, and second, its potential impact on expediting a first-passage process. Each of those two features requires an elaborate discussion on its own. In what follows, we shall briefly discuss two of the above-mentioned fundamental aspects of stochastic resetting with the simple example of Brownian motion as discussed, and also briefly review the current state of the art of the literature.

1.1.1 Harnessing non-equilibrium features with resetting

Since its origin from the time of Boltzmann, the theory of equilibrium statistical mechanics has rapidly evolved to date. Standing today, it provides clear-cut ways to formulate and solve any physical process under thermodynamic equilibrium. However, the living world around us is mostly comprised of processes which are constantly evolving, flowing and changing with time - or in *non-equilibrium*. The moment a process is driven out of equilibrium, most of the theory of equilibrium statistical mechanics breaks down. Nevertheless, pioneered by some seminal contributions from Kubo, Zwanzig and others, the linear response theory was developed, which treated such processes under small perturbations around the equilibrium. Needless to say, the analytical tractability of this theory is limited when considering processes which have a substantial amount of perturbation, or quite *far-from-equilibrium*. At this point, the route of stochastic processes came to the rescue. The detailed formalism primarily based on Brownian motion, Markov chains, Fokker-Planck equations, and Langevin equations, proved to be indispensable to infer statistical properties away from equilibrium. Today, it is perhaps the most sought-after technique in a vast area of non-equilibrium statistical mechanics (NESM). Notwithstanding the significant amount of research dedicated to understanding non-equilibrium systems, due to the lack of a unified picture, the study of the same remains largely elusive and subject to different pathways for distinct systems. The strategy of stochastic resetting serves as one of the simplest ways to generate non-equilibrium features in a statistical process. Moreover, its analytical tractability makes it an ideal Guinea pig to study NESM both in theory and experiments. Here we shall explicitly show how resetting induces rich non-equilibrium features in even the simplest case of Brownian motion.

The theory of Brownian motion was originally provided by Einstein in one of his papers in 1905 [6]. In here, it was shown that the probability density $P(x,t)$ of finding a randomly moving Brownian particle around x at time t is found from the diffusion equation given by

$$\frac{\partial P(x,t)}{\partial t} = D\frac{\partial^2 P(x,t)}{\partial x^2}, \tag{1.1}$$

where D is the diffusion coefficient, physically measuring the amount of randomness in the motion. To ensure the probability density and flux vanish at infinity, preserving normalization and preventing probability from leaking out of the system, we impose natural boundary conditions i.e., $P(x \to \pm\infty, t) = 0$. Furthermore, assuming the particle initially starts from the origin $x = 0$, we have $P(x, t = 0) = \delta(x)$ with δ being the Dirac-delta function. Then the solution of the above diffusion equation is a Gaussian function with mean zero and variance $\sigma^2(t) = 2Dt$. The exact form of the probability

density is given by

$$P(x,t) = \frac{e^{-\frac{x^2}{4Dt}}}{\sqrt{4\pi Dt}}. \tag{1.2}$$

Note that the distribution indefinitely spreads out with respect to time (see left panel of Fig. (1.2)).

Let us now study the same motion under the influence of stochastic resetting as depicted in Fig. (1.1). For convenience of illustration, we assume that the random time interval after which the particle is reset to the origin is drawn from an exponential distribution with rate r, so that $f_R(\tau) = re^{-r\tau}$. The choice of such an exponential distribution leads to a Markovian resetting implementation where the probability of reset in a small time window t to $t+\Delta t$ is simply $r\Delta t$, which is independent of the history of the process till t. Microscopically, the random position of the Brownian particle under resetting $x(t)$ at each time step Δt can then be written as follows

$$x(t+\Delta t) = \begin{cases} 0, & \text{with probability } r\Delta t, \\ \\ \text{follows standard Brownian motion}, & \text{with probability } (1-r\Delta t). \end{cases} \tag{1.3}$$

Let us denote the probability density of the resetting particle to be found around x at time t by $P_r(x,t)$. Under the resetting condition, the diffusion equation as in Eq. (1.1) is modified as

$$\frac{\partial P_r(x,t)}{\partial t} = D\frac{\partial^2 P_r(x,t)}{\partial x^2} - rP_r(x,t) + r\delta(x). \tag{1.4}$$

The addition of two extra terms in the above equation can be interpreted in the following way: The second term in the RHS of Eq. (1.4) accounts for the loss of probability due to resetting. At any time t the particle is removed from the position x at a rate r. Multiplying that rate by the probability of finding the particle at that position i.e., $P_r(x,t)$, gives the second term in the equation. The third term in Eq. (1.4) accounts for the accumulation of probability at the origin due to resetting. Each resettling event, which occurs at a rate r, brings the particle to the origin. This causes an instantaneous increase in the probability density of the particle at the origin in the form of a Dirac-delta function. Combinedly, both the loss and gain terms due to the resetting ensure the normalisation of the probability density. The Eq. (1.4) can be easily solved in Laplace domain, and the solution yields a non-trivial time-independent stationary form as $t \to \infty$ given by

$$P_r^{\text{ss}}(x) = P_r(x, t\to\infty) = \frac{1}{2}\sqrt{\frac{r}{D}}e^{-\sqrt{\frac{r}{D}}|x|}. \tag{1.5}$$

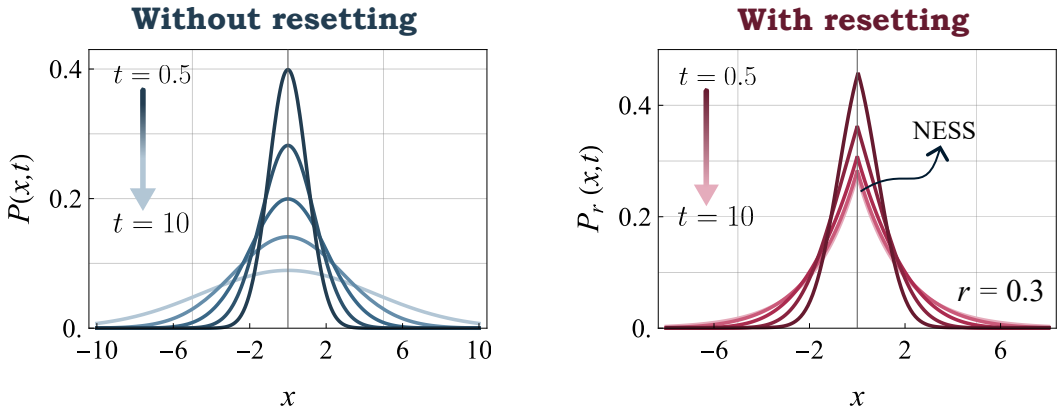

Figure 1.2: *Variation of probability density of a Brownian particle with time without resetting (left panel) and with resetting (right panel) at a resetting rate $r = 0.3$. Note that without resetting the density spreads indefinitely with time, whereas resetting stablilizes the distribution and a NESS is reached at $t \to \infty$ as in Eq. (1.5).*

The approach to this stationary state is shown in the right panel of Fig. (1.2). Note that the distribution becomes time-independent although the system is not in equilibrium due to constant violation of the detailed balance condition, which is a hallmark of equilibrium. In other words, the system is constantly driven out-of-equilibrium by means of resetting. Evidently, the system reaches a *non-equilibrium steady state* (NESS) at large enough times where a constant resetting current flows towards the origin from both directions. The existence of such a NESS is at the heart of NESM. Note two stark differences from the free Brownian motion: First, the reset-free Gaussian propagator evolves indefinitely with time, whereas resetting stabilizes the distribution and generates an exponential steady state. Second, the MSD for free Brownian motion increases as $\sim t$ at all times. In contrast, the MSD found for the Brownian particle under stochastic resetting has the form

$$\langle x_r^2(t)\rangle = \frac{2D}{r}(1 - e^{-rt}). \tag{1.6}$$

Evidently, the MSD for the reset-induced process saturates to the steady state value $2D/r$ as $t \to \infty$.

There have been numerous studies on the non-equilibrium features generated on the motion of Brownian particle induced by stochastic resetting. The study [7] particularly studies the relaxation properties to the NESS. In [8, 9, 10] the authors study the NESS generated by a stochastically reset Brownian motion under a variety of potential landscapes. Note that, our derivations assumed resetting epochs to occur at a fixed rate or following an exponential distribution. Generically, the resetting events can happen following any arbitrary distribution of $f_R(\tau)$. In [11] the authors study the resetting times drawn from a power-law distributed waiting time distribution. In contrast to the exponential resetting scenario, here it was shown that the existence of NESS is guaranteed only when the mean of the resetting time distribution is finite. The paper [12] investi-

gates Brownian motion under Gamma-distributed waiting times. Furthermore, the authors in [13] study the case where the resetting rates are time-dependent in nature. Apart from the theoretical progress, the non-equilibrium features of Brownian motion has also been verified in tabletop experiments [14, 15, 16]. We refer to [17] for a brief review of the Brownian motion under stochastic resetting.

Finally, one should note that Brownian motion represents only the most elementary case within a much broader class of stochastic processes. There are a plethora of processes where resettling plays a pivotal role in harnessing non-equilibrium properties. A few notable examples include activity-induced random motion [18, 19], random walk in lattice [20, 21] and network [22, 23], anomalous diffusion [24, 25], Ising model [26], quantum mechanics [27, 28, 29, 30, 31], stochastic thermodynamics [32, 33, 34] etc. Needless to mention, the quest to understand NESM is still ongoing in a full-fledged fashion, where stochastic resetting has proven to play a key role.

1.1.2 First-passage optimization with resetting

Besides providing new routes to study non-equilibrium physics, possibly one of the most significant outcomes of the strategy of resetting is its potential influence on a stochastic search process. Search processes are ubiquitous in nature. While searching for a lost key, locating a familiar person in the crowd, finding a particular product a supermarket or finding a particular topic in a book - we encounter many such search processes in our daily lives. In fact, search processes are equally prominent in a major share of scientific research. In chemistry, the enzyme molecules randomly move in the solvent to find the substrate to bind. In physics, one often searches for a desired minima or maxima in a complex potential landscape. In stock market, investors look for an optimal stock price to exit and book profit, to name a few. No wonder, the study of search processes has been a focal point for scientific research spanning across diverse contexts from physics [35, 2, 36], biology [37], chemistry [38, 39], ecology [40, 41, 42], computer science [43], finance [44] to aviation and marine navigation [45].

In context of statistical physics the search processes are termed as first-passage (FP) processes. Generically there are two main component of a FP process- a searcher and a target. One key aspect of the study of FP processes is to find suitable strategies for the searcher to locate the target in a minimal time span. For example, Animals have adapted several search strategies to find their home or resources in an optimal way [46, 47, 48]. In living systems, many living agents such as proteins seem to perform efficient universal navigation dynamics eg facilitated diffusion to optimally search the target sites [49, 50]. Likewise in physics, several search strategies have been explored as a potential way for facilitating the FP processes [2, 51, 36].

The seminal work of Evans and Majumdar [5] proposed stochastic resetting as a novel optimization technique in a FP process. It says, stopping a search process midway and restarting the enitre search process all over again from the initial position can

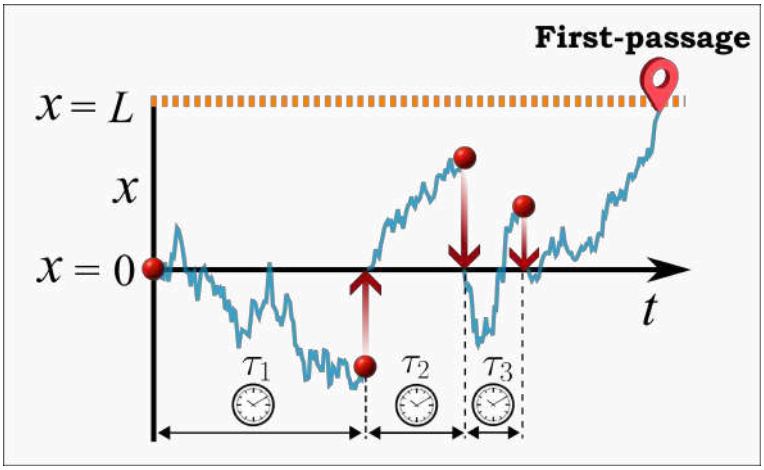

Figure 1.3: ***First-passage of a Brownian particle under stochastic resetting*** – *The particle starts from the origin $x = 0$ at time $t = 0$. It undergoes free diffusion until at random intervals of time $\{\tau_1, \tau_2, \tau_3 ...\}$ the particle gets reset to the origin again. This diffusion and reset motion continues until the particle reaches the target at $x = L$. Upon reaching this target the process is terminated and we call it a first-passage event.*

facilitate the FP process. Although seemingly counter-intuitive, resetting has emerged as one of the simplest yet powerful strategies in recent days to expedite a variety of FP processes ranging from statistical physics [52, 53, 54, 55], quantum mechanics [27, 56], molecular dynamics [57, 58, 59] to chemical [60] and biological processes [61, 62]. In this section, we shall try to understand the benefits of resetting a first-passage process with the example of Brownian motion in 1-d (one-dimension) as also discussed in the previous section. Consider a Brownian particle that starts its motion from the origin $x = 0$ at time $t = 0$. In between its random motion at stochastic time intervals drawn from the distribution $f_R(\tau)$ the particle is instantaneously brought back to the starting position. Till now this is the same set-up as considered in section (1.1.1). However, now consider a target is placed at the position $x = L$ (see Fig. (1.3)). The target acts as a sort of absorbing boundary. Whenever the particle reaches this target, it gets absorbed there, and the process is deemed to be completed. The event, when the particle reaches the target for the first time, is known as the first-passage (FP) and the corresponding random time for the process is known as the first passage time (FPT). Our next job is to quantify and understand the first-passage quantities of this reset-induced process.

***Unified renewal approach*:** As with the Fokker-Planck equation as in Eq. (1.4) for the propagator, to extract the first-passage quantities, one can write a *backward Fokker-Planck equation* (BFPE) in terms of the survival probability $Q_R(x_0, t)$ of the particle which is the probability that the particle starting from $x = x_0$ at $t = 0$ *will not* find the target or will survive up to time t while it performs the resetting dynamics. Note that, the variable in the BFPE is the initial position x_0 (instead of x as in Eq. (1.4)) with the boundary conditions $Q_R(x_0 \to -\infty, t) = 1, Q_R(x_0 = L, t) = 0$ and initial condition

$Q_R(x_0, t = 0) = 1$ (see [63]for a complete derivation of this method). We shall also discuss the BFPE approach in detail in chapter 2.

However, in this section, we take an orthogonal approach based on the renewal theory of random variables to find the desired quantities. This general formalism based on the renewal theory allows us to, first, find a universal description of the resetting mechanism irrespective of the kinds of dynamics under consideration or the resetting mechanism. Especially when the resetting dynamics are non-Markovian in nature (so that the distribution $f_R(\tau)$ is not an exponential function), the Fokker-Planck equations are hard to write. In such cases, the renewal approach comes to the rescue. Secondly, the formalism can also be extended to a more general scenario where the resetting events are non-instantaneous in nature, as seen in experiments and to be illustrated in the later parts of the thesis. In the following, we illustrate the renewal formalism in the case of stochastic resetting as originally proposed in [54, 53] and show the broader implications of the results obtained through this approach.

The main ingredient of the renewal formalism lies in identifying a repetitive pattern in the process under consideration. For e.g., in the resetting dynamics under consideration, the particle's motion starts afresh from the origin $x = 0$ after each resetting event and the entire process repeats itself. Such repetition of the process is called a *renewal event*. In Fig. (1.3) the process is renewed for the first time at time $t = \tau_1$ when the first resetting occurs. From this figure one can also see the last renewal has occurred at time $t = \tau_1 + \tau_2 + \tau_3$ just before the first-passage. Identifying these renewal events is the first important step in developing the renewal theory. In the following we shall mathematically express this renewal formalism in terms of the random variables associated with the FP quantities of the process. Let us fist define them systematically in the following list:

- T_R – Random variable standing for the FPT of the process under resetting i.e. the random time at which the particle reaches the target.
- T – Random variable denoting the FPT of the process in absence of resetting mechanism.
- R – Random variable standing for the random resetting times i.e., $\{\tau_1, \tau_2, \tau_3 ...\}$ which are drawn from the distribution $f_R(\tau)$.

With this identification, one can write the following renewal equation for the FPT of the entire process under resetting i.e., T_R, given by

$$T_R = \begin{cases} T & \text{if } \; T < R \, , \\ \\ R + T'_R & \text{if } \; R \leq T \, , \end{cases} \tag{1.7}$$

where T'_R is an independent and identically distributed (i.i.d.) copy of T_R. We also assume that resetting gets priority over FP, hence the equality in Eq. (1.7). The equation can be interpreted in the following fashion: The particle can make the first passage in two possible ways. In the first case, it does not experience any resetting events before

making the first passage. This is accounted by the first condition, where the FPT is of the reset-free process i.e., T, but occurs only if $T < R$. On the other hand, it can also experience multiple resetting events before the first-passage. In that case, we assume the first-resetting event occurs at time R, after which the entire process repeats and the FPT is T'_R, an i.i.d. copy of T_R. The latter scenario happens if $R \leq T$. Starting from the renewal equation Eq. (1.7) and after a bit of simplification, one arrives at the following expression for the mean first-passage time of the process, given by

$$\langle T_R \rangle = \frac{\langle \min(T, R) \rangle}{\Pr(T < R)}. \tag{1.8}$$

Here $\min(T, R)$ denotes the minimum of the two random variables R, T, and $\Pr(T < R)$ stands for the probability that $T < R$ (Appendix A.1). Note that the the above result is not specific to the Brownian motion but applies to any arbitrary stochastic dynamics under resetting. Moreover, the renewal equation Eq. (1.7) not only gives expression for the mean but the full generating function of the FPT T_R, which in turn allows extraction of all its moments.

Although, the above result generally holds for any arbitrary resetting protocol, for simplicity, let us illustrate the result with the exponential case, i.e., $f_R(\tau) = re^{-r\tau}$. Starting from Eq. (1.8), the MFPT for any generic stochastic process with a fixed resetting rate r has the following form (see Appendix A.1 for the detailed derivation)

$$\langle T_r \rangle = \frac{1 - \tilde{T}(r)}{r\tilde{T}(r)}, \tag{1.9}$$

where $\tilde{T}(r)$ is the Laplace transform of the first-passage time distribution $f_T(t)$ of the underlying reset-free process i.e., $\tilde{T}(r) = \int_0^\infty dt e^{-rt} f_T(t)$. The above result reveals that the MFPT of the reset-induced process can be found in terms of the FPT distribution of the reset-free process. Notably, in a variety of FP problems the FPT distribution is readily available in the Laplace space which, through (1.9), immediately determines the MFPT of the process with resetting. Moreover, the result is also not system-specific and holds for any generic stochastic process as well. For the specific choice of Brownian motion, the corresponding reset-free density is the very well-known Lévy-Smirnov distribution, which is given by [35]

$$f_T(t) = \frac{L}{\sqrt{4\pi D t^3}} e^{-L^2/4Dt}, \tag{1.10}$$

with the associated Laplace transform given by

$$\widetilde{T}(r) = e^{-\sqrt{rL^2/D}}. \tag{1.11}$$

Plugging the above expression into Eq. (1.9) we eventually arrive at the following result

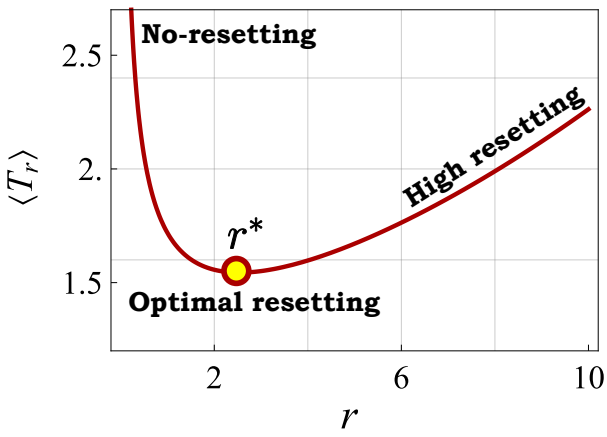

Figure 1.4: ***Mean first-passage time (MFPT) for diffusion under resetting –*** *The MFPT (as obtained from Eq. (1.12) with L = 1, D = 1) shows non-monotonic dependence on the resetting rate r. For low resetting rates the MFPT is infinite mimicking that of the reset-free process. On the other hand, too much of resetting also causes the MFPT to diverge. In between, there exist an optimal resetting rate r^* at which the MFPT is the lowest.*

for the MFPT of the diffusive Brownian motion under exponential resetting,

$$\langle T_r \rangle = \frac{1 - e^{-\sqrt{rL^2/D}}}{re^{-\sqrt{rL^2/D}}}. \tag{1.12}$$

In Fig. (1.4) we plot this MFPT that exhibits a non-monotonic behaviour with respect to the resetting rate r. Let us first understand the extreme limits of this equation. In the limit $r \to 0$ i.e., the reset-free limit, the MFPT diverges as $\sim \frac{1}{r}$. This is the classic free-diffusion limit where the MFPT is divergent in absence of resetting. Physically, when no resetting is there, the particle has a finite chance of moving continuously away from the target with time. Such detrimental trajectories may consume an huge amount of time to return to the target leading to a diverging MFPT [35, 5]. On the other hand, when resetting becomes too frequent such that $r \to \infty$ the MFPT again diverges exponentially as $\sim e^{\sqrt{rL^2/D}}/r$. In this limit, the resetting is so frequent that the particle remains around the origin most of the time and hardly gets a chance to even reach the target. In between these two extreme limits there exists an optimal amount of resetting such that the MFPT is lowest there. The exact value of the resetting rate $r = r^*$ at which the MFPT becomes lowest is known as the *optimal resetting rate* (ORR) which can be found from the equation

$$\left.\frac{\partial \langle T_r \rangle}{\partial r}\right|_{r=r^*} = 0 \tag{1.13}$$

Plugging the expression from Eq. (1.9) one then arrives at the following expression for

the ORR [5, 52, 54, 64]

$$r^* = 2.537 * D/L^2. \tag{1.14}$$

The emergence of such ORR can also be explained from simple arguments as follows. A very high value of resetting rate would confine the spread ($\Delta x = \sqrt{\langle x_r^2 \rangle}$) of the particle close to the origin so that $\Delta x = \sqrt{2D/r} \ll L$ and it hardly manages to reach the target. On the other hand, a very small value of the resetting rate would cause the particle to move further away from the target so that $\Delta x = \sqrt{2D/r} \gg L$. Evidently an ideal choice of ORR should be such that both the effects are suitable optimized which happens around the limit $\Delta x \approx L$ such that one finds $r^* \approx 2D/L^2$. For such choice of the ORR based on the diffusive time-scale the particle gets just enough time to locate the target without deviating further away from it. The choice of the ORR ensures that the MFPT is the lowest for the diffusion. The ORR plays a pivotal role in the theory of stochastic resetting.

Unlike the free-diffusion case discussed above, the existence of a ORR is not guaranteed if the dynamics of the particles are changed. For example, consider the drift-diffusive search process. In here, an additional drift velocity v toward the target is added to the particle on top its diffusive motion. The first-passage time density and its Laplace transform in that case is given by [35]

$$f_T(t) = \frac{Le^{-\frac{(L-tv)^2}{4Dt}}}{2\sqrt{\pi}\sqrt{D}t^{3/2}}, \quad \widetilde{T}(r) = e^{\frac{L\left(v-\sqrt{4Dr+v^2}\right)}{2D}}. \tag{1.15}$$

Plugging this expression in Eq. (1.9) we find the MFPT under resetting for the drift-diffusive case given by

$$\langle T_r \rangle = \frac{e^{\frac{L\left(-v+\sqrt{4Ds+v^2}\right)}{2D}} - 1}{r}. \tag{1.16}$$

Following the same procedure as in the free-diffusion case, in here, one finds that the ORR exists only for a certain choice of v as seen in Fig. (1.5). Note that when v exceeds a certain threshold value the ORR becomes zero. Physically, for very high values of the drift-velocity v the MFPT of the reset-free process L/v is small enough so that resetting the particle's motion only delays the first-passage. Such behavioural transition of the ORR with respect to the system parameters, is known as 'resetting transition' and has been studied quite rigorously in a variety of physically systems [65, 66, 67] Specifically, by expanding $\langle T_r \rangle$ in the limit of small r and setting the first-order correction term to be zero one can explicitly find the criterion for resetting to be beneficial for any arbitrary

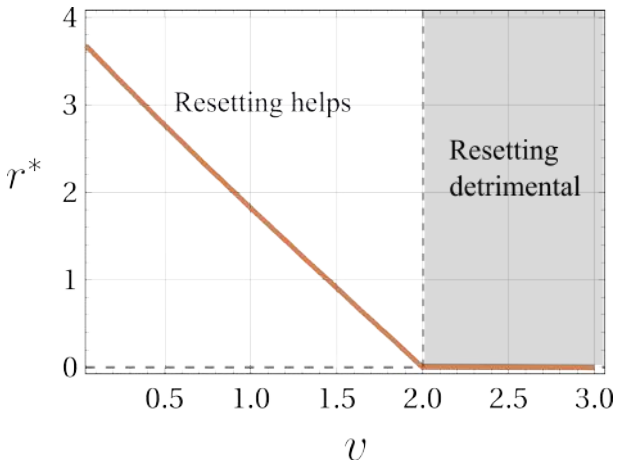

Figure 1.5: ***ORR for drift-diffusive process under resetting*** *– Note that the ORR r^* becomes zero when v is sufficiently large. In that case (shown by the shaded region), the reset-free process itself is the most optimised situation and adding any amount of resetting would only prolong the search process. The parameters for the plot are: $L = 1, D = 1$.*

stochastic process is given by [53]

$$CV = \sqrt{\frac{\langle T^2 \rangle - \langle T \rangle^2}{\langle T \rangle^2}} > 1, \tag{1.17}$$

where $\langle T \rangle, \langle T^2 \rangle$ are the mean and second moment of the FPT distribution of the reset-free process, respectively, and CV denotes the coefficient of variation. Physically, a higher value of CV is associated with a broader distribution. It turns out resetting reduces the broadness of a distribution but cutting off the tails emanating from trajectories which diverge far away from the target. For the specific case of drift-diffusive search process, the criterion is found to be

$$CV = \sqrt{\frac{2D}{Lv}} > 1. \tag{1.18}$$

Thus, the resetting transition in the drift-diffusive search process is governed by the Peclet-number $Pe = \frac{Lv}{2D}$ [65, 64, 66, 68]. We shall return to the explicit derivation and analysis of the CV criterion in chapter 5.

This concludes a very brief into to the two key aspects of stochastic resetting. Most of the content of this thesis will be built over the methodology provided in here. Before delving into the main body of this thesis let us briefly discuss the goal of this thesis and sketch out the structure at which they will be presented.

1.2 Goal of this thesis

The objectives of this thesis can be broadly classified into three categories. In the first, we illustrate the application of the theory of resetting into three different contexts,

namely, chemical reactions, viscoelastic media and queueing processes. Secondly, we propose a unifed formalism to extract the FPT statistics under resetting from an experimental perspective, where the return events are space-time coupled. Finally, we consider an alternative resetting strategy based on threshold crossing events to expedite a multi-agent correlated search process. Each of these categories are discussed below in detail.

1.2.1 Applications of stochastic resetting in diverse contexts

A significant part of this thesis has been devoted to exploring the possible real-life applications of stochastic resetting across a wide spectrum of physical processes—from chemical reactions and viscoelastic media to problems in operations research. These studies collectively demonstrate how resetting can act as a universal strategy to optimise efficiency, stabilise dynamics, and control fluctuations in complex systems. The main findings are summarised below.

Rate enhancement of gated chemical reactions

How long does it take for a chemical reaction to be complete? The conventional approach to this problem was given by Michaelis and Menten in their seminal paper in 1913 [69]. However, a seemingly possible backdrop of the Michaelis-Menten theory lies in the fact that it treats the chemical reaction in the time domain, whereas most reactions in laboratory or biology occur in space, with the reactant molecules randomly diffusing in the solution. This gap was filled by Smoluchowski in 1917 in the paper [70]. Since then, the study of diffusion-controlled chemical reactions has seen extensive development, leading to a promising understanding of the underlying mechanism (see [71] for a review).

An important aspect of the diffusion-controlled reaction revolves around the study of 'gated' chemical reactions. Due to the nature of the solution, the physical/chemical configurations, two reactants might not always form a product whenever they bind. 'Gated' reactions refer to such chemical processes in which the reactant molecules fluctuate between active and inactive phases. The product can only be formed when both of them meet in an 'active' state. Although such reactions have seen a substantial progress starting from the seminal contribution from Szabo et. al. [72, 73, 39], recent studies [74, 75, 76] have enabled us to consider a more unified theory of gated reactions. In addition to the 'gated' component, a formed complex can also unbind spontaneously to go back to its constituent molecules, which mimics a resetting event. Furthermore, the molecules have a certain affinity to move towards their correct complement to form product, which can be thought of as a drift towards the reaction target. Building upon the foundational works on gated kinetics [72, 73], we investigate how stochastic resetting influences such drift–diffusive transport processes toward a stochastically gated target in chapter 2.

The central quest in our study is to identify parameter regimes where resetting accelerates the overall reaction rate. Our analysis shows that resetting can substantially

enhance the completion rate of diffusion-limited reactions by curbing long excursions in phase space that delay binding events. Conversely, in drift-dominated regimes, resetting may slow the process, giving rise to a clear crossover governed by the interplay of drift, diffusion, and gating timescales. These findings allowed us to map out three characteristic regimes: (i) resetting-enhanced reactions, (ii) partially beneficial regions, and (iii) regimes where resetting provides no gain. Beyond its analytical clarity, the study offers insights into enzyme kinetics and other reaction networks where stochastic interruptions can be engineered to improve efficiency.

Resetting in viscoelastic media

The classical theory of Brownian motion by Einstein had the underlying assumption that the timescale of observation is much larger than the timescale of collision between the particles. That in principle implies that the correlation between the particle's movement at each time step decays instantaneously and is independent of its history. In many systems, however, the time scale of the molecular motion is not very much shorter than the time scale of the motion of the suspended particle. In such cases, the Einstein's description of Brownian motion has to be suitably modified to take into account the nature of the medium and how the correlations between successive collisions decay with time. Such media are also known as 'viscoelastic' in physics where the viscous motion follows Einstein's theory of Brownian motion and the elastic property takes into account the non-instantaneous decays of correlations between the particle and the media.

How to treat a viscoelastic medium then? Kubo and Mori first proposed the theory of generalized Langevin equation (GLE) to incorporate the memory effect into the particle's dynamics [77, 78]. They showed that introducing a time-dependent memory kernel into the Langevin description of the Brownian motion, indeed gives rise a rich statistical behaviour of the particle's dynamics. A plethora of studies have been followed till now to study the statistical properties of GLE under various theoretical and experimental setups.

We next study the role of stochastic resetting in viscoelastic systems, where the dynamics are inherently non-Markovian due to the persistence of memory in the medium in chapter 3. To address this, we extended the renewal approach to the generalized Langevin equation (GLE) with arbitrary friction kernels, enabling the exact derivation of mean-squared displacements (MSD) and two-time correlation functions under resetting.

As a concrete example, we analysed a particle moving in a Jeffreys fluid [79, 80], a model that has been shown to be a good approximation in many experimental systems. Without resetting, the MSD exhibits an intermediate saturation plateau due to slow relaxation of the viscoelastic bath. Introducing resetting drastically modifies this behaviour—the plateau is suppressed, correlations decay faster, and in the limit of frequent resetting, the system effectively recovers normal diffusive behaviour. These results, supported by

numerical simulations via Markovian embedding, demonstrate that resetting provides an effective external control parameter for manipulating non-Markovian dynamics. This could have potential implications for microrheology experiments, intracellular transport, and diffusion in crowded or active environments.

Optimizing queue length via service resetting

Finally, we applied the concept of stochastic resetting to queuing systems, a cornerstone of operations research and performance optimisation in chapter 4. Queues are ubiquitous — from super market, telecommunications, computer networks to biological and enzymatic processes. However, they are often constrained by intrinsic fluctuations in service times. A central challenge is a queuing theory is, how to find optimal strategies to mitigate a long queue? Traditional control strategies are generally effective only for extrinsic fluctuations but fail when the randomness originates from the service mechanism itself [81, 82].

In our study, we introduced a framework of *service resetting*, where the server intermittently restarts its operation after a random overhead period. Modelling the system as an M/G/1 queue with overhead, we developed a renewal formulation that generalises the classical Pollaczek–Khinchin results. The analysis revealed that the efficiency of resetting strongly depends on the distribution of overhead times. For systems with broad or heavy-tailed service fluctuations, an optimally tuned resetting rate can substantially reduce the mean queue length by simultaneously lowering the average service time and suppressing stochastic variability. Interestingly, we also found that periodic resetting performs better than random resetting under certain conditions. These insights may inspire new approaches to managing congestion and optimizing service efficiency in stochastic networks, computational systems, and biochemical processes.

1.2.2 Towards experimental realization of stochastic resetting

A key assumption in the resetting model discussed till now is that the particle/searcher resets to the initial position instantaneously. Notwithstanding the simplicity of the model, question arises about its practical applicability. In practice or in an experiment, any return event of the searcher to its starting position must take a finite amount of time. Previous studies have made such attempt either by adding an overhead time after each reset [83, 84, 85, 1] or making the return process space-time correlated [12, 86, 87, 88, 89, 88, 90]. Since the return motion of the searcher was *deterministic* and was always directed to the resetting location, such protocols have always contributed addition time penalty to the FPT in comparison to the classical instantaneous return processes.

To understand this further, let us discuss how a Brownian particle is actually reset in tabletop experiments. In Fig. (1.6)(a) we show the actual trajectory of a resetting Brownian motion studied in experiments by Tal-Friedman et. al. [14]. Under this set-up, an optical tweezer is turned on around the instantaneous position of the particle. The

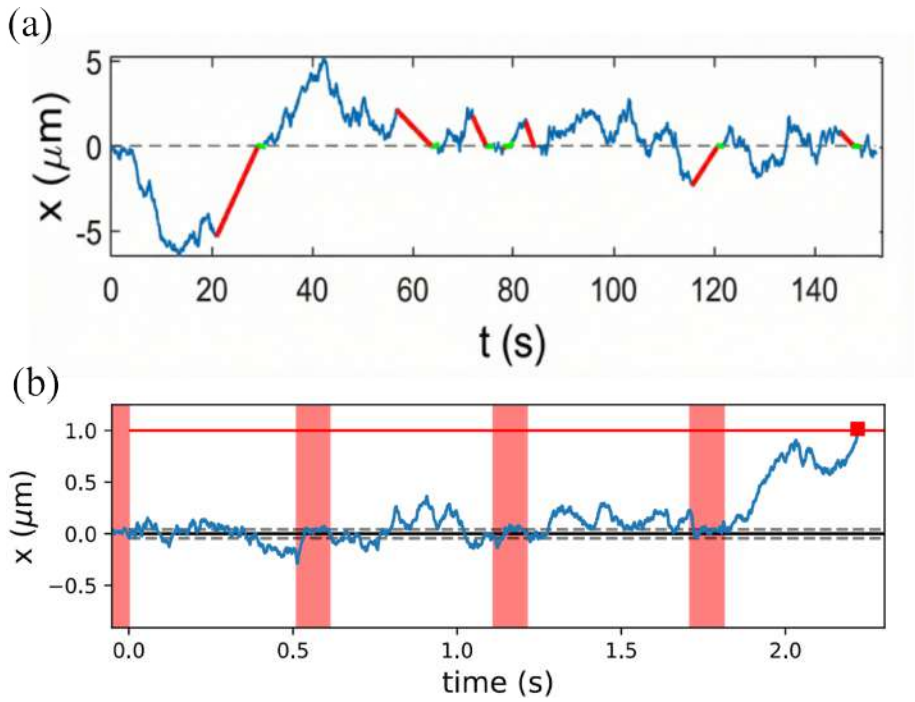

Figure 1.6: *Experimental trajectory of a resetting Brownian particle from the study of (a) Tal-Friedman et. al. [14] (b) Besga. et. al. [15]. Unlike the theoretical model as shown in Fig. (1.3) where the particle resets instantaneously to the origin, in experiments, it always costs a finite time penalty.*

electro-magnetic field created by optical tweezers effectively gives rise to a confining harmonic trap around the particle. For a sufficiently high values of the trap stiffness the particle is essentially trapped and cannot get out of the confining potential. This gives the experimentalists access to move the particle at will (keeping some constraint on the velocity). At each resetting phase, the particle is brought back to the origin with a constant velocity (shown by the red lines). In another experiment by Besga et. al. [15] the Brownian particle was reset by turning on an optical tweezer around the origin as shown in Fig. (1.6)(b) (in contrast to the instantaneous position of the particle in the earlier experiment). When the tweezer is on, the particle feels a drag force towards the origin under the effect of the potential and comes back to the origin, mimicking a complete resetting phase (shown by the red shaded region in the figure). Besides resetting taking a finite amount of time, another key feature of both these experiments is that the particle cannot find the target during the return phase. But this condition need not be true in a generic search process. For example, in the experiments by Besga et. al. [15], the trajectories where the particle escaped to the target while the trap is on, were filtered out. In general search process a more realistic case would be to make the searcher active even during the return phase so the target could be detected.

In chapter 5, we provide a unified theory of a generic first-passage process under stochastic resetting with *non-instantaneous return*. The theory incorporates any given choice of the return motion followed by the searcher, either deterministic (with constant velocity, acceleration) or stochastic (as followed by the Brownian particle under the

potential). In particular, we shall show that when the resetting phase is stochastic in nature so that target detection is possible during the resetting phase, it not only resembles the most physical picture of the experiment but also can serve a superior strategy than the classical instantaneous return. Furthermore, we shall see how the stochastic return of the searcher while resetting can do a better job in first-passage optimization than the instantaneous resetting at its best (at ORR as discussed previously).

1.2.3 A novel target search optimization strategy based on threshold resetting

Threshold-crossing phenomena play a central role in many natural and engineered systems. For example, integrate-and-fire neurons are triggered when a certain action potential threshold is crossed [91]. In stock market, threshold price based strategies like stop-loss or stop-profit are very popular [92]. In immunology, the kinetic proofreading model suggests a threshold number of reaction steps to be completed for rare antigen detection [93]. Despite its natural prevalence, the first study of event-driven resetting was taken up very recently by Falcao and Evans [94] where two Brownian particles biased towards each other reset to their respective initial positions upon collision. In here, when the distance between the two particles acts as the variable with the threshold at zero. Thereafter, De Bruyne et. al. [95] proposed a general formalism for a threshold-based resetting strategy for a generic stochastic process. In here, the process is reset after hitting a certain pre-specified threshold. Unlike the traditional resetting, threshold resetting (TR) is an event-based resetting mechanism where resetting events are solely dependent on the system parameters. Although such TR events are very common in nature, the study of them remains comparatively underexplored. For e.g., a few natural questions arise - how would such TR strategy alter the FP statistics of a stochastic process? How a multi-agent target search would be affected by TR? Is there an optimization protocol based on TR on a FP process?

Motivated by this, we develop a unified theoretical framework for FP processes under a threshold-resetting mechanism in chapter 6. In this framework, a system of one or more searchers resets whenever any one of them crosses a predefined threshold, with all agents returning to their starting positions and the search resuming. This collective resetting naturally couples the dynamics of the agents, inducing correlations that influence the search efficiency.

To illustrate the formalism, we consider N independent ballistic searchers moving in one dimension with constant speeds and randomly oriented initial velocities. Our analysis shows a non-trivial optimisation of the mean first-passage time (MFPT): frequent threshold resets can minimise the MFPT, providing a clear performance advantage. By further introducing a cost function associated with the resetting process, we demonstrate that the collective threshold-resetting protocol achieves an optimal balance between efficiency and resource expenditure. Importantly, the framework also allows the computation of higher-order moments of the search time. Overall, this threshold-

resetting mechanism emerges as a simple yet effective strategy for target search problems, offering insights into the control of collective stochastic processes and providing a foundation for potential applications in diverse contexts where event-driven resetting naturally arises.

To summarise, a significant part of the thesis is devoted to bridging the gap between the theory of stochastic resetting and its potential applications. First, we show how the theory can be implemented in gated chemical reactions by modelling with a drift-diffusive search process. Interestingly, we find that a certain unbinding rate of the enzyme-substrate compound modelled as a resetting event enhances the product formation rate of the reaction. Next, we apply the resetting strategy to queuing theory and show how it can mitigate long queues and prevent prolonged waiting times. Then, we study the resetting dynamics in a non-Markovian system, namely a microscopic particle in a viscoelastic medium. By analysing the generalised Langevin equation describing the media under resetting dynamics, we find the emergence of novel time-scales and NESS. Next, we propose a unified renewal theory for resetting that incorporates any generic non-instantaneous return motion of the searcher. By corroborating the results from the theory with actual parameter sets taken from experiments, we show a stochastic component in the return motion of the searcher can facilitate the search process. Finally, we propose a novel first-passage optimization technique based on a threshold crossing resetting strategy. By considering a parallel multi-agent search process, we show that such a threshold resetting strategy can indeed generate rich optimization features in a FP process. Overall, this thesis advances the role of stochastic resetting in nonequilibrium statistical mechanics and opens new directions for applying these concepts to complex dynamical processes.

2

Stochastic resetting in gated chemical reactions

(The content of this chapter has been published in [96])

2.1 Introduction

In biochemistry, the term 'gating' generally denotes the transition between the *open* and *closed* states of an ion channel, allowing ions to pass only when the channel is open [97]. Similarly, in a gated chemical reaction, reactant molecules alternate between reactive and non-reactive forms; a successful reaction occurs only when collisions involve the reactive states. Consequently, gating represents a hallmark of constrained reaction or transport processes, whether it involves an enzyme locating the correct substrate, a protein binding to a specific DNA site, or a peptide encountering its cleavage site. Due to their broad relevance, gated processes are found in diverse contexts ranging from chemistry [98, 99, 72, 100], physics [73, 101, 102, 103, 104, 105, 106], to biology [107, 108, 76].

Following the seminal studies of Szabo *et al.* [72, 73, 39], gated processes have attracted substantial attention across a variety of applications, including 1D gated continuous-time and discrete-space random search in confined domains [102], intermittent switching dynamics of proteins undergoing facilitated diffusion along DNA [39], 3D gated diffusive searches with heterogeneous diffusivities [103], and gated active particles [109]. Gopich and Szabo analyzed models with multiple gated particles or targets exhibiting intrinsic reversible binding [105], while Lawley and Keener established connections between reactive/radiative boundaries and gated boundaries in diffusion-controlled reactions [110]. Recent renewed interest stems from the works of Mercado-Vásquez and Boyer on 1D gated diffusion on an infinite line [75], Scher and Reuveni on gated reactions across arbitrary networks, including both continuous- [74] and discrete-time [111] random walks, and Kumar *et al.* on threshold crossing events and inference of first-passage times in gated diffusive processes [112, 113]. In this work, we extend these

studies by examining design principles to optimize the efficiency of a gated reaction [see Fig. (2.1)].

Completion of a gated diffusive process requires meeting a condition that mimics the open-gate scenario, imposed either on the diffusing particle or on the target. This gating restriction increases selectivity, essential for proper biochemical function, but it also slows the process relative to an ungated counterpart. Nature, however, often compensates for this by facilitating reactions through mechanisms such as unbinding or resetting from metastable states, as illustrated in Fig. (2.1). The impact of such resetting has been demonstrated in chemical reactions [1, 66], RNA polymerase backtracking [114], and RhoA disassociation kinetics in membranes [115]. Reactant or morphogen motion, with continuous production and finite lifetime, can similarly be treated as stochastically restarted processes [116]. Pioneering work by Evans and Majumdar [5] showed that stochastic resetting can significantly accelerate 1D diffusive search processes. This finding has inspired numerous studies demonstrating benefits of intermittent resetting in both diffusion-controlled [13, 68, 9, 117, 10, 118, 119, 120, 121, 122] and non-diffusive stochastic processes [61, 53, 55, 123], reviewed comprehensively in [17]. Experiments with optical traps further validated these concepts [14, 15]. Despite these advances, understanding resetting in gated processes remained limited until recent studies demonstrated its role in reducing average completion times in 1D gated diffusive processes [124, 125].

Resetting benefits purely *diffusive* transport in unbounded domains, but its effect in *drift-diffusive* search processes is more nuanced. Resetting helps only if diffusion dominates drift; when drift exceeds diffusion, resetting can increase transit times. This interplay is captured by the Péclet number, comparing diffusion- and drift-dominated timescales [65, 126, 127, 128]. Resetting can also be quantified using the universal first-passage under restart framework, showing it is advantageous when the coefficient of variation of the completion time (standard deviation divided by mean) exceeds unity [53, 129, 54]. These results motivate our study of resetting in gated drift-diffusive processes, which, to our knowledge, has not yet been explored. Specifically, we aim to determine whether resetting can accelerate completion and under what conditions, analyzing the combined effects of drift, diffusion, gating, and resetting.

To illustrate our setup, consider a diffusive transport process on the positive semi-infinite line with constant drift toward a target that switches randomly between open and closed states at a constant rate. This mimics, for example, the chemical reaction in Fig. (2.1), where collisions between CR_1 and R_2 yield a product only if at least one reactant is activated ($R_2^\star$). Since resetting is integral to reversible reactions (e.g., C binding/unbinding from R_1), this system can be described as gated drift-diffusion with resetting. We analyze the completion time statistics, explore optimal resetting to accelerate transport, and construct a phase diagram distinguishing regimes where (i) resetting accelerates gated drift-diffusion beyond the ungated process, (ii) resetting improves gated

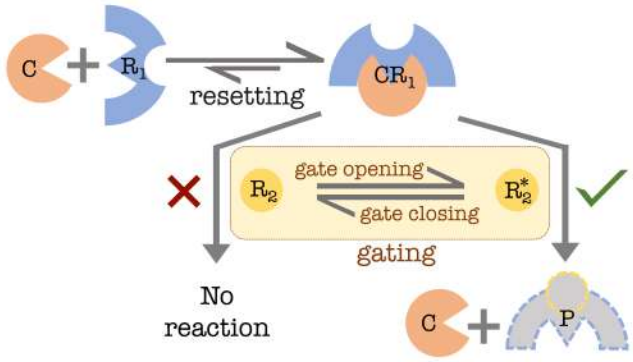

Figure 2.1: *Scheme for a gated chemical reaction between two reactants R_1 and R_2, catalysed by C. In the first step, the catalyst binds reversibly with R_1 to form a metastable intermediate CR_1: $C + R_1 \rightleftharpoons CR_1$. Next, CR_1 reacts selectively with $R_2^\star$ (the reactive or open-gate state of R_2) to form the product P and release the catalyst: $CR_1 + R_2^\star \rightarrow C + P$. This step is modeled as gated drift-diffusion, while unbinding of C from R_1 represents resetting.*

drift-diffusion but not beyond the ungated rate, and (iii) resetting fails to expedite the process.

The chapter is organized as follows. Section 2.2 introduces the model and derives the Fokker-Planck equations for gated drift-diffusion under resetting. We solve for the mean completion time $\langle T_r^G \rangle$, determine the optimal resetting rate $r^\star$, and identify conditions for accelerated completion in Section 2.3, including various limiting cases. Section 2.4 quantifies the maximal speedup achievable via optimal resetting. Section 2.5 presents the full phase diagram characterizing the influence of resetting. Section 2.8 concludes with a brief summary and outlook.

2.2 Completion time statistics

We begin by framing the problem of a gated chemical reaction [$CR_1 + R_2^\star \rightarrow C + P$, introduced in Fig. (2.1)] in terms of gated drift-diffusion. One convenient way to implement this mapping is to associate the reaction coordinate of the reactants $CR_1 + R_2^\star$ with the initial position $x_0 > 0$ of a particle undergoing Brownian motion [see Fig. (2.2)]. Similarly, the products $C + P$ are represented by a target located at the origin. The chemical potential driving the reaction can be translated into a constant bias λ acting on the particle as it diffuses toward the target with diffusion coefficient D. Positive λ corresponds to drift towards the target, while negative λ represents drift away from it. This effective one-dimensional representation of an enzyme or protein energy landscape is commonly employed in the literature [130, 131, 132].

Several key assumptions are made in this mapping. First, it is well-established that chemical master equations for discrete states can be coarse-grained into Fokker-Planck equations for continuous reaction coordinates using a system-size expansion [133, 134]. This coarse-graining generally introduces spatial dependence in the drift and diffusion coefficients. In other words, the reaction coordinate associated with $CR_1 + R_2^\star \rightarrow C + P$

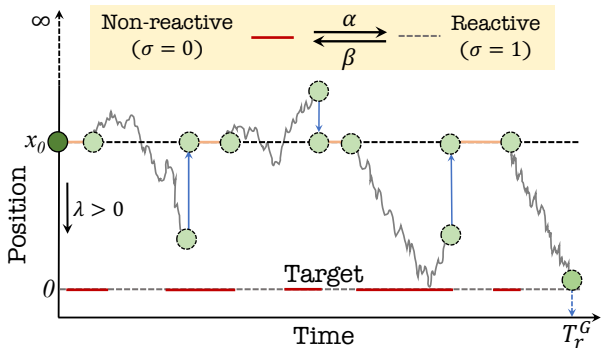

Figure 2.2: *Schematic diagram of a gated drift-diffusion process in semi-infinite space with resetting, where the target (placed at the origin) switches stochastically between a reactive state ($\sigma = 1$) and a non-reactive state ($\sigma = 0$). The transition from the non-reactive to the reactive state takes place with a constant rate $\alpha > 0$, and the opposite transition takes place with a constant rate $\beta > 0$. When the particle, starting at x_0, hits the target in its reactive state (dashed line), the process ends. T_r^G marks the random completion time of the gated drift-diffusion process with resetting.*

typically evolves in an arbitrary energy landscape, with the product state $C + P$ as the global minimum. To simplify the analysis, we approximate this potential as linear, leading to a constant drift velocity λ toward (or away from) the target. This approximation allows for analytical tractability while preserving the essential interplay between the gated boundary and the resetting/unbinding mechanism.

To incorporate gating, the target is assumed to switch stochastically between a reactive state ($\sigma = 1$ in Fig. (2.2), corresponding to $R_2^\star$ in Fig. (2.1)) and a non-reactive state ($\sigma = 0$ in Fig. (2.2), corresponding to R_2 in Fig. (2.1)). Transitions from non-reactive to reactive occur at rate $\alpha > 0$, and from reactive to non-reactive at rate $\beta > 0$ [Fig. (2.2)]. The probability that the target is reactive is then $p_r := \alpha/(\alpha+\beta)$, and the probability that it is non-reactive is $p_{nr} := 1 - p_r = \beta/(\alpha + \beta)$. The process completes only when the particle reaches the target in the reactive state; if the target is non-reactive, the particle is reflected and continues to diffuse.

As discussed in the Introduction, catalyst unbinding (C from R_1) can be represented as resetting to x_0. Here, we assume Poissonian resetting at a constant rate r, meaning the particle returns to x_0 after exponentially distributed intervals with mean r^{-1}. Resetting is considered instantaneous, with the particle immediately resuming drift-diffusion. Any refractory period after resetting is neglected, since the time required for C to rebind R_1 [as in Fig. (2.1)] is assumed negligible compared to the timescales of drift-diffusion or resetting. The stochastic dynamics of the target are assumed independent of resetting [124].

The central quantity of interest is the random completion time, or *first-passage time* [35], for the particle to reach the target. Let $Q_\sigma(t|x_0)$ denote the survival probability, i.e., the probability that the particle has not reached the target by time t given initial position x_0 and target state σ. The backward Fokker-Planck equations for Q_σ are then

[124]:

$$\begin{aligned}\frac{\partial Q_0(t|x_0)}{\partial t} =& -\lambda\frac{\partial Q_0(t|x_0)}{\partial x_0} + D\frac{\partial^2 Q_0(t|x_0)}{\partial x_0^2} + \alpha[Q_1(t|x_0) \\ & - Q_0(t|x_0)] + r[Q_0(t|x_r) - Q_0(t|x_0)], \\ \frac{\partial Q_1(t|x_0)}{\partial t} =& -\lambda\frac{\partial Q_1(t|x_0)}{\partial x_0} + D\frac{\partial^2 Q_1(t|x_0)}{\partial x_0^2} + \beta[Q_0(t|x_0) \\ & - Q_1(t|x_0)] + r[Q_1(t|x_r) - Q_1(t|x_0)], \end{aligned} \tag{2.1}$$

where recall that λ is the drift velocity towards the origin and D is the diffusion constant. It should be noted that for simplicity of calculations, the direction of the positive drift is assumed to be along the negative x direction, leading to a negative sign in Eq. (2.1), which is opposite to the usual convention. Here, x_r is the resetting position, which is set self-consistently to x_0 at the end. The initial conditions are $Q_\sigma(0|x_0) = 1$, with boundary conditions

$$Q_1(t|0) = 0, \quad \left[\frac{\partial Q_0(t|x_0)}{\partial x_0}\right]_{x_0=0} = 0, \tag{2.2}$$

representing absorption for $\sigma = 1$ and reflection for $\sigma = 0$. The average survival probability is

$$Q_r^G(t|x_0) = p_r\ Q_1(t|x_0) + (1-p_r)Q_0(t|x_0), \tag{2.3}$$

with Laplace transform

$$\tilde{Q}_r^G(s|x_0) = p_r\ \tilde{Q}_1(s|x_0) + (1-p_r)\tilde{Q}_0(s|x_0), \tag{2.4}$$

where $\tilde{Q}_r^G(s|x_0) = \int_0^\infty e^{-st}Q_r^G(t|x_0)dt$ and $\tilde{Q}_\sigma(s|x_0) = \int_0^\infty e^{-st}Q_\sigma(t|x_0)dt$. The mean first-passage time (MFPT) is

$$\langle T_r^G(x_0)\rangle = p_r\langle T_1(x_0)\rangle + (1-p_r)\langle T_0(x_0)\rangle, \tag{2.5}$$

with $\langle T_\sigma(x_0)\rangle = \int_0^\infty Q_\sigma(t|x_0)dt = \tilde{Q}_\sigma(s|x_0)|_{s=0}$ [134, 35]. Here $\langle T_\sigma(x_0)\rangle$ stands for the MFPT of the particle to the origin starting from the position x_0 and initial state σ. Finally, we arrive at the expression for the overall MFPT

$$\langle T_r^G(x_0)\rangle = \int_0^\infty dt\ Q_r^G(t|x_0) = \tilde{Q}_r^G(s|x_0)|_{s=0}. \tag{2.6}$$

For brevity, we will denote $\langle T_r^G\rangle$ instead of $\langle T_r^G(x_0)\rangle$.

Solving Eq. (2.1) in Laplace space and substituting into Eq. (2.4) with $s = 0$ [see

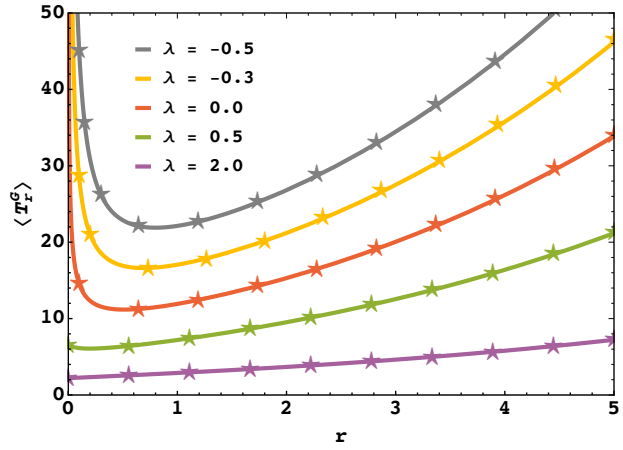

Figure 2.3: *The average MFPT, $\langle T_r^G \rangle$, vs the resetting rate r for different values of the drift velocity λ. The lines represent analytical results following Eq. (2.7) and the symbols represent results from numerical simulations [see section 2.7 for details]. The curves with $\lambda > 0$ denote cases where the drift acts towards the gated target and that with $\lambda < 0$ denote otherwise. The variation of $\langle T_r^G \rangle$ with r is always non-monotonic for $\lambda \leq 0$, however, for $\lambda > 0$ it is non-monotonic for lower values of λ, but monotonic for sufficiently high values of λ. Here we take $x_0 = 2$, $D = 1$, $\alpha = 0.5$, and $\beta = 0.5$ for all cases.*

Appendix B.1 for details] yields

$$\langle T_r^G \rangle = \frac{1}{r}\left(e^{\mu_1 x_0} - 1\right) + \frac{\beta\mu_1}{\alpha\mu_2}\left(\frac{1}{r} + \frac{e^{-\mu_2 x_0}}{\alpha+\beta}\right)e^{\mu_1 x_0}, \tag{2.7}$$

with $\mu_1 = (-\lambda + \sqrt{\lambda^2 + 4Dr})/2D > 0$ and $\mu_2 = (-\lambda + \sqrt{\lambda^2 + 4D(\alpha+\beta+r)})/2D > 0$. In the diffusion limit ($\lambda \to 0$), Eq. (2.7) reduces to [124]

$$\langle T_r^G \rangle = \frac{e^{\sqrt{\frac{r}{D}}x_0} - 1}{r} + \frac{\beta e^{\sqrt{\frac{r}{D}}x_0}}{\alpha\sqrt{r[r+\alpha+\beta]}}\left[1 + \frac{re^{-\sqrt{\frac{r+\alpha+\beta}{D}}x_0}}{(\alpha+\beta)}\right]. \tag{2.8}$$

For ungated drift-diffusion ($\beta \to 0$), Eq. (2.7) recovers

$$\langle T_r \rangle = \frac{\exp\left(x_0(\sqrt{\lambda^2 + 4Dr} - \lambda)/2D\right) - 1}{r} \tag{2.9}$$

as also discussed in the section 1.1.2 [65].

Fig. (2.3) shows $\langle T_r^G \rangle$ as a function of r for different drift velocities λ, keeping p_r fixed. For $\lambda > 0$, the MFPT exhibits non-monotonic behavior at low λ, implying that resetting accelerates first-passage in diffusion-controlled scenarios. At higher λ, $\langle T_r^G \rangle$ increases monotonically with r, meaning resetting delays first-passage in drift-controlled cases. When diffusion dominates, resetting truncates long trajectories, reducing MFPT; when drift dominates, resetting hinders directed motion. If drift opposes the target ($\lambda < 0$), resetting can still accelerate first-passage.

In summary, for $\lambda \leq 0$, the MFPT always shows non-monotonic dependence on r, making resetting beneficial. The resetting transition occurs only for $\lambda > 0$, whereas

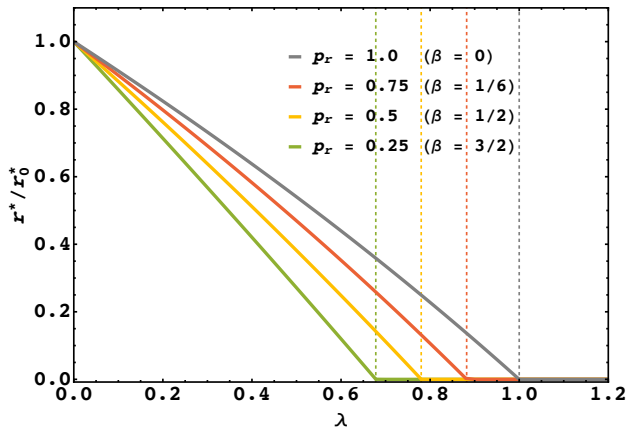

Figure 2.4: *The scaled optimal resetting rate, $r^\star/r_0^\star$, vs λ for different values of p_r. Resetting transition in each case is observed at $\lambda = \lambda_c$, where the scaled ORR becomes zero, marked by dashed lines of the same color as the curve. For $\lambda < \lambda_c$, resetting expedites transport, whereas for $\lambda \geq \lambda_c$ it can not. Here we take $D = 1$, $x_0 = 2$, and $\alpha = 0.5$ [which leads to $p_r = 1/(2\beta + 1)$] for all cases. For ungated drift-diffusion [given by $p_r = 1$, since $\beta \to 0$], the resetting transition is observed at $\lambda_c = 1$ (gray curve). For gated drift-diffusion with $p_r < 1$, λ_c decreases below unity.*

for pure diffusion or drift away from the target, resetting is always advantageous [5, 13, 124]. We focus on drift towards the target and determine the conditions where resetting is helpful. Situations with an additional reflecting boundary can mimic high energy barriers; as discussed in section 2.6.

2.3 The optimal resetting rate and a phase diagram for expedited completion

The concept of the resetting transition is generally characterized by the so-called optimal resetting rate (ORR), denoted $r^\star$, which is defined as the resetting rate that produces the minimal mean first-passage time (MFPT). As illustrated in Fig. (2.3), the optimal resetting rate is positive for the pure diffusion case ($\lambda = 0$), represented by $r^\star = r_0^\star$ (though this value is not explicitly labeled in the figure). As the drift parameter λ in the direction of the target is increased, the ORR diminishes steadily, becoming zero once a critical drift value λ_c (not indicated in Fig. (2.3)) is reached, signifying the point of the resetting transition. Beyond this critical drift λ_c, further increases in λ lead to an ORR that remains at zero. On the other hand, for drift away from the target ($\lambda < 0$), $r^\star$ grows as the drift magnitude increases. Therefore, $r^\star$ serves as an order parameter in much the same way as in conventional phase transitions, facilitating the analysis of the resetting transition.

Since the ORR yields the minimum of $\langle T_r^G \rangle$, it is determined by the stationarity condition $d\langle T_r^G \rangle / dr|_{r=r^\star} = 0$, which results in a transcendental equation with no closed-form analytic solution. By employing numerical techniques to solve this equation, $r^\star$ can be found for values $\lambda > 0$. Analogously, the optimal resetting rate under pure dif-

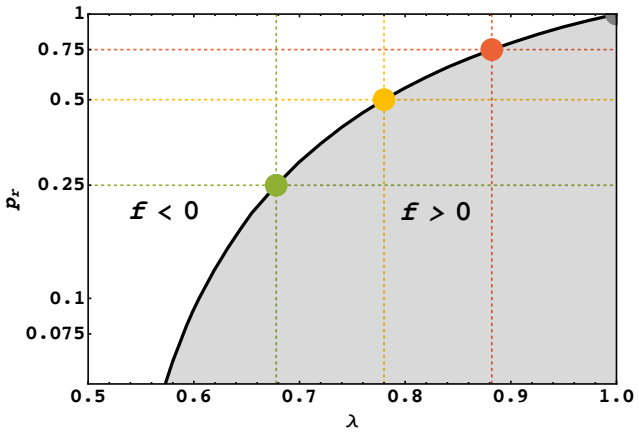

Figure 2.5: *A phase diagram of p_r vs. λ based on the qualitative effect of resetting on gated drift-diffusion. The black line represents the condition for resetting transition (λ_c), which divides the entire phase space in two parts. For $\lambda < \lambda_c$ resetting expedites transport (white regime), whereas for $\lambda \geq \lambda_c$ resetting fails to expedite transport (gray regime). Here we take $D = 1$, $x_0 = 2$ and $\alpha = 0.5$ [i.e., $p_r = 1/(2\beta + 1)$] for all cases. For the ungated process ($p_r = 1$), $\lambda_c = 1$ and it decreases with p_r. The colored discs on the black line present the cases shown in Fig. (2.4). Following the analysis of $\langle T_r^G \rangle$ in the limit $r \to 0$ [see Eq. (2.10) and Eq. (2.12)], the separatrix (black line) is also obtained by plotting $f = 0$ (as defined by Eq. (2.12)). Resetting is beneficial for $f < 0$ (white regime), but not for $f > 0$ (gray regime).*

fusion ($\lambda = 0$, labeled as $r_0^\star$) is similarly calculated, and from this the normalized ORR $r^\star/r_0^\star$ is obtained.

In Fig. (2.4), the plot shows how this scaled ORR changes with λ for a variety of values for the reactive occupancy p_r (with α fixed and p_r tuned by varying β only). For $\lambda < \lambda_c$, nonzero values of the normalized ORR in Fig. (2.4) indicate that resetting can speed up first-passage events in this regime. In marked contrast, when $\lambda \geq \lambda_c$, the scaled ORR drops to zero, meaning resetting fails to provide benefit in that regime. In the particular case of the process without gating ($p_r = 1$), we find $\lambda_c = 1$ for the chosen parameters, which exactly matches previous results as found in [65]. Examination of Fig. (2.4) also reveals that decreasing p_r results in a smaller λ_c; this implies that when gating is present, the critical drift up to which resetting provides faster completion is reduced compared to the no-gating scenario.

To further clarify the relationship between the critical drift λ_c and the effective reactivity p_r of the target, we determine λ_c as a function of p_r numerically. In Fig. (2.5), this produces a phase diagram with p_r and the drift velocity λ as axes, where the curve for λ_c forms a separatrix, dividing the space into two distinct regions: for $\lambda < \lambda_c$ (white area), resetting enhances first-passage efficiency, while for $\lambda \geq \lambda_c$ (gray area), no such benefit is attained. The findings from Fig. (2.4) are fully echoed in Fig. (2.5) as follows: for any value of p_r within $[0, 1]$ (traversing horizontally in Fig. (2.5)), if λ is smaller than λ_c the mechanism is governed primarily by diffusion and resetting brings a benefit, while for $\lambda \geq \lambda_c$ transport becomes dominated by drift, causing resetting to lose its utility. It is obvious from Fig. (2.5) that as p_r increases, λ_c approaches unity, ultimately

matching the result for no gating ($p_r = 1$). Thus, Fig. (2.5) offers a comprehensive yet concise depiction of the parameters under which resetting is advantageous for gated drift-diffusion. The next part discusses an alternative method that reconstructs this phase diagram by systematic analysis of the resetting criterion in the regime where $r \to 0$.

Returning to Fig. (2.3), it is clear that when the small-r (as $r \to 0$) slope of the $\langle T_r^G \rangle$ versus r curve is negative, resetting yields a reduction in average MFPT, hence proving beneficial. Alternatively, if the slope is positive in the limit of vanishing resetting rate, then introducing resetting actually increases the average MFPT. Motivated by this, we seek to establish the precise criterion under which resetting expedites gated drift-diffusion, by studying the small-r expansion of the mean first-passage time:

$$\langle T_r^G \rangle \approx \langle T^G \rangle + r \left[\frac{\partial \langle T_r^G \rangle}{\partial r} \right]_{r=0} + O(r^2), \tag{2.10}$$

where $\langle T^G \rangle$ denotes the MFPT without resetting. Utilizing Eq. (2.7) and consulting Appendix B.2 for another derivation, we find

$$\langle T^G \rangle = \frac{1}{\lambda} \left[x_0 + \frac{2\beta D}{\alpha \left(\sqrt{4\alpha \mathrm{D} + 4\beta \mathrm{D} + \lambda^2} - \lambda \right)} \right]. \tag{2.11}$$

Importantly, in the absence of gating ($p_r = 1$, which corresponds to $\beta = 0$), Eq. (2.11) becomes simply $\langle T \rangle = x_0/\lambda$ following [35], showing that $\langle T^G \rangle$ always exceeds $\langle T \rangle$ since the second term of Eq. (2.11) is unconditionally positive.

Although the second term of Eq. (2.10) is rather involved, using newly defined quantities $\gamma := \lambda^2/2D$, $Pe := x_0\lambda/2D$, and $\kappa := \sqrt{1 + [4D(\alpha+\beta)/\lambda^2]} - 1$, the result becomes

$$f := \left. \frac{\partial \langle T_r^G \rangle}{\partial r} \right|_{r=0} = \frac{\beta}{2\gamma^2 \alpha} \left[\frac{2Pe - 1}{\kappa} - \frac{2}{\kappa^2(\kappa+1)} + \frac{2\gamma e^{-\kappa Pe}}{\kappa(\alpha+\beta)} \right] + \frac{1}{2\gamma^2} Pe(Pe-1). \tag{2.12}$$

Here, Pe defined in Eq. (2.12) is the Péclet number, quantifying the ratio of advective to diffusive transport, while γ^{-1} corresponds to the minimal decay time (the fastest first-passage time) in the strong drift limit, as previously highlighted in [35].

By examining Eq. (2.10), it follows that for $r \to 0$, resetting is expected to bring about faster process completion (i.e., $\langle T_r^G \rangle < \langle T^G \rangle$) whenever $f < 0$. This provides a sufficient (though not necessary) condition for resetting to have utility. Conversely, if $f > 0$, introducing resetting will make completion slower ($\langle T_r^G \rangle > \langle T^G \rangle$). Therefore, the phase diagram in (λ, p_r) space should be separated by the line $f = 0$ into two

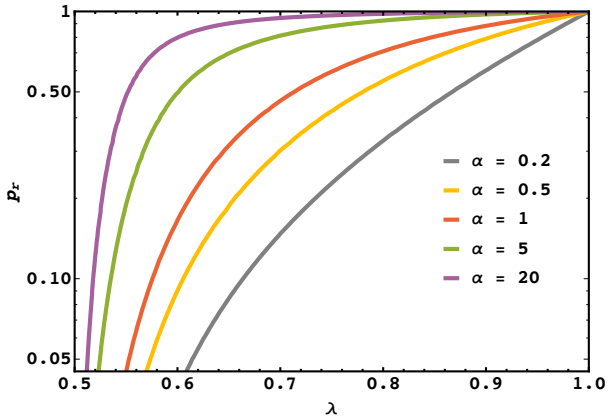

Figure 2.6: *A phase diagram of p_r vs. λ for different values of α. Each phase boundary (obtained for a certain value of α, shown by the curves) divides the phase space into a "resetting-beneficial" phase (left to the curve) and a "resetting-detrimental" phase (right to the curve). For large values of α, the "resetting-beneficial" phase becomes considerably smaller as the "resetting-detrimental" phase occupies the majority of the phase space.*

regimes, one where resetting is helpful ($f < 0$) and one where it is not ($f > 0$). Plotting $f = 0$ as specified by Eq. (2.12) on Fig. (2.5) yields a curve that precisely matches the previously drawn separatrix obtained from the numerics for λ_c as a function of p_r. Thus, $f < 0$ marks the regime in which adding resetting accelerates transport (white area), while $f > 0$ designates the region where resetting actually retards it (gray area), as anticipated. Notably, if we focus on the limit $p_r \to 1$ (i.e., $\beta \to 0$), only the final term in Eq. (2.12) remains, so $f < 0$ condenses to the familiar $Pe < 1$ condition (with $Pe = 1$ marking the transition). This again matches earlier established results for the ungated process [126, 65, 128].

The diagram in Fig. (2.5) was produced for just a single value of α. To generalize, we repeat this construction for several other α values, as displayed in Fig. (2.6). From Fig. (2.6), we observe that the separatrix—the curve dividing the "resetting-beneficial" domain on the left from the "resetting-detrimental" phase on the right—depends noticeably on α. Specifically, increasing α causes the beneficial region to shrink, with the detrimental region occupying nearly the whole parameter space, meaning that the practical effectiveness of resetting is quite constrained in that large-α regime. Next, we proceed to analyze two relevant limits of the gating rates, namely $\alpha \to 0$ and $\alpha, \beta \to \infty$.

2.3.1 The limit $\alpha \to 0$

Taking the limit $\alpha \to 0$ means that, for most of the time, the target behaves as a reflecting boundary. As we show below, this is a subtle scenario and must be treated with attention. Strictly, setting $\alpha \to 0$ is interpreted as operating in a regime where $\beta \gg \alpha$, so the likelihood of the target being in the non-reactive state far exceeds that of being reactive.

Substituting this limit into Eq. (2.7) yields

$$\langle T_r^G \rangle = \frac{1}{r}\left(e^{\mu_1 x_0} - 1\right) + \frac{\beta\mu_1}{r\alpha\mu_2} e^{\mu_1 x_0}, \tag{2.13}$$

where, as before, $\mu_1 = (-\lambda + \sqrt{\lambda^2 + 4Dr})/2D > 0$ and $\mu_2 = (-\lambda + \sqrt{\lambda^2 + 4D(\alpha+\beta+r)})/2D > 0$. Furthermore, for any finite resetting rate r and in the regime $\beta \gg r$, the first term on the right of Eq. (2.13) becomes negligible, and we arrive at

$$\langle T_r^G \rangle = \frac{\beta\left(\sqrt{4Dr+\lambda^2} - \lambda\right) e^{\frac{x_0\left(\sqrt{4Dr+\lambda^2}-\lambda\right)}{2D}}}{\alpha r\left(\sqrt{4\beta D + \lambda^2} - \lambda\right)}. \tag{2.14}$$

To clarify the behavior of $\langle T_r^G \rangle$, Fig. (2.7) displays its dependence on the resetting rate r, considering large β and small α with $\beta/\alpha \gg 1$. Interestingly, in this limit, the MFPT exhibits both monotonic and non-monotonic trends as r is varied for different λ values. Specifically, non-monotonicity signals the existence of an optimal resetting rate that minimizes $\langle T_r^G \rangle$. The minimum condition is found by setting $\frac{d\langle T_r^G \rangle}{dr}\Big|_{r=r^\star} = 0$, leading to

$$r^\star = \frac{D}{x_0^2} - \frac{\lambda}{x_0}, \tag{2.15}$$

which simply depends on the diffusion coefficient, starting position, and drift velocity. Notably, $r^\star$ varies linearly with λ. For the particular case $\lambda = 0$, one regains $r^\star = D/x_0^2$, aligning with the findings of [124].

The emergence of a finite ORR when $\alpha \to 0$ i.e., when the target is nearly always non-reactive (the so-called *cryptic* regime [75, 74])—is a surprising result, especially when compared to the scenario $\alpha = 0$ (a strictly reflecting boundary). One can interpret this as follows: a particle undergoing diffusion (and drift) typically encounters the target multiple times, regardless of its instantaneous reactivity. Although the particle is usually unable to find the target in the reactive state, it still stands a chance of eventual absorption if the target ever becomes reactive. For further background on cryptic targets and their occurrence in chemical, biological, and ecological settings, see [98, 75, 126, 135].

2.3.2 The limit $\alpha, \beta \to \infty$

For the case where both α and β are very large, recalling the expression in Eq. (2.12), we can make the approximation $\kappa \approx \sqrt{4D(\alpha+\beta)}/\lambda$. This allows us to safely discard terms of order $O(1/\kappa^2)$ and the exponential expression. Under these considerations, imposing

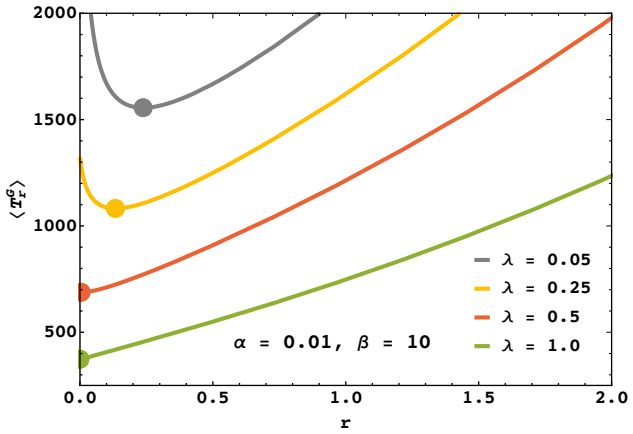

Figure 2.7: *Monotonic and non-monotonic behaviour of the MFPT in the limit $\alpha \to 0$ (i.e., $\beta/\alpha \gg 1$), as obtained from Eq. (2.14). The non-monotonic behaviour gradually vanishes as λ goes beyond the resetting transition point $\lambda_c = D/x_0 = 0.5$. This can be obtained by setting $r^\star$ in Eq. (2.15) to zero.*

$f = 0$ in Eq. (2.12) yields a closed formula for the critical drift:

$$\lambda_c = \frac{2D}{x_0}\left[\frac{D + x_0\frac{\alpha}{\beta}\sqrt{\alpha+\beta}\sqrt{D}}{2D + x_0\frac{\alpha}{\beta}\sqrt{\alpha+\beta}\sqrt{D}}\right]. \tag{2.16}$$

We find that even in this asymptotic regime, the parameter p_r alone does not completely dictate the system's dynamics. Physically, this limit corresponds to a partially reactive boundary: the target flips rapidly between states, so quickly (relative to the drift-diffusion time scale) that the particle perceives a time-averaged reactivity and interacts probabilistically, the case which was previously studied in [136]—see also [98, 75].

With this, we have thoroughly examined how resetting influences gated drift-diffusion dynamics. In the next section, we will focus on the maximum attainable speedup using optimal resetting protocols.

2.4 The maximal speedup for process completion

The quantity known as maximal speedup—i.e., the gain one achieves by resetting optimally, can be defined as the ratio of the MFPT for the base process (without resetting) to that for the same process under resetting at the optimal rate. Thus, selecting $r = r^\star$ in Eq. (2.7) and using Eq. (2.11), we obtain the maximal speedup for the *gated* drift-diffusion system as

$$\frac{\langle T^G\rangle}{\langle T^G_{r^\star}\rangle} = \begin{cases} \dfrac{r^\star(\alpha+\beta)(2D\beta+x_0\alpha\mu_2^\star)}{\lambda\left[r\beta\mu_1^\star e^{\frac{x_0}{2D}\left(\mu_1^\star+\mu_2^\star\right)}+(\alpha+\beta)\left[e^{\frac{x_0\mu_1^\star}{2D}}(\beta\mu_1^\star+\alpha\mu_2^\star)-\alpha\mu_2^\star\right]\right]} & \text{for } \lambda < \lambda_c \\ 1 \qquad \text{for } \lambda \geq \lambda_c, \end{cases} \tag{2.17}$$

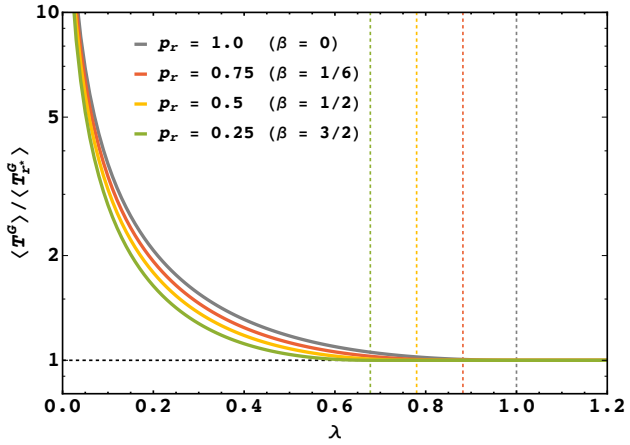

Figure 2.8: *The maximal speedup for the gated process with resetting compared to the gated process without resetting, $\langle T^G\rangle/\langle T^G_{r^\star}\rangle$, vs the drift velocity λ, for different values of the reactive occupancy, p_r. The vertical dashed lines mark the points of resetting transitions for curves of same color, denoted λ_c, such that $\langle T^G\rangle/\langle T^G_{r^\star}\rangle > 1$ for $\lambda < \lambda_c$, and $\langle T^G\rangle/\langle T^G_{r^\star}\rangle = 1$ at $\lambda \geq \lambda_c$. We take $D = 1$, $x_0 = 2$ and $\alpha = 0.5$ [i.e., $p_r = 1/(2\beta+1)$] for all cases. In the absence of gating ($p_r = 1$, gray curve), the resetting transition is observed at $\lambda_c = 2D/x_0 = 1$, and λ_c decreases when gating is introduced ($p_r < 1$).*

where $\mu_1^\star = \mu_1(r^\star)$ and $\mu_2^\star = \mu_2(r^\star)$, with μ_1 and μ_2 as defined previously after Eq. (2.7). In Fig. (2.8), we display $\langle T^G\rangle/\langle T^G_{r^\star}\rangle$ for multiple p_r values. The figure shows that maximal speedup is highest when the drift towards the target is weak, and diminishes as λ increases, becoming unity at the critical value λ_c. For the situation without gating ($p_r = 1$), the transition occurs at $\lambda_c = 1$, which matches [65]; decreasing p_r shifts the transition to smaller λ as previously seen in Fig. (2.5).

To go further, we compare the optimally reset gated MFPT $\langle T^G_{r^\star}\rangle$ with $\langle T\rangle$, the MFPT for the *ungated* system without resetting, to check whether the gating-induced MFPT increase can be counteracted by optimal resetting. The MFPT for ungated drift-diffusion is simply $\langle T\rangle = x_0/\lambda$; using Eq. (2.7) with $r = r^\star$, we have

$$\frac{\langle T\rangle}{\langle T^G_{r^\star}\rangle} = \begin{cases} \dfrac{r^\star x_0\alpha(\alpha+\beta)\mu_2^\star}{\lambda\left[r\beta\mu_1^\star e^{\frac{x_0}{2D}\left(\mu_1^\star+\mu_2^\star\right)}+(\alpha+\beta)\left[e^{\frac{x_0\mu_1^\star}{2D}}(\beta\mu_1^\star+\alpha\mu_2^\star)-\alpha\mu_2^\star\right]\right]} & \text{for} \quad \lambda < \lambda_c \\ \dfrac{x_0\alpha\mu_2^\star}{2D\beta+x_0\alpha\mu_2^\star} & \text{for} \ \ \lambda \geq \lambda_c. \end{cases} \tag{2.18}$$

By plotting $\langle T\rangle/\langle T^G_{r^\star}\rangle$ as a function of λ (see Fig. (2.9)), we recognize that for low drift, optimal resetting can yield a speedup in excess of a factor of ten compared to the original ungated process! The curve indicates that the speedup is infinite at zero drift and decreases with λ as expected. Hence, when the system is primarily diffusion-driven, optimal resetting can more than offset framing delays introduced by gating, providing a transport rate (the reciprocal of MFPT) exceeding that of the original ungated process. Additionally, in the scenario $p_r = 1$ (no gating), the minimum $\langle T\rangle/\langle T^G_{r^\star}\rangle$ equals one and is reached for $\lambda \geq \lambda_c$ [65]. For $p_r < 1$, this ratio falls below unity even before the resetting transition. If we define λ_c^0 as the value of λ (shown by colored discs in

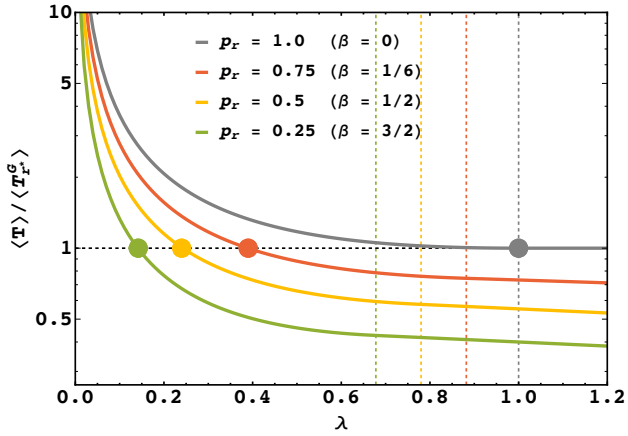

Figure 2.9: *The maximal speedup for the gated process with resetting compared to the ungated process without resetting, $\langle T\rangle / \langle T^G_{r\star}\rangle$, vs λ, for different values of p_r. The vertical dashed lines mark the points of resetting transition (λ_c) for curves of same color, whereas the colored discs mark the values of λ_c^0, such that optimal resetting expedites gated process beyond the original ungated process only when $\lambda < \lambda_c^0$. Here $D = 1$, $x_0 = 2$ and $\alpha = 0.5$ [i.e., $p_r = 1/(2\beta + 1)$] for all cases. In the absence of getting ($p_r = 1$, gray curve), the point of resetting transition ($\lambda_c = 2D/x_0 = 1$) coincides with λ_c^0.*

Fig. (2.9)) where $\langle T\rangle/\langle T^G_{r\star}\rangle = 1$ for a fixed p_r, then $\lambda_c^0 \leq \lambda_c$, with equality only in the ungated process; for low p_r the gap widens. These observations motivate the classification of all distinct regions where resetting helps completion in gated drift-diffusion. In the following, we synthesize a complete phase diagram encompassing the full range of resetting effects.

2.5 The complete phase diagram

To synthesize the global phase diagram, we revisit Fig. (2.5) and Fig. (2.8). Recall that the (λ, p_r) plane divides into the domain where $\langle T^G_{r\star}\rangle < \langle T^G\rangle$ (optimal resetting assists transport) and where $\langle T^G_{r\star}\rangle \geq \langle T^G\rangle$ (resetting does not enhance transport), the dividing line being set by λ_c. Scrutinizing the maximal speedup in Section IV, we see the former region can be further split: one subdomain where $\langle T^G_{r\star}\rangle < \langle T\rangle$ (optimal resetting in the gated system produces greater transport rates than the original ungated system) and another where $\langle T^G_{r\star}\rangle \geq \langle T\rangle$. The boundary between these appears at $\lambda = \lambda_c^0 \leq \lambda_c$. Since, without resetting, gating slows drift-diffusion [$\langle T\rangle < \langle T^G\rangle$ per Eq. (2.11)], we can, consolidating all observations, build a phase diagram (Fig. (2.10)) featuring three regimes: (i) phase I: optimal resetting in the gated process yields faster completion than both the original gated and ungated processes [$\langle T^G_{r\star}\rangle < \langle T\rangle < \langle T^G\rangle$]; (ii) phase II: optimal resetting expedites the gated process over its original value, but not relative to the ungated system [$\langle T\rangle \leq \langle T^G_{r\star}\rangle < \langle T^G\rangle$]; and (iii) phase III: resetting does not accelerate the gated system over either baseline [$\langle T\rangle < \langle T^G\rangle \leq \langle T^G_{r\star}\rangle$]. Boundaries λ_c^0 and λ_c demarcate the transitions between these regimes. For $p_r = 1$, $\lambda_c^0 = \lambda_c$ so phases I and II are contiguous, aligning with the no-gating case. Accordingly, the

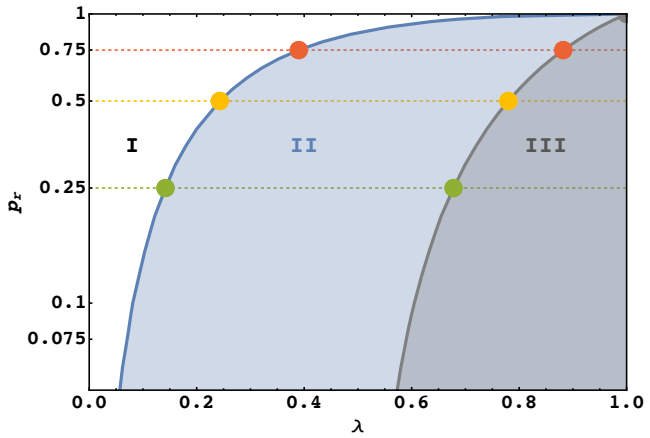

Figure 2.10: *A complete phase diagram of p_r vs. λ showing three distinct phases; (i) phase I: where optimal resetting enhances the rate of gated drift-diffusion beyond the original (without resetting) ungated process, given by $\langle T^G_{r^\star}\rangle < \langle T\rangle < \langle T^G\rangle$, (ii) phase II: when optimal resetting improves the rate of the gated process, but not compared to the original ungated process, given by $\langle T\rangle \leq \langle T^G_{r^\star}\rangle < \langle T^G\rangle$, and (iii) phase III: when resetting can not improve the rate of gated process, given by $\langle T\rangle < \langle T^G\rangle \leq \langle T^G_{r^\star}\rangle$. The horizontal colored lines mark the cases shown in Fig. (2.9). Here we consider $\alpha = 0.5$ [such that $p_r = 1/(2\beta+1)$], $D = 1$ and $x_0 = 2$. Phases I and II merge together at $\lambda_c = 2D/x_0 = 1$, the point of resetting transition for drift-diffusion in the absence of gating ($p_r = 1$).*

diagram in (p_r, λ) specifies how resetting impacts process completion, guiding optimal parameter choices and offering maximal benefit with precise, preemptive knowledge of the parameter space.

2.6 The case of confined geometry

Here we consider the case of a bounded system, i.e., where the particle remains in a finite confinement. This is also highly relevant from the context of chemical reactions, since a high energy barrier can mimic a reflecting boundary (in the reaction coordinate space) that pushes the particle away from it. We construct this finite domain by considering the same set-up as in the main text, with an additional reflecting wall at $x = L > x_0$. If the particle hits the wall it gets reflected back. Intuitively, the barrier or the reflecting boundary prevents the particle from going too far from the target placed at the origin. This is in sharp contrast to the semi-infinite case, where the particle is allowed to diffuse away from the target. This leads to a few key changes in the dynamics that are reflected in the average MFPT.

On the technical ground, we can find the survival probability in Laplace space using the same method as discussed in Appendix B.1 with the new boundary condition $\left[\frac{\partial Q_\sigma(t|x_0)}{\partial x_0}\right]_{x_0=L} = 0$. For this reason, all the eigenvalues will exist unlike in the previous case. In particular, one can show that the eigenvector corresponding to m_3 is the same as m_1, i.e., $\Phi_1 = \binom{1}{1}$ and that of m_4 is same as m_2 i.e. $\Phi_2 = \binom{-\alpha/\beta}{1}$. Recalling the decomposition $\tilde{Q}_\sigma(s) = \tilde{Q}^h_\sigma(s) + \tilde{Q}^{inh}_\sigma(s)$ from Eq. (B.2), we first try to obtain the solu-

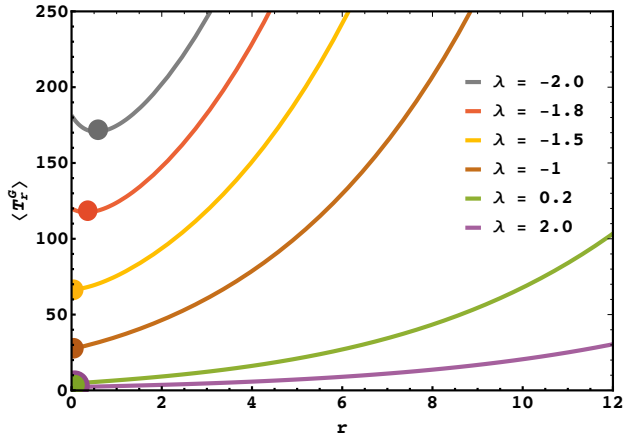

Figure 2.11: *The average MFPT $\langle T_r^G \rangle$ as a function of the resetting rate r for different values of λ in the case of bounded domain. Here, the reflecting boundary is placed at $L = 3$, where the resetting/initial location is at $x_0 = 2$. The colored discs mark the optimal resetting rate ($r^\star$) in each case. Notably, resetting may not always be helpful ($r^\star = 0$) even when $\lambda < 0$ (e.g., yellow and brown curves).*

tions for the homogeneous part. As before taking $\Psi = \begin{pmatrix} \tilde{Q}_0^h & \tilde{Q}_1^h \end{pmatrix}^T$ and using Eq. (B.7) we find

$$\Psi = c_1 \Phi_1 e^{m_1 x_0} + c_2 \Phi_2 e^{m_2 x_0} + c_3 \Phi_1 e^{m_3 x_0} + c_4 \Phi_2 e^{m_4 x_0}, \tag{2.19}$$

so that

$$\tilde{Q}_0^h = c_1 e^{m_1 x_0} - \frac{\alpha}{\beta} c_2 e^{m_2 x_0} + c_3 e^{m_3 x_0} - \frac{\alpha}{\beta} c_4 e^{m_4 x_0}, \tag{2.20}$$

$$\tilde{Q}_1^h = c_1 e^{m_1 x_0} + c_2 e^{m_2 x_0} + c_3 e^{m_3 x_0} + c_4 e^{m_4 x_0}. \tag{2.21}$$

The inhomogeneous part $\tilde{Q}_\sigma^{inh}(s)$ has the same solution as given in Eq. (B.5). In addition to the boundary conditions $\tilde{Q}_1(s|0) = 0$ and $\frac{\partial \tilde{Q}_0^h(s|x_0)}{\partial x_0}|_{x_0=0} = 0$ at the gated target, we also have two additional boundary conditions namely $\frac{\partial \tilde{Q}_0(s|x_0)}{\partial x_0}|_{x_0=L} = 0$ and $\frac{\partial \tilde{Q}_1(s|x_0)}{\partial x_0}|_{x_0=L} = 0$. These four boundary conditions give four linear equations

$$\begin{aligned}
&c_1 + c_2 + c_3 + c_4 + \tilde{Q}_1^{inh}(s) = 0, \\
&c_1 m_1 e^{m_1 L} + c_2 m_2 e^{m_2 L} + c_3 m_3 e^{m_3 L} + c_4 m_4 e^{m_4 L} = 0, \\
&c_1 m_1 e^{m_1 L} - \frac{\alpha}{\beta} c_2 m_2 e^{m_2 L} + c_3 m_3 e^{m_3 L} - \frac{\alpha}{\beta} c_4 m_4 e^{m_4 L} = 0, \\
&c_1 m_1 - \frac{\alpha}{\beta} c_2 m_2 + c_3 m_3 - \frac{\alpha}{\beta} c_4 m_4 = 0,
\end{aligned} \tag{2.22}$$

which completely determine the constants c_1, c_2, c_3, c_4. From this, we can find a closed-form expression for the survival probabilities in Laplace space (and subsequently the MFPT by setting $s \to 0$). The expression for the MFPT is quite lengthy to present here; check [137] for the *Mathematica* file where all the derivations are given. In what follows, we perform a comprehensive analysis of this MFPT and point out the key dif-

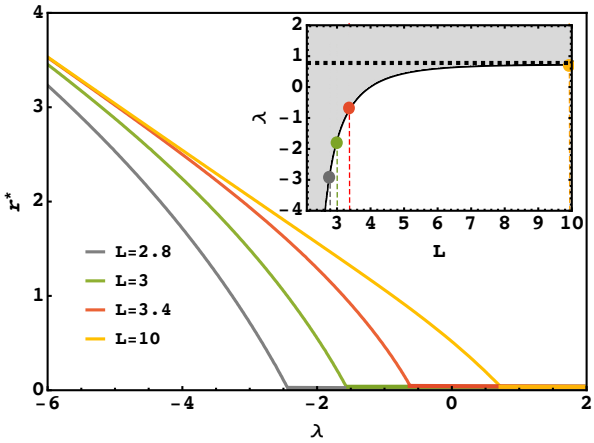

Figure 2.12: *Main: Variation of ORR ($r^\star$) as a function of λ for different domain size L. For $\lambda < \lambda_c$, resetting proves itself beneficial, as indicated by the non-zero values of $r^\star$, whereas for $\lambda \geq \lambda_c$, resetting becomes detrimental, as indicated by $r^\star = 0$. The resetting transition is thus marked by λ_c. Inset: Phase diagram with reflecting barrier at L, by plotting λ_c that acts as the separatrix (black line; the colored discs mark the specific cases shown in the main panel) that divides the phase space in two parts; one where resetting is beneficial (white regime) and the other where resetting is detrimental (gray regime). Existence of negative λ_c essentially implies that resetting can be detrimental even when $\lambda < 0$. The dashed horizontal line corresponds to $\lambda_c = 0.78$, obtained for the semi-infinite case (i.e. $L \to \infty$), as displayed in Fig. (2.5) for $p_r = 0.5$. Note that we consider $\alpha = 0.5, \beta = 0.5$ and $D = 1$ for each case in the main panel and in the inset.*

ferences in comparison to the that obtained for the semi-infinite domain.

Fig. (2.11) showcases the variation of the MFPT, $\langle T_r^G \rangle$, as a function of the resetting rate r for different values of the drift λ. One crucial observation is that the non-monotonic behaviour of $\langle T_r^G \rangle$ is *not always present* even when the drift is away from the target (i.e., $\lambda < 0$). This is in complete contrast to the semi-infinite case where resetting is guaranteed to help whenever the drift is away from the target [see Fig. (2.3)]. To understand this better, we plot the optimal resetting rate $r^\star$ as a function of λ for various domain sizes L in Fig. (2.12), which clearly shows that the critical values of λ that marks the resetting transition (denoted λ_c in the main text; the minimal value of λ for which $r^\star = 0$), can be negative for considerably smaller domains. With increasing L, however, λ_c starts to increase and for sufficiently large values of L it saturates to the value of λ_c for the semi-infinite case, as displayed Fig. (2.5) of the main text. Simply put, if the reflecting boundary starts moving sufficiently away from the target, the MFPT starts to increase and resetting renders a more effective search in that case.

To elaborate this further, one can expand the MFPT (for finite domain) in the limit of small resetting rate $r \to 0$ and find the first order correction in r [in similar spirit as in Eq. (2.10) – see the discussion for the semi-infinite case in section 2.3, particularly around Eq. (2.12)]. The arguments on the function f as discussed there still holds for the present case (of course, the exact form of the function will be different here). Thus, setting $f = 0$ gives us the separatrix distinguishing between the region where resetting helps ($f < 0$) and where it hinders ($f > 0$). Utilizing this fact, we generate a phase dia-

gram by plotting λ_c as a function of L, the distance between the reflecting barrier and the origin, and present the same in the inset of Fig. (2.12). The semi-infinite limit is obtained by taking $L \to \infty$, where λ_c saturates to the corresponding value calculated/presented in the main text. For example, we see from Fig. (2.12) that when $p_r = 0.5$, λ_c saturates to 0.78, the critical value of λ for $p_r = 0.5$ (marked in Fig. (2.5) by the vertical yellow line).

2.7 Details of numerical simulations

In this section, we sketch out the basic steps used for the numerical simulations. We recall that the particle starts from and resets to x_0 at a rate r. In between reset events, it diffuses in the presence of a drift λ. Evolution of this particle in microscopic time scale Δt can be written in the form of a Langevin dynamics such as

$$x(t+\Delta t) = \begin{cases} x_0 & \text{w.p.} \quad r\Delta t \\ \\ x(t) - \lambda\Delta t + \sqrt{2D\Delta t}\,\eta(t) & \text{w.p.} \quad (1 - r\Delta t) \end{cases} \tag{2.23}$$

where $\eta(t)$ is a δ-correlated white noise i.e., a Gaussian random variable with zero mean and unit variance. Note that the abbreviation w.p. in Eq. (2.23) has full-form *with probability*. We evolve the particle at each time step Δt in our simulation according to Eq. (2.23) until the particle reaches the target at $x = 0$. However, to implement the gating condition to the target, we define a state variable $\sigma = (0, 1)$ representing the non-reactive and reactive states of the target, respectively. If the target is initially at the non-reactive state, it switches to the reactive state with probability $\alpha\Delta t$. Similarly, it is switched from the active state to the inactive one with probability $\beta\Delta t$.

To compute the first passage time, we simultaneously track two events: (i) the instant when the particle crosses the origin to the negative side i.e., $x \leq 0$ and (ii) note whether the target is in active state i.e., $\sigma = 1$. If both the conditions are satisfied, the particle gets absorbed and the process ends. We measure the corresponding time and put it into the first passage statistics. However, if $x \leq 0$ and $\sigma = 0$ then the particle gets reflected from the boundary, and the process continues till the next absorption occurs. The reflecting boundary condition is implemented by simply reversing the position of the particle i.e. $x \to -x$. The initial target state σ is chosen from the steady state i.e.,

$$\sigma(t=0) = \begin{cases} 1 & \text{with probability} \quad p_r, \\ 0 & \text{with probability} \quad (1 - p_r), \end{cases} \tag{2.24}$$

where $p_r = \alpha/(\alpha+\beta)$. In our simulations, $\Delta t = 10^{-5}$ and the averaging was done for 10^5 successful trajectories for each value of λ. The results are displayed in Fig. (2.3) with the star symbols, which show excellent agreement with the analytical results presented

by the solid lines of same color.

2.8 Conclusions

In this study, we undertook a comprehensive examination of the completion time statistics for drift-diffusive transport toward a stochastically gated target in the presence of Poissonian resetting. Specifically, we systematically investigated the regimes in which resetting can accelerate transport rates, extending existing results on ungated systems where resetting is known to stabilize non-equilibrium dynamics [5, 17, 8, 138, 32] by eliminating the unfavorable long excursions that slow down overall transport. By mapping the broader dynamics of gated drift-diffusion with resetting onto the case of a gated chemical reaction triggered by a catalyst [as illustrated in Fig. (2.1)], the central findings of our work can be summarized as follows.

We established that the rate of product generation is governed by an intriguing balance between the chemical driving force for the reaction (λ), the likelihood (p_r) that the gated reactant is found in its active configuration [i.e., R_2 being in the $R_2^\star$ state], and the unbinding rate (or resetting rate, r) for the catalyst C detaching from CR_1. In settings where the drive toward product ($\lambda > 0$) is weak or moderate so that the system is diffusion-limited, the reaction rate is maximized at an optimal catalyst unbinding rate ($r^\star$). Conversely, when λ is large—indicative of drift-dominated kinetics—detaching the catalyst (C) from CR_1 actually reduces the reaction rate. This crossover is marked by a critical value of the drive, λ_c, which increases with p_r and attains its maximum at $p_r = 1$ (corresponding to the ungated scenario). Remarkably, for $\lambda < \lambda_c^0$ [with $\lambda_c^0 \leq \lambda_c$ another critical drift value that is an increasing function of p_r and saturates at $\lambda_c^0 = \lambda_c$ when $p_r = 1$], tuning the unbinding to its optimum ($r^\star$) can make the reaction more than an order of magnitude (> 10 times) faster than the ungated reaction in the nearly irreversible binding limit ($r \to 0$).

As a consequence of these findings, we constructed a complete phase diagram characterizing both the *qualitative* and *quantitative* impacts of optimal catalyst unbinding (resetting) on gated chemical reactions—modeled as drift-diffusion toward a gated target—and identified three distinct operational regimes. Recalling that the product formation rate is inversely proportional to the mean reaction completion time [132], these regimes are distinguished as: (i) $\langle T_{r^\star}^G \rangle < \langle T \rangle < \langle T^G \rangle$, where optimal catalyst unbinding accelerates the gated reaction beyond both ungated and gated reactions in the irreversible binding limit ($r \to 0$); (ii) $\langle T \rangle \leq \langle T_{r^\star}^G \rangle < \langle T^G \rangle$, where unbinding with optimal resetting still improves the gated reaction rate, but not beyond that of the ungated case as $r \to 0$; and (iii) $\langle T \rangle < \langle T^G \rangle \leq \langle T_{r^\star}^G \rangle$, where catalyst unbinding does not succeed in accelerating the gated process relative to either baseline (ungated/gated) in the regime of nearly irreversible binding. Intuitively, gating acts as a bottleneck to the ungated chemical reactions. However, we show that optimal unbinding of the enzyme from the substrate often renders a faster product formation rate in the gated chemical reactions compared

to the ungated one.

The theoretical framework developed here is broadly applicable to analysis of gated drift-diffusion influenced by resetting. Beyond being analytically tractable, it also offers valuable insight into the complex interplay between gating and resetting, both of which are crucial elements within chemical reaction networks. Extending this model to more general, space-dependent diffusion processes in arbitrary potential landscapes with randomly switching targets is an exciting direction for future work—with detailed numerical investigations especially promising. Importantly, this theoretical paradigm is also very relevant for experiments probing completion time statistics in biological systems, such as protein folding monitored via gated fluorescence quenching. In such setups, a fluorophore-labeled protein undergoes reversible binding (unbinding corresponding to resetting), which imparts measurable fluorescence [139]. Once the labeled protein adopts its native fold, a quencher reacts specifically with its active site in the fluorescent conformation, but only when that site is exposed (open). When the active site is closed (hidden), the quencher cannot interact, a direct analog of gating. Successful quenching and thus a mark of process completion occur only if the folded protein exposes the active site, reflecting the interplay of stochastic gating and reaction [140]. We believe our theoretical findings offer new perspectives for understanding and leveraging various gating and resetting control strategies in such complex biological and chemical processes.

3

Stochastic resetting in operation research

(The content of this chapter has been published in [84])

3.1 Introduction

Operations Research is a field that helps people make better decisions by studying how to organize work in the best possible way. It looks at real-life problems—like how to save time, use resources wisely, or make a process run more smoothly using maths and logic to find good solutions. Queuing theory is a branch of operations research devoted to the mathematical study of waiting lines, focusing on the formation, behavior, and related properties of queues that develop ahead of service points [81, 141, 142, 82]. Queues are found throughout nature and engineering, and they emerge across diverse domains such as supermarkets, banks, and call centers [143, 144], telecommunications [145, 146], airplane boarding procedures [147, 148, 149], computer systems [150, 151], emergency response, transport processes [152, 153, 154], and even in models of gene expression [155, 156, 157, 158, 159] or metabolic and enzymatic pathways [160, 161, 162, 163, 164]. Each queueing system is governed by its own operational principles. For instance, a teller at a supermarket or bank may typically serve at a roughly constant pace, whereas computer servers or biological entities such as genes or enzymes often display greater variability in their service times [165, 166, 167, 168]. In fact, it is now well appreciated that queue efficiency hinges not only on average service rates but also on the magnitude of intrinsic fluctuations in service times, to which queuing performance is highly sensitive. Significant stochastic fluctuations can cause severe congestion or delays in queues, sometimes halting operations entirely [151].

There is an ongoing effort to develop broad strategies for mitigating or controlling the adverse effects introduced by these random fluctuations, particularly in queues with heavy-tailed workloads [169]. Various scheduling protocols exist; for example, prioritizing small jobs ahead of larger ones instead of the commonly used first-come-first-

serve policy. Although proven to be optimal under certain conditions, such schemes may be criticized for lacking fairness [151]. It is also worth noting that these strategies are most effective when fluctuations are external, arising from variation in job size or item number, as in supermarkets. However, they are less effective when randomness in service times is rooted within the server itself, as in stochastic optimization algorithms, genetic regulation, or enzymatic processes [170, 171, 172]. In such contexts, conventional queuing policies are insufficient, highlighting the need for alternative approaches.

In recent work [173], a novel queuing control mechanism was proposed based on the application of resetting (restart) to alleviate problems due to service time fluctuations. It was demonstrated that the expected queue length can be reduced significantly by implementing policies that reset service at suitable times. To explain the principle of resetting, one may consider a generic stochastic process designed to accomplish a certain task within a random duration. The process can be interrupted and restarted—forced to begin anew—at random times before it completes [5, 52, 17, 129, 53, 126, 55, 123, 174, 8, 14, 15, 16]. This cycle continues until the task is finally finished, resulting in a completion time influenced by both the process dynamics and the resetting protocol. Analogously, for a single-server queue where each task's service time is drawn from an intrinsic random process, resetting can be operationalized by intermittently stopping the server and assigning a new service time to the current job.

At first glance, it may seem paradoxical that restarting a process from the beginning could speed up the completion of complex random tasks. However, substantial research in statistical physics and the theory of stochastic processes over the last decade has shown that resetting systematically eliminates long-duration trajectories and allows for the exploration of alternative, potentially faster, paths [5, 52, 17, 129, 53, 126, 175, 83, 176, 177, 127, 178]. Identifying new trajectories can notably accelerate completion, especially when the non-reset process is characterized by substantial variability in completion times. This is a striking observation, since resetting can transform the disadvantage of large fluctuations into a beneficial effect. Accordingly, resetting strategies have become widespread across a spectrum of search and optimization processes, ranging from stochastic optimization [43, 179, 58], first-passage phenomena [67, 117, 68, 180, 27], foraging models [86], reaction kinetics [1, 96], and even in studies of income dynamics [181, 44].

This chapter aims to introduce the essential concepts of queuing and resetting, present the formulation of a single-server queue with instantaneous service resetting, and present new insights when resetting is noninstantaneous and involves a finite overhead or buffering period. We will examine the consequences of this additional overhead and its interplay with the service time in determining the queue length and waiting times. The treatment is pedagogical, intended for readers without specialized prior knowledge.

The remainder of this chapter is arranged as follows. In Sec. 3.2 ("Preliminaries"), we offer a succinct introduction to the M/G/1 queue, featuring general service

time distribution and Markovian arrivals—the central model studied herein. We review the Pollaczek-Khinchin formula for the mean steady-state number of jobs in an M/G/1 queue, highlighting its dependence on service time variability. Section 3.3 ("Service with resetting") develops the M/G/1 queue model incorporating service resetting, including a refractory (overhead) time for each reset event. Effectively, this model can be recast as a standard M/G/1 queue with a composite service time that encapsulates both service and reset overhead, allowing direct application of the Pollaczek-Khinchin formula to determine the mean occupation. Section 3.4 ("M/G/1 Queues with Poissonian service resetting") studies the influence of Poissonian resetting (i.e., resets at a fixed rate) on the mean queue size, leading to substantial simplifications. In Section 3.5 ("Service at an optimal resetting rate"), we discuss the mean number of jobs under optimal Poissonian resetting and address how resetting may decrease the queue size depending on overhead variability. Section 3.6 ("Application") applies our methods to log-normal service distributions and various overhead time statistics. The final section 3.7 ("Discussion and Summary") synthesizes the main outcomes and perspectives. Technical calculations are deferred to the appendices for completeness.

In what follows, we use the notations $f_X(t)$, $\langle X \rangle$, $\sigma^2(X)$, $\widetilde{X}(s) \equiv \langle e^{-sX} \rangle$ and CV_X to denote, respectively, the probability density function, expectation, variance, Laplace transform and coefficient of variation of a non-negative random variable X.

3.2 Preliminaries

Consider a single-server queue, where jobs form a single line and are processed one at a time on a first-come, first-served basis. This system is classified in Kendall's notation as an M/G/1 queue: here, "M" signifies Markovian (memoryless) arrivals, meaning jobs enter the system according to a Poisson process with rate λ. The "G" indicates that service times are drawn from a general, possibly arbitrary, distribution. We denote the random service time as S, characterized by the density $f_S(t)$. The final "1" specifies that only one server is available to handle jobs sequentially. It is also assumed in this framework that the server incurs an overhead (or setup) period after each service or reset. Such overhead is commonplace, for example, in computing where a buffer or initialization time is required between tasks, as well as in natural scenarios like chemical reactions or facilitated diffusion. We represent the overhead duration as a random variable S_{on}. Thus, the complete service time per task, denoted S_u, is given by the sum $S + S_{on}$, and has its own probability density $f_{S_u}(t)$. The effective service rate becomes $\eta = 1/\langle S_u \rangle$. Additionally, the queue's utilization factor is $\rho = \lambda/\eta$, reflecting the fraction of time the server is occupied in the long-run. For a well-defined steady-state to exist, the job arrival rate λ must be less than the mean effective service rate ($\rho < 1$); otherwise, when $\rho > 1$, the system is overloaded and the queue length diverges.

The overall state of the M/G/1 queue is described by the set $N = \{0, 1, 2, 3, ...\}$, where N records the total number of jobs in the system, including any currently in ser-

vice. Because arrivals and completions are stochastic, N fluctuates in time. One principal quantity of interest is the average number of jobs, $\langle N \rangle$, present in the system (both queue and server); its steady-state value is given by the celebrated Pollaczek-Khinchin formula [151]:

$$\langle N \rangle = \frac{\rho}{1-\rho} + \frac{\rho^2}{2(1-\rho)} \left(CV_u^2 - 1 \right) \ , \tag{3.1}$$

where the first term accounts for the mean queue length of an M/M/1 queue, and the second term captures the impact of service time variability. Here,

$$CV_u^2 = \frac{\sigma^2(S_u)}{\langle S_u \rangle^2}, \tag{3.2}$$

defines the squared coefficient of variation (SCV) of the total service time distribution. Some notable features follow: (1) $\langle N \rangle$ grows monotonically with increasing utilization ρ and diverges as $\rho \to 1$, signaling congestion. (2) The average queue size is extremely sensitive to the degree of service time fluctuations: if $CV_u^2 < 1$, the correction in Eq. (3.1) is negative, leading to shorter queues; if $CV_u^2 > 1$, fluctuations inflate system size. This sensitivity illustrates the crucial role played by service time noise in M/G/1 queues and suggests similar consequences in related queuing models.

The mean waiting time in the system, $\langle T \rangle$—that is, the average time a given job spends from entry to completion—connects directly to $\langle N \rangle$ through Little's law: $\langle T \rangle = \lambda^{-1} \langle N \rangle$ [151]. This results in

$$\langle T \rangle = \frac{1/\eta}{1-\rho} + \frac{\rho/\eta}{2(1-\rho)} \left(CV_u^2 - 1 \right) \ , \tag{3.3}$$

showing again that waiting times depend crucially on both the mean and the variability of the total service time. Variability in service time may be extrinsic or intrinsic to the server. For instance, if job sizes vary while the server processes all jobs at a fixed rate, then S is determined extrinsically by the jobs themselves—as in supermarket checkouts, where the number of items purchased sets service duration. Conversely, intrinsic randomness arises when service times fluctuate for reasons internal to the server: catalytic cycles of enzymes, for instance, can require varying intervals even for identical substrate and product molecules. For further discussion on the origins and implications of service time fluctuations in queueing, see [173].

3.3 Service with resetting

When the fluctuations in service times originate from intrinsic properties of the server, a resetting strategy can be introduced as follows. Once more, let us consider the M/G/1 queue, where the server processes jobs sequentially. Assume the server begins servic-

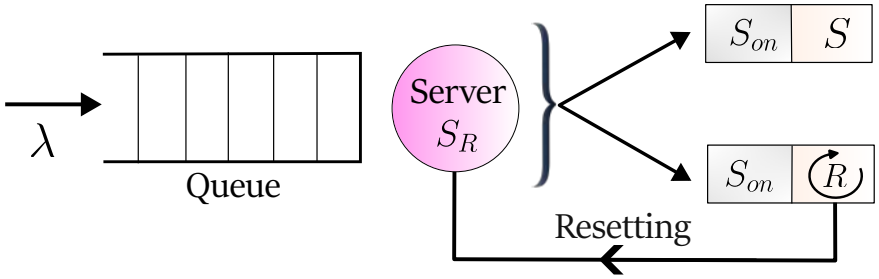

Figure 3.1: *Schematic of a queuing system under resetting. Jobs arrive at the queue with a rate λ and they are being served at the service station according to a first-come, first-served policy. The server has two components: a service time S followed by an overhead time S_{on}. It can complete a task in time $S_u = S + S_{on}$ prior to resetting (upper branch). Otherwise, resetting can occur in time R (lower branch), following which the service is renewed. The process repeats by itself until the task is completed which is possible only via the upper branch.*

ing a job at time zero and, if uninterrupted, finishes after a random duration $S_{on} + S$. However, at a random time R, the service may instead be reset, after which the process restarts. Denoting by S_R the random variable for the total service time in this compound process, the dynamics can be described as

$$S_R = S_{on} + \begin{cases} S & \text{if } S < R\,, \\ R + S'_R & \text{if } R \leq S\,, \end{cases} \tag{3.4}$$

where S_{on} is a random overhead period (sampled from a general distribution) preceding either completion or resetting, and S'_R denotes an independent copy of S_R. To interpret this, notice that if the service completes before a reset occurs ($S < R$), then $S_R = S_{on}+S = S_u$. If, on the other hand, resetting takes place first ($R \leq S$), the process restarts with a new overhead and service period, resulting in $S_R = S_{on}+R+S'_R$. This formulation reveals a renewal structure reminiscent of renewal theory. As discussed in [173], this set-up can be viewed as a first-passage process under intermittent resetting, and the broad theoretical framework for first-passage processes with resetting is developed in [182, 53]. We briefly review these results in (Appendix C.1), while focusing here on the main conclusions. Rewriting Eq. (3.4), we can express this as

$$S_R = S_{on} + \min(S, R) + I(R \leq S)S'_R, \tag{3.5}$$

where $\min(S, R)$ denotes the smaller of the two times and $I(R \leq S)$ is an indicator variable equal to one when resetting occurs before service is complete, and zero otherwise. This representation facilitates calculation of the moment generating function for S_R, which we discuss in the Appendix. However, the first and second moments can be

evaluated directly by taking expected values:

$$\langle S_R \rangle = \frac{\langle \min(S,R) \rangle + \langle S_{on} \rangle}{\Pr(S < R)}, \tag{3.6}$$

$$\langle S_R^2 \rangle = \frac{\langle (\min(S,R) + S_{on})^2 \rangle}{\Pr(S < R)} + \frac{2\Pr(R \leq S)\big(\langle R_{min} \rangle + \langle S_{on} \rangle\big)\left(\langle \min(S,R) \rangle + \langle S_{on} \rangle\right)}{\Pr(S < R)^2}. \tag{3.7}$$

Here, $\Pr(S < R)$ is the probability that service concludes before a reset, and $R_{\min} = \{R | R < S\}$ represents the resetting time, conditional on occurring before service completion. Recall the variance of the compound service time is $\sigma^2(S_R) = \langle S_R^2 \rangle - \langle S_R \rangle^2$. Once the precise distributions for S and R are specified, all averages in Eq. (3.6) and Eq. (3.7) can be evaluated directly, as detailed in the next section.

3.4 M/G/1 Queues with Poissonian service resetting

Many possible combinations of resetting and service mechanisms are possible. Of particular interest is Poissonian resetting, which has been extensively analyzed in recent literature [5, 52, 67, 183, 54, 53, 117, 68, 14, 55, 8]. In this setting, reset events occur with a fixed average rate r, so the number of resets in a time interval t is Poisson distributed with mean rt, and each reset time R is sampled from an exponential distribution $f_R(t) = re^{-rt}$. Utilizing (3.6) and (3.7) (see Appendix C.2 for derivations), the mean and second moment of the compound service time become

$$\langle S_r \rangle = \frac{1 - \widetilde{S}(r) + r\langle S_{on} \rangle}{r\widetilde{S}(r)}, \tag{3.8}$$

$$\langle S_r^2 \rangle = \frac{2r\frac{d\widetilde{S}(r)}{dr}(1 + r\langle S_{on} \rangle) + 2(1 - \widetilde{S}(r))(1 + r\langle S_{on} \rangle)^2 + r^2\widetilde{S}(r)\langle S_{on}^2 \rangle}{r^2\widetilde{S}(r)^2}, \tag{3.9}$$

where $\widetilde{S}(r) = \int_0^\infty dt\, e^{-rt} f_S(t)$ is the Laplace transform of f_S evaluated at r. The corresponding utilization is $\rho_r = \lambda\langle S_r \rangle$, and the squared coefficient of variation becomes $CV_r^2 = \sigma^2(S_r)/\langle S_r \rangle^2$.

Owing to resetting, the effective service time is now S_r. Thus, in the Pollaczek-Khinchin result, ρ and CV_u^2 are replaced by ρ_r and CV_r^2, yielding:

$$\langle N_r \rangle = \frac{\rho_r}{1 - \rho_r} + \frac{\rho_r^2}{2(1 - \rho_r)}\left(CV_r^2 - 1\right). \tag{3.10}$$

Similarly, the mean waiting time with resetting $\langle T_r \rangle$ follows directly from Little's Law [184, 151], taking the same form as Eq. (3.3). To illustrate how resetting and overhead time affect the M/G/1 queue, Fig. 3.2(a) shows a prototypical example (with further details in Sec. 3.6). Starting with a chosen service time distribution, it is found that introducing

resetting leads to a non-monotonic curve for $\langle S_r \rangle$ as a function of r under multiple overhead distributions. Specifically, $\langle S_r \rangle$ initially decreases, reaching a minimum at some optimal r^*, before rising again. This optimal rate r^* is noteworthy, as it both lessens and globally minimizes the mean service time. The next section examines r^* in more depth and explores how it relates to the generic properties of service and overhead distributions.

3.5 Service at an optimal resetting rate

The resetting rate that minimizes the mean service time is determined by the condition

$$\left.\frac{d\langle S_r \rangle}{dr}\right|_{r=r^*} = 0. \tag{3.11}$$

Plugging the explicit formula for $\langle S_r \rangle$ from Eq. (3.8) into this stationarity condition yields

$$\widetilde{S}(r^*)(\widetilde{S}(r^*) - 1) - r^*\widetilde{S}'(r^*)(1 + r^*\langle S_{on} \rangle) = 0, \tag{3.12}$$

where $\widetilde{S}'(r)$ is the derivative of $\widetilde{S}(r)$ with respect to r. Substituting $\widetilde{S}'(r^*)$ into Eq. (3.9), and rearranging, one obtains for the variability of the optimally restarted process [54]

$$CV_{r^*} = \frac{\sigma(S_{r^*})}{\langle S_{r^*} \rangle} = \sqrt{1 + \frac{\langle S_{on} \rangle^2}{\widetilde{S}(r^*)\langle S_r^* \rangle^2}\left(CV_{on}^2 - 1\right)}, \tag{3.13}$$

Here, $CV_{on} = \frac{\sigma(S_{on})}{\langle S_{on} \rangle}$ is the coefficient of variation of the overhead time, and the total service SCV can be written

$$CV_u = \sqrt{\frac{\sigma^2(S) + \sigma^2(S_{on})}{\langle S + S_{on} \rangle^2}}. \tag{3.14}$$

Notably, the expression in Eq. (3.13) is universal—it holds for arbitrary underlying service and overhead time distributions. Our aim is now to investigate how the mean queue length changes when the service rate is set optimally.

For the optimally restarted process, the mean queue length from the Pollaczek-Khinchin formula reads

$$\langle N_{r^*} \rangle = \frac{\rho_{r^*}}{1 - \rho_{r^*}} + \frac{\rho_{r^*}^2}{2(1 - \rho_{r^*})}(CV_{r^*}^2 - 1). \tag{3.15}$$

Substituting (3.13) gives

$$\langle N_{r^*}\rangle = \frac{\rho_{r^*}}{1-\rho_{r^*}} + \frac{\lambda^2}{2(1-\rho_{r^*})}\frac{\langle S_{on}\rangle^2}{\widetilde{S}(r^*)}\left(CV_{on}^2 - 1\right), \tag{3.16}$$

where we used $\rho_{r^*} = \lambda\langle S_{r^*}\rangle$. This result shows that the mean system size depends crucially on the variability of the overhead process. In the following, we consider several regimes distinguished by the value of CV_{on}.

In the above, it was assumed that a finite optimal rate r^* actually exists. To be more precise, the criterion for the existence of such an optimum is (Appendix C.3)

$$CV_u^2 > 1 + \frac{\langle S_{on}\rangle^2}{\langle S_u\rangle^2}(CV_{on}^2 - 1), \tag{3.17}$$

highlighting again the dependence on the overhead variability.

3.5.1 Resetting with no overhead

First, let us revisit the limiting case where the resetting generates no overhead—the service restarts instantaneously, as thoroughly analyzed in [173]. For $S_{on} = 0$, $S_u = S$ and equations (3.8) and (3.9) reduce to [173]

$$\langle S_r\rangle = \frac{1-\widetilde{S}(r)}{r\widetilde{S}(r)}, \tag{3.18}$$

$$\langle S_r^2\rangle = \frac{2r\frac{d\widetilde{S}(r)}{dr} - \widetilde{S}(r) + 1}{r^2\widetilde{S}(r)^2}, \tag{3.19}$$

and the universal relation (3.13) simplifies to $CV_r^* = 1$. In this scenario, the average queue size becomes

$$\langle N_{r^*}\rangle = \frac{\rho_{r^*}}{1-\rho_{r^*}}, \tag{3.20}$$

which satisfies the inequality $\langle N_{r^*}\rangle < \langle N\rangle$, establishing that an optimal resetting policy reduces congestion. Moreover, existence of a minimum is guaranteed if $CV_u > 1$ [173].

3.5.2 Overhead time with $CV_{on} < 1$

Next, consider the case where overhead times are narrowly distributed, meaning $CV_{on} < 1$. Denoting the queue length in this regime as $\langle N_{r^*}^I\rangle$, we have

$$\langle N_{r^*}^I\rangle = \frac{\rho_{r^*}}{1-\rho_{r^*}} + \frac{\lambda^2}{2(1-\rho_{r^*})}\frac{\langle S_{on}\rangle^2}{\widetilde{S}(r^*)}\left(CV_{on}^2 - 1\right) \tag{3.21}$$

where the second term is negative, so that $\langle N^I_{r^*}\rangle < \frac{\rho_{r^*}}{1-\rho_{r^*}}$. According to (3.17), for $CV_{on} < 1$ a sufficient (but not necessary) condition for optimal resetting is $CV_u > 1$.

If such a finite r^* is found, it follows that $\langle S_{r^*}\rangle < \langle S_u\rangle$, or equivalently, $\rho_{r^*} < \rho$, recalling $\rho = \lambda\langle S_u\rangle$, $\rho_{r^*} = \lambda\langle S_{r^*}\rangle$. Because $\frac{\rho}{1-\rho}$ is monotonically increasing in ρ, this implies $\frac{\rho_{r^*}}{1-\rho_{r^*}} < \frac{\rho}{1-\rho}$. Collecting results,

$$\langle N^I_{r^*}\rangle < \frac{\rho_{r^*}}{1-\rho_{r^*}} < \frac{\rho}{1-\rho} \leq \frac{\rho}{1-\rho} + \frac{\rho^2}{2(1-\rho)}\left(CV_u^2 - 1\right) = \langle N\rangle, \tag{3.22}$$

which always holds so long as $CV_u > 1$, confirming that optimal resetting provides relief from queue buildup.

Because the threshold $CV_u > 1$ is not strictly necessary, r^* can still exist (and reduce queue size) before this holds (see Appendix C.3.1 for more on this). This demonstrates that the advantages of service resetting persist even when a finite overhead is present.

3.5.3 Overhead time with $CV_{on} = 1$

Let us now examine the special case where the coefficient of variation in the overhead time equals unity, $CV_{on} = 1$. Under this condition, the correction term in Eq. (3.16) disappears, so the mean queue size, denoted $\langle N^{II}_{r^*}\rangle$, reduces to

$$\langle N^{II}_{r^*}\rangle = \frac{\rho_{r^*}}{1-\rho_{r^*}}. \tag{3.23}$$

Following the argument developed for previous cases, we readily establish that

$$\langle N^{II}_{r^*}\rangle = \frac{\rho_{r^*}}{1-\rho_{r^*}} \leq \frac{\rho}{1-\rho} \leq \frac{\rho}{1-\rho} + \frac{\rho^2}{2(1-\rho)}\left(CV_u^2 - 1\right) = \langle N\rangle, \tag{3.24}$$

where we have followed similar logic as before, and note that the existence of a finite r^* again requires $CV_u > 1$ (see Appendix C.3.2 for further discussion).

3.5.4 Overhead time with $CV_{on} > 1$

Finally, consider the situation where the overhead times are widely dispersed and thus $CV_{on} > 1$. In this setting, one arrives at

$$\langle N^{III}_{r^*}\rangle = \frac{\rho_{r^*}}{1-\rho_{r^*}} + \frac{\lambda^2}{2(1-\rho_{r^*})}\frac{\langle S_{on}\rangle^2}{\widetilde{S}(r^*)}\left(CV_{on}^2 - 1\right), \tag{3.25}$$

where now the correction arising from the overhead variability is strictly positive. However, in contrast to the previous cases, the condition $CV_u > 1$ by itself no longer guarantees that $\langle N^{III}_{r^*}\rangle < \langle N\rangle$. A closer analysis reveals that a sufficient (though not necessary)

criterion for this inequality is (see Appendix C.3.3 for details):

$$CV_u^2 > 1 + \left(\frac{\langle S_{on}\rangle}{\langle S_u\rangle}\right)^2 \frac{1}{\widetilde{S}(r^*)}(CV_{on}^2 - 1). \tag{3.26}$$

As CV_u can be manipulated as a control parameter, this condition may be used to ensure a tangible reduction in queue length due to resetting.

3.6 Application

To illustrate the practical relevance of our theory, let us analyze an M/G/1 queue where the service times follow a log-normal distribution—a distribution frequently encountered in queuing studies [185, 186]. We will explore how resetting influences this system under several types of overhead time distributions. The specific form of the log-normal distribution employed is

$$f_S(t) = \frac{1}{\sqrt{2\pi}\alpha t}\, e^{-\frac{(\ln t-\mu)^2}{2\alpha^2}}, \tag{3.27}$$

for $t > 0$, where μ is a real parameter and $\alpha > 0$. The mean and variance of the service time, S, in this case read

$$\langle S\rangle = e^{\mu+\frac{\alpha^2}{2}}, \tag{3.28}$$

$$\sigma(S) = \left(e^{\alpha^2} - 1\right) e^{2\mu+\alpha^2}, \tag{3.29}$$

which yields

$$CV^2 = e^{\alpha^2} - 1\,, \tag{3.30}$$

independent of μ. The previous sections developed general conclusions for arbitrary overhead distributions, mainly in terms of CV_{on}. We now focus on three illustrative cases with distinct values of CV_{on}, all with the mean overhead time $\langle S_{on}\rangle$ held constant, before finally considering scenarios where $\langle S_{on}\rangle$ is itself variable.

3.6.1 Case I: $CV_{on} < 1$

Let us begin with the situation where $CV_{on} = 0 < 1$, meaning the overhead distribution is highly localized about its mean, i.e., $f_{S_{on}}(t) = \delta(t - \langle S_{on}\rangle)$. The overall variability of the total service process is then

$$CV_u^2 = \frac{e^{\alpha^2} - 1}{(1 + \langle S_{on}\rangle)^2}. \tag{3.31}$$

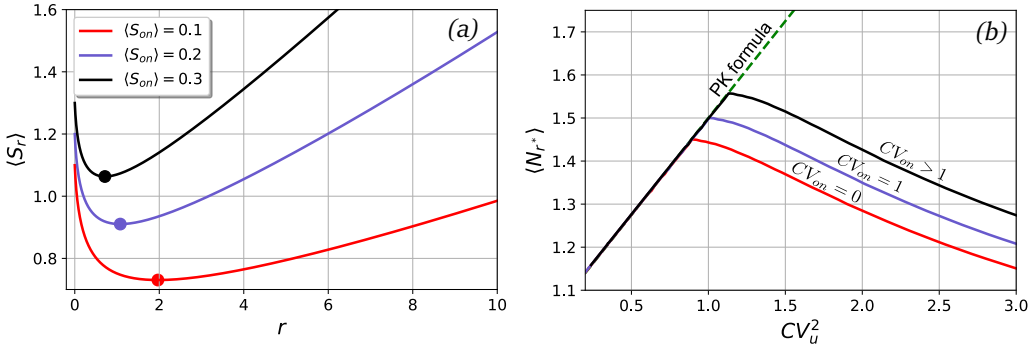

Figure 3.2: *(a) Mean service time $\langle S_r \rangle$ from Eq. (3.8) as a function of resetting rate for different choices of $\langle S_{on} \rangle$. The underlying service time S is sampled from the log-normal distribution (3.27) with $\langle S \rangle = 1$ and $\alpha = 1.5$. Circles mark the optimal resetting rate r^* for each value where $\langle S_r \rangle$ attains its minimum. (b) Mean queue length at optimal resetting, $\langle N_{r^*} \rangle$, versus squared CV_u. Here, $\langle S \rangle$ is fixed at unity and α is varied to tune CV_u in Eqs. (3.31), (3.32), and (3.35). Results are shown for deterministic ($CV_{on} = 0$), exponential ($CV_{on} = 1$), and Weibull ($CV_{on} > 1$) overheads, all with $\langle S_{on} \rangle = 0.5$. Dashed lines indicate the standard Pollaczek–Khinchin result (3.1) at $r^* = 0$. For larger CV_u, optimal resetting becomes nonzero, causing $\langle N_{r^*} \rangle$ to dip below the standard value, and the transition points agree with theoretical predictions. Optimal resetting efficiently reduces queue lengths for any S_{on} and CV_{on}, and all results here use $\lambda = 0.4$.*

In Fig. 3.2(a), we plot the mean service time $\langle S_r \rangle$ versus resetting rate r for different $\langle S_{on} \rangle$ values, fixing $\langle S \rangle = 1$ and $\alpha = 1.5$. Each curve displays a minimum at a specific r^* which depends on $\langle S_{on} \rangle$. Turning to the mean queue length, we keep $\langle S \rangle = 1$ and $\langle S_{on} \rangle = 0.5$ fixed, but vary α to scan different CV_u. For each α, $\langle S_r \rangle$ is minimized over r to find r^*, which is then used to compute the optimal queue length using Eq. (3.21). Note that the emergence of a finite r^* is not always guaranteed (see Sec. 3.5.2). When $r^* = 0$, $\langle N^I_{r^*} \rangle$ matches the unreset queue $\langle N \rangle$, but for finite r^*, the deviation clearly shows $\langle N^I_{r^*} \rangle < \langle N \rangle$. The lowest curve in Fig. 3.2(b) highlights how the mean queue length drops sharply as CV_u increases.

3.6.2 Case II: $CV_{on} = 1$

In this regime, S_{on} is exponentially distributed such that $f_{S_{on}}(t) = \gamma e^{-\gamma t}$, with $\gamma > 0$. Here, $\langle S_{on} \rangle = 1/\gamma$ and $\sigma^2(S_{on}) = 1/\gamma^2$, thus $CV_{on} = 1$. The total process variability is then

$$CV_u^2 = \frac{e^{\alpha^2} - 1 + \frac{1}{\gamma^2}}{(1 + \frac{1}{\gamma})^2}. \tag{3.32}$$

We again fix $\langle S_{on} \rangle = 0.5$ and use α to sweep CV_u. For each α, we seek r^* by minimizing $\langle S_r \rangle$ and substitute in Eq. (3.23). For $CV_u < 1$, the optimal and baseline queue lengths coincide, but as CV_u increases, $\langle N^{II}_{r^*} \rangle$ falls below $\langle N \rangle$, with $CV_u = 1$ marking the transition. This boundary is visible in the middle curve of Fig. 3.2(b).

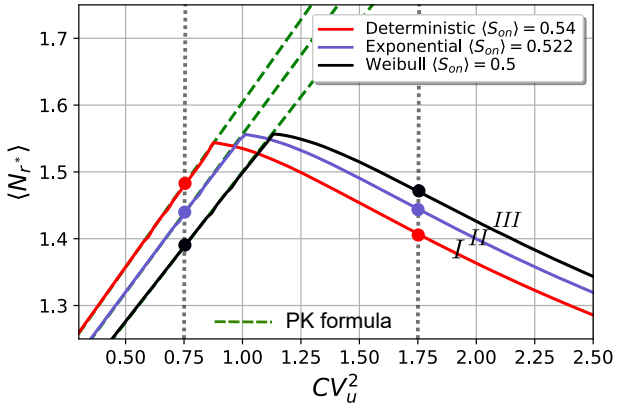

Figure 3.3: *Mean queue length at optimal Poisson resetting as a function of squared CV_u for multiple choices of $\langle S_{on}\rangle$ and variability, taking deterministic ($CV_{on} = 0$), exponential ($CV_{on} = 1$), and Weibull ($CV_{on} = 1.4624$) overheads. The underlying service distribution is log-normal [Eq. (3.27)] with $\langle S\rangle = 1$ and variable α setting CV_u via Eq. (3.31), Eq. (3.32), Eq. (3.35). Dashed lines show standard PK formula ($r^* = 0$). Left vertical dashed line at $CV_u < 1$ reflects the order $\langle N^I_{r^*=0}\rangle > \langle N^{II}_{r^*=0}\rangle > \langle N^{III}_{r^*=0}\rangle$, tracking $\langle S_{on}\rangle$ from largest to smallest. Resetting has no effect here. When r^* becomes nonzero (right dashed line, $CV_u > 1$), the order reverses: $\langle N^I_{r^*}\rangle < \langle N^{II}_{r^*}\rangle < \langle N^{III}_{r^*}\rangle$ for a fixed CV_u. This means queues with smaller overhead fluctuations (but larger mean overhead) are most impacted by optimal resetting.*

3.6.3 Case III: $CV_{on} > 1$

Finally, for the case $CV_{on} > 1$, we use the Weibull distribution: $f_{S_{on}}(t) = \frac{k}{\nu}(\frac{t}{\nu})^{k-1}\exp[-(t/\nu)^k]$, for $t \geq 0$, where $k > 0$ is the shape parameter and $\nu > 0$ the scale parameter. The mean and variance become

$$\langle S_{on}\rangle = \nu\Gamma(1+\frac{1}{k}), \tag{3.33}$$

$$\sigma^2(S_{on}) = \nu^2\left[\Gamma(1+\frac{2}{k}) - (\Gamma(1+\frac{1}{k}))^2\right], \tag{3.34}$$

with $\Gamma(z)$ denoting the Gamma function. If $k = 0.7$, $\langle S_{on}\rangle = 1.2658\nu$ and $CV_{on} = 1.4624 > 1$. The overall variability is then

$$CV_u^2 = \frac{e^{\alpha^2} - 1 + 3.4268\nu^2}{(1+1.2658\nu)^2}. \tag{3.35}$$

We pick $\nu = 0.395$ to fix $\langle S_{on}\rangle = 0.5$ and repeat the optimization as before. When the criterion (3.26) is met, we see $\langle N^{III}_{r^*}\rangle < \langle N\rangle$. Critically, in this scenario the deviation from the standard PK result arises only for larger CV_u (*i.e.*, for larger fluctuations), as seen in Fig. 3.2(b).

Thus, optimal resetting has a stronger impact on queues with low-overhead variability, even if the mean overhead is larger.

3.6.4 Mean queue length for different $\langle S_{on}\rangle$

So far, our analysis has held $\langle S_{on}\rangle$ constant while varying CV_{on} to study the mean queue length. Let's now examine the interplay when both $\langle S_{on}\rangle$ and CV_{on} vary. Recall, from

the PK formula, that for a fixed $r^* = 0$, the mean queue length increases linearly with CV_u^2, i.e. $\langle N_{r^*} \rangle = \langle N \rangle$; for fixed CV_u, increasing $\langle S_{on} \rangle$ also increases queue size. For example, at $CV_u = \sqrt{0.75}$ in Fig. (3.3), increasing $\langle S_{on} \rangle$ raises $\langle N_{r^*=0} \rangle$, as shown by the colored circles, and we have:

$$\langle N^I_{r^*=0} \rangle > \langle N^{II}_{r^*=0} \rangle > \langle N^{III}_{r^*=0} \rangle. \tag{3.36}$$

But how does queue length compare for different $\langle S_{on} \rangle$ values under optimal resetting? Strikingly, a queue with higher $\langle S_{on} \rangle$ may see a much larger reduction from resetting than one with lower $\langle S_{on} \rangle$—*if* the former has a smaller CV_{on}. This reversal of order is clear at $CV_u = \sqrt{1.75}$ (for which $r^* > 0$) in Fig. (3.3):

$$\langle N^I_{r^*>0} \rangle < \langle N^{II}_{r^*>0} \rangle < \langle N^{III}_{r^*>0} \rangle, \tag{3.37}$$

so that, for fixed CV_u, the queue with the lowest overhead variability (and largest mean overhead) is most susceptible to shortening by reset. Full details are shown in Fig. (3.3). Here, we focused on log-normal service times, but the conclusions are likely general for other service distributions as well.

3.7 Discussion and Summary

The task of devising methods to minimize queue lengths is a central concern in queuing theory. Crucially, it is the management of substantial stochastic fluctuations in service durations that poses a significant challenge for queue efficiency. This phenomenon has often been highlighted, particularly in contexts such as computing workloads where service time distributions display high variability, for instance in UNIX process lifetime studies [151, 187]. This chapter has reviewed a notable development focused on improving the performance of systems with high-variability workloads [173, 188, 189]. We have demonstrated that *service resetting* stands as a powerful tool to counteract such inefficiencies. Specifically, our analysis has centered on the M/G/1 queue model, where jobs arrive at a fixed rate and the server encompasses both a processing time and an additional overhead (or buffer) period. By intermittently resetting the service, we explored the consequences for queue dynamics. Employing a renewal approach for service times that include overhead and resetting, we showed how the modified process can be seamlessly incorporated into the classic Pollaczek-Khinchin formula to yield the expected average number of jobs in the queue.

Our study identifies three distinct regimes for the overhead time distribution: tightly concentrated, marginally dispersed, and broadly distributed. Across all these cases, we established that an optimally designed resetting protocol can make the queue at least as efficient, or even substantially more so, than its non-resetting counterpart. In particular, we found that a resetting strategy can dramatically decrease queue lengths—especially

for servers with inherently high service-time variance. Thus, resetting not only shortens the mean service time but also dampens relative stochastic fluctuations, providing a double benefit.

While our main discussion focuses on Poissonian resetting, the general framework developed extends naturally to alternative strategies, including sharp (deterministic) resetting [13, 53, 190], in which resets are performed at fixed intervals. This periodic resetting mechanism is strongly motivated by earlier work in the stochastic resetting literature, where sharp resets frequently outperform random counterparts regardless of the process being controlled. To illustrate this, suppose resetting is scheduled deterministically after every τ time units:

$$f_R(t) = \delta(t - \tau). \tag{3.38}$$

By applying Eqs. (3.6) and (3.7), one can directly compute the mean and second moment of the reset service time (Appendix C.4):

$$\langle S_\tau \rangle = \frac{\int_0^\tau q_S(t)dt + \langle S_{on} \rangle}{1 - q_S(\tau)}, \tag{3.39}$$

$$\langle S_\tau^2 \rangle = \frac{2\int_0^\tau t\, q_S(t)dt + 2\langle S_{on} \rangle \int_0^\tau q_S(t)dt + \langle S_{on}^2 \rangle}{1 - q_S(\tau)} + \frac{2q_S(\tau)(\tau + \langle S_{on} \rangle)\left(\int_0^\tau q_S(t)dt + \langle S_{on} \rangle\right)}{(1 - q_S(\tau))^2}, \tag{3.40}$$

where $q_S(t) = \int_t^\infty f_S(t')dt'$ is the survival function for the service, i.e., the probability that service has not yet finished by time t; for the log-normal case (Sec. 3.6), this is given by

$$q_S(t) = \frac{1}{2}\left[1 + \mathrm{erf}\left(\frac{\mu - \log(t)}{\sqrt{2}\alpha}\right)\right]. \tag{3.41}$$

To find the mean queue length, plug the moments of the modified service into Eq. (3.10):

$$\langle N_\tau \rangle = \frac{\rho_\tau}{1 - \rho_\tau} + \frac{\rho_\tau^2}{2(1 - \rho_\tau)}\left(CV_\tau^2 - 1\right), \tag{3.42}$$

where $\rho_\tau = \lambda\langle S_\tau \rangle$ and CV_τ measures the service time variability after sharp resetting. The optimal interval τ^* is found by solving $d\langle S_\tau \rangle / d\tau|_{\tau=\tau^*} = 0$. Using this approach, Fig. 3.4(b) shows the mean queue length $\langle N_{\tau^*} \rangle$ as a function of underlying service time variability CV_u for several overhead time distributions. One sees that sharp resetting robustly reduces queue length, regardless of the specific CV_{on} values.

It is also illuminating to directly compare the mean queue lengths for optimal Poissonian versus sharp resetting. Drawing from general results in first-passage resetting, we know that sharp resetting always matches or outperforms Poissonian resetting in minimizing mean completion time. Our findings confirm that this hierarchy persists even in the presence of overheads (see Fig. 3.4(a)). In Fig. 3.5, we plot the difference

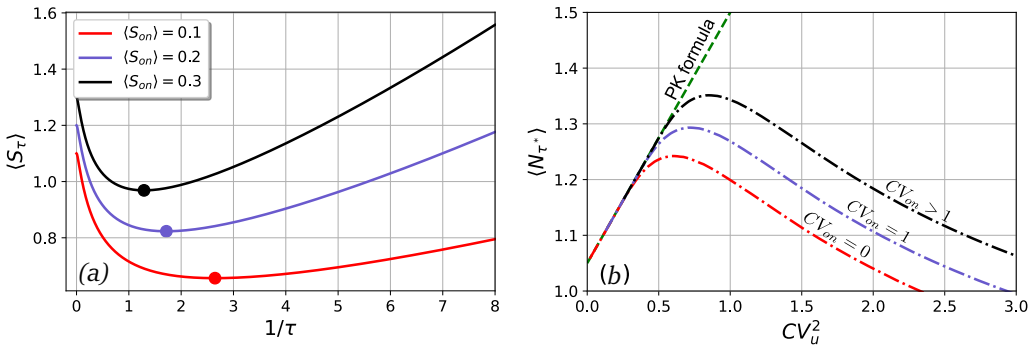

Figure 3.4: *Panel (a): The mean service time from Eq. (3.39) as a function of resetting period τ for various overhead S_{on} values, with service S drawn from a log-normal distribution (Eq. (3.27)). In each curve, the global minimum at τ^* (shown by a solid circle) marks the optimal resetting. We use $\langle S\rangle = 1$, $\alpha = 1.5$, and $\lambda = 0.4$. Panel (b): $\langle N_{\tau^*}\rangle$ as a function of CV_u^2 (tuned via α). The dashed line is the classical PK formula, valid when $\tau^* = 0$. Once τ^* becomes positive, the mean queue length falls below the baseline: evidence for the improved performance enabled by sharp resetting. Overhead times S_{on} are sampled from three distributions with differing CV_{on} as indicated.*

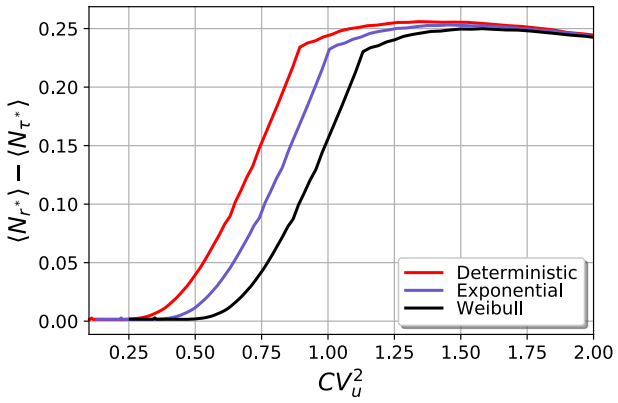

Figure 3.5: *The difference in mean queue length between optimal Poisson and sharp resetting as a function of squared CV_u. The service S is log-normal (Eq. (3.27)) with $\langle S\rangle = 1$ and $\langle S_{on}\rangle = 0.5$, and α is varied to tune CV_u. Overhead S_{on} is drawn from deterministic ($CV_{on} = 0$), exponential ($CV_{on} = 1$) and Weibull ($CV_{on} > 1$) distributions. In all scenarios, $\langle N_{r^*}\rangle - \langle N_{\tau^*}\rangle > 0$ for all CV_u, confirming that sharp resetting universally outperforms Poisson resetting. Here, $\lambda = 0.4$.*

$\langle N_{r^*}\rangle - \langle N_{\tau^*}\rangle$ versus CV_u, for various overhead distributions (deterministic, exponential, Weibull). Strikingly, this difference remains strictly positive, establishing that optimal sharp resetting always achieves lower queue lengths than even the best Poissonian strategy. This finding is significant for real-world systems, as it demonstrates further gains in queue performance achievable through deterministic resetting protocols.

The analytical approach established here for service times incorporating overhead and resetting is not limited to the M/G/1 context, but can also be extended to more general queueing models, such as G/G/1, where arrivals lack Markovian structure [151]. Renewal methods of a similar flavor may be applied to analyze situations where each job's service time consists of both extrinsic (job size) and intrinsic (server fluctuations) components [188], for which resetting has also been shown to reduce queue size [173]. Exploring the interplay between overhead and resetting in such generalized systems remains an important avenue for future research. For instance, in an M/G/n queue (a

multi-server queue), each server could, in principle, follow its own resetting protocol, provided each job's modified service time is consistent. Yet, in practice, scenarios in which several servers undergo coordinated resetting or correlated failures are common, presenting more complex dependencies that may not be directly tractable using the tools developed here. Further work will be required to generalize resetting theory to such coupled and correlated queueing networks.

In summary, we believe this chapter has highlighted the feasibility and value of employing resetting-based strategies in queueing systems. Our hope is that these concepts may foster a stronger connection between the queuing theory and stochastic resetting communities, spurring new research efforts toward developing resetting-based solutions in queues with potential applications spanning computer science, randomized algorithms, and active living systems.

4

Stochastic resetting in a viscoelastic medium

(The content of this chapter has been published in [191])

4.1 Introduction

The classical framework of Brownian motion describes, for instance, the erratic movement of a heavy particle suspended in a fluid, as was first noted by Robert Brown in 1827 while observing pollen and dust grains in water. This stochastic motion results from the thermal agitation of the molecules in the fluid, whose individual masses are much smaller than the mass of the suspended particle. Paul Langevin characterized the dynamics of such a Brownian particle with mass m by invoking Newton's second law, where the particle experiences viscous friction $-\gamma_0 v(t)$, an external deterministic potential $V(x)$, and a stochastic internal force $\xi(t)$, *i.e.*, [192]

$$m\dot{v}(t) + \gamma_0 v(t) + \frac{dV(x)}{dx} = \xi(t), \quad \dot{x}(t) = v(t), \tag{4.1}$$

where $x(t)$ and $v(t)$ denote the particle's displacement and velocity, respectively, and γ_0 stands for the friction coefficient. The stochastic force $\xi(t)$ is assumed to be a Gaussian process with zero mean ($\langle \xi(t) \rangle = 0$) and correlation function $\langle \xi(t)\xi(t') \rangle = 2\gamma_0 k_B T \delta(t-t')$, where $\langle \cdot \rangle$ specifies ensemble averaging. This framework identifies the noise as internal white noise, ensuring that fluctuations and dissipation originate from a common source. In this regime, the timescale associated with molecular motion is much less than the timescale for Brownian movement of the particle. As a result, the mean squared displacement (MSD) $\sigma^2(t) = \langle x^2(t) \rangle - \langle x(t) \rangle^2$, in the absence of an external potential ($V(x) = 0$), exhibits a linear time dependence in the long-time limit, $\sigma^2(t) \sim t$, which is emblematic of normal diffusion, although at short times the inertia causes the motion to be ballistic. The crossover from ballistic to normal diffusion is determined by the characteristic timescale m/γ_0.

In many physical systems, the mass of the embedded particle is not necessarily much greater than that of the surrounding fluid molecules, implying that the timescales for the microscopic and Brownian motions are not well separated. In these cases, it becomes necessary to generalize the Langevin equation by introducing a memory-dependent friction term, leading to the generalized Langevin equation with a friction kernel [77, 78, 193, 194], which is central to the present work.

The generalized Langevin equation is often used to describe anomalous diffusion by incorporating a power-law friction memory kernel [195, 196, 197, 198, 199, 200]. This anomalous diffusion manifests as a power-law dependence of the MSD on time, $\sigma^2(t) \sim t^\alpha$, $\alpha \neq 1$, as has been measured in systems ranging from single-protein electron transfer [201, 202], to models with a solute particle in a fast-moving solvent [203], or particles in viscoelastic environments [204]. The GLE framework has found applications in the study of protein conformational fluctuations [205, 206], in microscopic models of tracer dynamics in one-dimensional systems with two-body interactions [207], in generalized elastic models for membranes and semiflexible polymers [208], and in polymer translocation studies [209]. As an illustrative example, the emergence of exponential memory is seen in the context of Brownian motion in a harmonic potential, i.e., the Ornstein-Uhlenbeck (OU) process [210, 211, 212]. In this chapter, we focus on the Jeffreys fluid model for a particle in a viscoelastic medium, which represents another instance of a non-Markovian system [79, 80, 213, 214, 215, 216, 217, 218, 219]. Our objective is to study the motion of a particle in such a medium under stochastic resetting, as will be described in the following sections.

In contrast to the extensive body of work devoted to analyzing various types of diffusion and anomalous transport described by (generalized) diffusion and Fokker-Planck equations for homogeneous and heterogeneous systems with stochastic resetting [52, 63, 8, 178, 220, 221, 222, 223, 224, 25, 64], studies treating the generalized Langevin equation under stochastic resetting are scarce. In a resetting scenario, a particle is brought back to its initial or some fixed position at either regular or random times. Notably, this resetting mechanism can stabilize the dynamics by recurrently returning the system to a fixed point. This phenomenon was first demonstrated by Evans and Majumdar for the case of normal diffusion, where the absence of resetting leads to a non-stationary process, but the introduction of resetting induces stationarity [52]. Similar effects have been observed in the aforementioned diffusion and Fokker-Planck models, where stochastic resetting steers the system towards a non-equilibrium stationary state (NESS) [52, 63, 64, 21, 225, 138, 226, 10], and the path to the steady state can be highly nontrivial [7, 63, 9].

In this work, we investigate a process governed by the generalized Langevin equation with Poissonian resetting. This setup implies that the process is restarted at random times drawn from an exponential distribution $f_R(t) = re^{-rt}$, where $1/r$ specifies the average resetting time (here, r denotes the resetting rate). We present a thorough analy-

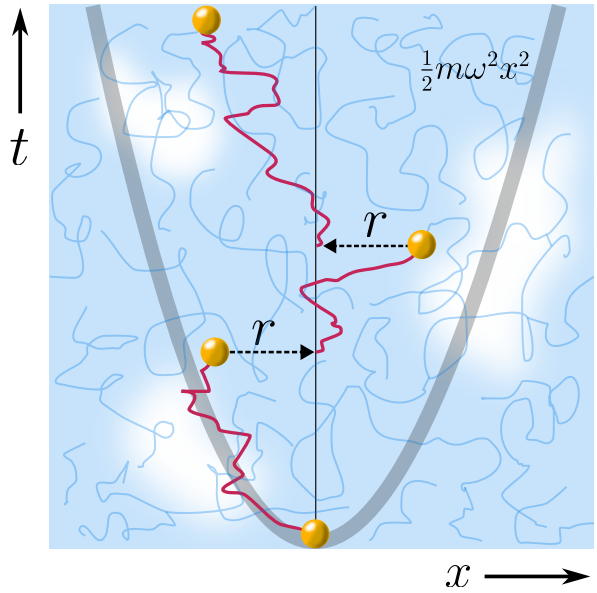

Figure 4.1: *Schematic representation of a colloidal particle diffusing in a viscoelastic bath under harmonic trapping. The motion of the particle is governed by the generalized Langevin equation (GLE) as in Eq. (4.5). In addition, the particle undergoes stochastic resetting at random time intervals drawn from an exponential distribution with mean* $1/r$.

sis of the mean squared displacement and correlation functions for an arbitrary friction memory kernel. We then apply these general results to the Jeffreys fluid memory kernel, corroborating our analytical expressions with numerical simulations.

The structure of this chapter is as follows: first, in Section 4.2, we offer a detailed exposition of the generalized Langevin equation (GLE), obtaining the mean squared displacement and correlation function for particle dynamics in a viscoelastic medium with an arbitrary kernel. In Section 4.3, we elaborate on the renewal approach to stochastic resetting to obtain general expressions for the mean and correlation function under GLE dynamics with resetting at rate r. In Section 4.4, we consider as a specific example the Jeffreys fluid model for the viscoelastic bath, examining in detail the mean and correlation function both with and without resetting. We validate our theoretical predictions by numerical simulation using the Markovian embedding scheme, as described in Section 4.5. The chapter concludes with a concise summary and a perspective on future directions in Section 4.6.

4.2 Generalized Langevin equation

Consider a particle of mass m situated in a viscoelastic environment and subjected to correlated thermal noise $\xi(t)$. Additionally, the particle is constrained by an external potential $V(x)$. The dynamics of this system are governed by the generalized Langevin

equation (GLE), which takes the following form [78, 210]

$$m\ddot{x}(t) + m\int_0^t \gamma(t-t')\dot{x}(t')dt' + \frac{dV(x)}{dx} = \xi(t). \tag{4.2}$$

Here, $\gamma(t)$ is the generalized friction kernel, accounting for the memory effects in the particle's velocity over time. In other words, this kernel captures the non-Markovian response of fluid particles. The generalized fluctuation-dissipation relation corresponding to the GLE is provided by [78, 210]

$$\langle \xi(t)\xi(t')\rangle = k_B T m\gamma(|t-t'|). \tag{4.3}$$

When $\gamma(t-t') = 2\gamma_f\delta(t-t')$, we recover the usual Langevin equation with a constant friction coefficient γ_f (here, the factor of 2 disappears upon integration in Eq. (4.2) because the upper limit of the integral coincides with the delta function argument). The corresponding noise correlation then simplifies to the usual form $\langle \xi(t)\xi(t')\rangle = 2k_B T m\gamma_f\delta(t-t')$. Throughout, we assume the external potential to be harmonic so that

$$V(x) = \frac{1}{2}m\omega^2 x^2. \tag{4.4}$$

In many experimental settings, the inertial contribution $m\ddot{x}(t)$ in the underdamped GLE Eq. (4.2) is negligible, which physically corresponds to a regime of strong damping. This so-called overdamped limit [227]—where friction dominates inertia—is frequently adopted for modeling the motion of driven colloids in aqueous polymer solutions (such as poly-ethylene oxide), which combines elasticity with substantial viscosity and thus forms a viscoelastic yet strongly damped medium [213, 214]. By the same reasoning, protein macromolecules in solution also experience very high friction, and so their movement is appropriately described as overdamped (see, e.g., Refs. [228, 229]). Moreover, the confined environment inside proteins is well approximated by a harmonic potential, making the overdamped GLE for a harmonic oscillator an accurate model for intramolecular dynamics [228, 229, 202].

Applying these approximations, we obtain the overdamped GLE:

$$m\int_0^t \gamma(t-t')\dot{x}(t')dt' + m\omega^2 x = \xi(t). \tag{4.5}$$

Our primary goal is to investigate the overdamped GLE dynamics under the influence of stochastic resetting. Nevertheless, before introducing resetting, it is useful to revisit the standard solution techniques for the GLE without resetting and derive the central statistical quantities of interest. This will lay the groundwork for our subsequent generalization to the case with resetting.

GLE in Laplace space: Correlation function and MSD

To proceed, we apply the Laplace transform to both sides of equation Eq. (4.5) and divide through by m, yielding

$$\widetilde{\gamma}(s)(s\widetilde{X}(s) - x_0) + \omega^2\widetilde{X}(s) = \frac{\widetilde{\Xi}(s)}{m}, \tag{4.6}$$

where we abbreviate the Laplace transforms as

$$\widetilde{X}(s) = \int_0^\infty dt\ e^{-st}x(t),\ \widetilde{\Xi}(s) = \int_0^\infty dt\ e^{-st}\xi(t),\ \widetilde{\gamma}(s) = \int_0^\infty dt\ e^{-st}\gamma(t), \tag{4.7}$$

and set $x_0 = x(t = 0)$ as the initial condition. Rearranging, the general solution reads

$$\widetilde{X}(s) = \left[\frac{1}{s} - \omega^2\widetilde{I}_0(s)\right] x_0 + \frac{1}{m}\widetilde{\Xi}(s)\widetilde{G}_0(s), \tag{4.8}$$

where the functions $G_0(t)$ and $I_0(t)$ are the so-called relaxation kernels, defined as

$$G_0(t) = \mathcal{L}^{-1}\left[\widetilde{G}_0(s)\right] = \mathcal{L}^{-1}\left[\frac{1}{s\widetilde{\gamma}(s) + \omega^2}\right], \tag{4.9}$$

$$I_0(t) = \mathcal{L}^{-1}\left[\widetilde{I}_0(s)\right] = \mathcal{L}^{-1}\left[\frac{s^{-1}}{s\widetilde{\gamma}(s) + \omega^2}\right]. \tag{4.10}$$

where $\mathcal{L}^{-1}[\widetilde{f}(s)]$ denotes the inverse Laplace transform of $\widetilde{f}(s)$. Equation Eq. (4.8) can be inverted to yield the following integral representation for $x(t)$:

$$x(t) = \langle x(t)\rangle + \frac{1}{m}\int_0^t dt'\ G_0(t - t')\xi(t'), \tag{4.11}$$

with the average trajectory given by

$$\langle x(t)\rangle = \left[1 - \omega^2 I_0(t)\right] x_0. \tag{4.12}$$

From Eq. (4.8), we see that the two-point correlation function in Laplace space can be expressed as

$$\langle\widetilde{X}(s)\widetilde{X}(s')\rangle = \langle\widetilde{X}(s)\rangle\langle\widetilde{X}(s')\rangle + \frac{1}{m^2}\widetilde{G}_0(s)\widetilde{G}_0(s')\langle\widetilde{\Xi}(s)\widetilde{\Xi}(s')\rangle, \tag{4.13}$$

where

$$\langle\widetilde{X}(s)\rangle = \left[\frac{1}{s} - \omega^2\widetilde{I}_0(s)\right] x_0, \tag{4.14}$$

which is just the Laplace-transformed mean $\langle x(t)\rangle$. The noise correlation term $\langle\widetilde{\Xi}(s)\widetilde{\Xi}(s')\rangle$ can be determined via a double Laplace transform of the fluctuation-dissipation relation

Eq. (4.3) (see [230]):

$$\langle\widetilde{\Xi}(s)\widetilde{\Xi}(s')\rangle = k_BTm\left(\frac{\widetilde{\gamma}(s)+\widetilde{\gamma}(s')}{s+s'}\right). \tag{4.15}$$

Using expressions for $\widetilde{\gamma}(s)$ in terms of the relaxation functions (Eq. (4.9)-Eq. (4.10)) and some algebraic manipulation, we finally find

$$\langle\widetilde{X}(s)\widetilde{X}(s')\rangle = \langle\widetilde{X}(s)\rangle\langle\widetilde{X}(s')\rangle + \frac{k_BT}{m}\left[\frac{\widetilde{I}_0(s)}{s'}+\frac{\widetilde{I}_0(s')}{s}-\frac{\widetilde{I}_0(s)+\widetilde{I}_0(s')}{s+s'}-\omega^2\widetilde{I}_0(s)\widetilde{I}_0(s')\right]. \tag{4.16}$$

Transforming to the time domain, the two-time correlation function $C(t,t') = \langle x(t)x(t')\rangle$ is given by

$$C(t,t') = \langle x(t)\rangle\langle x(t')\rangle + \frac{k_BT}{m}\left[I_0(t)+I_0(t')-I_0(|t-t'|)-\omega^2 I_0(t)I_0(t')\right]. \tag{4.17}$$

The mean squared displacement, $\sigma^2(t) = \langle x^2(t)\rangle - \langle x(t)\rangle^2$, can be extracted by setting $t = t'$ in the above, which yields

$$\sigma^2(t) = \frac{k_BT}{m}\left[2I_0(t)-\omega^2 I_0^2(t)\right]. \tag{4.18}$$

We have omitted the term $I_0(0)$ since, by the initial value theorem, $I_0(t=0) = \lim_{s\to\infty} s\tilde{I}_0(s) = 0$. For any specified friction kernel, these results can be employed to explicitly determine the GLE correlation function; we will discuss this in detail for the Jeffreys fluid further in the chapter. In the next section, we proceed to include stochastic resetting in the GLE and develop the theoretical framework to derive explicit results for the mean squared displacement and the correlation function.

4.3 GLE with stochastic resetting

In the context of resetting dynamics, the motion of a particle governed by a GLE is intermittently interrupted—at which point, the particle is instantly relocated to its initial position $x = x_0$. These resets occur randomly at time intervals determined by an exponential distribution $f_R(t) = re^{-rt}$ with an average interval of $1/r$. Between successive resets, the particle evolves according to the GLE specified in Eq. (4.5), always starting anew from the same position. We define $P(x,t)$ as the probability density for finding the particle at position x at time t, having started at x_0 at $t = 0$ in the absence of resetting. By employing renewal theory [231, 232, 63, 64], the propagator for the resetting

process, $P_r(x,t)$, can be written as

$$P_r(x,t) = e^{-rt}P(x,t) + r\int_0^t d\tau e^{-r\tau}P(x,\tau). \tag{4.19}$$

This formula admits a simple interpretation: the first term represents the scenarios where the particle experiences no resetting up to time t, an event with probability e^{-rt}, multiplied by the propagator in the absence of resetting, $P(x,t)$. The second term accounts for all paths in which at least one resetting event takes place. Specifically, if the most recent reset happened at time $t-\tau$, the probability for a reset to occur in the interval $[\tau, \tau+d\tau]$ is $rd\tau$, combined with the survival probability $e^{-r\tau}$ for no further reset following $t-\tau$. For the period after the most recent reset, the propagator reverts to $P(x,\tau)$.

A crucial point here is that the renewal formulation in Eq. (4.19) remains valid only when the complete state of the particle—including both its position and the memory of the friction kernel—is reset at each resetting event. Because the kernel $\gamma(t)$ is time-dependent, each resetting requires restarting $\gamma(t)$ from its initial value. This ensures that although the process between resets is non-Markovian (due to memory effects), the resetting events themselves are genuinely Markovian, so that the full renewal approach is appropriate. We further discuss this point in Section 4.5 when presenting the simulation methods. Next, we will derive explicit formulas for the mean squared displacement (MSD) and the correlation function in the presence of resetting.

4.3.1 MSD in presence of resetting

The MSD of the process with resetting can be defined as

$$\begin{aligned}\sigma_r^2(t) &= \langle x^2(t)\rangle_r - \langle x(t)\rangle_r^2 \\ &= \int_{-\infty}^{\infty} dx\, x^2 P_r(x,t) - \left(\int_{-\infty}^{\infty} dx\, x\, P_r(x,t)\right)^2,\end{aligned} \tag{4.20}$$

where $\langle x(t)\rangle_r$ and $\langle x^2(t)\rangle_r$ denote the first and second moments of the position in the presence of resetting, respectively. Using the result for $P_r(x,t)$ given by Eq. (4.19), a renewal equation for the MSD in the resetting protocol can be readily derived [21, 225]:

$$\sigma_r^2(t) = e^{-rt}\sigma^2(t) + r\int_0^t d\tau\, e^{-r\tau}\sigma^2(\tau), \tag{4.21}$$

where $\sigma^2(t) = \int_{-\infty}^{\infty} dx\, x^2 P(x,t) - \left(\int_{-\infty}^{\infty} dx\, x\, P(x,t)\right)^2$ is the MSD of the non-reset process, as previously derived in Eq. (4.18). Substituting the exact form of $\sigma^2(t)$ from Eq. (4.18) into Eq. (4.21), one arrives at the precise expression for the MSD under re-

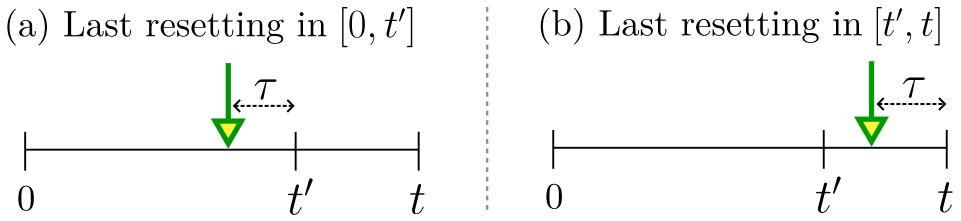

Figure 4.2: *A simple schematic illustrating the contribution to the correlation function from two different scenarios depending on the event of the last resetting (shown by the arrow). In (a) the last resetting happens in* $[0, t']$ *whereas in (b) the last resetting happens in* $[t', t]$.

setting,

$$\sigma_r^2(t) = \left(\frac{k_B T}{m}\right)\left(e^{-rt}\left[2I_0(t) - \omega^2 I_0^2(t)\right] + r\int_0^t d\tau e^{-r\tau}\left[2I_0(\tau) - \omega^2 I_0^2(\tau)\right]\right). \quad (4.22)$$

This formula is fully general and is valid for any choice of memory kernel. In the long-time limit, the system reaches a non-equilibrium steady state (NESS), and this is reflected in the asymptotic behavior of the MSD. Specifically, taking $t \to \infty$ in Eq. (4.22), the first term vanishes, yielding the steady-state value of the MSD as

$$\left(\sigma_r^2\right)_{ss} = \sigma_r^2(t \to \infty) = \left(\frac{k_B T r}{m}\right)\left[2\widetilde{I}_0(r) - \omega^2 \widetilde{I}_0^2(r)\right], \quad (4.23)$$

where $\widetilde{I}_0(r)$ is the Laplace transform of $I_0(t)$ and $\widetilde{I_0^2}(r)$ is the Laplace transform of $I_0^2(t)$, both evaluated at r. It is worth noting that the steady-state MSD, whether in Eq. (4.22) or Eq. (4.23), is entirely independent of the initial (resetting) position x_0. Thus, the results hold for a fixed initial/resetting position, or for an initial/resetting position drawn randomly from a given distribution, as long as these coincide. However, if the initial and resetting positions are independent draws from two different probability distributions, the renewal formula for $P_r(x, t)$ requires modification. Here, for simplicity, we concentrate on the case where the resetting coordinate is fixed. In addition to the MSD, one is also often interested in the autocorrelation function for the GLE under resetting; to obtain this, one needs to write a corresponding renewal equation for the two-point correlator, as discussed next.

4.3.2 Correlation function with resetting

Recently, the temporal autocorrelation function for stochastic resetting processes has been studied in the context of diffusion [233], fractional Brownian motion [234], and geometric Brownian motion [235]. Here, we follow a renewal formalism inspired by [235], and briefly summarize its derivation. For a process $x(t)$ subject to resetting, the auto-

correlation function is $C_r(t,t') = \langle x(t)x(t')\rangle_r$ (for $t > t'$), and it satisfies

$$\begin{aligned} C_r(t,t') =& e^{-rt}C(t,t') + r\int_0^{t'} d\tau e^{-r(t-t'+\tau)}C(\tau, t-t'+\tau) \\ &+ r\int_0^{t-t'} d\tau e^{-r\tau}\langle x(t')\rangle_r\langle x(\tau)\rangle, \end{aligned} \tag{4.24}$$

where $C(t,t')$ is the correlation function of the non-reset process.

The three terms on the right-hand side of Eq. (4.24) have distinct interpretations. The first term accounts for trajectories that do not experience any reset during $[0,t]$, with survival probability e^{-rt}, multiplied by the process correlation function. The second term sums over all cases where the most recent reset occurs at time $t'-\tau$, before t', so that after this event the system evolves afresh, with a probability $rd\tau$ for the reset and $e^{-r(t-t'+\tau)}$ for no further reset up to t. The correlation between t' and t is now simply $C(\tau, t-t'+\tau)$ after relabeling time with $t'-\tau$ as the new origin. The third term covers scenarios where the latest reset takes place within $[t',t]$ at $t-\tau$; in this case, the correlation reduces to the product of expectation values $\langle x(t')\rangle_r\langle x(\tau)\rangle$ due to the loss of memory across the reset. The factor $e^{-r\tau}$ enforces no further resets in $[t-\tau,t]$, and integrating over all possible τ completes the term. Setting $x_0 = 0$ (so that both $\langle x(\tau)\rangle$ and $\langle x(t)\rangle_r$ vanish), the last term drops out, leaving

$$C_r(t,t') = e^{-rt}C(t,t') + r\int_0^{t'} d\tau e^{-r(t-t'+\tau)}C(\tau, t-t'+\tau). \tag{4.25}$$

This compact renewal formula allows us to obtain the correlation function under resetting simply by substituting $C(t,t')$ from Eq. (4.17). Evaluating the MSD (Eq. (4.22)) and the correlation function (Eq. (4.25)) for explicit examples requires specifying the kernel $\gamma(t)$ and thus the required relaxation functions. As an illustration, we next consider the Jeffreys fluid model for viscoelastic environments.

4.4 Jeffreys fluid as a viscoelastic bath

The Jeffreys fluid has been widely utilized to model viscoelastic baths in experimental contexts [79, 80, 236, 213, 214, 216]. This model cohesively incorporates both viscous and elastic features of the bath: the purely viscous response enters as a delta-function term, while elasticity enters via an exponential memory kernel, making the model both analytically tractable and amenable to simulation.

Within the Jeffreys model, the friction kernel $\gamma(t)$ is given by [79, 80, 236, 213, 214, 216]

$$\gamma(t) = 2\gamma_f\delta(t) + \frac{\gamma_s}{\tau_s}\exp\left(-\frac{t}{\tau_s}\right). \tag{4.26}$$

Here, γ_f quantifies viscous damping, while γ_s and τ_s characterize the elastic timescale and strength, respectively. Physically, a larger τ_s signals a more sluggish relaxation of the fluid, and γ_s measures the degree to which elasticity modifies the particle's motion. When $\gamma_s = 0$, one recovers the standard Langevin result with diffusion constant $D = \frac{k_B T}{m\gamma_f}$.

Laplace transforming Eq. (4.26) yields $\widetilde{\gamma}(s) = \gamma_f + \frac{\gamma_s}{1+s\tau_s}$. Using this in Eq. (4.10), we obtain

$$\widetilde{I}_0(s) = \frac{s^{-1}}{s\left(\gamma_f + \frac{\gamma_s}{1+s\tau_s}\right) + \omega^2}, \tag{4.27}$$

which can be inverted to the time domain:

$$I_0(t) = \frac{1}{\omega^2}\left(1 - e^{-\alpha t/\tau_s}\cosh\left[\frac{t}{\tau_s}\sqrt{\alpha^2-\beta^2}\right] - \frac{\alpha-\beta^2}{\sqrt{\alpha^2-\beta^2}}e^{-\alpha t/\tau_s}\sinh\left[\frac{t}{\tau_s}\sqrt{\alpha^2-\beta^2}\right]\right), \tag{4.28}$$

where the dimensionless parameters are defined as

$$\alpha = \frac{\gamma_f + \gamma_s + \tau_s\omega^2}{2\gamma_f}, \quad \beta = \sqrt{\frac{\omega^2\tau_s}{\gamma_f}}. \tag{4.29}$$

By substituting this result into Eq. (4.22) and Eq. (4.25), we can compute the MSD and correlation function for the GLE with resetting in the Jeffreys fluid.

4.4.1 MSD

We now provide a detailed analysis of the dynamic regimes and crossover timescales that arise in the MSD for both the underlying process (without resetting) and in the resetting protocol. Let us first consider the reset-free case.

Underlying reset-free process

Plugging Eq. (4.28) into Eq. (4.18) gives the exact MSD for the underlying process:

$$\langle x^2(t)\rangle = \frac{k_B T}{m\omega^2}\left[1 - e^{-\frac{2\alpha t}{\tau_s}}\cosh^2\left(\sqrt{\alpha^2-\beta^2}t/\tau_s\right)\right.$$
$$\left.\times\left\{1 + \left(\frac{\alpha-\beta^2}{\sqrt{\xi}}\right)\tanh\left(\sqrt{\alpha^2-\beta^2}t/\tau_s\right)\right\}^2\right]. \tag{4.30}$$

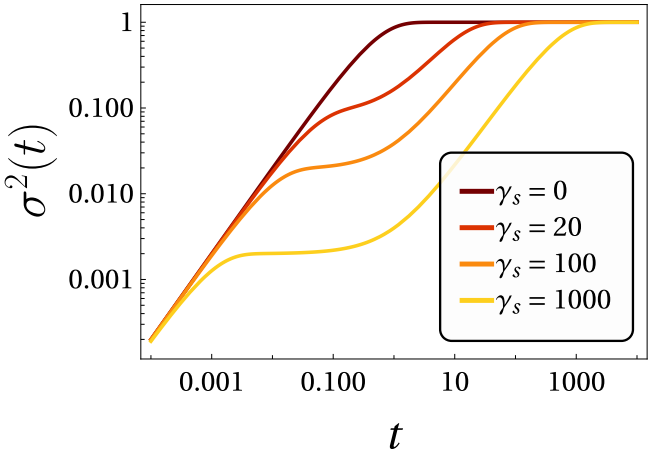

Figure 4.3: *MSD of the underlying reset-free process for the Jeffreys fluid model as a function of time for different values of γ_s. The circles represent results from the simulation. For $\gamma_s = 0$, the MSD is the same as that of an OU process. The plots indicate the existence of two distinct time scales for a non-zero value of γ_s with the emergence of a plateau. In Fig. 4.4, we discuss the origin of these characteristics and illustrate further. The parameters for this simulation are set at: $\gamma_f = 1, \omega = 1, \tau_s = 1$.*

In Fig. (4.3), we display the MSD versus time for different γ_s. Setting $\gamma_s = 0$ collapses the result to

$$\langle x^2(t)\rangle = \frac{k_B T}{m\omega^2}\left(1 - e^{-\frac{2t\omega^2}{\gamma_f}}\right), \tag{4.31}$$

which corresponds to the MSD of the Ornstein-Uhlenbeck process. At short times ($t \ll \gamma_f/\omega^2$), the MSD grows linearly as $\langle x^2(t)\rangle \sim \frac{2k_BTt}{m\gamma_f}$. At long times ($t \gg \gamma_f/\omega^2$), it saturates at the equilibrium value $\langle x^2(t)\rangle \sim \frac{k_BT}{m\omega^2}$.

Here, the influence of memory arises from the exponential term in the kernel (Eq. (4.26)), i.e., for $\gamma_s \neq 0$. As shown in Fig. (4.3), for the GLE with $\gamma_s \neq 0$, an intermediate plateau emerges in the MSD—a feature absent for the classical Langevin case ($\gamma_s = 0$). The MSD displays linear growth at early times, reaches a plateau, then resumes growth before finally saturating. Our task is to determine the characteristic timescales for transitions between these regimes and to analyze the precise asymptotic behavior of the MSD. For simplicity, we will set $k_BT/m = 1$ to focus purely on dynamical features.

Setting $\omega = 0$ further simplifies the discussion since the confining potential becomes relevant only at very long times. For time durations short enough such that the particle does not sense the trap, the cases $\omega = 0$ and $\omega \neq 0$ yield nearly identical MSDs (see Fig. (4.4)).

Case without a confining potential ($\omega = 0$):

In the limit $\omega \to 0$, or $\beta \to 0$, the expression for α becomes

$$\alpha_0 = \alpha(\omega \to 0) = \frac{\gamma_f + \gamma_s}{2\gamma_f}. \tag{4.32}$$

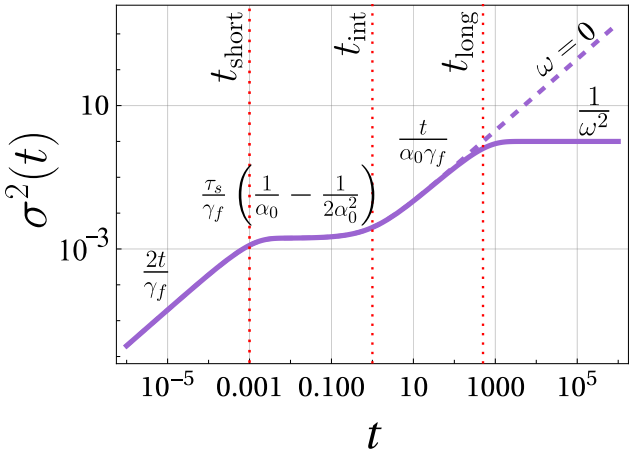

Figure 4.4: *Variation of the MSD of the underlying process (the solid line) as a function of time and emergence of the plateaus for parameters fixed at* $\gamma_s = 1000, \gamma_f = 1, \omega = 1, \tau_s = 1$. *This is the bottom-most curve for the MSD as borrowed from Fig. 4.3. The vertical dotted lines represents three three different timescales as in Eq. (4.34), Eq. (4.38) and Eq. (4.42). The asymptotic behaviour of the MSD at different timescales is also shown above the curve in each region. The dashed line shows the MSD with* $\omega = 0$ *as in Eq. (4.33).*

Substituting this into the MSD, we obtain a more tractable result:

$$\langle x^2(t)\rangle_{w\to 0} = \frac{\tau_s}{\gamma_f}\left(\frac{1}{\alpha_0} - \frac{1}{2\alpha_0^2}\right) + \frac{t}{\alpha_0\gamma_f} - e^{-2t\alpha_0/\tau_s}\frac{\tau_s}{\gamma_f}\left(\frac{1}{\alpha_0} - \frac{1}{2\alpha_0^2}\right). \tag{4.33}$$

This formula reveals two distinct time scales. At early times, $t \ll \frac{\tau_s}{2\alpha_0}$, expanding the exponential indicates that the shortest timescale is

$$t_{\text{short}} = \frac{\tau_s}{2\alpha_0}. \tag{4.34}$$

For this regime,

$$\langle x^2(t)\rangle_{w\to 0} \approx \frac{2t}{\gamma_f}, \quad \text{when } t \ll t_{\text{short}}. \tag{4.35}$$

The memory effect is negligible, and the MSD grows diffusively, $D = \frac{1}{\gamma_f}$, as seen in Fig. (4.3). At longer times $t \gg t_{\text{short}}$, the exponential decays to zero, and we find

$$\langle x^2(t)\rangle_{w\to 0} \approx \frac{\tau_s}{\gamma_f}\left(\frac{1}{\alpha_0} - \frac{1}{2\alpha_0^2}\right) + \frac{t}{\alpha_0\gamma_f}, \text{ when } t \gg t_{\text{short}}. \tag{4.36}$$

This regime also reveals an *intermediate* timescale t_{int} between these behaviors. By rearranging, we write

$$\begin{aligned}\langle x^2(t)\rangle_{w\to 0} &\approx \frac{\tau_s}{\gamma_f}\left(\frac{1}{\alpha_0}-\frac{1}{2\alpha_0^2}\right)\left[1+\frac{t}{\tau_s\left(1-\frac{1}{2\alpha_0}\right)}\right]\\ &\approx \frac{\tau_s}{\gamma_f}\left(\frac{1}{\alpha_0}-\frac{1}{2\alpha_0^2}\right)\left[1+\frac{t}{t_{\text{int}}}\right],\end{aligned} \tag{4.37}$$

with t_{int} given by

$$t_{\text{int}} = \tau_s\left(1-\frac{1}{2\alpha_0}\right). \tag{4.38}$$

In the plateau regime $t_{\text{short}} \ll t \ll t_{\text{int}}$, the MSD becomes

$$\langle x^2(t)\rangle_{w\to 0} \approx \frac{\tau_s}{\gamma_f}\left(\frac{1}{\alpha_0}-\frac{1}{2\alpha_0^2}\right), \text{ when } t_{\text{short}} \ll t \ll t_{\text{int}}. \tag{4.39}$$

This gives an analytic result for the first plateau (see Fig. (4.3)). When $t \gg t_{\text{int}}$, time dependence dominates again:

$$\langle x^2(t)\rangle_{w\to 0} \approx \frac{t}{\alpha_0\gamma_f}, \text{ when } t \gg t_{\text{int}}. \tag{4.40}$$

The MSD thus resumes linear growth beyond the intermediate regime, as observed in Fig. (4.3). In the next subsection, we move on to analyze the trapped case ($\omega \neq 0$).

The case with potential ($\omega \neq 0$):

To identify the longest characteristic timescale, t_{long}, consider that the mean squared displacement (MSD) saturates at late times ($t \gg t_{\text{long}}$) to the equilibrium steady-state value $1/\omega^2$. This can be checked explicitly by taking the $t \to \infty$ limit of the MSD in Eq. (4.30). Furthermore, corrections to this saturation can be estimated in the same limit, yielding the following approximation:

$$\langle x^2(t\to\infty)\rangle \approx \frac{1}{\omega^2} - Ae^{-\frac{2t\left(\alpha-\sqrt{\alpha^2-\beta^2}\right)}{\tau_s}}, \tag{4.41}$$

where A is a constant prefactor determined by α, β, τ_s, and ω. This result immediately reveals the longest relaxation timescale,

$$t_{\text{long}} = \frac{\tau_s}{2\left(\alpha-\sqrt{\alpha^2-\beta^2}\right)}. \tag{4.42}$$

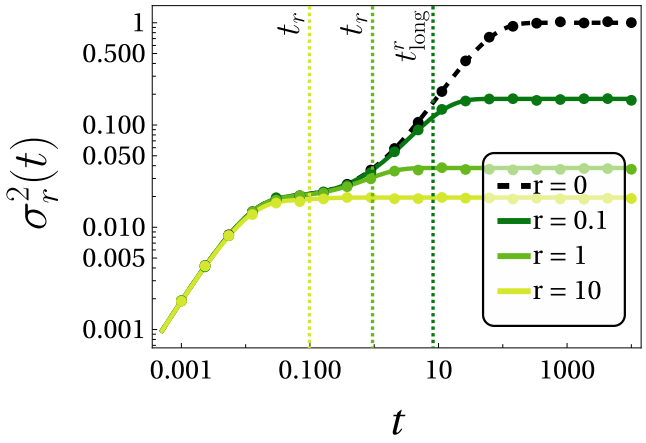

Figure 4.5: *Variation of MSD with time for the resetting system for different values of resetting rate r. The parameters are fixed at: $\gamma_f = 1, \gamma_s = 100, \tau_s = 1, \omega = 1$. The circles represent results from the simulation. The dashed curve represents the result for the underlying reset-free process, i.e., $r = 0$. The solid circles represent the results from numerical simulation. The rightmost vertical dashed line represents the longest timescale of the system under resetting while the other two vertical dashed lines are associated with the timescales t_r for different values of r (color-codes represent the values of r respectively). At sufficiently short times $t \ll t_r, t_{long}^r$, the curves follow the MSD of the underlying reset-free process.*

For $t \gg t_{\text{long}}$, the MSD approaches its steady-state value. Collecting all earlier results, the MSD exhibits the following behavior across different regimes ($k_BT/m = 1$ throughout):

$$\langle x^2(t)\rangle \approx \begin{cases} \frac{2t}{\gamma_f} & \text{when } t \ll t_{\text{short}} \\ \frac{\tau_s}{\gamma_f}\left(\frac{1}{\alpha_0} - \frac{1}{2\alpha_0^2}\right) & \text{when } t_{\text{short}} \ll t \ll t_{\text{int}} \\ \frac{t}{\alpha_0\gamma_f} & \text{when } t_{\text{int}} \ll t \ll t_{\text{long}} \\ \frac{1}{\omega^2} & \text{when } t \gg t_{\text{long}} \end{cases} \tag{4.43}$$

To highlight these different timescales, the lowest curve from Fig. (4.3) is replotted in Fig. (4.4), with parameters $\gamma_s = 1000$, $\gamma_f = 1$, $\omega = 1$, and $\tau_s = 1$; this results in $\alpha = 501$, $\alpha_0 = 500.5$, $\beta = 1$. In Fig. (4.4) we mark the various regime boundaries and show the MSD's asymptotic forms. It is worth noting that the dashed curve for $\omega = 0$ matches exactly with the $\omega \neq 0$ result at $t \ll t_{\text{long}}$, affirming the earlier discussion.

Resetting induced process

Let us now focus on the behavior of the MSD when stochastic resetting is introduced into the dynamics. By substituting Eq. (4.28) into Eq. (4.22), one can obtain the explicit expression for the MSD in the presence of resetting. Due to its length and complexity, the full form is presented in the appendix (see Eq. (D.11)). The evolution of the MSD as a function of time is displayed in Fig. (4.5). The dashed curve indicates the underlying, reset-free behavior. It is prudent to recognize that the introduction of resetting adds a

new timescale

$$t_r = 1/r, \tag{4.44}$$

which represents the mean interval between successive resetting events. This additional timescale is set externally and is not intrinsic to the system itself. As observed from Fig. (4.5), the influence of resetting emerges only at the longest timescales. An asymptotic expansion for the MSD at long times $t \to \infty$, as obtained from Eq. (D.11), yields

$$\langle x^2(t \to \infty)\rangle_r \approx \langle x^2\rangle_r^{ss} - Be^{-\frac{t\left(2\alpha-2\sqrt{\alpha^2-\beta^2}+r\tau_s\right)}{\tau_s}}, \tag{4.45}$$

where the steady-state value under resetting is given by

$$\langle x^2\rangle_r^{ss} = \frac{2\beta^2\left[4\alpha\left(r\tau_s+1\right)+r\tau_s\left(1+r\tau_s-\beta^2\right)\right]}{\omega^2\left(2\alpha+r\tau_s\right)\left[4\beta^2+r\tau_s\left(4\alpha+r\tau_s\right)\right]}, \tag{4.46}$$

with B a time-independent constant. In the limit $r \to 0$, one recovers $\langle x^2\rangle_{r\to 0}^{ss} = 1/\omega^2$, which is consistent with the stationary value in absence of resetting. Importantly, the steady-state obtained under resetting is genuinely non-equilibrium, as the continual injection of particles to the resetting location maintains a nonzero probability current at stationarity. From Eq. (4.45), the modified longest timescale of relaxation under resetting t_{long}^r can be read off as

$$t_{\text{long}}^r = \frac{\tau_s}{2\left(\alpha-\sqrt{\alpha^2-\beta^2}\right)+r\tau_s}. \tag{4.47}$$

If the resetting rate is sufficiently low, such that $1/r \gg t_{\text{long}}$ or $t_r \gg t_{\text{long}}$, then $t_{\text{long}}^r \approx t_{\text{long}}$. Thus, the approach to steady state is dictated by the intrinsic dynamics, with resetting playing a negligible role in the timescale. Yet, even so, the steady-state value of the MSD is distinct for the two cases.

Conversely, for finite values of r, $t_{\text{long}}^r < t_{\text{long}}$, so the relaxation to steady state in the presence of resetting is speeded up. At early times $t \ll t_{\text{long}}^r$, the particle does not experience the impact of resetting and the MSD tracks that of the underlying process (Fig. (4.5)). For high resetting rates where r is large, t_{long}^r becomes $t_r = 1/r$, so the steady state is effectively reached after $t \gg t_r$, as demonstrated in Fig. (4.5). For such rapid resetting (r large), the preexisting timescales (e.g., t_{int} or t_{short}) may not manifest, as the system is dominated by resetting. For instance, in the $r = 10$ curve of Fig. (4.5), $t_r = 0.1$ is shorter than the intermediate timescale $t_{\text{int}} = 1$, so the plateau is suppressed and steady state is reached much sooner. In the limit $r \to \infty$, the steady-state MSD

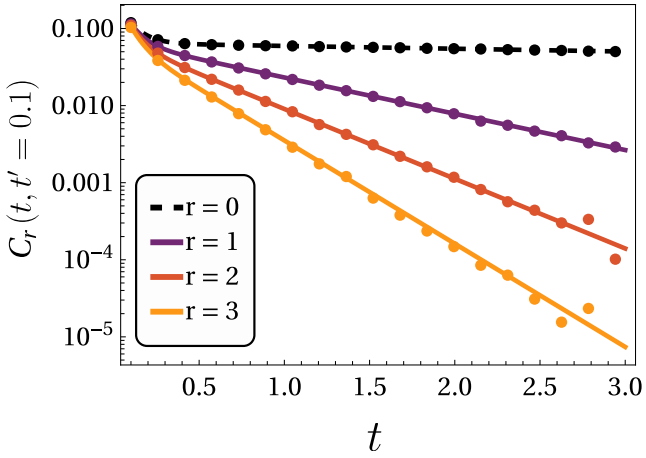

Figure 4.6: *Variation of the correlation function with time under resetting for Jeffreys fluid model. The parameters chosen are:* $\gamma_f = 1, \gamma_s = 10, \omega = 1, \tau_s = 1$. *As before, the dashed line represents the reset-free process (*$r = 0$*) and the solid circles represent data points from numerical simulation. Note that the correlation decays exponentially with time as given by Eq. (4.50).*

converges to

$$\langle x^2 \rangle_{r\to\infty} = \frac{2}{\gamma_f r}, \tag{4.48}$$

matching the known result for free Brownian motion with resetting, associated with diffusion constant $D = 1/\gamma_f$ [52].

4.4.2 Correlation function

Next, let us analyze the behavior of the correlation function $C(t, t')$ in the Jeffreys fluid scenario. Plugging Eq. (4.28) into Eq. (4.17) gives the non-reset correlation function. At long times $t \gg t'$,

$$C(t, t';\ t \gg t') \sim e^{-\frac{\left(\alpha-\sqrt{\alpha^2-\beta^2}\right)t}{\tau_s}}, \tag{4.49}$$

where, as earlier, $\alpha = \frac{\gamma_f+\gamma_s+\tau_s\omega^2}{2\gamma_f}$ and $\beta = \sqrt{\frac{\omega^2\tau_s}{\gamma_f}}$. The presence of the trap ensures exponential decay; for $\omega \to 0$, the correlation approaches a nonzero limiting value, signaling the absence of a stationary state (see also Fig. (4.4) where MSD is linear). With resetting, one uses Eq. (4.17) and Eq. (4.25) (and $I_0(t)$ from Eq. (4.28)) to evaluate the explicit correlation function, whose closed form appears in the appendix. As displayed in Fig. (4.6), the autocorrelation under resetting exhibits accelerated decay, described in the asymptotic regime by

$$C_r(t, t';\ t \gg t') \sim e^{-rt-\frac{\left(\alpha-\sqrt{\alpha^2-\beta^2}\right)t}{\tau_s}}. \tag{4.50}$$

Importantly, even when $\omega \to 0$, under resetting the correlation ultimately vanishes due to the ongoing returns, reflecting the establishment of a steady state—even for otherwise unconfined motion. This highlights the essential role of resetting in stabilizing systems where the potential is absent.

4.5 Simulation scheme for GLE with resetting

We have so far concentrated on exact analytical formulas for the MSD and correlation functions. In this section, we outline numerical methods for simulating GLE systems. Unlike the standard Langevin equation (Eq. (4.1)), solving the GLE (Eq. (4.2)) can be quite challenging—various numerical strategies have been proposed in the literature [237, 238, 239, 240]. Our approach employs the Markovian embedding technique, which is particularly effective for simulating non-Markovian systems like the GLE for colloids in viscoelastic fluids [240, 241, 242, 213].

To clarify the discussion, consider the overdamped GLE for Jeffreys fluid, as in Eq. (4.26):

$$\gamma_f \dot{x}(t) + \frac{\gamma_s}{\tau_s} \int_0^t \exp\left(-\frac{t-t'}{\tau_s}\right) \dot{x}(t')dt' + \omega^2 x(t) = \xi(t), \tag{4.51}$$

where we take $m = 1$. Directly integrating this evolution is challenging for two main reasons:

- The integral term requires knowledge of all past velocities, which is computationally intensive to store and repeatedly convolve at each time step.
- Generating the correlated noise $\xi(t)$ as required by Eq. (4.3) entails keeping track of the full noise history, unlike the Markovian case where each increment is independent. For time steps of size $\Delta t = 10^{-4}$ and trajectory durations of order $t = 10^4$, a single path involves 10^8 data points, and many independent runs are needed for statistical accuracy—making storage and computation expensive.

To address both obstacles, we employ the Markovian embedding procedure:

Markovian embedding

To eliminate the need for full memory storage, we introduce an auxiliary variable:

$$W(t) = \frac{\gamma_s}{\tau_s} \int_0^t \exp\left(-\frac{t-t'}{\tau_s}\right) \dot{x}(t')dt'. \tag{4.52}$$

Taking the time derivative gives

$$\dot{W}(t) = -\frac{1}{\tau_s} W(t) + \frac{\gamma_s}{\tau_s} \dot{x}(t). \tag{4.53}$$

Consequently, the original non-Markovian dynamics (Eq. (4.51)) become a coupled pair of first-order Markovian equations:

$$\begin{aligned}\dot{x} &= -\frac{1}{\gamma_f}W(t) - \frac{\omega^2}{\gamma_f}x(t) + \frac{1}{\gamma_f}\xi(t),\\ \dot{W}(t) &= -\frac{1}{\tau_s}\left(1+\frac{\gamma_s}{\gamma_f}\right)W(t) - \frac{\omega^2}{\tau_s}\frac{\gamma_s}{\gamma_f}x(t) + \frac{1}{\tau_s}\frac{\gamma_s}{\gamma_f}\xi(t).\end{aligned} \tag{4.54}$$

Addressing the second challenge—the correlated noise—I model $\xi(t)$ as the sum of two independent processes: an Ornstein-Uhlenbeck (OU) process $\eta(t)$ and a standard white noise $\zeta_0(t)$. Define $\eta(t)$ via

$$\dot{\eta}(t) = -\frac{1}{\tau_s}\eta(t) + \frac{1}{\tau_s}\zeta(t), \tag{4.55}$$

where $\zeta(t)$ is white noise with $\langle\zeta(t)\zeta(t')\rangle = 2\gamma_s k_B T\delta(t-t')$. The autocorrelation function of $\eta(t)$ is then

$$\langle\eta(t)\eta(t')\rangle = k_B T\frac{\gamma_s}{\tau_s}\exp\left(-\frac{|t-t'|}{\tau_s}\right). \tag{4.56}$$

Therefore, the full noise is

$$\xi(t) = \zeta_0(t) + \eta(t), \tag{4.57}$$

with $\zeta_0(t)$ having correlation $\langle\zeta_0(t)\zeta_0(t')\rangle = 2\gamma_f k_B T\delta(t-t')$.

All together, the evolution can now be written as a set of Markovian stochastic differential equations:

$$\begin{aligned}\dot{x}(t) &= -\frac{1}{\tau_s}W(t) - \frac{\omega^2}{\gamma_f}x(t) + \frac{1}{\gamma_f}\zeta_0(t) + \frac{1}{\gamma_f}\eta(t),\\ \dot{W}(t) &= -\frac{1}{\tau_s}\left(1+\frac{\gamma_s}{\gamma_f}\right)W(t) - \frac{\omega^2}{\tau_s}\frac{\gamma_s}{\gamma_f}x(t) + \frac{1}{\tau_s}\frac{\gamma_s}{\gamma_f}\zeta_0(t) + \frac{1}{\tau_s}\frac{\gamma_s}{\gamma_f}\eta(t),\\ \dot{\eta}(t) &= -\frac{1}{\tau_s}\eta(t) + \frac{1}{\tau_s}\zeta(t),\end{aligned} \tag{4.58}$$

along with noise statistics

$$\langle\zeta(t)\zeta(t')\rangle = 2\gamma_s k_B T\delta(t-t'), \tag{4.59}$$

$$\langle\zeta_0(t)\zeta_0(t')\rangle = 2\gamma_f k_B T\delta(t-t'). \tag{4.60}$$

For simulation, we use the initial condition $\overrightarrow{X}(0) = (x(0), W(0), \eta(0)) = (0, 0, \eta_0)$, where η_0 is sampled from a zero-mean normal distribution with variance $\sqrt{\gamma/\tau_s}$.

Stochastic resetting

In our framework, resetting events require not only resetting the particle's position, but also restoring the friction kernel of the viscoelastic medium to its initial state. Accordingly, for each resetting, we return all system variables—namely, the position and auxiliary variables—to their starting configuration, i.e., $\overrightarrow{X}(t) = (x(t), W(t), \eta(t)) = \overrightarrow{X}(0) \equiv (0, 0, \eta_0)$ at the times of reset. Since resets happen randomly, with intervals governed by an exponential distribution of rate r, the update rule for the system at each timestep Δt is:

$$\overrightarrow{X}(t + \Delta t) = \begin{cases} \overrightarrow{X}(0), & \text{with probability } r\Delta t, \\ \text{solutions of Eq. (4.58)}, & \text{with probability } (1 - r\Delta t), \end{cases} \tag{4.61}$$

where "with probability" is abbreviated as w.p. In our simulations, we used $\Delta t = 10^{-4}$ and averaged observables over approximately 10^4 trajectories for the MSD and about 10^6 trajectories for the correlation function, respectively.

4.6 Discussion and outlook

In recent years, stochastic resetting has become a topic of great interest in statistical physics, the study of stochastic processes, and various interdisciplinary fields such as chemistry and biology. There have been significant advances both in theoretical developments [52, 8, 243, 244] and experimental investigations [14, 15, 16]; for comprehensive reviews, see [63, 64, 129, 245]. Meanwhile, generalized Langevin equations with a variety of memory kernels have proven useful for understanding the motion of biomolecules in crowded environments and colloids in elastic media [205, 206, 204].

Here, we present a first effort to bridge these two fields, aiming to elucidate the statistical properties of the GLE subject to stochastic resetting and to stimulate advances analogous to those in diffusion under resetting protocols.

To begin, we generalized the renewal formalism to encompass Langevin systems with memory. Leveraging this approach, we derived exact, closed-form results for the MSD and the correlation function of a resetting particle within a viscoelastic medium, for arbitrary friction kernels. These general findings are exemplified using the Jeffreys fluid model. Without resetting, the Jeffreys model displays an intermediate time regime in which the MSD exhibits a plateau, reflecting the slow relaxation timescale inherent to the viscoelastic environment. Our work demonstrates that stochastic resetting truncates this plateau and, for large resetting rates, restores the dynamics to those characteristic of normal diffusion. We further showed that the correlation function decays more rapidly under resetting. All analytical results for the GLE with resetting were validated against detailed simulations using the Markovian embedding strategy.

We believe that our study will open up multiple exciting research opportunities. A

natural extension involves exploring other forms of friction kernels—such as those governed by power laws (common in models of anomalous diffusion [229, 246, 247, 248])—to investigate how resetting modifies steady-state and dynamic properties. There has also been noteworthy progress in considering non-Markovian resetting mechanisms [13, 53, 12], as well as more experimentally motivated space-time coupled resetting schemes [249, 250, 251, 86, 252]; analyzing such variants for the GLE would constitute an important direction. Finally, recent optical trapping and viscoelastic colloid experiments [214, 213, 216, 217] provide promising avenues for experimental verification of our predictions for resetting effects in complex environments.

5

Towards experimental realization of stochastic resetting

(The content of this chapter has been published in [251, 253])

5.1 Introduction

A key assumption of the resetting model discussed till now is that the resetting is an instantaneous event so that the particle comes back to the starting position in *zero time*. This is, however, a major hindrance to practical realisation or experimental verification in the field since 'resetting' should be considered as a finite time process. Moreover, resetting a particle from far should require more time than to reset it from a nearby location. These presumptions seek for a more realistic viewpoint where resetting should be considered as a spatio-temporally coupled process and not just a mere teleportation.

An important step to this direction was taken recently by considering the fact that there is a finite time return process that brings the searcher/particle back to a preferred location/home upon resetting [86, 14]. It was, however, assumed that the return process is deterministic with absolute precision and moreover, the searcher is blind and thus can not locate a target during the return (see also [87, 254, 249, 88, 255, 256, 89, 257, 232, 12, 258]). In realistic search processes as well as in experiments, the return motion or the driving protocols are never completely deterministic or perfect and will always be accompanied by uncontrollable random fluctuations [259, 252, 260, 258]. Importantly, precise return controls with regard to the energetics may be costly as the thermodynamic trade-off relations have taught us [261, 262, 263, 264]. It is therefore important to understand how the errors or fluctuations in return process can be incorporated and secondly, their ramifications to the overall search. The content of this chapter will be devoted to the purpose of deriving an unified first passage theory under resetting where the searcher returns to its starting position following any generic stochastic/deterministic dynamics. In particular, we shall illustrate important ramification to the first-passage statistics of the process especially when the return is governed by some stochastic dynamics. Fur-

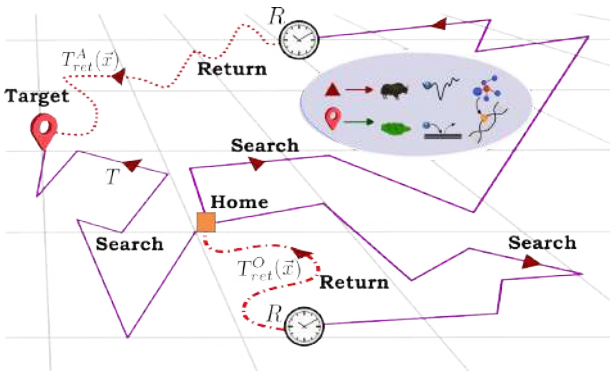

Figure 5.1: *Schematic diagram of an agent (could be a foraging animal, colloid or a bio-molecule) searching for targets (could be resources, sticky surface or a defected site along DNA). The agent can find the target during the search phase (violet solid trajectory). Otherwise, after a random resetting time R the agent, currently located at $\vec{x}$, switches to a return phase (facilitated e.g., by a chemical or potential gradient or simply, by choice) when it either returns to its home or relocates to a new location in finite time $T^O_{ret}(\vec{x})$ (red dot-dashed trajectory). The agent also has a finite probability to find the target during its return phase (red dotted trajectory) in time $T^A_{ret}(\vec{x})$. Target detection marks the completion of the global search regardless of its phase. We ask: Whether search with a finite-time home return can perform better than the instantaneous return process?*

thermore we shall also strengthen the results based on data used in tabletop experiments on resetting.

5.2 General framework

Consider a prototypical random search process where a searcher starts at the origin O, its home, of a d-dimensional arena at time zero (Fig. (5.1)). The arena may contain one or multiple targets. The searcher can locate one of these targets following a random T which we denote as the first passage time. However, during the search phase, if the target is not found up to a random time R (which we denote as the resetting time), the searcher decides to return to its home. Crucially, the return process can be stochastic and it is assumed moreover that the searcher has the ability to detect the target(s) even during the return phase. If the searcher returns to O, failing to detect the target, the search process restarts afresh to the next attempt. Overall, the process is said to be completed once the target is detected irrespective of the searcher's phase (see Fig. (5.1)).

The time it takes for the searcher to either find the target or the origin (home) during return will typically depend on the searcher's position $\vec{x}$ at the time of resetting R. Furthermore, various demographical or physical constraints may compel the searcher to follow different routes hence there can be more nontrivial dependence between the position of the searcher and the stochastic return time either to the origin (denoted by $T^O_{ret}(\vec{x})$) or to any of the targets A (denoted by $T^A_{ret}(\vec{x})$). In the former case, the searcher resumes its search phase upon returning to the origin while in the latter case the process ends. Denoting the overall completion time by a random variable T_R and considering

the above-mentioned possibilities, we can write a renewal equation as follows

$$T_R = \begin{cases} T & \text{if } T < R \\ R + T^A_{ret}(\vec{x}) & \text{if } R \leq T \ \& \ T^A_{ret}(\vec{x}) < T^O_{ret}(\vec{x}) \\ R + T^O_{ret}(\vec{x}) + T'_R & \text{if } R \leq T \ \& \ T^O_{ret}(\vec{x}) \leq T^A_{ret}(\vec{x}) \end{cases} \tag{5.1}$$

where we have assumed that return will be prioritized if $R = T$ (although the probability of $R = T$ for the continuous problem as considered in the following is exactly zero, we include it for completeness and also its potential importance in the discrete problem where the formalism equally holds valid). Here, T'_R is a statistically independent and identically distributed copy of T_R. Eq. (5.1) can be written in a more concise form as

$$\begin{aligned} T_R = & \, min(T, R) + I(R \leq T) min(T^A_{ret}(\vec{x}), T^O_{ret}(\vec{x})) \\ & + I(R \leq T) I(T^O_{ret}(\vec{x}) \leq T^A_{ret}(\vec{x})) T'_R, \end{aligned} \tag{5.2}$$

where $min(u, v)$ is the minimum of two random variables u & v and $I(u \leq v)$ is an indicator function that takes value unity when $u \leq v$, and zero otherwise. Thus, $\langle I(u \leq v) \rangle = Pr(u \leq v)$ i.e, the probability that $u \leq v$. Crucially, the indicator function $I(T^O_{ret}(\vec{x}) \leq T^A_{ret}(\vec{x}))$ also depends on the coordinate $\vec{x}$ of the searcher at the time of resetting. This implies that the expectations on Eq. (5.2) need to be performed over the underlying stochastic process, the resetting time density $f_R(t)$ and the return protocols. For instance, the expectation $\mathcal{E} \equiv \langle I(R \leq T) I(T^O_{ret}(\vec{x}) \leq T^A_{ret}(\vec{x})) T'_R \rangle$ can be computed as follows

$$\begin{aligned} \mathcal{E} &= \int_0^\infty dt f_R(t) \frac{Pr(T \geq t) \int_{\mathcal{D}} d\vec{x} G(\vec{x}, t) \langle I(T^O_{ret}(\vec{x}) \leq T^A_{ret}(\vec{x})) \rangle_{\text{traj}}}{Q(t)} \langle T'_R \rangle \\ &= \langle T_R \rangle \int_0^\infty dt f_R(t) \int_{\mathcal{D}} d\vec{x} G(\vec{x}, t) Pr(T^O_{ret}(\vec{x}) \leq T^A_{ret}(\vec{x})), \end{aligned} \tag{5.3}$$

where $\mathcal{D}$ is the domain of search in arbitrary dimension that can contain one or multiple targets and $G(\vec{x}, t)$ is the underlying time-dependent propagator in the presence of targets so that $Q(t) = Pr(T \geq t) = \int_{\mathcal{D}} d\vec{x} \ G(\vec{x}, t)$ becomes the survival probability [35]. Note that the notation $\langle ... \rangle$ denotes expectation over both the random resetting times and the random trajectories of the searcher. However, by $\langle ... \rangle_{\text{traj}}$ we denote the expectation only over the random trajectory of the searcher. In the first line of Eq. (5.3), we have taken averages over $f_R(t)$ and the underlying search propagator. Computing similar expectations from Eq. (5.2), we obtain the mean first passage time (MFPT) to be

$$\langle T_R \rangle = \frac{\langle min(T, R) \rangle + \langle min \left(T^A_{ret}, T^O_{ret} \right) \rangle}{1 - \int_{\mathcal{D}} d\vec{x} \ \widetilde{G}_R(\vec{x}) Pr(T^O_{ret}(\vec{x}) \leq T^A_{ret}(\vec{x}))}, \tag{5.4}$$

where

$$\widetilde{G}_R(\vec{x}) \equiv \int_0^\infty G(\vec{x},t) f_R(t) dt, \tag{5.5}$$

$$\langle min\left(T^A_{ret}, T^O_{ret}\right)\rangle = \int_{\mathcal{D}} d\vec{x} \widetilde{G}_R(\vec{x}) \langle min\left(T^A_{ret}(\vec{x}), T^O_{ret}(\vec{x})\right)\rangle_{\text{traj}}. \tag{5.6}$$

On the other hand, $Pr(T^O_{ret}(\vec{x}) \leq T^A_{ret}(\vec{x}))$ is the splitting probability that the searcher, starting from $\vec{x}$, reaches the origin before hitting any of the targets during the return phase.

Eq. (5.4) is central to this study and is remarkably general since it holds for a) any kind of underlying first passage process (beyond diffusion) conducted in any dimension in the presence of arbitrary target(s) regardless of their variation in size, shape or nature (purely absorbing or partial), b) arbitrary resetting time distributions, and c) generic returning motion such as instantaneous, deterministic or stochastic and their various modes of return.

5.3 A universal criterion for the trade-off between instantaneous and stochastic return

Various optimization questions could be asked given the generality of the formalism. Specifically, we ask whether stochastic returns can over-perform the search compared to the instantaneous returns irrespective of the underlying process. Our analysis shows that stochastic return will be beneficial only if

$$\langle T_R \rangle < \langle T_R^{inst} \rangle, \tag{5.7}$$

where

$$\langle T_R^{inst} \rangle = \frac{\langle min(T,R)\rangle}{Pr(T<R)} \tag{5.8}$$

is the MFPT for the instantaneous return [53] and can be obtained by noting that the searcher always returns to the origin in zero time so that $Pr(T^O_{ret} \leq T^A_{ret}) = 1$. Evidently, the condition in Eq. (5.7) yields

$$\mathcal{T} \equiv \frac{\langle min\left(T^A_{ret}, T^O_{ret}\right)\rangle}{Pr(T^A_{ret} < T^O_{ret})} < \langle T_R^{inst} \rangle, \tag{5.9}$$

where $Pr(T^A_{ret} < T^O_{ret}) = \int_{\mathcal{D}} d\vec{x}\ \widetilde{G}_R(\vec{x}) Pr(T^A_{ret}(\vec{x}) < T^O_{ret}(\vec{x}))$. The quantity $\mathcal{T}$ can be understood as the scaled time (with the splitting probability $Pr(T^A_{ret} < T^O_{ret})$) it takes, on an average, for the process to either return to the origin or to complete the search, starting from the location at the time of resetting. Clearly, to understand this trade-

off, one needs to consider many realizations of such a process and compare between the time $\mathcal{T}$ and the time $\langle T_R^{inst} \rangle$ that it would have taken for the instantaneous return. This is rather intriguing since the former accumulates time only during the post-resetting return phase, while the latter does so only during the pre-resetting phase. Thus, the relation (5.9) puts a strong constraint on the average return time $\mathcal{T}$ regardless of the final destination. Notably, this relation is quite universal for it does not depend on the particular choice of the underlying first passage process, resetting time density or the return protocol. Furthermore, the relation can be used as a guiding principle to design search-efficient protocols as will be shown below.

5.4 Diffusive search with resetting and stochastic return via controlled potential trap.

To demonstrate the power of our approach, we examine the paradigm of a 1d diffusive search process (characterised by the diffusion constant D) in which a particle starts at the origin O and continues to diffuse until it hits a stationary target at a location L. In addition, assume that the process is reset at a constant rate r (i.e., resetting time density $f_R(t) = re^{-rt}$) upon which a potential $U(x)$ centered at the origin is turned on. The particle diffuses through the potential and it is switched off when the particle makes a first return to the origin. Subsequently, the particle resumes its diffusive search phase (see [259, 252] where non-equilibrium steady state and the relaxation properties were studied under this protocol). However, since the return is not purely deterministic, there is always a chance to find the target during the return phase (Fig. (5.2) inset). Below, we demonstrate how this could expedite the overall search time.

We start by recalling the diffusive propagator of this process given by [35]

$$G(x,t) = \frac{1}{\sqrt{4\pi D t}} \left(e^{-\frac{x^2}{4Dt}} - e^{-\frac{(2L-x)^2}{4Dt}} \right). \tag{5.10}$$

For diffusive search process, the underlying first passage times (T) are sampled from the Lévy-Smirnov distribution so that

$$\langle min(T,R) \rangle = \frac{1}{r} \left(1 - e^{-\sqrt{rL^2/D}} \right) \tag{5.11}$$

(see Appendix A.1 for derivation). During the return phase, the particle has the possibility to hit either O or L starting from position x which is the coordinate of the particle exactly at the time of resetting. Considering that the return phase is facilitated by a linear potential $U(x) = \lambda|x|$, we can compute the average time for the particle to reach either

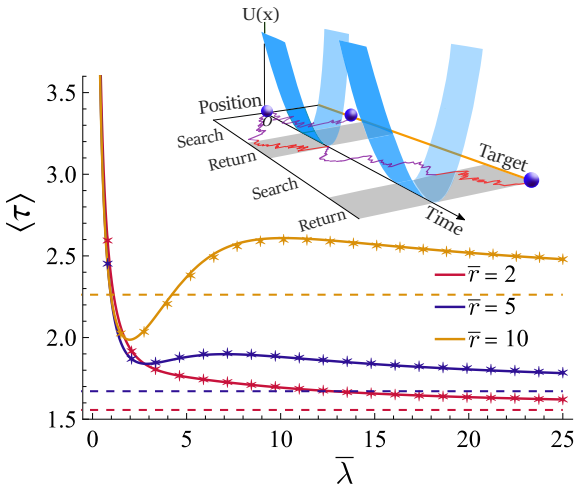

Figure 5.2: *Variation of the MFPT $\langle\tau(\bar{r},\bar{\lambda})\rangle$ from (5.15), shown by the solid curves, as a function of $\bar{\lambda}$ for different resetting rate $\bar{r}$. The horizontal dashed lines represent $\langle\tau_{inst}(\bar{r})\rangle$ for respective $\bar{r}$. Evidently, stochastic return can both reduce ($\bar{r}=10$) or prolong ($\bar{r}=5$) the completion time compared to the instantaneous returns. This behavioural transition occurs at $\bar{r}^*$ which is strictly a function of $\bar{\lambda}$. Numerical data (depicted by the stars) shows an excellent agreement with the theory. Inset schematic: Possible trajectories of a diffusive searcher under resetting and stochastic return facilitated by a potential trap. Violet (red) trajectory corresponds to search & trap-off (return & trap-on) phase.*

of the boundaries namely [35]

$$\langle t_2(x)\rangle = \frac{L(1-e^{\lambda x/D})+x(e^{\lambda L/D}-1)}{\lambda(e^{\lambda L/D}-1)} \quad \text{for } x>0, \tag{5.12}$$

$$\langle t_1(x)\rangle = |x|/\lambda \quad \text{for } x<0. \tag{5.13}$$

It is worth noting that for $x<0$ the particle can only reach the origin at $x=0$ first, whereas for $x>0$ it may reach either the target at $x=L$ or the origin first. Using this idea, one can write the following expectation

$$\langle min\left(T^L_{ret}(x),T^O_{ret}(x)\right)\rangle_{\text{traj}} = \theta(-x)\langle t_1(x)\rangle + \theta(x)\langle t_2(x)\rangle, \tag{5.14}$$

where $\theta(x)$ is the step-function. In addition, the splitting probability is given by $Pr(T^O_{ret}(x)\leq T^L_{ret}(x)) = \left[\theta(x)\frac{e^{\lambda x/D}-e^{\lambda L/D}}{1-e^{\lambda L/D}}+\theta(-x)\right]$ [35]. Substituting these expressions into Eq. (5.4), we arrive at the following expression for the MFPT $\langle T_R\rangle = D/L^2\langle\tau(\bar{r},\bar{\lambda})\rangle$, where

$$\langle\tau(\bar{r},\bar{\lambda})\rangle = \frac{1}{\bar{r}\bar{\lambda}^2}\left(2\bar{\lambda}^2+2e^{\bar{\lambda}}\bar{r}-2e^{\bar{\lambda}}\bar{\lambda}^2-\bar{r}\bar{\lambda}-2\bar{r}+\frac{2\left(e^{\bar{\lambda}}-1\right)\bar{\lambda}\left(\left(2e^{\bar{\lambda}}-1\right)e^{\sqrt{\bar{r}}}-1\right)\left(\bar{\lambda}^2-\bar{r}\right)}{2e^{\bar{\lambda}+\sqrt{\bar{r}}}\bar{\lambda}-e^{2\sqrt{\bar{r}}}\left(\bar{\lambda}+\sqrt{\bar{r}}\right)-\bar{\lambda}+\sqrt{\bar{r}}}\right), \tag{5.15}$$

and $\bar{r}=\frac{rL^2}{D}, \bar{\lambda}=\frac{\lambda L}{D}$ are the scaled (dimensionless) resetting rate and potential strength respectively. Fig. (5.2) shows corroborated plots (theory & simulations) of $\langle\tau(\bar{r},\bar{\lambda})\rangle$ as

a function of $\overline{\lambda}$. Eq. (5.15) reproduces

$$\langle \tau_{inst}(\overline{r}) \rangle = \langle \tau(\overline{r}, \overline{\lambda} \to \infty) \rangle = \frac{e^{\sqrt{\overline{r}}} - 1}{\overline{r}} \tag{5.16}$$

which is the MFPT for instantaneous resetting [5] – shown in Fig. (5.2) by the horizontal dashed lines for different resetting rates.

Intriguingly, Fig. (5.2) shows a key feature that the MFPT for the stochastic return can be reduced further than the instantaneous resetting (see e.g., the $\overline{r} = 10$ curve). In fact, Eq. (5.15) reveals the existence of a critical resetting rate $\overline{r}^*$, which is a function of $\overline{\lambda}$, beyond which stochastic return always supersedes the instantaneous return in optimizing the search time (see later for the exact evaluation of $\overline{r}^*$). However, for $\overline{r} < \overline{r}^*$ (see e.g., the $\overline{r} = 5$ curve), the MFPT always stays above the instantaneous (dashed) line indicating that no advantage can be gained from the stochastic return for any resetting rate or $\overline{\lambda}$.

5.4.1 A universal phase diagram for diffusive search

The inequality in Eq. (5.9) allows us to construct a universal phase diagram, spanned by the system parameters, that governs the dominance of stochastic return over the classical instantaneous return. Such a phase diagram is graphically illustrated in Fig. (5.3) for the 1d diffusion. The red dashed line, obtained by setting $\mathcal{T} = \langle T_R^{inst} \rangle$, separates the two phases namely stochastic return -'beneficial' and -'detrimental' than the instantaneous return. The separatrix is the locus of the set of critical resetting rate $\overline{r}^*$ for each $\overline{\lambda}$ obtained from the above equality.

To gain further insights into the trade-off between two phases, we study $\mathcal{T}$ given by Eq. (5.9) and discuss some of the limiting cases. For *very low resetting rate* ($\overline{r} \to 0$) and finite $\overline{\lambda}$, one has $\mathcal{T} \sim \frac{1}{\overline{r}} \left(\frac{2\overline{\lambda}\left(1-e^{\overline{\lambda}}\right)}{\overline{\lambda}(\overline{\lambda}+2)-2e^{\overline{\lambda}}+2} \right)$ whereas $\langle \tau_{inst}(\overline{r}) \rangle \propto 1/\sqrt{\overline{r}}$. Clearly, the LHS diverges faster than RHS nullifying the criterion (5.9) for any $\overline{\lambda}$. Indeed, the trajectories that go away from the target accumulate more time during the stochastic return than the instantaneous return making the former strategy detrimental. In contrast for $\overline{r} \gg O(1)$ - *frequent resets* - and finite $\overline{\lambda}$, the RHS diverges as $\propto e^{\sqrt{\overline{r}}}/\overline{r}$ while the LHS is bounded as $\mathcal{T} = \frac{2e^{\overline{\lambda}}-\overline{\lambda}-2}{\overline{\lambda}^2}$ which is identical to $\langle \tau(\overline{r} \to \infty, \overline{\lambda}) \rangle$. Here, the pre-resetting phase is very short and the particle is effectively in the return phase. Thus, it has a finite probability to find the target during return phase while the instantaneous return almost always keeps the particle close to the origin eliminating the target-detection. Clearly, this is a favourable situation for the stochastic returns.

For the intermediate case of *finite* $\overline{r}$, there are two limiting cases of $\overline{\lambda}$. For large $\overline{\lambda}$, one finds $\mathcal{T} \sim \overline{\lambda} \left(\frac{2\sinh\left(\sqrt{\overline{r}}\right)}{\overline{r}^{3/2}} - \frac{1}{\overline{r}} \right)$ to be divergent while the RHS is finite. Note that in this limit the return probability to the origin (having return time $\approx \sqrt{D/r}/\lambda$) is almost close

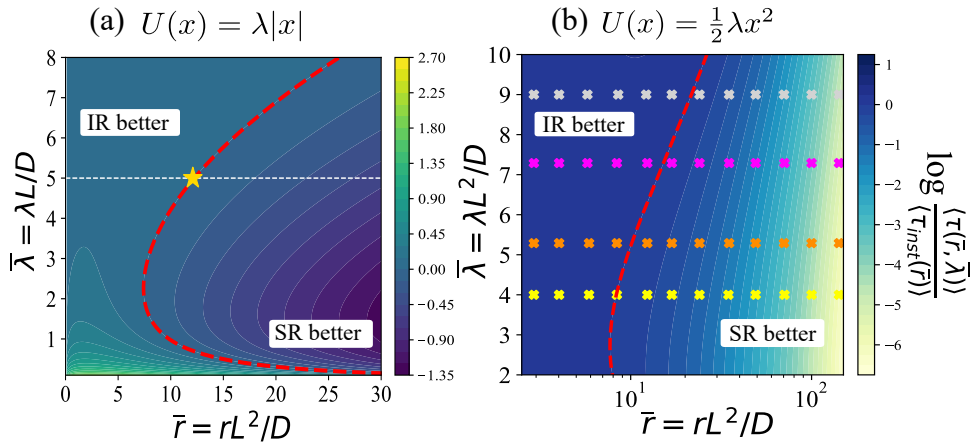

Figure 5.3: *Phase diagram for diffusive search with stochastic returns driven by linear- (panel a) and harmonic- (panel b) potentials: The region right to the phase boundary (red dashed curve) is where condition (5.9) is satisfied and stochastic return (SR) supersedes instantaneous return (IR). The red curve is obtained by setting (5.9) to an equality. The side colorbar is an estimation of search efficiency, defined by the ratio* $\frac{\langle \tau(\bar{r},\bar{\lambda})\rangle}{\langle \tau_{inst}(\bar{r})\rangle}$*; values in log-scale - positive (negative) for slow-down (speed-up) by the stochastic return. In panel (a), the yellow star indicates the critical* $\bar{r}^*$ *which is obtained from the intersection of the separatrix and the horizontal white line spanned by each* $\bar{\lambda}$ *(here,* $\bar{\lambda} = 5$*,* $\bar{r}^* \approx 12$*). In panel (b), we have superimposed the data points (marked as crosses) from the experimental parameter sets* $\left(\bar{\lambda}, \bar{r}\right)$ *from [15].*

to unity and the return phase only adds time penalties. Naturally, instantaneous returns are more efficient. For small $\bar{\lambda}$, however, the average return time is large (specifically from the trajectories in the $x < 0$ region) as can be seen from $\mathcal{T} \sim \frac{1}{\bar{\lambda}} \frac{1}{1-\sqrt{\bar{r}}\,\mathrm{csch}\left(\sqrt{\bar{r}}\right)} \propto \frac{1}{\bar{\lambda}}$ which diverges invalidating the condition (5.9). This ensures that instantaneous returns are more beneficial. In the bulk, the competing effect is non-trivial due to the intricate interplay between $\bar{r}$ and $\bar{\lambda}$. The results have also been summarized in the table below.

Table 1: *Demonstration of criterion in Eq. (5) for 1d diffusion in different limits of* $\bar{r}$ *and* $\bar{\lambda}$

Quantity	$\bar{r} \to 0$, Finite $\bar{\lambda}$	$\bar{r} \to \infty$, Finite $\bar{\lambda}$	$\bar{\lambda} \to 0$, Finite $\bar{r}$	$\bar{\lambda} \to \infty$, Finite $\bar{r}$
$\mathcal{T}(\bar{r},\bar{\lambda})$	$\frac{1}{\bar{r}}\left(\frac{2\bar{\lambda}\left(1-e^{\bar{\lambda}}\right)}{\bar{\lambda}(\bar{\lambda}+2)-2e^{\bar{\lambda}}+2}\right)$	$\frac{2e^{\bar{\lambda}}-\bar{\lambda}-2}{\bar{\lambda}^2}$	$\frac{1}{\bar{\lambda}}\frac{1}{1-\sqrt{\bar{r}}\,\mathrm{csch}\left(\sqrt{\bar{r}}\right)}$	$\bar{\lambda}\left(\frac{2\sinh\left(\sqrt{\bar{r}}\right)}{\bar{r}^{3/2}}-\frac{1}{\bar{r}}\right)$
$\langle \tau_{inst}(\bar{r})\rangle$	$\frac{1}{\sqrt{\bar{r}}}$	$\frac{e^{\sqrt{\bar{r}}}}{\bar{r}}$	$\frac{e^{\sqrt{\bar{r}}}-1}{\bar{r}}$	$\frac{e^{\sqrt{\bar{r}}}-1}{\bar{r}}$
$\frac{\mathcal{T}(\bar{r},\bar{\lambda})}{\langle \tau_{inst}(\bar{r})\rangle}$	> 1, IR better	< 1, SR better	> 1, IR better	> 1, IR better

5.5 A pragmatic application of the phase diagram

In this section, we employ the formalism developed in the work to test the efficiency of the stochastic return protocol in the experimentally realizable parameter regimes. In experiments, returns are modulated by turning on an optical tweezer around the center of the particle which gives rise to an harmonic confining potential. In the following we provide the detailed theory to find the MFPT under this return protocol as well as the

methodologies to connect the result to experimental datasets.

5.5.1 Theoretical result for MFPT with return by harmonic trap

Let us now consider a 1d diffusive search process where returns are facilitated by a harmonic trap $U(x) = \frac{1}{2}\lambda x^2$ (replacing the linear trap) that can be easily fabricated in experiments [15, 265]. Let us define the dimensionless variables in this case as where

$$\overline{\lambda} = \frac{\lambda L^2}{D}, \quad \overline{r} = \frac{rL^2}{D}, \quad \overline{x} = x/L. \tag{5.17}$$

For this process the splitting probabilities are found to be

$$\epsilon_L(\overline{x}) = \frac{\text{erfi}\left(\frac{\overline{x}\sqrt{\overline{\lambda}}}{\sqrt{2}}\right)}{\text{erfi}\left(\frac{\sqrt{\overline{\lambda}}}{\sqrt{2}}\right)}, \quad \epsilon_O(\overline{x}) = 1 - \frac{\text{erfi}\left(\frac{\overline{x}\sqrt{\overline{\lambda}}}{\sqrt{2}}\right)}{\text{erfi}\left(\frac{\sqrt{\overline{\lambda}}}{\sqrt{2}}\right)}, \tag{5.18}$$

where $\text{erfi}(z) = \text{erf}(iz)/i$ is the imaginary error function with $\text{erf}(z) = \frac{2}{\sqrt{\pi}}\int_0^z dt e^{-t^2}$. The unconditional mean first passage times for this case can also be computed in a similar manner and they read

$$\langle t_1(x)\rangle = \frac{L^2}{D}\mathcal{G}_1(\overline{\lambda}, \overline{x}), \quad \langle t_2(x)\rangle = \frac{L^2}{D}\mathcal{G}_2(\overline{\lambda}, \overline{x}), \tag{5.19}$$

where

$$\mathcal{G}_1(\overline{\lambda}, \overline{x}) = \frac{\overline{\lambda}\overline{x}^2\, {}_2F_2\left(1, 1; \frac{3}{2}, 2; -\frac{1}{2}\left(\overline{x}^2\overline{\lambda}\right)\right) - \pi\left(\text{erf}\left(\frac{\sqrt{\overline{\lambda}}\overline{x}}{\sqrt{2}}\right) - 1\right)\text{erfi}\left(\frac{\sqrt{\overline{\lambda}}\overline{x}}{\sqrt{2}}\right)}{2\overline{\lambda}}, \tag{5.20}$$

$$\mathcal{G}_2(\overline{\lambda}, \overline{x}) = \frac{1}{2}\Bigg(-\frac{\text{erfi}\left(\frac{\sqrt{\overline{\lambda}}\overline{x}}{\sqrt{2}}\right)\, {}_2F_2\left(1, 1; \frac{3}{2}, 2; -\frac{\overline{\lambda}}{2}\right)}{\text{erfi}\left(\frac{\sqrt{\overline{\lambda}}}{\sqrt{2}}\right)} + \overline{x}^2\, {}_2F_2\left(1, 1; \frac{3}{2}, 2; -\frac{1}{2}\left(\overline{x}^2\overline{\lambda}\right)\right)$$
$$+ \frac{\pi}{\overline{\lambda}}\left(\text{erf}\left(\frac{\sqrt{\overline{\lambda}}}{\sqrt{2}}\right) - \text{erf}\left(\frac{\sqrt{\overline{\lambda}}\overline{x}}{\sqrt{2}}\right)\right)\text{erfi}\left(\frac{\sqrt{\overline{\lambda}}\overline{x}}{\sqrt{2}}\right)\Bigg), \tag{5.21}$$

and ${}_2F_2\,(a, b; c, d; z)$ is the generalized hypergeometric function. The underlying free range propagator in Laplace space ($\widetilde{G}(x, r)$) is given by

$$\widetilde{G}(x, r) = \frac{L}{D}\frac{1}{\sqrt{4\overline{r}}}\left(e^{-\sqrt{\overline{r}}|\overline{x}|} - e^{-\sqrt{\overline{r}}(2-\overline{x})}\right) = \frac{L}{D}\widetilde{G}(\overline{x}, \overline{r}), \tag{5.22}$$

which we have rewritten in terms of the dimensionless parameter $\overline{r}$. Finally, following the same proceedure as in the previous case, we find the MFPT here to be given by

$$\langle \tau(\overline{r},\overline{\lambda})\rangle = \frac{D}{L^2}\langle T_R\rangle = \frac{\frac{1}{\overline{r}}\left(1-e^{-\sqrt{\overline{r}}}\right) + \overline{r}\int_{-\infty}^{1} d\overline{x}\widetilde{G}(\overline{x},\overline{r})\left[\theta(-\overline{x})\mathcal{G}_1(\overline{\lambda},\overline{x}) + \theta(\overline{x})\mathcal{G}_2(\overline{\lambda},\overline{x})\right]}{1-\overline{r}\int_{-\infty}^{1} d\overline{x}\ \widetilde{G}(\overline{x},\overline{r})\left[\theta(-\overline{x}) + \theta(\overline{x})\epsilon_O(\overline{x})\right]}, \tag{5.23}$$

where the integrals can be computed numerically. We can now employ the criterion Eq. (5.9) to generate the phase diagram for this dynamics. In here, we vary the resetting rate and the potential strength to generate the phase diagram. Such a phase diagram, spanned by the system parameters, allows us to identify the parameter regimes where the stochastic return can be more useful over the classical instantaneous return with regard to an efficient search in Fig. 5.3(b). Note however that in this case, we have not arbitrarily varied these parameters, rather we have used a list of the parameters with the exact values that were used in the experiments [15, 265].

5.5.2 The phase diagram for search efficiency: identification of realistic range of parameters

In the following, we briefly revisit the experimental set-up by Besga *et al* [15, 265]. This will be useful to interlace the resetting experiment with our theoretical modeling. In the experiment, the authors considered an overdamped Brownian particle fluctuating inside a harmonic trap with potential $U(x) = \frac{1}{2}\lambda_e x^2$, where Γ is the damping constant and the λ_e stands for the potential strength as obtained from an optical tweezer by controlling its power. $\zeta(t)$ is a Delta correlated white noise with strength D. Here, $D = k_B T_B/\Gamma$ is the diffusion constant where k_B is the Boltzmann constant and T_B is the ambient temperature. The value of Γ can be found from the Stoke's law as $\Gamma = 6\pi\eta r$, where $r \approx 1\mu m$ is the radius of the particle (as in the experiment) and η is the viscosity of water. Given long enough time the particle equilibrates inside the harmonic trap and its position gets distributed according to the Gibbs–Boltzmann distribution $P_{eq}(x) = \frac{e^{-x^2/2\sigma^2}}{\sqrt{2\pi\sigma^2}}$, where $\sigma = \sqrt{k_B T_B/\lambda_e}$. The authors design an "instantaneous resetting" protocol using the harmonic trap that brings the particle to a fluctuating location (close to the origin) distributed according to the $P_{eq}(x)$ [15, 265]. We do not delve deeper into the experimental details here besides stressing the fact that the resetting there was conducted by the harmonic trap. Moreover, resetting was made "instantaneous" by throwing away the so-called pulling/equilibration time while in our case, we assume that the return time can not be thrown away (generically this should be true for any arbitrary stochastic process) and thus by its inclusion we have unveiled new physics as illustrated this chapter. This is a notable distinction between our work and majority of the existing works.

To summarize this part, our return protocol is facilitated by the same harmonic trap as proposed by the experiments (and thus we use their experimentally accessible parame-

ters); however, the return is not instantaneous but a finite-time process. In the following, we demonstrate how the theoretical and experimental variables are related to each other.

The dimensionless potential strength: In the experiments [15, 265], the authors introduced

$$b = L/\sigma, \tag{5.24}$$

where L is the distance to the target and recall that $\sigma = \sqrt{k_B T_B/\lambda_e}$ which is also the equilibrium length scale of the particle under the harmonic trap with strength λ_e. This can be connected to the dimensionless potential strength $\overline{\lambda}$ that we have defined in the theoretical modeling such as

$$\overline{\lambda} = \lambda L^2/D = \frac{\lambda_e L^2}{D\Gamma} = \frac{k_B T_B}{D\Gamma} b^2 = b^2, \tag{5.25}$$

where $D\Gamma = k_B T_B$ and the potential strength λ, in our theoretical model, is related to the same from the experiment as $\lambda = \lambda_e/\Gamma$. This dimensionless relation is quite useful as it allows us to scale D or L without specifying their exact values. In the experiment, b is varied in between 2 to 3 which corresponds to an approximated range of $\overline{\lambda} \in (4, 9)$.

The dimensionless resetting rate: In a similar vein, the authors in [15, 265] constructed a dimensionless resetting rate in the following way

$$c = \frac{\sqrt{r}L}{\sqrt{D}}, \tag{5.26}$$

which upon taking squares on both the sides yield the non-dimensional resetting rate $\overline{r}$ for our theory i.e.,

$$\overline{r} = rL^2/D = c^2. \tag{5.27}$$

In their experiment, c was varied roughly between 0 and 14 which corresponds to the following range for our resetting rate: $\overline{r} \in (0, 196)$.

Data extraction and the phase diagram: We have used Fig. 5 from Ref [15] and Fig. 6 from Ref [265] to extract the parameters (b, c). Using the mapping shown by Eqs. 5.25 and 5.27, we have generated a corresponding list of parameters $(\overline{\lambda}, \overline{r})$. We have used the parameters from this list to generate the phase diagram in Fig. 5.3(b). The red dashed line is the separatrix (generated from the equality of Eq. (5.9)) that distinguishes between two regimes: (i) left regime where the instantaneous returns are more useful, (ii) right regime where stochastic returns (SR) are found to be more beneficial than the instantaneous return (IR). For each coordinate $(\overline{\lambda}, \overline{r})$ in the phase diagram, we compute

the log ratio between $\langle\tau(\overline{r},\overline{\lambda})\rangle$ and $\langle\tau_{inst}(\overline{r})\rangle = \langle\tau(\overline{r},\overline{\lambda}\to\infty)\rangle$. Cumulatively, this is shown using colorbars in Fig. 5.3(b). It is evident from the figure that in the stochastic return dominated regime, there is a significant improvement in the search efficiency as the mean search times can differ by the order of magnitude.

This phase space plot is effective in two ways: (i) to identify the parameter range where one needs to design stochastic return protocols, and (ii) to quantify the corresponding speed-up in the search time for each parameter coordinate in the phase space especially pertaining to (i). Thus, in an attempt to verify our results (with proposed stochastic return protocols) experimentally in similar set-ups as in [15, 265], Fig. (5.3)(b) would be the guiding phase diagram to selectively choose parameters for showcasing various trade-offs. Finally, we emphasize that the phase diagram also quantifies the speed-up in search efficiency that can be gained by implementing stochastic return protocols for a range of experimentally accessible parameters.

5.6 Optimal speed-up for the drift-diffusive search process

The MFPT of a free diffusive particle in 1d as discussed till now, is infinite [266] and thus it is expected that any finite resetting rate will render the MFPT finite [5, 53, 129]. But what happens when the underlying reset-free process has a finite MFPT? Is resetting useful there? This was first studied in [53] where it was shown that whenever the ratio of fluctuation to mean of FPT, known as the coefficient of variation (CV), is greater than unity, resetting with the instantaneous return is guaranteed to help. This condition, however, also suggests that there are scenarios where resetting with instantaneous return can not be beneficial. This leaves us with a set of intriguing questions: Whether resetting with stochastic return can be an advantageous strategy in the latter case? Furthermore, can stochastic return perform better than an optimally restarted instantaneous process? Can one find suitable conditions where stochastic return can be useful than both the instantaneous return and the underlying process? Understanding these aspects is the central goal of this section. In parallel to developing the general theory, we will extensively study one canonical model set-up namely drift-diffusion in 1d where the MFPT is finite. We will assume that the search will be conducted by a drift-diffusive process while the stochastic return motion will be modulated by turning on a potential trap around the origin. The aim will be to analyze the MFPT as a function of various system parameters and then to delve deeper into some of the questions raised above.

5.6.1 Problem set-up and MFPT

We consider the same problem as described in the section 5.4. However, here there is an additional drift velocity v present in the system that drives the particle toward the target at $x = L$. Note that, due to the constant nature of the drift velocity the return motion is now also a drift-diffusive process similar to the underlying motion (search phase).

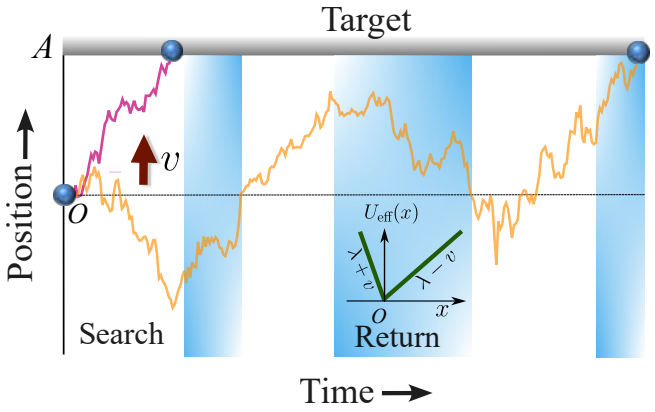

Figure 5.4: *Illustrative representation of drift-diffusive resetting search process under stochastic return. A drift of magnitude v (red arrow) always acts on the particle, biasing its motion towards a fixed target located at A. Once a resetting time is set (drawn randomly from a distribution), a potential $U(x) = \lambda|x|$ with $\lambda > 0$ is turned on at the resetting location which is denoted by O here (shown by the blue strips). This potential causes an additional drift of magnitude λ towards the origin. Overall, an effective potential $U_{\text{eff}}(x)$ as in Eq. (5.30) acts on the particle during the return. After the particle reaches the origin the potential is turned off marking the completion of one resetting event. The search process can end in two ways: either the target is found during the search phase (potential turned off - shown by the violet trajectory) or during the return phase (potential turned on - shown by the yellow trajectory).*

However, the direction and magnitude are now changed. For $x > 0$, the net drift now becomes

$$\lambda_+ = \lambda - v, \tag{5.28}$$

towards the origin (assuming $\lambda > v$). Quite evidently, when $\lambda < v$ the net drift acts towards the target in the region $x > 0$. On the other hand for $x < 0$ the drift always is

$$\lambda_- = \lambda + v, \tag{5.29}$$

towards the target (or origin, as both fall on the same side). In another way, one can construct an effective potential $U_{\text{eff}}(x)$ as below

$$U_{\text{eff}}(x) = \begin{cases} \lambda_+ x & \text{if } x > 0, \\ -\lambda_- x & \text{if } x < 0, \end{cases} \tag{5.30}$$

which acts on the particle during the return phase. Fig. (5.4) depicts a trajectory of the particle schematically. Note that in the limit $\lambda \to \infty$ one expects to recover the results for the classical instantaneous return for a drift-diffusive system [65, 86].

Note that the relevant quantities to evaluate the MFPT in this as required by Eq. (5.4)

and Eq. (5.14) are given as

$$\widetilde{G}(x,s) = \frac{e^{\frac{vx}{2D}}\left(e^{-\frac{|x|\sqrt{4Ds+v^2}}{2D}} - e^{-\frac{(2L-x)\sqrt{4Ds+v^2}}{2D}}\right)}{\sqrt{4Ds+v^2}}. \tag{5.31}$$

$$\langle t_2(x)\rangle = \frac{L(1-e^{\lambda_+ x/D}) + x(e^{\lambda_+ L/D}-1)}{\lambda_+(e^{\lambda_+ L/D}-1)}, \tag{5.32}$$

$$\tag{5.33}$$

$$\langle t_1(x)\rangle = \frac{|x|}{\lambda_-}, \tag{5.34}$$

$$\epsilon_L(x) = 1-\epsilon_O(x) = \frac{1-e^{\lambda_+ x/D}}{1-e^{\lambda_+ L/D}}, \tag{5.35}$$

$$\langle min(T,R)\rangle = \frac{1-e^{\frac{L\left(v-\sqrt{4Ds+v^2}\right)}{2D}}}{r}. \tag{5.36}$$

It turns out that the overall MFPT can be written in a dimensionless form

$$\langle \tau(\overline{r},\overline{\lambda},\overline{v})\rangle = \frac{D}{L^2}\langle T_R(r,\lambda,v)\rangle, \tag{5.37}$$

where we introduce the scaled quantities

$$\overline{r} = rL^2/D,\ \overline{\lambda} = \lambda L/D,\ \overline{v} = vL/D. \tag{5.38}$$

The exact expression for $\langle \tau(\overline{r},\overline{\lambda},\overline{v})\rangle$ is quite cumbersome and provided in Appendix E.1 and also in the Mathematica file in the GitHub link [267]. Fig. (5.5) shows its variation with respect to the potential strength $\overline{\lambda}$ and resetting rate $\overline{r}$ for two distinct values of $\overline{v} = 0.2$ and 3.

The behaviour with respect to potential strength is quite intricate as can be seen from Fig. (5.5)(a,c). Let us first discuss two important limiting cases of the MFPT $\langle \tau(\overline{r},\overline{\lambda},\overline{v})\rangle$ that we shall frequently refer to in the rest of the chapter.

MFPT of the underlying (reset-free) process: In the limit $\overline{\lambda} \to 0$ no effect of resetting potential is there and the process effectively goes back to the simple reset-free drift-diffusion. One can check that in this limit the MFPT is given by

$$\langle \tau(\overline{r},\overline{\lambda}\to 0,\overline{v})\rangle = \frac{1}{\overline{v}}, \tag{5.39}$$

which is the MFPT of the underlying drift-diffusive process [35]. Note that this is also equivalent to setting $\overline{r} \to 0$. Both the limits correspond to the same underlying reset-free process.

MFPT with instantaneous return: On the other hand when $\overline{\lambda} \to \infty$ the potential strength is so high that the particle returns almost instantaneously to the origin. The

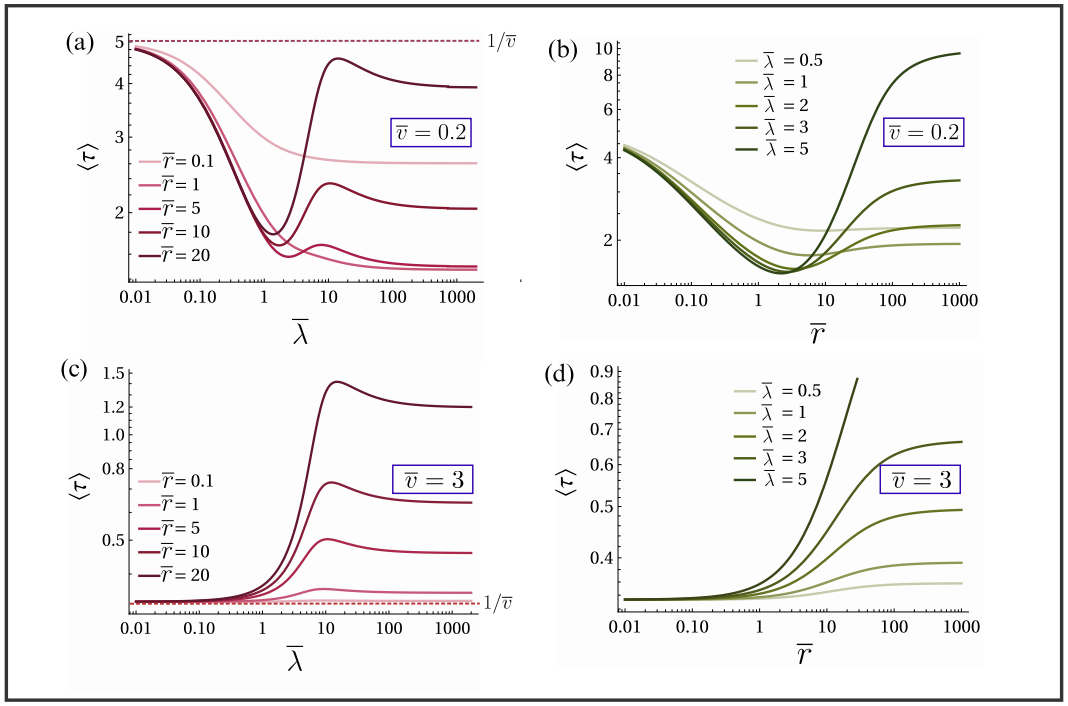

Figure 5.5: *Variation of the MFPT $\langle \tau(\overline{r}, \overline{\lambda}, \overline{v}) \rangle$ with potential strength $\overline{\lambda}$ (panel a,c) and resetting rate $\overline{r}$ (panel b,d) for exponentially distributed resetting times. Panel (a,b) are for $\overline{v} = 0.2$ and panel (c,d) are shown for $\overline{v} = 3$. The limit $\overline{\lambda} \to 0$ gives the MFPT of the underlying process i.e. $\frac{1}{\overline{v}}$ shown by the dashed horizontal lines. Note the contrasting behaviour for different values of $\overline{v}$. For lower value of $\overline{v}$ each plot shows a non-monotonic behaviour implying the utility of resetting compared to the reset-free process. However, as $\overline{v}$ becomes higher MFPT for a finite value of $\overline{r}$ and $\overline{\lambda}$ is always greater than that of the underlying process. Also in some of the curves in panel (a) and in each of the curves in panel (c), there exists a range of $\overline{\lambda}$ where MFPT becomes lower than the instantaneous return limit ($\overline{\lambda} \to \infty$).*

resulting expression of the MFPT in this limit indeed reduces to the result for the instantaneous return case

$$\langle \tau(\overline{r}, \overline{v}) \rangle_{\text{inst}} = \langle \tau(\overline{r}, \overline{\lambda} \to \infty, \overline{v}) \rangle = \frac{e^{\frac{1}{2}\left(\sqrt{\overline{v}^2 + 4\overline{r}} - \overline{v}\right)} - 1}{\overline{r}}, \tag{5.40}$$

as derived in [65]. Here we have denoted the MFPT associated with instantaneous return protocol by $\langle \tau(\overline{r}, \overline{v}) \rangle_{\text{inst}}$.

Quantification of MFPT for intermediate values of $\overline{\lambda}$ is highly non-trivial. Note that depending on the magnitude of the drift $\overline{v}$ of the underlying process the plots show two distinct kinds of behaviour. Let us first focus on Fig. (5.5)(a) which is for $\overline{v} = 0.2$. For lower values of resetting rates (e.g. $\overline{r} = 0.1, 1$), the curves monotonically go down and saturate to the instantaneous return MFPT given by Eq. (5.40). On the other hand, when resetting rates are high it shows non-monotonic behaviour with $\overline{\lambda}$. Particularly, for $\overline{r} = 10, 20$ it is evident from the plots that, for a range of $\overline{\lambda}$ *MFPT can be reduced below that of both the underlying reset-free process and the instantaneous return limit*. In contrast, for the value of $\overline{v} = 3$, we see from Fig. (5.5)(c) that MFPT never goes below the MFPT of the underlying reset-free process for any values of $\overline{\lambda}$. However, in this case

also one can find the set of $\overline{\lambda}$ values where MFPT is lower than that of instantaneous resetting.

With resetting rate $\overline{r}$ MFPT shows a non-monotonic variation for lower values of $\overline{v}$ (look at Fig. (5.5)(b)). In the absence of resetting $\overline{r} \to 0$ one gets

$$\langle \tau(\overline{r} \to 0, \overline{\lambda}, \overline{v}) \rangle = \frac{1}{\overline{v}}, \tag{5.41}$$

the same as in Eq. (5.39) as they are physically equivalent. When resetting is too frequent *i.e.* in the limit $\overline{r} \to \infty$, the potential is almost always turned on, and the MFPT resembles that of a particle in the potential $U_{\text{eff}}(x)$ (as defined in Eq. (5.30)), given by

$$\langle \tau(\overline{r} \to \infty, \overline{\lambda}, \overline{v}) \rangle = \frac{\overline{v}^2 - \overline{\lambda}\left(-2e^{\overline{\lambda}-\overline{v}} + \overline{\lambda} + 2\right)}{(\overline{\lambda} - \overline{v})^2(\overline{\lambda} + \overline{v})}. \tag{5.42}$$

Once $\overline{v}$ is increased this non-monotonous behaviour goes away and MFPT starts increasing with $\overline{r}$ for any value of $\overline{\lambda}$ (see Fig. (5.5)(d)).

From the above discussion, it is evident that resetting is not guaranteed to expedite the search process for any arbitrary parameters. Fig. (5.5)(a,b) are the cases where it indeed helps. On the contrary, Fig. (5.5)(c,d) depicts that any amount of resetting is detrimental. In the next section, we delve deeper into this and try to find a criterion for resetting to be helpful.

5.6.2 Speed up over underlying process - the *CV criterion*

To ensure that the stochastic return process is more beneficial than the underlying process, one should have

$$\langle T_R(\delta r, \lambda, v) \rangle < \langle T \rangle, \tag{5.43}$$

where $\langle T \rangle$ is the MFPT of the underlying reset-free process and $\langle T_R(\delta r, \lambda, v) \rangle$ can be found from Eq. (5.8). Here we should emphasize that the above condition is sufficient for resetting to be helpful but not a necessary one. A Taylor series expansion of $\langle T_R(\delta r, \lambda, v) \rangle$ up to $O(\delta r)$ and simple rearrangement leads to (detailed derivation in Appendix E.2)

$$CV^2 > \frac{2}{\langle T \rangle}\overline{\langle t^{ret}(x) \rangle} + 2\overline{\epsilon_O^{ret}(x)} - 1, \tag{5.44}$$

where CV is the coefficient of variation of the underlying reset-free process defined as

$$CV = \frac{\sqrt{\langle T^2 \rangle - \langle T \rangle^2}}{\langle T \rangle}. \tag{5.45}$$

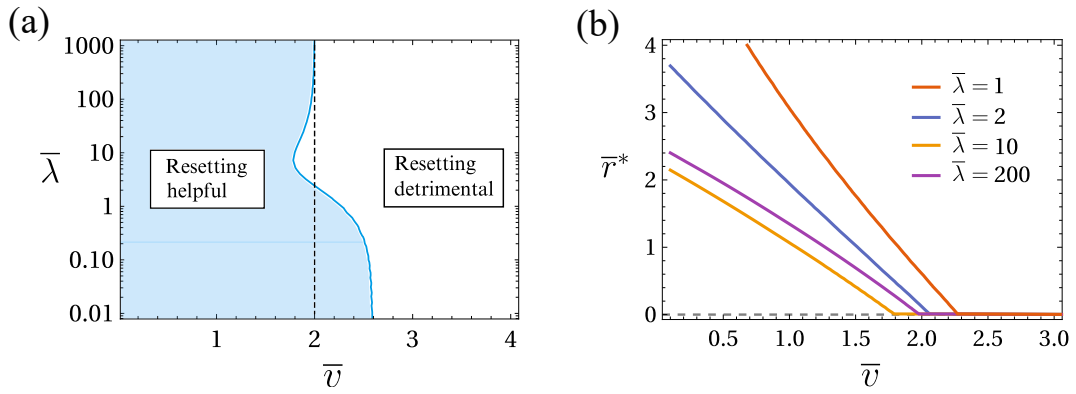

Figure 5.6: *(a) Phase space obtained from the CV criterion (5.44) for the drift-diffusive system with return via $U_{eff}(x)$. The blue-shaded region is where resetting will help to reduce the MFPT beyond the underlying process. The black dashed line at $\overline{v} = 2$ refers to the phase boundary in the instantaneous limit ($\overline{\lambda} \to \infty$). (b) Variation of the ORR with respect to $\overline{v}$ for several values of $\overline{\lambda}$.*

This is a measure of the relative fluctuation of the first passage time of the underlying reset-free process. The quantities $\langle t^{ret}(x)\rangle$ and $\epsilon_O^{ret}(x)$ are defined as

$$\langle t^{ret}(x)\rangle = \theta(-x)\langle t_1(x)\rangle + \theta(x)\langle t_2(x)\rangle, \tag{5.46}$$

$$\epsilon_O^{ret}(x) = \theta(-x) + \theta(x)\epsilon_O(x). \tag{5.47}$$

The overbar $\overline{(...)}$ in Eq. (5.44) implies an average that has to be taken with respect to $G_0(x)$ so that $\overline{f(x)} = \int_{-\infty}^{L} dx\, G_0(x) f(x)$. The quantity $G_0(x)$ is defined as

$$G_0(x) = \frac{1}{\langle T\rangle}\int_0^\infty dt G(x,t), \tag{5.48}$$

which is normalized by construction so that $\int_{-\infty}^{L} G_0(x)dx = 1$. The condition in Eq. (5.44) is not limited to the drift-diffusive system considered here, but applies to any arbitrary first passage system in 1d. For the drift-diffusive system considered in this chapter, the mean and the second moment are given, respectively, by $\langle T\rangle = L/v$ and $\langle T^2\rangle = \frac{L(2D+Lv)}{v^3}$. The CV thus becomes

$$CV = \sqrt{\frac{2D}{Lv}} = \frac{1}{\sqrt{\text{Pe}}}, \tag{5.49}$$

where $\text{Pe} = \frac{Lv}{2D} = \frac{\overline{v}}{2}$ is the so-called Peclet number. It is simply the ratio of the diffusion and drift time scales. Eq. (5.44) is quite useful since without any prior knowledge of the resetting rates one can infer from here if resetting will be helpful. One can generate the phase space spanned by the CV criterion mentioned above, over $\overline{\lambda} - \overline{v}$ plane as shown in Fig. (5.6)(a). If the parameters are chosen from the blue-shaded region, then resetting is bound to decrease the MFPT of this process further below the underlying drift-diffusive limit *i.e.* $1/\overline{v}$ (see Eq. (5.41)). The black dashed line ($\text{Pe} = 1$ or $\overline{v} = 2$) represents

the phase boundary for the instantaneous resetting limit as obtained previously. Note that, keeping a fixed value of $\overline{\lambda}$ if one gradually increases $\overline{v}$, then at some finite value $\overline{v}$ one crosses from the region where resetting helps to where resetting does not. This behavioural transition is known as *restart transition* (recall the discussion in section 1.1.2) and is of second order in nature [66]. When $\overline{v}$ is low enough, note that the MFPT becomes the lowest at some finite value of $\overline{r} = \overline{r}^*$ Fig. (5.5). This resetting rate $\overline{r}^*$ is formally known as the *optimal resetting rate* (ORR). Mathematically, this can be found by setting

$$\left.\frac{\partial\langle\tau(\overline{r},\overline{\lambda},\overline{v})\rangle}{\partial\overline{r}}\right|_{\overline{r}=\overline{r}^*} = 0. \tag{5.50}$$

A non-zero value of $\overline{r}^*$ ensures that resetting can benefit the search process in lowering the MFPT to its lowest. In contrast, one observes in Fig. (5.5), that for a higher value of $\overline{v}$ resetting only increases the MFPT. Consequently, the reset-free process performs at its best and the optimal resetting rate $\overline{r}^*$ is zero. Solving Eq. (5.50) numerically, we can now probe this behavioural transition as depicted in Fig. (5.6)(b). We find that $\overline{r}^*$ undergoes a second-order transition as $\overline{v}$ is gradually increased, for any values of $\overline{\lambda}$. For very high potential strength ($\overline{\lambda} = 200$) the transition occurs at $\overline{v} = 2$, commensurate with the instantaneous return limit [65].

The physical origin behind these two distinct regions in Fig. (5.6)(a) can be understood as follows. For very low values of the drift $\overline{v}$ the particle can disperse very far from the origin. These diverging trajectories in the direction opposite to the target can lead to a very high value of the MFPT. Return (any finite value of $\overline{\lambda} > 0$) in those cases prohibits the particle from wandering off too far away from the target consequently reducing the MFPT. In contrast, when the drift $\overline{v}$ is sufficiently high, then the MFPT of the underlying process is itself very short. The diverging trajectories as mentioned previously are already very rare in this case. Any kind of resetting in this case would only hinder the trajectories which were supposed to find the target in a shorter time span and cause a delay in the process completion.

5.6.3 Speed up over instantaneous resetting- the *SR criterion*

Similar to the discussion in section 5.4 here too, one can generate the phase plot using the criterion Eq. (5.9). However, this condition along with the CV criterion as in Eq. (5.44) generates a combined phase-diagram from which one can easily infer the parameter spaces where the stochastic return is either better than the instantaneous return or the underlying reset-free process as shown in Fig. (5.7). The region left to the solid (red) separatrix is where the CV criterion is satisfied. On the other hand, the region below the dashed separatrix is where the SR criterion is satisfied. This immediately presents us with 4 distinct phases in the parameter space. We mark them from I-IV and discuss each of them below in detail.

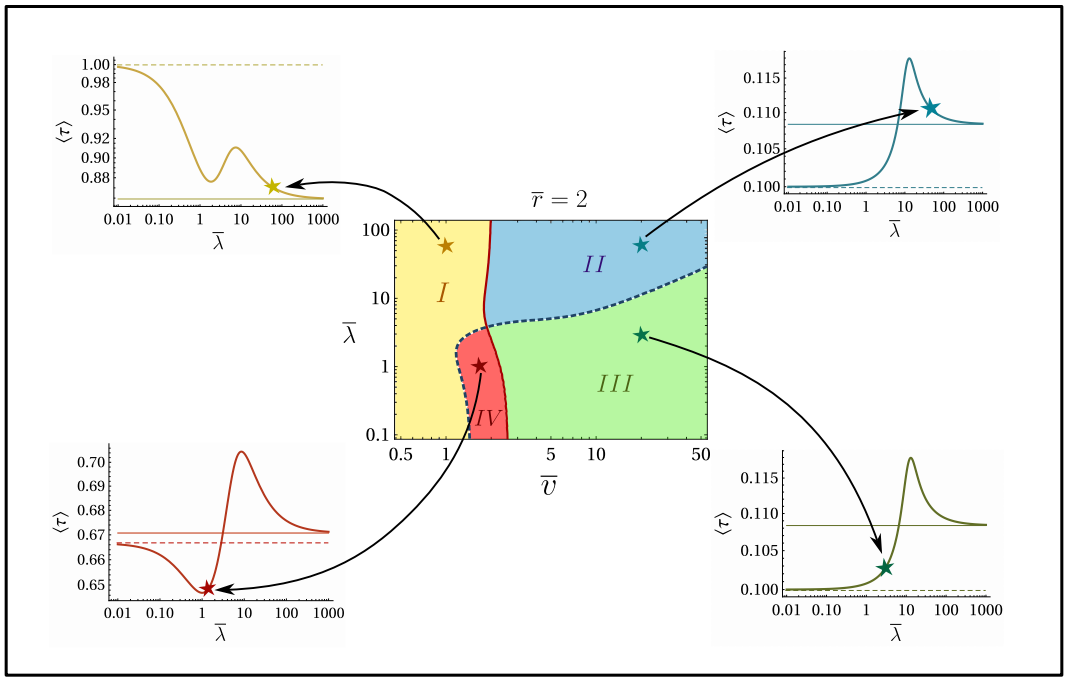

Figure 5.7: *A unified phase diagram for the drift-diffusive search process for exponential resetting with rate $\overline{r} = 2$. Different regions in this parameter space represent the regions where either of the CV criteria in Eq. (5.44) or the SR criteria as in Eq. (5.9) is satisfied. The most important is region IV (the red-shaded region) where both the criteria are satisfied, and stochastic return facilitates the process beyond both the underlying process and also that of resetting with instantaneous return. The behaviour of the MFPT for a sample point (star) in each of these regions is shown in the corners. In these plots, the horizontal solid lines represent the MFPT that with instantaneous return and the dashed horizontal line represents the MFPT of the underlying reset-free process.*

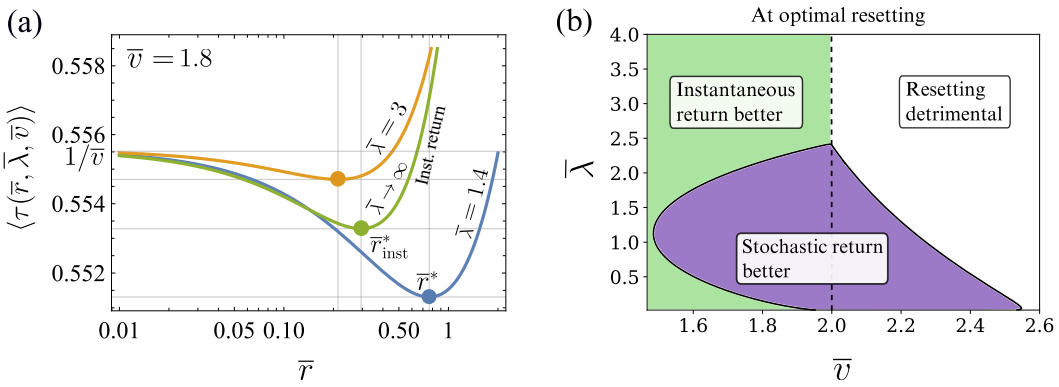

Figure 5.8: *(a) MFPT with stochastic return i.e.* $\langle \tau(\overline{r}, \overline{\lambda}, \overline{v}) \rangle$ *(blue and orange curves) and instantaneous return i.e.* $\langle \tau(\overline{r}, \overline{v}) \rangle_{inst} = \langle \tau(\overline{r}, \overline{\lambda} \to \infty, \overline{v}) \rangle$ *(green curve) are plotted with respect to the resetting rate* $\overline{r}$*, for a fixed drift velocity* $\overline{v} = 1.8$*. Remarkably, for* $\overline{\lambda} = 1.4$ *we find that optimal stochastic return can lower the MFPT (the blue circle) even beyond the optimal instantaneous return (the green circle). (b) Phase space showing regions where stochastic (or instantaneous) return is better at the optimal resetting rate (which is different in general for both the protocols). The blue shaded region (obtained by setting the speed-up parameter* γ^* *as in Eq. (5.54), to be greater than unity) is where stochastic return performs better than the optimal instantaneous return.*

Region I (yellow): Here, the CV criterion is met but not the SR one. Stochastic return (SR) accelerates the search compared to the reset-free case but remains slower than instantaneous return (IR). For $(\overline{v}, \overline{\lambda}) = (1, 60)$ (yellow star in Fig. (5.7)), the MFPT lies between those of the reset-free (solid line) and IR (dashed line) processes.

Region II (blue): Neither criterion holds, making SR the least efficient. At $(\overline{v}, \overline{\lambda}) = (20, 60)$ (blue star), MFPT exceeds both IR and reset-free values (top-right panel of Fig. (5.7)).

Region III (green): Only the SR criterion is satisfied. SR outperforms IR but not the reset-free case. For $(\overline{v}, \overline{\lambda}) = (20, 2)$ (green star), MFPT lies below IR yet above the reset-free line (bottom-right panel).

Region IV (red): Both criteria are fulfilled, making SR optimal—it yields the shortest MFPT, even outperforming IR. For $(\overline{v}, \overline{\lambda}) = (1.5, 1)$ (red star, bottom-left panel), MFPT is lower than both IR and reset-free processes; notably, IR here increases search time.

In summary, SR can expedite searches even where IR fails. The phase diagram in Fig. (5.7) corresponds to $\overline{r} = 2$; varying $\overline{r}$ shifts the phase boundaries.

In the previous section, we have already described in detail the physical conditions when stochastic return strategy can beat both the instantaneous return and the underlying process. Here, we explore even a more ambitious question: Can stochastic return perform better than an optimally restarted instantaneous process?

5.6.4 Speed-up beyond optimal instantaneous return

In the previous section, we have already described in detail the physical conditions when stochastic return strategy can beat both the instantaneous return and the underlying pro-

cess. Here, we explore a even more ambitious question: Can stochastic return perform better than an optimally restarted instantaneous process?

MFPT at optimal resetting rate

We start by defining the optimal resetting rate (ORR) $\overline{r}^*$ that can be obtained by minimizing the MFPT ie,

$$\left.\frac{\partial\langle\tau(\overline{r},\overline{\lambda},\overline{v})\rangle}{\partial\overline{r}}\right|_{\overline{r}=\overline{r}^*}=0, \tag{5.51}$$

where $\overline{r}^*$ will be a function of $\overline{\lambda},\overline{v}$ in general. In the limit $\overline{\lambda}\to\infty$, the ORR coincides with that of the instantaneous case

$$\overline{r}^*_{\rm inst}=\overline{r}^*(\overline{\lambda}\to\infty,\overline{v}), \tag{5.52}$$

which can also be found from Eq. (5.40) as

$$\left.\frac{\partial\langle\tau(\overline{r},\overline{v})\rangle_{\rm inst}}{\partial\overline{r}}\right|_{\overline{r}=\overline{r}^*_{\rm inst}}=0. \tag{5.53}$$

We recall from Sec. 5.6.2 that for $\overline{v}>2$ instantaneous return fails to expedite the underlying process. Consequently, $\overline{r}^*_{\rm inst}$ is exactly zero there. On the other hand, a careful look at Fig. (5.6)(a) reveals that there is a certain blue shaded region even at $\overline{v}>2$. This is where stochastic return is actually able to enhance the search process compared to the underlying process, in spite of instantaneous return failing to do so. Evidently, $\overline{r}^*$ is non-zero in this region. Interestingly, there also exists a set of values of $\overline{v}$ (which is less than 2) where despite having a finite $\overline{r}^*_{\rm inst}$, stochastic return at $\overline{r}^*$ can perform better. We turn attention to Fig. (5.8)(a) where we plot the MFPT for both the protocols with respect to $\overline{r}$ keeping $\overline{v}=1.8$. Note that the blue curve, corresponding to the MFPT with stochastic return for $\overline{\lambda}=1.4$, shows a minima at $\overline{r}^*$. The MFPT at this minima is lower than the optimal MFPT obtained for the instantaneous return at $\overline{r}^*_{\rm inst}$ (the green curve). However, we observe a inverse effect for $\overline{\lambda}=3$ where the optimal MFPT obtained with stochastic return is higher than that of instantaneous return (the orange curve).

Thus for the given problem of drift-diffusion process, we have found a parameter space in $(\overline{v},\overline{\lambda})$ where stochastic return at the optimality can indeed outperform the instantaneous resetting at the optimality. To quantify this region, we calculate the speed-up parameter γ^* at the optimal resetting rate, defined as

$$\gamma^*=\frac{\langle\tau(\overline{r}^*_{\rm inst},\overline{v})\rangle_{\rm inst}}{\langle\tau(\overline{r}^*,\overline{\lambda},\overline{v})\rangle}. \tag{5.54}$$

The $\gamma^*>1$ condition indicates the blue shaded region in Fig. (5.8)(b) where optimal

stochastic return is better than optimal instantaneous return. The inverse condition $\gamma^* < 1$ depicts the complementary region (marked by green in Fig. (5.8)(b)). Finally, resetting of any kind is detrimental in the white region in Fig. (5.8)(b).

Plausible physical explanations

We now discuss the mechanisms behind the observed speed-up of stochastic return (SR) over instantaneous resetting (IR). The main effects governing SR are:

(a) For $x < 0$, the effective drift $\lambda_- = \lambda + v$ exceeds v, pulling trajectories back toward the origin and suppressing long excursions.
(b) For $x > 0$, the drift $\lambda_+ = \lambda - v$ either opposes or weakens the motion toward the target, slowing the search.
(c) In IR, return to the origin is instantaneous, adding no return time to the MFPT.
(d) In SR, however, some trajectories can reach the target during the return phase—an advantage absent in IR.

The interplay among these effects determines which protocol performs better for a given $(\overline{v}, \overline{\lambda})$. We examine the main limits below.

1) Very high $\overline{v} \gg 2$*:* Strong drift quickly drives particles to the target, so any resetting—instantaneous or stochastic—only delays arrival. Both protocols are detrimental.

2) Intermediate $\overline{v} \gtrsim 2$*:* In this range, IR no longer helps, but SR can outperform both IR and the reset-free process (violet region in Fig. (5.8)). Moderate return strengths allow some trajectories to reach the target during return, while the enhanced leftward drift ($\lambda_- > \overline{v}$) prevents excessive wandering. For large $\overline{\lambda}$, the benefit fades as long return times dominate.

3) Intermediate $\overline{v} \lesssim 2$*:* Both IR and SR can improve search efficiency, but SR achieves the lowest MFPT for suitable $\overline{\lambda}$. At small $\overline{v}$, diverging trajectories dominate; SR remains effective as long as the target-hitting probability during return (effect d) outweighs the finite return-time penalty (effect c). For very small or very large $\overline{\lambda}$, SR again becomes less efficient.

4) Very low $\overline{v} \ll 2$*:* Most trajectories move away from the target, leading to large return times even at optimal parameters. Instantaneous return is therefore superior here.

5.7 Discussion

In this chapter, we have developed a unified framework for first-passage processes under resetting with stochastic return dynamics, where the return to the origin occurs over a finite time governed by a random process. This generalizes the classical instantaneous resetting models [5, 249, 86, 259] by allowing the searcher to encounter the target even during the return phase. Counterintuitively, we find that such finite-time stochastic

returns can reduce the mean completion time, sometimes performing better than instantaneous returns that take no time at all. To quantify this, we derived two fundamental criteria: the CV criterion, ensuring that stochastic resetting expedites the search relative to the underlying reset-free process, and the SR criterion, which guarantees superiority over the instantaneous return protocol for a given resetting rate. By combining these, we identified a phase space of optimality where stochastic return (SR) emerges as the most efficient search strategy. The physical origin of this improvement lies in the finite probability of target capture during the return motion—an effect absent in instantaneous resetting.

Importantly, we corroborate our theoretical predictions with experimental observations in systems where resetting is implemented by activating a potential trap at the origin, such as in colloidal particle experiments [15, 265]. The data show clear signatures of accelerated search times consistent with our theoretical phase diagram and MFPT scaling. This connection between theory and experiment underscores the practical relevance and testability of stochastic return dynamics.

Our general framework is universal and versatile, offering predictive insights not only for mean search times but also for fluctuations and potentially full distributions. Beyond its analytical merit, it provides a realistic and energetically favorable resetting mechanism, eliminating the need for active tracking or instantaneous repositioning of agents. Such features make SR particularly relevant for practical applications in biochemical search, molecular transport, and robotic exploration [2, 268, 127, 269].

Several promising directions remain open. Extending this study to higher dimensions, multiple targets, or non-diffusive processes could further test the robustness of the SR and CV criteria. Determining the optimal resetting time distribution that globally minimizes the search time under stochastic returns is another outstanding challenge. Overall, this study establishes stochastic return as a powerful and experimentally validated strategy that can outperform both instantaneous resetting and the underlying search process itself.

6

First-passage optimization with collective threshold resetting

(The content of this chapter has been published in [270])

6.1 Introduction

The aim of this chapter is to introduce *target search optimization* under a *threshold resetting* (TR) mechanism. In contrast to the prototypical scenario where resetting is imposed by an external time clock, TR is an event driven phenomenon in which resetting occurs when the system operates under "safety covenant" or broadly, meets certain "threshold rules". Thresholds play a crucial role in governing transitions across numerous systems, acting as critical points that trigger significant changes. In neuroscience, integrate-and-fire neurons accumulate stimuli until their membrane potential crosses a threshold, leading to an action potential before resetting to their initial state [91, 271, 272, 273]. Financial strategies like stop-loss and take-profit rely on preset thresholds to limit losses or secure gains [92, 274, 275, 276]. In software engineering, circuit breakers operate similar to threshold-based reset mechanisms, preventing an application to access an unresponsive server [277, 278, 279]. In physics, fiber bundle models describe how materials distribute stress until a rupture threshold is met, after which the load is redistributed among the remaining fibers [280, 281]. Simple stroboscopic threshold mechanisms have also been employed to obtain sustained temporal regularity in chaotic systems with applications to laser modeling [282, 283, 284, 285].

The concept of event-driven resetting was pioneered by Falcao and Evans [94], who investigated a system of two Brownian particles that reset to their starting positions upon meeting. This scenario is mathematically equivalent to monitoring the distance between the particles and triggering a reset once that distance reaches a threshold of zero. In the recent past, De Bruyne *et al* investigated spatial properties of a single diffusing particle under TR mechanism (referred as *first-passage resetting* there) disclosing dynamic nonstationarity of the process [95, 286]. Yet, another unexplored aspect of the problem

is the *target search optimization* – the study of which is at the heart of this chapter. To put things in perspective, consider a first passage process that is conducted by a group of agents, setting off from a certain location and looking for a target until it is found [35, 36, 287, 288, 289, 290]. The process is, however, restarted at some random time whenever one of the agents reaches a pre-assigned threshold. At that time all the searchers are reset simultaneously to the initial locations from which they renew their search. This collective resetting couples the degrees of freedom and makes the system strongly correlated [291, 292, 293]. Such collective TR mechanism has natural justifications as earlier instances of experiments with fish school [294, 295, 296] and swarming robots [297, 298] have demonstrated event-triggered collective transitions—where a local individual event (such as the detection of a fault or hazard by a single agent) prompts a coordinated adjustment in navigation strategy or "reset" across the population. Similarly, in individuals or groups of agents such as clonal raider ants (*Ooceraea biroi*), sensory thresholds shaped by factors like environment, and external stimuli influence decisions vital for survival and reproduction [299]. Inspired by these connections, this chapter aims to analyze the statistical signatures of the random completion time for this correlated multi-agent search process under threshold controlled resetting. To this end, we develop a unified framework for generic governing dynamics and show that TR can also be used as a potent mechanism to facilitate improved target search dynamics and efficiency. Finally, inspired from the control-management problem, we define a cost objective function that interpolates between the successful search time and the effective penalty owing to resetting events and examine whether this can be minimized.

6.2 General formalism

Consider a system of N non-interacting searchers, each governed by the same stochastic dynamics which is generic, with position coordinates $\{x_i\}$, starting from x_0. The searchers are confined in an interval $[0, L]$ where origin is the target location. If any of the N searchers reaches this target we mark the process complete. The TR mechanism is introduced by placing another boundary at L, which hereafter is referred to as the *threshold* (see Fig. (6.1)). Whenever one of the searchers hits the threshold, all of them are collectively reset to the initial position x_0 from where the search is renewed – for a higher dimensional embedding interpretation, see [1]. This procedure repeats until

[1] One natural way to interpret collective resetting is through the dynamics of a single ballistic searcher in N dimensions, initialized at the point $(x_0, x_0, \ldots, x_0)$. For simplicity, let us consider the case $N = 2$. Imagine a square domain $(0, L) \times (0, L)$ with $0 \leq x_0 \leq L$. The target is located on two adjacent sides of the square: (1) $x_2 = 0$ with $0 \leq x_1 \leq L$, and (2) $x_1 = 0$ with $0 \leq x_2 \leq L$. The threshold, which triggers resetting, is defined by the other two sides: (3) $x_1 = L$ with $0 \leq x_2 \leq L$, and (4) $x_2 = L$ with $0 \leq x_1 \leq L$. A single particle begins at (x_0, x_0) and moves with independently chosen velocities along the x_1 and x_2 directions. If it hits either of the threshold sides, it is reset to the initial point (x_0, x_0) with new velocities — effectively resetting both coordinates *simultaneously*. If it hits one of the target sides, the process ends. This setup allows us to interpret the dynamics of two independent 1D walkers (in our model) as the two components of a single 2D walker undergoing simultaneous resetting. This interpretation generalizes naturally to higher dimensions: N independent walkers correspond to the N components of a single walker in N dimensions, with the simultaneous resetting occurring when any coordinate

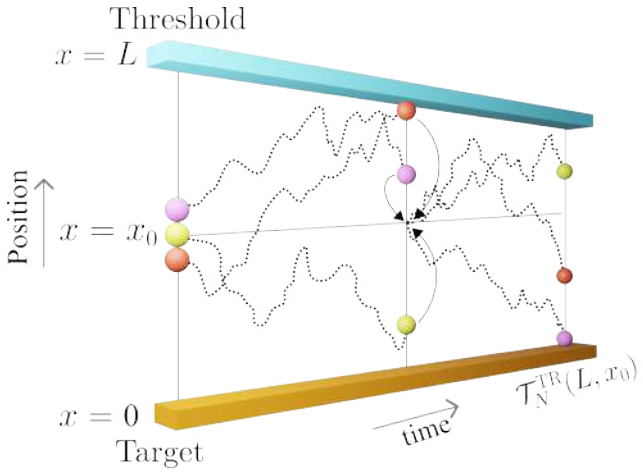

Figure 6.1: *Schematic representation of the TR mechanism with N searchers (here, N = 3) starting from x_0 and undergoing generic stochastic dynamics. The process is considered complete when any of the searchers reaches the target located at the origin, and the corresponding first passage time is denoted by $\mathcal{T}_N^{TR}(L, x_0)$. However, if any searcher reaches the resetting threshold at position L before the target is found, all searchers are collectively returned to their initial positions, and the search process is restarted.*

the target at the origin is found, with the process considered complete as soon as any one searcher locates it. We show that despite the presence of strong correlations, the mean search/first-passage time (MFPT) can be exactly calculated and furthermore, a nontrivial optimization is discovered due to the threshold resetting and the emerging collective nature of the searchers. Note that the model assumes instantaneous information transfer among searchers: whenever one reaches the threshold, all reset simultaneously; likewise, when one finds the target, all are immediately informed and the search ends.

We start by introducing the survival probability under TR as $Q_N^{\mathrm{TR}}(L, x_0, t)$ which estimates the probability that none of the N-particles has found the target at the origin, starting from x_0, up to time t although they may remain confined without hitting the resetting threshold or they can hit the threshold once or multiple times. Summing over all these possibilities, we can write the following renewal equation for the survival probability

$$Q_N^{\mathrm{TR}}(L, x_0, t) = q_N(L, x_0, t) + \int_0^t dt' j_{L,N}(L, x_0, t') Q_N^{\mathrm{TR}}(L, x_0, t - t'), \quad (6.1)$$

where $q_N(L, x_0, t)$ as the survival probability that none of the searchers has hit either of the boundaries at $x = 0$ or $x = L$ up to time t and $j_{L,N}(L, x_0, t')$ is the probability flux at the resetting threshold L from any incoming searcher reaching at time $t' < t$. Eq. (6.1) renders the following interpretation: Starting from x_0, the searchers can survive the target up to time t in two ways. In one plausible set of events, the searchers survive without hitting any of the boundaries which occurs with the probability $q_N(L, x_0, t)$ – this is the "no resetting" scenario and the first term on the RHS. In the second case,

reaches its respective threshold. This provides an intuitive and unified perspective on the simultaneous resetting mechanism explored in our work.

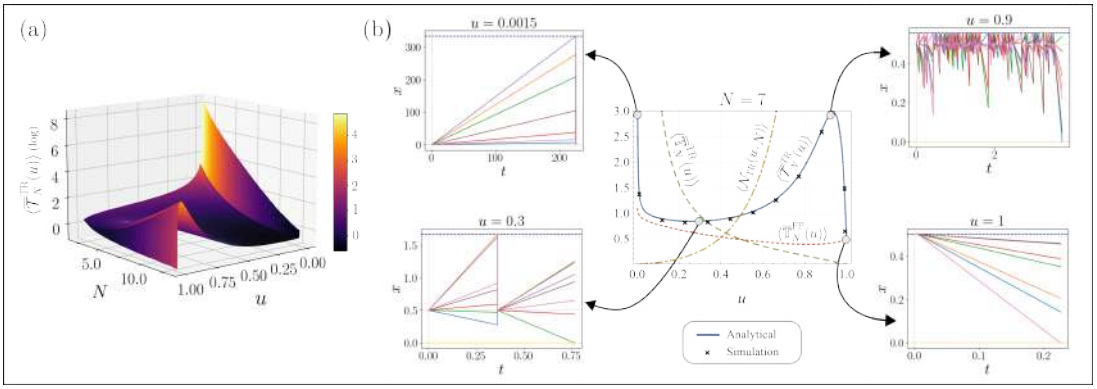

Figure 6.2: *Panel (a): Variation of the scaled MFPT (6.20) with respect to u and N. The plot shows a global minima in the MFPT at $u = 1$ for any $N > 1$. A cross section for $N = 7$ is shown in panel (b). Panel (b) - central figure: Optimization of $\langle \overline{\mathcal{T}}_N^{TR}(u) \rangle$ as a function of u (shown by the solid blue curve) – superimposed with individual components as given by the RHS of (6.23) namely $\langle \mathcal{N}_{TR}(u, N) \rangle$ (shown by orange dotted-dashed line), $\langle \overline{\mathbb{T}}_N^{TR}(u) \rangle$ (shown by green dashed line) and $\langle \overline{\mathbb{T}}_N^{FP}(u) \rangle$ (shown by red dotted line). Simulation results are shown by the cross markers demonstrating an excellent match. The accompanying subpanels showcase typical stochastic trajectories (with x and t standing for the position and time, respectively) generated for different values of u (marked by the circles) showing disparate behavior (global minima, local maxima & minima, divergence) as explained in the main text. In this analysis, we fix $x_0 = 0.5$ and vary L within the range $[0.5, 333.33]$ to explore the regime corresponding to $u \in (0.0015, 1)$.*

whenever any one of the N searchers hits the resetting threshold for the very *first time* (say at t'), all are instantaneously reset to the starting position x_0 renewing the next trial for the search. The contribution for any particle hitting the resetting threshold at L is essentially the flux $j_{L,N}(L, x_0, t')$ followed by the survival probability $Q_N^{\rm TR}(L, x_0, t - t')$ for the remaining duration. Taking the Laplace transform of Eq. (6.1) with respect to t and rearranging, we find

$$\widetilde{Q}_N^{\rm TR}(L, x_0, s) = \frac{\widetilde{q}_N(L, x_0, s)}{1 - \widetilde{j}_{L,N}(L, x_0, s)}, \tag{6.2}$$

where we have defined $\widetilde{Z}(\cdot, s) = \int_0^\infty dt\ e^{-st}\ Z(\cdot, t)$ as the Laplace transform of the function $Z(\cdot, t)$. Eq. (6.2) can be used to obtain all the moments of the completion times. For instance, the MFPT can be defined as

$$\langle \mathcal{T}_N^{\rm TR}(L, x_0) \rangle \equiv \int_0^\infty dt\ Q_N^{\rm TR}(L, x_0, t) = \frac{\langle T_N(L, x_0) \rangle}{\epsilon_0(L, x_0, N)}, \tag{6.3}$$

where $\langle T_N(L, x_0) \rangle = \int_0^\infty dt\ q_N(L, x_0, t)$ is the mean fastest first passage time out of N searchers to reach either the target or the resetting threshold and $\epsilon_0(L, x_0, N) = 1 - \int_0^\infty dt\ j_{L,N}(L, x_0, t)$ is the splitting probability that any of the N searchers reaches the target first before hitting the threshold.

Since the searchers are non-interacting and identical in nature, we can write

$$q_N(L, x_0, t) = [Q(L, x_0, t)]^N \tag{6.4}$$

where $Q(L, x_0, t)$ is the survival probability of a single searcher, starting at $x_0 \in [0, L]$ up to time t, with absorbing boundaries at both 0 and L [300]. On the other hand, $j_{L,N}(L, x_0, t)$ consists of current to the resetting threshold from a single searcher i.e. $j_{L,1}(L, x_0, t)$ barring the rest $N-1$ of them which survive with probability $[Q(L, x_0, t)]^{N-1}$ so that

$$j_{L,N}(L, x_0, t) = N j_{L,1}(L, x_0, t) \, [Q(L, x_0, t)]^{N-1} \, , \tag{6.5}$$

where the factor N accounts for the fact that any of the N searchers can contribute to $j_{L,1}(L, x_0, t)$. Substituting these statistical metrics into Eq. (6.3), we arrive at

$$\langle \mathcal{T}_N^{\rm TR}(L, x_0) \rangle = \frac{\int_0^\infty dt \, [Q(L, x_0, t)]^N}{1 - \int_0^\infty dt \, N j_{L,1}(L, x_0, t) [Q(L, x_0, t)]^{N-1}}, \tag{6.6}$$

which is a general expression for the MFPT and a key result of this chapter. Importantly, the derivation does not rely on specific dynamics of the searchers or target configurations, and moreover, the framework can be generalized to higher-dimensional search processes.

6.3 Ballistic search under TR mechanism

To illustrate the theoretical framework developed above, we examine the paradigmatic case of ballistic searchers with randomized velocity. Such models have been commonly used to describe navigation pattern for some foragers such as microzooplankton, jackals and marine predators [301, 302], to scrutinize optimal strategies for identifying randomly located target sites [303, 304] and also in statistical physics [305, 293, 306, 307, 308]. Crucially, its analytical tractability offers valuable insights that enhance our understanding of TR-facilitated target search processes.

We assume that each ballistic searcher moves with a random initial velocity drawn from a distribution $\phi(v)$. If the target is found *a priori*, the process therein ends. However, if the resetting threshold is encountered prior to the target, all the searchers are simultaneously reset to x_0 following which they draw new random velocities from the same distribution. As outlined above, we first derive the survival probability and the

probability current for a single ballistic searcher (Appendix F.1)

$$Q(L, x_0, t) = \Phi\left(\frac{L - x_0}{t}\right) + \Phi\left(\frac{x_0}{t}\right), \tag{6.7}$$

$$j_{L,1}(L, x_0, t) = \frac{L - x_0}{t^2}\, \phi\left(\frac{L - x_0}{t}\right), \tag{6.8}$$

where $\Phi(v) = \int_0^v dv' \phi(v')$; and substitute these into Eq. (6.6) to obtain the MFPT. Let us now explicitly derive the formula for the MFPT for a single ballistic searcher.

6.3.1 MFPT

MFPT for single searcher ($N = 1$***)***: For symmetric velocity distribution and $N = 1$, we start by deriving the numerator of Eq. (6.6) by setting $N = 1$ which yields the unconditional MFPT for a single particle to reach either the resetting threshold or the target

$$\begin{aligned}\langle T_1(L, x_0)\rangle &= \int_0^\infty dt\; Q(L, x_0, t) \\ &= \int_0^\infty dv\; \phi(v)\left(\frac{L - x_0}{v}\right) + \int_{-\infty}^0 dv\; \phi(v)\left(\frac{x_0}{|v|}\right).\end{aligned} \tag{6.9}$$

Using the symmetry property of the velocity distribution i.e. $\phi(-v) = \phi(v)$, we can further simplify the above equation to find

$$\begin{aligned}\langle T_1(L, x_0)\rangle &= \int_0^\infty dv\; \phi(v)\left(\frac{L - x_0}{v}\right) + \int_0^\infty dv\; \phi(v)\left(\frac{x_0}{v}\right) \\ &= L\int_0^\infty dv\; \frac{\phi(v)}{v}.\end{aligned} \tag{6.10}$$

Let us turn our attention to compute the denominator of Eq. (6.6) for $N = 1$. We first note that it is just the splitting probability $\epsilon_0(L, x_0, 1)$ of a single searcher to reach the target located at the origin before hitting the threshold. For a symmetric velocity distribution, $\epsilon_0(L, x_0, 1)$ is simply $1/2$ since any searcher can acquire a positive (negative) velocity with probability $1/2$ indifferent to the initial coordinate x_0. This can also be seen formally as

$$\begin{aligned}\epsilon_0(L, x_0, 1) &= 1 - \int_0^\infty dt\; j_{L,1}(L, x_0, t) = \int_0^\infty dt\; j_{0,1}(L, x_0, t) \\ &= \int_0^\infty dt\; \frac{x_0}{t^2}\, \phi(x_0/t)s = \frac{1}{2}.\end{aligned} \tag{6.11}$$

Putting together both the numerator and denominator in Eq. (3) of the main text, the

MFPT under TR mechanism for a single searcher takes the form

$$\langle \mathcal{T}_1^{\mathrm{TR}}(L, x_0)\rangle = 2L \int_0^\infty dv\, \frac{\phi(v)}{v}. \tag{6.12}$$

Remarkably, the MFPT does not depend on the starting point x_0 for any symmetric velocity distribution $\phi(v)$. Notably, the integral in Eq. (6.12) converges only when $\phi(v) \to 0$ as $v \to 0$ so that $\phi(v)/v$ becomes integrable around $v = 0$. Simply put, if $\phi(v)$ does not vanish as $v \to 0$, there is a nonzero probability of observing realizations with searchers acquiring an almost vanishing velocity. These searchers will hit either the target or the resetting threshold in an exceedingly large timescale resulting in a divergent MFPT.

MFPT for multiple searchers ($N > 1$): To continue the analysis for multiple searchers, we will assume that the velocities are chosen from a probability distribution given by $\phi(v) = \frac{1}{2v_0} e^{-|v|/v_0}$. While the MFPT for a single searcher is diverging, as evident from Eq. (6.12), the MFPT for the collective walkers e.g., $N \geq 2$ turns out to be a finite quantity. For the exponential kernel, the MFPT can be scaled as $\langle \overline{\mathcal{T}}_N^{\mathrm{TR}}(u \equiv \frac{x_0}{L})\rangle = \frac{v_0}{x_0}\langle \mathcal{T}_N^{\mathrm{TR}}(L, x_0)\rangle = \mathcal{F}(u, N)$, where $\mathcal{F}$ is the scaling function and depends only on N and a dimensionless ratio $0 \leq u \leq 1$. First note that, for the exponential velocity distribution $\phi(v) = \frac{1}{2v_0} e^{-|v|/v_0}$, we have $\Phi(v) = \frac{1}{2}\left(1 - e^{-v/v_0}\right)$. We define the following variables

$$u = x_0/L, \quad \tau_b = L/v_0, \tag{6.13}$$

where τ_b is the timescale of a ballistic walker with speed v_0. The dimensionless variable u effectively governs the frequency of resetting. For instance, the limit $u \to 1$ corresponds to *high resetting frequency* where the searchers start close to the threshold ($L \to x_0$), while $u \to 0$ captures the *low frequency* regime where the threshold is practically at infinity ($L \to \infty$). Using Eq. (6.7) and Eq. (6.8), we can now compute the survival probability and the currents to the resetting threshold and the target respectively which take the following form

$$Q(u, t) = 1 - \frac{1}{2}\exp\left(-\frac{\tau_b(1-u)}{t}\right) - \frac{1}{2}\exp\left(-\frac{\tau_b u}{t}\right), \tag{6.14}$$

$$j_{L,1}(u, t) = \frac{\tau_b(1-u)}{2t^2}\exp\left(-\frac{\tau_b(1-u)}{t}\right), \tag{6.15}$$

$$j_{0,1}(u, t) = \frac{\tau_b u}{2t^2}\exp\left(-\frac{\tau_b u}{t}\right). \tag{6.16}$$

We now recall that the splitting probability for any of the N particles to hit the target is

given by

$$\begin{aligned}\epsilon_0(L,x_0,N) &= 1-\int_0^\infty dt\ j_{L,N}(L,x_0,t)\\ &= 1-\int_0^\infty dt\ N j_{L,1}(L,x_0,t)[Q(L,x_0,t)]^{N-1}\\ &= \int_0^\infty dt\ N j_{0,1}(L,x_0,t)[Q(L,x_0,t)]^{N-1}. \end{aligned} \tag{6.17}$$

Plugging the results from Eq. (6.14)-(6.17) into Eq. (6.6), we find

$$\langle \mathcal{T}_N^{\rm TR}(L,x_0)\rangle = \frac{\int_0^\infty dt\ \left[1-\frac{1}{2}\exp\left(-\frac{[1-u]\tau_b}{t}\right)-\frac{1}{2}\exp\left(-\frac{\tau_b u}{t}\right)\right]^N}{\int_0^\infty dt\ N\left[\frac{\tau_b u}{2t^2}\exp\left(-\frac{u\tau_b}{t}\right)\right]\left[1-\frac{1}{2}\exp\left(-\frac{[1-u]\tau_b}{t}\right)-\frac{1}{2}\exp\left(-\frac{\tau_b u}{t}\right)\right]^{N-1}}. \tag{6.18}$$

Now we make the change of variable as $t\to\frac{\tau_b}{t}$ to obtain

$$\langle \mathcal{T}_N^{\rm TR}(L,x_0)\rangle = \frac{\tau_b\int_0^\infty dt\ \left[1-\frac{1}{2}\exp\left(-\frac{1-u}{t}\right)-\frac{1}{2}\exp\left(-\frac{u}{t}\right)\right]^N}{Nu\int_0^\infty dt\ \left[\frac{1}{2t^2}\exp\left(-\frac{u}{t}\right)\right]\left[1-\frac{1}{2}\exp\left(-\frac{1-u}{t}\right)-\frac{1}{2}\exp\left(-\frac{u}{t}\right)\right]^{N-1}}. \tag{6.19}$$

Noting $\tau_b=\frac{1}{u}\frac{x_0}{v}$ from Eq. (6.13) and substituting into the above expression for MFPT, we find

$$\begin{aligned}\langle \mathcal{T}_N^{\rm TR}(L,x_0)\rangle &= \frac{\frac{x_0}{v}\int_0^\infty dt\ \left[1-\frac{1}{2}\exp\left(-\frac{1-u}{t}\right)-\frac{1}{2}\exp\left(-\frac{u}{t}\right)\right]^N}{Nu^2\int_0^\infty dt\ \left[\frac{1}{2t^2}\exp\left(-\frac{u}{t}\right)\right]\left[1-\frac{1}{2}\exp\left(-\frac{1-u}{t}\right)-\frac{1}{2}\exp\left(-\frac{u}{t}\right)\right]^{N-1}},\\ \implies \mathcal{F}(u,N) &= \frac{v_0}{x_0}\langle \mathcal{T}_N^{\rm TR}(L,x_0)\rangle\\ &= \frac{\int_0^\infty dt\ \left[1-\frac{1}{2}\exp\left(-\frac{1-u}{t}\right)-\frac{1}{2}\exp\left(-\frac{u}{t}\right)\right]^N}{Nu^2\int_0^\infty dt\ \left[\frac{1}{2t^2}\exp\left(-\frac{u}{t}\right)\right]\left[1-\frac{1}{2}\exp\left(-\frac{1-u}{t}\right)-\frac{1}{2}\exp\left(-\frac{u}{t}\right)\right]^{N-1}}. \end{aligned} \tag{6.20}$$

For $N=2$, a closed form expression can be obtained following a non-trivial computation (Appendix F.2)

$$\mathcal{F}(u,2)=\frac{2}{u\,(3-2u)}\left[\ln 2-u\,\ln u-(1-u)\,\ln(1-u)\right], \tag{6.21}$$

while for $N>2$, we can extract the following asymptotic forms which will be useful in

later analysis

$$\mathcal{F}(u,N) \approx \begin{cases} \frac{a_N}{2^N-1}\frac{1}{u} & \text{as} \quad u \to 0 \\ a_N - N\,(1-u)\,\ln(1-u) & \text{as} \quad u \to 1, \end{cases} \tag{6.22}$$

where $a_N = \int_0^\infty \frac{dx}{x^2}\,(1-e^{-x})^N$ is a constant. The scaling function $\mathcal{F}(u,N)$, evaluated as a function of u for fixed N, diverges as $u \to 0$, and decreases monotonically with increasing u when $N < 4$. Interestingly, for $N \geq 4$, the function exhibits non-monotonic behavior: it first develops a local minimum, followed by a local maximum, and eventually approaches a global minimum as $u \to 1$, see Fig. (6.2)(a) and a representative case for $N = 7$ in Fig. (6.2)(b) (solid curve).

Optimization and limiting behavior of the MFPT.– To study the optimal behavior, we rewrite the MFPT by summing over the stochastic timescales

$$\langle \overline{\mathcal{T}}_N^{\rm TR}(u)\rangle = \langle \mathcal{N}_{\rm TR}(u,N)\rangle \times \langle \overline{\mathbb{T}}_N^{\rm TR}(u)\rangle + \langle \overline{\mathbb{T}}_N^{\rm FP}(u)\rangle, \tag{6.23}$$

where $\langle \mathcal{N}_{\rm TR}(u,N)\rangle = \frac{1-\epsilon_0(u,N)}{\epsilon_0(u,N)}$ is the mean number of TR events up to the completion, and $\langle \overline{\mathbb{T}}_N^{\rm TR}(u)\rangle$ is the mean conditional waiting time between consecutive TR events and $\langle \overline{\mathbb{T}}_N^{\rm FP}(u)\rangle$ is the mean time for the first-passage to the target conditioned on *no* TR events. Numerical plots of these quantities are given in Fig. (6.2)(b) (explicit calculations in Appendix F.4).

In the limit $u \to 1$ when the resetting threshold is at the closest proximity to x_0, the resetting events are frequent and we find $\langle \mathcal{N}_{\rm TR}(u \to 1, N)\rangle = 2^N - 1$. However, since all such resetting events consume almost no time with $\langle \overline{\mathbb{T}}_N^{\rm TR}(u \to 1)\rangle \to 0$, the cumulative contribution to the MFPT from TR events becomes almost negligible. Notably, the finite contribution to the MFPT in this case comes solely from those correlated events where all the ballistic searchers collectively sample negative velocities right after the resetting or at the inception to drift right toward the target, marking a successful completion. Thus, $\langle \overline{\mathbb{T}}_N^{\rm FP}(u \to 1)\rangle$ effectively contributes to the MFPT whose asymptotic form is given by Eq. (6.22). The typical trajectories in this limit (see the bottom-right panel in Fig. (6.2)b) confirm this observation. Quite interestingly, this emergent global optimality at $u \to 1$ aligns with a widely used threshold control strategy in chaos theory [282, 285].

However, when the searchers start from a finite distance away from the resetting threshold ($u \lessapprox 1$), $\langle \overline{\mathbb{T}}_N^{\rm TR}(u)\rangle$ become finite (recall that it is exactly zero for the $u \to 1$ limit) and $\langle \mathcal{N}_{\rm TR}(u,N)\rangle$ remains large enough so that the first term in Eq. (6.23) dominates the MFPT leading to the local maxima observed in Fig. (6.2)(b) (corresponding trajectories shown in the top-right figure for $u = 0.9$). Further tuning initial configuration of the searchers in the direction of the target (i.e. reducing u further) ensures $\epsilon_0 > 1/2$ and subsequently, we see a gradual decrease in the MFPT up to a local minimum. Stochastic realizations at the bottom-left of Fig. (6.2)(b) depict this scenario.

Moreover, in the limit $u \to 0$ where the threshold is far away from the starting position, each searcher can acquire a positive or negative velocity with probability $1/2$ for the symmetric velocity distribution and thus, there is a finite probability $\frac{1}{2^N}$ that all the N-searchers possess a positive velocity that is away from the target. The probability of selecting a unfavorable positive velocity, albeit vanishingly small, remains finite and yield in MFPT with a diverging form $\sim 1/u$ given by Eq. (6.22) (Appendix F.3). Contributing realizations (for instance, shown in the top-left panel in Fig. (6.2)b for $u = 0.0015$) corroborate this observation.

6.4 First-passage distribution as optimality

In this section, we present a detailed study of the FPT density of the collective search in the absence and presence of threshold resetting. The large time behavior of the FPT density becomes particularly useful to understand and compare the first-passage time moments between the processes.

6.4.1 FPT distribution of the ballistic searchers without TR ($u \to 0$)

The survival probability for a single ballistic searcher (starting from x_0 and target at $x = 0$) in absence of the threshold is given by

$$\begin{aligned} Q_0(x_0, t) &= \int_0^\infty dv\ \phi(v) + \int_{-\infty}^0 dv\ \phi(v)\ \theta(x_0 - |v|t) \\ &= \frac{1}{2} + \int_0^{\frac{x_0}{t}} dv\ \phi(v) \\ &= \frac{1}{2} + \Phi\left(\frac{x_0}{t}\right). \end{aligned} \tag{6.24}$$

Thus, the survival probability for N independent ballistic searchers are given by

$$Q_0^N(x_0, t) = [Q_0(x_0, t)]^N = \left[\frac{1}{2} + \Phi\left(\frac{x_0}{t}\right)\right]^N, \tag{6.25}$$

which can be used to deduce the FPT distribution as follows

$$\begin{aligned} f_{T_0}(x_0, t) &= -\frac{\partial Q_0^N(x_0, t)}{\partial t} \\ &= N\left[\frac{1}{2} + \Phi\left(\frac{x_0}{t}\right)\right]^{N-1}\left[\frac{x_0}{t^2}\phi\left(\frac{x_0}{t}\right)\right]. \end{aligned} \tag{6.26}$$

For the exponential velocity distribution i.e., $\phi(v) = \frac{1}{2v_0}e^{-v/v_0}$ we have $\Phi(v) = \frac{1}{2}(1 - e^{-v/v_0})$. Finally plugging this expressions into the above results (setting $v_0 = 1$ without

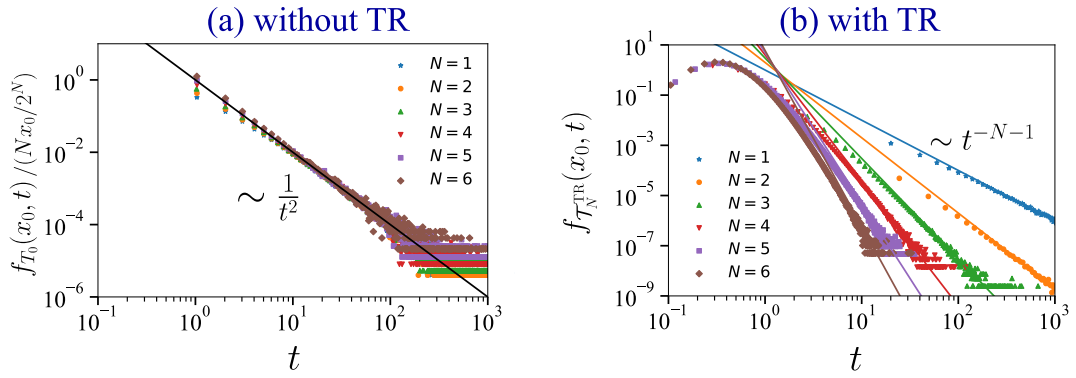

Figure 6.3: *(a) The scaled FPT density $f_{T_0}(x_0,t)/\frac{Nx_0}{2^N}$ for the ballistic searchers (without TR) exhibits $\sim 1/t^2$ decay for any values of N. The markers represents results from numerical simulation. The solid black line is the asymptotic result as in Eq. (6.28). (b) The FPT density $f_{\mathcal{T}_N^{TR}}(L = x_0, t)$ under optimal TR. Note that the tail exponent becomes N-dependent in this case as mentioned in the main text – see Eq. (6.35).*

loss of generality) we have

$$f_{T_0}(x_0,t) = N\left(1-\frac{1}{2}e^{-x_0/t}\right)^{N-1}\left(\frac{x_0}{2t^2}e^{-x_0/t}\right). \tag{6.27}$$

In the limit $t \to \infty$ it has the following asymptotic behavior

$$f_{T_0}(x_0, t\to\infty) \sim \frac{Nx_0}{2^N t^2}. \tag{6.28}$$

The exponent of t at asymptotic limit is 2 (i.e., N independent) leading to a diverging MFPT for any given values of N. The variation of the FPT density with t is shown in Fig. 6.3(a) which shows an excellent agreement with numerical simulations.

6.4.2 FPT distribution of the ballistic searchers under optimal TR

We have noted from the main text that the optimal MFPT occurs for the ballistic case when $u = 1$ so that $L = x_0$. In here, we provide an exact derivation for the FPT distribution of the ballistic searchers at this optimality. To this end, we start from the renewal equation for the survival probability as in Eq. (6.1). At the optimal case of $u = 1$ or $L = x_0$, the particles can survive in two possible ways. First is the the no-resetting case in which the survival probability is simply $q_N(L = x_0) = [Q(L,t)]^N$. In the other possible scenario, one or multiple resetting events can happen. This implies that at least one of the searchers will attain a positive velocity so that resetting will surely take place – the probability of such occurrence is given by $1 - \frac{1}{2^N}$. Since the resetting here takes no time to occur as $u = 1$, the probability current is simply given $j_{L,N}(L = x_0, t') = \left(1 - \frac{1}{2^N}\right)\delta(t')$, where $\delta(t')$ is the Dirac-delta function. Combining both these possibilities, the renewal equation for the survival probability at $L = x_0$ takes

the form

$$Q_N^{\mathrm{TR}}(L = x_0, t) = [Q(L, t)]^N + \left(1 - \frac{1}{2^N}\right) Q_N^{\mathrm{TR}}(L = x_0, t). \tag{6.29}$$

Rearranging, we obtain an exact expression for the survival probability at the optimality i.e. $L = x_0$ as

$$Q_N^{\mathrm{TR}}(L = x_0, t) = [2Q(L, t)]^N, \tag{6.30}$$

which is a very interesting result since it holds for arbitrary symmetric velocity distribution of the ballistic searchers. The single particle survival probability $Q(L = x_0, t)$ for a symmetric velocity distribution is given by

$$Q(L, t) = \Phi\left(\frac{L}{t}\right), \tag{6.31}$$

where $\Phi(v) = \int_0^v dv\phi(v)$. Thus the survival probability has the final form

$$Q_N^{\mathrm{TR}}(L = x_0, t) = \left[2\Phi\left(\frac{L}{t}\right)\right]^N. \tag{6.32}$$

Recall that, for the exponential velocity distribution i.e., $\phi(v) = \frac{1}{2v_0} e^{-v/v_0}$ we have $\Phi(v) = \frac{1}{2}(1 - e^{-v/v_0})$. Thus the survival probability in this case has the form (setting $v_0 = 1$ without any loss of generality)

$$Q_N^{\mathrm{TR}}(L = x_0, t) = \left(1 - e^{-L/t}\right)^N, \tag{6.33}$$

from which the FPT distribution can be obtained via the relation $f_{\mathcal{T}_N^{\mathrm{TR}}}(L = x_0, t) = -\frac{\partial Q_N^{\mathrm{TR}}(L=x_0,t)}{\partial t}$ and is given by

$$f_{\mathcal{T}_N^{\mathrm{TR}}}(L = x_0, t) = \frac{NL}{t^2} e^{-L/t} \left(1 - e^{-L/t}\right)^{N-1}, \tag{6.34}$$

with the following asymptotic behavior

$$f_{\mathcal{T}_N^{\mathrm{TR}}}(L = x_0, t) \sim NL^N t^{-N-1} \text{ as } t \to \infty. \tag{6.35}$$

Thus the distribution of the FPT distribution under optimal TR for the ballistic walkers with exponential velocities follows a power tail $\sim t^{-N-1}$. This exponent makes sure that the MFPT is finite immediately when $N \geq 2$. This result is verified against numerical simulations and is shown in Fig. 6.3(b).

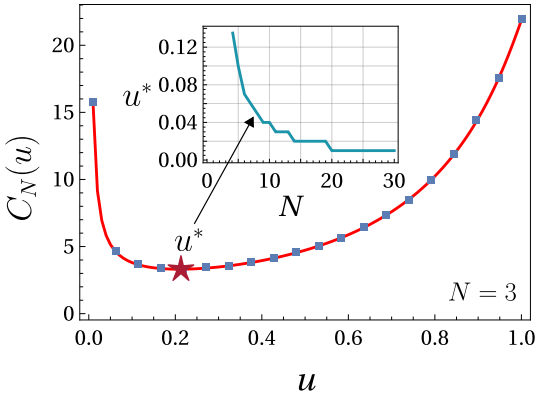

Figure 6.4: *Behavior of the cost function with respect to $u = x_0/L$ for $N = 3$ and $\beta = 1$. The cost attains a minimum at an optimal u^* – the variation of which as a function of N is shown in the inset panel. The squares represent data from simulations.*

6.5 Cost of TR mechanism

A central quest in the resetting discipline is to harness the cost, whether it be dynamic [95, 309, 310] or thermodynamic [14, 311, 312, 32, 264], of the overall process. Imitating the penalty during a power grid breakdown [313, 314], we posit, for each resetting event, a cost that is proportional to the MFPT as well as the total number of TR events. Henceforth, the goal is to determine the optimal operation of this system, for which the cost function

$$C_N(u) = \langle \overline{\mathcal{T}}_N^{\mathrm{TR}}(u) \rangle + \beta N \langle \mathcal{N}_{\mathrm{TR}}(u, N) \rangle, \tag{6.36}$$

is minimal. Here, β is a constant that can be thought of cost per resetting event for a single particle and thus, we multiply by N to enumerate the total cost for the "reset operation". For the ballistic searchers, Fig. (6.4) shows that $C_N(u)$ attains a minimum for an optimal $u = u^*$ for a fixed N. Note that unlike the MFPT, the cost function is not globally minimized at $u \to 1$ since in this limit the resetting frequency is significantly high and the second term in Eq. (6.36) dominates. On the other hand, if the resetting threshold is far away from the starting position, the MFPT gradually increases, contributing to diverging cost. In the inset of Fig. (6.4), we show the variation of u^* with respect to N, further noting that large number of searchers can systematically reduce the optimal distance $u^* \to 0$. Evidently, this collective cost optimization is different than that of the MFPT, indicating that a judicious choice of optimal u can leverage to a decision based biasing between the MFPT and the cost function.

6.6 Conclusions

Motivated by threshold-driven phenomena that refer to processes or events that occur only when a system surpasses a critical threshold, we study the first passage properties of an arbitrary search dynamics under threshold resetting mechanism.We develop a general

theoretical framework and study the optimization properties of the MFPT which is a useful metric in learning the efficiency of a target search process. The optimization reported here also resonates with the performance maximization by the agents (robots or foraging animals) that collaborate and achieve tasks (for instance finding the desired target between many competitive ones by a fish school in [295]) in an optimal way.

In a classical foraging model where the searchers move ballistically, we discover a non-trivial optimization that suggests that persistent resetting to the threshold can render the MFPT globally minimum – an effect reminiscent to the threshold mechanism in nonlinear chaotic systems [282, 285]. By defining a cost function for such systems, we further demonstrate that the collective TR mechanism can achieve optimal cost.

To extend the formalism to capture more realistic scenarios, we can incorporate an overhead time for information transfer. This can be done in two ways: First, we can add a random (or deterministic) information passing time $\mathcal{T}^O$ whenever a searcher hits the threshold, after which all of them are reset to the initial position. In this case, one can show that the overall MFPT of the system would increase (however, this computation excludes the time required to transfer information to the others once a searcher successfully locates the target). A more involved extension would be to consider space–time coupled return protocols, where after a TR event searchers return to the initial configuration via finite-time spatial dynamics [86, 14, 251].

Finally, it is worth noting that the formalism can also be applied to extract higher order moments of the search time in higher dimensions and to the dynamics of non-coordinate variables like a fluctuating potential as in the case of firing neurons where the membrane potential of an individual synapse can reset after reaching a critical value [91, 273]. Ongoing works also include characterizing nonequilibrium stationary states for such long-range systems under TR. Given its simple implementation yet achieving target functionality makes the TR mechanism a promising avenue in the target search problem which can have far reaching implications beyond statistical physics to foraging, control theory, finance, structural failure-repair analysis and in computing systems.

7
Conclusions

The focus of this thesis was threefold: i) application and effects of stochastic resetting on physical in a variety of processes, namely, chemical reactions, operations research and viscoelastic media, ii) a unified renewal approach to experimental realisation of resetting, and iii) proposing a novel FP optimization strategy based on threshold resetting. In the following, we summarise the primary results emanated out of this thesis.

The chapters 2-4 are dedicated to the understanding of applications of resetting in several fields. In Chapter 2, we study how a gated chemical reaction can be facilitated with resetting. Resetting a chemical reaction refers to the unbinding of the enzyme-substrate complex, after which the reaction is started afresh. As a primary result, we find, a certain unbinding rate can indeed expedite the product formation of a chemical reaction, especially when the target is 'gated' in nature, which models the active-inactive phase of the substrate. We modelled the chemical reaction with a one-dimensional drift-diffusion process with a gated target. By doing so, we find a parameter space in terms of diffusion and drift coefficients where the reaction rate can be enhanced with stochastic resetting. In Chapter 3, we discuss how service resetting can reduce the queue length. Considering the vast fields of applications of queuing theory, strategies to effectively manage a queue remain a pivotal challenge. With analytical formulations, we explicitly find the mean queue length of an M/G/1 queue subjected to the service resetting strategy, where resetting consumes a random period of overhead time. We show that depending on the fluctuations of the overhead time, one can suitably choose an optimal resetting rate that can reduce the mean queue length to its best. Furthermore, we find that periodic resetting does a better optimization in contrast to resetting at random times. In Chapter 4 we study the effects of resetting in a particle embedded in a viscoelastic medium. Viscoelastic medium are different from the traditional viscous medium since the collisions between the particles are not forgotten instantaneously. Due to the memory dependence of the particle's trajectory, the system is highly non-Markovian in nature. Our study reveals that, resetting a particle in such a medium generates non-trivial non-equilibrium steady states and correlations. It also gives rise to a resetting rate-dependent timescale

in the system that can help the external agent to gain control over the dynamics of the particle in such a highly non-Markovian system.

In Chapter 5, we propose an experimentally amenable approach to stochastic resetting. Although the idea of resetting being a subject to extensive studies, a majority of them (along with the models considered in the previous section) consider resetting to be an instantaneous event. In reality, a resetting event is space-time coupled so that a finite time is consumed when the particle heads back to the starting position. We propose a universal framework of stochastic resetting where the agent returns to the starting position in a space-time coupled non-instantaneous fashion. By considering the paradigmatic example of diffusion, we show that a stochastic component in the return motion of the particle can indeed enhance the search efficiency in a FP process. Furthermore, we corroborate our theory with experimental parameters and identify suitable parameter regimes where stochastic return can indeed be beneficial than the classical instantaneous return. By adding a drift to the particle dynamics, we also show that stochastic return can outperform the underlying reset-free process as well as the optimal instantaneous return protocol. In summary, we demonstrate that search with stochastic returns provides not only a physically realizable approach to resetting but also can be more advantageous.

In Chapter 6, we propose a novel approach to the collective search process optimization based on threshold resetting. Under this set-up, the system resets only when any one of many searchers hits a pre-defined threshold value. Although the resetting epochs are still stochastic in time, it is now governed by some space-dependent threshold, leading to an event-driven process resetting strategy. We explicitly analyse the effect of such a resetting strategy in a multi-agent search process. Note that all the search agents are reset to the initial position at each resetting epoch, which introduces long-range correlations among the searchers. We show that the mean FPT of the process shows rich optimisation features with respect to the threshold distance and the number of searchers. We also quantify the cost of maintaining such a threshold-dependent search process and find an interesting optimisation of the cost function.

Despite the extensive progress achieved through the studies presented in this thesis, stochastic resetting continues to be a fertile ground for exploration. Its remarkable ability to induce nonequilibrium steady states, optimise search and reaction efficiencies, and generate novel dynamical correlations underscores its fundamental and applied importance. Future studies could explore resetting in systems with spatial or temporal disorder, active matter, and biological networks, where feedback-controlled or adaptive resetting rules may yield richer dynamics. Moreover, extending resetting concepts to quantum systems, machine learning algorithms, or complex supply-chain models could open exciting interdisciplinary avenues. The insights obtained here not only advance our understanding of resetting as a universal control mechanism but also lay the groundwork for its potential exploitation in experimental and technological contexts—from microscale transport processes to large-scale optimisation problems.

This page intentionally left blank.

References

[1] Shlomi Reuveni, Michael Urbakh, and Joseph Klafter. “Role of substrate unbinding in Michaelis–Menten enzymatic reactions”. In: *Proceedings of the National Academy of Sciences* 111.12 (2014), pp. 4391–4396.

[2] Olivier Bénichou et al. “Intermittent search strategies”. In: *Reviews of Modern Physics* 83.1 (2011), p. 81.

[3] Ilya Loshchilov and Frank Hutter. “SGDR: Stochastic Gradient Descent with Warm Restarts”. In: *ICLR (Poster)*. 2017. URL: https://openreview.net/forum?id=Skq89Scxx.

[4] Emily Baird et al. “The dung beetle dance: an orientation behaviour?” In: *PloS one* 7.1 (2012), e30211.

[5] Martin R. Evans and Satya N. Majumdar. “Diffusion with Stochastic Resetting”. In: *Physical Review Letters* 106 (2011), p. 160601.

[6] Albert Einstein. “Über die von der molekularkinetischen Theorie der Wärme geforderte Bewegung von in ruhenden Flüssigkeiten suspendierten Teilchen”. In: *Annalen der physik* 4 (1905).

[7] Satya N Majumdar, Sanjib Sabhapandit, and Grégory Schehr. “Dynamical transition in the temporal relaxation of stochastic processes under resetting”. In: *Physical Review E* 91.5 (2015), p. 052131.

[8] Arnab Pal. “Diffusion in a potential landscape with stochastic resetting”. In: *Physical Review E* 91.1 (2015), p. 012113.

[9] RK Singh, R Metzler, and T Sandev. “Resetting dynamics in a confining potential”. In: *Journal of Physics A: Mathematical and Theoretical* 53.50 (2020), p. 505003.

[10] Somrita Ray and Shlomi Reuveni. “Diffusion with resetting in a logarithmic potential”. In: *The Journal of chemical physics* 152.23 (2020).

[11] Apoorva Nagar and Shamik Gupta. “Diffusion with stochastic resetting at power-law times”. In: *Physical Review E* 93.6 (2016), p. 060102.

[12] Mattia Radice. “Diffusion processes with Gamma-distributed resetting and non-instantaneous returns”. In: *Journal of Physics A: Mathematical and Theoretical* 55.22 (2022), p. 224002.

[13] Arnab Pal, Anupam Kundu, and Martin R Evans. “Diffusion under time-dependent resetting”. In: *Journal of Physics A: Mathematical and Theoretical* 49 (2016), p. 225001.

[14] Ofir Tal-Friedman et al. “Experimental realization of diffusion with stochastic resetting”. In: *The Journal of Physical Chemistry Letters* 11.17 (2020), pp. 7350–7355.

[15] Benjamin Besga et al. “Optimal mean first-passage time for a Brownian searcher subjected to resetting: experimental and theoretical results”. In: *Physical Review Research* 2.3 (2020), p. 032029.

[16] Somnath Paramanick et al. “Uncovering universal characteristics of homing paths using foraging robots”. In: *PRX Life* 2.3 (2024), p. 033007.

[17] Martin R. Evans, Satya N. Majumdar, and Grégory Schehr. “Stochastic resetting and applications”. In: *Journal of Physics A: Mathematical and Theoretical* 53 (2020), p. 193001.

[18] Martin R Evans and Satya N Majumdar. “Run and tumble particle under resetting: a renewal approach”. In: *Journal of Physics A: Mathematical and Theoretical* 51.47 (2018), p. 475003.

[19] Vijay Kumar, Onkar Sadekar, and Urna Basu. “Active Brownian motion in two dimensions under stochastic resetting”. In: *Physical Review E* 102.5 (2020), p. 052129.

[20] Andrea Falcón-Cortés et al. “Localization transition induced by learning in random searches”. In: *Physical review letters* 119.14 (2017), p. 140603.

[21] Vicenç Méndez and Daniel Campos. “Characterization of stationary states in random walks with stochastic resetting”. In: *Physical Review E* 93.2 (2016), p. 022106.

[22] Alejandro P Riascos et al. “Random walks on networks with stochastic resetting”. In: *Physical Review E* 101.6 (2020), p. 062147.

[23] Hanshuang Chen and Yanfei Ye. “Random walks on complex networks under time-dependent stochastic resetting”. In: *Physical Review E* 106.4 (2022), p. 044139.

[24] Tian Zhou, Pengbo Xu, and Weihua Deng. “Continuous-time random walks and Lévy walks with stochastic resetting”. In: *Physical Review Research* 2.1 (2020), p. 013103.

[25] Vicenç Méndez et al. “Continuous time random walks under Markovian resetting”. In: *Physical Review E* 103.2 (2021), p. 022103.

[26] Matteo Magoni, Satya N Majumdar, and Grégory Schehr. “Ising model with stochastic resetting”. In: *Physical Review Research* 2.3 (2020), p. 033182.

[27] Ruoyu Yin and Eli Barkai. “Restart expedites quantum walk hitting times”. In: *Physical Review Letters* 130.5 (2023), p. 050802.

[28] B Mukherjee, K Sengupta, and Satya N Majumdar. “Quantum dynamics with stochastic reset”. In: *Physical Review B* 98.10 (2018), p. 104309.

[29] Manas Kulkarni and Satya N Majumdar. “Generating entanglement by quantum resetting”. In: *Physical Review A* 108.6 (2023), p. 062210.

[30] Gabriele Perfetto et al. “Designing nonequilibrium states of quantum matter through stochastic resetting”. In: *Physical Review B* 104.18 (2021), p. L180302.

[31] Dominic C Rose et al. “Spectral properties of simple classical and quantum reset processes”. In: *Physical Review E* 98.2 (2018), p. 022129.

[32] Deepak Gupta, Carlos A Plata, and Arnab Pal. “Work fluctuations and Jarzynski equality in stochastic resetting”. In: *Physical Review Letters* 124.11 (2020), p. 110608.

[33] Jaco Fuchs, Sebastian Goldt, and Udo Seifert. “Stochastic thermodynamics of resetting”. In: *Europhysics Letters* 113.6 (2016), p. 60009.

[34] Arnab Pal and Saar Rahav. “Integral fluctuation theorems for stochastic resetting systems”. In: *Physical Review E* 96.6 (2017), p. 062135.

[35] Sidney Redner. *A Guide to First-Passage Processes*. Cambridge University Press, 2001.

[36] Alan J Bray, Satya N Majumdar, and Grégory Schehr. “Persistence and first-passage properties in nonequilibrium systems”. In: *Advances in Physics* 62.3 (2013), pp. 225–361.

[37] Tom Chou and Maria R D’Orsogna. “First passage problems in biology”. In: *First-passage phenomena and their applications*. World Scientific, 2014, pp. 306–345.

[38] Olivier Bénichou et al. “Geometry-controlled kinetics”. In: *Nature Chemistry* 2.6 (2010), pp. 472–477.

[39] Attila Szabo, Klaus Schulten, and Zan Schulten. “First passage time approach to diffusion controlled reactions”. In: *The Journal of chemical physics* 72.8 (1980), pp. 4350–4357.

[40] Cordula V Mora et al. “Magnetoreception and its trigeminal mediation in the homing pigeon”. In: *Nature* 432.7016 (2004), pp. 508–511.

[41] Hans G Wallraff. “Navigation by homing pigeons: updated perspective”. In: *Ethology Ecology & Evolution* 13.1 (2001), pp. 1–48.

[42] Charles Walcott. “Pigeon homing: observations, experiments and confusions”. In: *Journal of Experimental Biology* 199.1 (1996), pp. 21–27.

[43] Michael Luby, Alistair Sinclair, and David Zuckerman. “Optimal speedup of Las Vegas algorithms”. In: *Information Processing Letters* 47.4 (1993), pp. 173–180.

[44] Petar Jolakoski et al. “A first passage under resetting approach to income dynamics”. In: *Chaos, Solitons & Fractals* 175 (2023), p. 113921.

[45] Charles E Billings. *Aviation automation: The search for a human-centered approach*. CRC Press, 2018.

[46] Frederic Bartumeus et al. “Animal search strategies: a quantitative random-walk analysis”. In: *Ecology* 86.11 (2005), pp. 3078–3087.

[47] W John O’brien, Howard I Browman, and Barbara I Evans. “Search strategies of foraging animals”. In: *American Scientist* 78.2 (1990), pp. 152–160.

[48] Shan He, Q Henry Wu, and Jon R Saunders. “Group search optimizer: an optimization algorithm inspired by animal searching behavior”. In: *IEEE transactions on evolutionary computation* 13.5 (2009), pp. 973–990.

[49] Leonid Mirny et al. “How a protein searches for its site on DNA: the mechanism of facilitated diffusion”. In: *Journal of Physics A: Mathematical and Theoretical* 42.43 (2009), p. 434013.

[50] Olivier Bénichou et al. “Facilitated diffusion of proteins on chromatin”. In: *Physical review letters* 106.3 (2011), p. 038102.

[51] Michael A Lomholt et al. “Lévy strategies in intermittent search processes are advantageous”. In: *Proceedings of the National Academy of Sciences* 105.32 (2008), pp. 11055–11059.

[52] Martin R Evans and Satya N Majumdar. “Diffusion with optimal resetting”. In: *Journal of Physics A: Mathematical and Theoretical* 44.43 (2011), p. 435001.

[53] Arnab Pal and Shlomi Reuveni. “First Passage under Restart”. In: *Physical Review Letters* 118 (2017), p. 030603.

[54] Shlomi Reuveni. “Optimal stochastic restart renders fluctuations in first passage times universal”. In: *Physical review letters* 116.17 (2016), p. 170601.

[55] A Chechkin and IM3845437 Sokolov. “Random search with resetting: a unified renewal approach”. In: *Physical Review Letters* 121.5 (2018), p. 050601.

[56] Pallabi Chatterjee, S Aravinda, and Ranjan Modak. “Quest for optimal quantum resetting: Protocols for a particle on a chain”. In: *Physical Review E* 110.3 (2024), p. 034132.

[57] Ofir Blumer, Shlomi Reuveni, and Barak Hirshberg. “Combining stochastic resetting with Metadynamics to speed-up molecular dynamics simulations”. In: *Nature Communications* 15.1 (2024), p. 240.

[58] Ofir Blumer, Shlomi Reuveni, and Barak Hirshberg. “Stochastic resetting for enhanced sampling”. In: *The journal of physical chemistry letters* 13.48 (2022), pp. 11230–11236.

[59] Jonathan R Church et al. “Accelerating molecular dynamics through informed resetting”. In: *Journal of Chemical Theory and Computation* ().

[60] Tal Rotbart, Shlomi Reuveni, and Michael Urbakh. “Michaelis-Menten reaction scheme as a unified approach towards the optimal restart problem”. In: *Physical Review E* 92.6 (2015), p. 060101.

[61] Paul C Bressloff. “Modeling active cellular transport as a directed search process with stochastic resetting and delays”. In: *Journal of Physics A: Mathematical and Theoretical* 53.35 (2020), p. 355001.

[62] Paul C Bressloff. “Stochastic resetting and the mean-field dynamics of focal adhesions”. In: *Physical Review E* 102.2 (2020), p. 022134.

[63] Martin R Evans, Satya N Majumdar, and Grégory Schehr. “Stochastic resetting and applications”. In: *Journal of Physics A: Mathematical and Theoretical* 53.19 (2020), p. 193001.

[64] Arnab Pal, Viktor Stojkoski, and Trifce Sandev. “Random resetting in search problems”. In: *arXiv preprint arXiv:2310.12057. Springer Nature, 2024* (2023).

[65] Somrita Ray, Debasish Mondal, and Shlomi Reuveni. “Péclet number governs transition to acceleratory restart in drift-diffusion”. In: *Journal of Physics A: Mathematical and Theoretical* 52.25 (2019), p. 255002.

[66] Arnab Pal and V. V. Prasad. “Landau-like expansion for phase transitions in stochastic resetting”. In: *Physical Review Research* 1.3 (2019), p. 032001.

[67] Lukasz Kusmierz et al. “First order transition for the optimal search time of Lévy flights with resetting”. In: *Physical Review Letters* 113.22 (2014), p. 220602.

[68] Saeed Ahmad et al. “First passage of a particle in a potential under stochastic resetting: A vanishing transition of optimal resetting rate”. In: *Physical Review E* 99.2 (2019), p. 022130.

[69] Leonor Michaelis, Maud L Menten, et al. “Die kinetik der invertinwirkung”. In: *Biochem. z* 49.333-369 (1913), p. 352.

[70] M v Smoluchowski. “Versuch einer mathematischen Theorie der Koagulationskinetik kolloider Lösungen”. In: *Zeitschrift für physikalische Chemie* 92.1 (1918), pp. 129–168.

[71] Subrahmanyan Chandrasekhar. “Stochastic problems in physics and astronomy”. In: *Reviews of modern physics* 15.1 (1943), p. 1.

[72] Attila Szabo et al. “Stochastically gated diffusion-influenced reactions”. In: *The Journal of Chemical Physics* 77.9 (1982), pp. 4484–4493.

[73] Huan-Xiang Zhou and Attila Szabo. “Theory and simulation of stochastically-gated diffusion-influenced reactions”. In: *The Journal of Physical Chemistry* 100.7 (1996), pp. 2597–2604.

[74] Yuval Scher and Shlomi Reuveni. “Unified approach to gated reactions on networks”. In: *Physical review letters* 127.1 (2021), p. 018301.

[75] Gabriel Mercado-Vásquez and Denis Boyer. “First Hitting Times to Intermittent Targets”. In: *Phys. Rev. Lett.* 123 (25 2019), p. 250603.

[76] Jürgen Reingruber and David Holcman. “Gated narrow escape time for molecular signaling”. In: *Physical review letters* 103.14 (2009), p. 148102.

[77] Hazime Mori. “Transport, collective motion, and Brownian motion”. In: *Progress of Theoretical Physics* 33.3 (1965), pp. 423–455.

[78] Rep Kubo. “The fluctuation-dissipation theorem”. In: *Reports on Progress in Physics* 29.1 (1966), p. 255.

[79] Brandon R Ferrer, Juan Ruben Gomez-Solano, and Alejandro V Arzola. “Fluid viscoelasticity triggers fast transitions of a Brownian particle in a double well optical potential”. In: *Physical Review Letters* 126.10 (2021), p. 108001.

[80] Juan Ruben Gomez-Solano and Clemens Bechinger. “Transient dynamics of a colloidal particle driven through a viscoelastic fluid”. In: *New Journal of Physics* 17.10 (2015), p. 103032.

[81] Ivo Adan and Jacques Resing. “Queueing theory”. In: *Eindhoven University of Technology* 180 (2002), p. 10.

[82] C Newell. “Applications of queueing theory, vol. 4”. In: *Springer Science & Business Media* 11 (2013), p. 12.

[83] Martin R Evans and Satya N Majumdar. “Effects of refractory period on stochastic resetting”. In: *Journal of Physics A: Mathematical and Theoretical* 52.1 (2018), 01LT01.

[84] Reshmi Roy, Arup Biswas, and Arnab Pal. “Queues with resetting: a perspective”. In: *Journal of Physics: Complexity* 5.2 (2024), p. 021001.

[85] Gregorio García-Valladares et al. “Stochastic resetting with refractory periods: pathway formulation and exact results”. In: *Physica Scripta* 99.4 (2024), p. 045234.

[86] Arnab Pal, Lukasz Kusmierz, and Shlomi Reuveni. “Search with home returns provides advantage under high uncertainty”. In: *Physical Review Research* 2 (2020), p. 043174.

[87] Arnab Pal, Łukasz Kuśmierz, and Shlomi Reuveni. “Invariants of motion with stochastic resetting and space-time coupled returns”. In: *New Journal of Physics* 21.11 (2019), p. 113024.

[88] Anna S Bodrova and Igor M Sokolov. “Brownian motion under noninstantaneous resetting in higher dimensions”. In: *Physical Review E* 102.3 (2020), p. 032129.

[89] Paul C Bressloff. “Search processes with stochastic resetting and multiple targets”. In: *Physical Review E* 102.2 (2020), p. 022115.

[90] Connor Roberts, Emir Sezik, and Eloise Lardet. “Ratchet-mediated resetting: Current, efficiency, and exact solution”. In: *Journal of Physics A: Mathematical and Theoretical* (2024).

[91] Anthony N Burkitt. “A review of the integrate-and-fire neuron model: I. Homogeneous synaptic input”. In: *Biological cybernetics* 95 (2006), pp. 1–19.

[92] Perry J Kaufman. *Trading Systems and Methods,+ Website*. Vol. 591. John Wiley & Sons, 2013.

[93] Timothy W McKeithan. “Kinetic proofreading in T-cell receptor signal transduction.” In: *Proceedings of the national academy of sciences* 92.11 (1995), pp. 5042–5046.

[94] Ricardo Falcao and Martin R Evans. “Interacting Brownian motion with resetting”. In: *Journal of Statistical Mechanics: Theory and Experiment* 2017.2 (2017), p. 023204.

[95] B De Bruyne, J Randon-Furling, and S Redner. “Optimization in first-passage resetting”. In: *Physical Review Letters* 125.5 (2020), p. 050602.

[96] Arup Biswas et al. “Rate enhancement of gated drift-diffusion process by optimal resetting”. In: *The Journal of Chemical Physics* 159.5 (2023).

[97] Christopher Maffeo et al. “Modeling and simulation of ion channels”. In: *Chemical reviews* 112.12 (2012), pp. 6250–6284.

[98] Paul C Bressloff. *Stochastic processes in cell biology*. Vol. 41. Springer, 2014.

[99] Paul C Bressloff. “Diffusion in cells with stochastically gated gap junctions”. In: *SIAM Journal on Applied Mathematics* 76.4 (2016), pp. 1658–1682.

[100] Scott H Northrup, Fahimeh Zarrin, and J Andrew McCammon. “Rate theory for gated diffusion-influenced ligand binding to proteins”. In: *The Journal of Physical Chemistry* 86.13 (1982), pp. 2314–2321.

[101] Yurii A Makhnovskii et al. “Stochastic gating influence on the kinetics of diffusion-limited reactions”. In: *The Journal of chemical physics* 108.3 (1998), pp. 971–983.

[102] Jaeoh Shin and Anatoly B Kolomeisky. “Molecular search with conformational change: One-dimensional discrete-state stochastic model”. In: *The Journal of chemical physics* 149.17 (2018).

[103] Aljaž Godec and Ralf Metzler. “First passage time statistics for two-channel diffusion”. In: *Journal of Physics A: Mathematical and Theoretical* 50.8 (2017), p. 084001.

[104] John L Spouge, Atilla Szabo, and George H Weiss. “Single-particle survival in gated trapping”. In: *Physical Review E* 54.3 (1996), p. 2248.

[105] Irina V Gopich and Attila Szabo. “Reversible stochastically gated diffusion-influenced reactions”. In: *The Journal of Physical Chemistry B* 120.33 (2016), pp. 8080–8089.

[106] Alexander M Berezhkovskii et al. “Smoluchowski-type theory of stochastically gated diffusion-influenced reactions”. In: *The Journal of chemical physics* 106.17 (1997), pp. 6985–6998.

[107] J Andrew McCammon and Scott H Northrup. “Gated binding of ligands to proteins”. In: *Nature* 293.5830 (1981), pp. 316–317.

[108] David D Boehr, Ruth Nussinov, and Peter E Wright. “The role of dynamic conformational ensembles in biomolecular recognition”. In: *Nature chemical biology* 5.11 (2009), pp. 789–796.

[109] Gabriel Mercado-Vásquez and Denis Boyer. “First hitting times between a run-and-tumble particle and a stochastically gated target”. In: *Physical Review E* 103 (2021), p. 042139.

[110] Sean D Lawley and James P Keener. “A new derivation of Robin boundary conditions through homogenization of a stochastically switching boundary”. In: *SIAM Journal on Applied Dynamical Systems* 14.4 (2015), pp. 1845–1867.

[111] Yuval Scher and Shlomi Reuveni. “Gated reactions in discrete time and space”. In: *The Journal of chemical physics* 155.23 (2021).

[112] Aanjaneya Kumar, Aniket Zodage, and MS Santhanam. “First detection of threshold crossing events under intermittent sensing”. In: *Physical Review E* 104.5 (2021), p. L052103.

[113] Aanjaneya Kumar et al. “Inference from gated first-passage times”. In: *Physical Review Research* 5.3 (2023), p. L032043.

[114] Édgar Roldán et al. “Stochastic resetting in backtrack recovery by RNA polymerases”. In: *Physical Review E* 93.6 (2016), p. 062411.

[115] Srikanth Budnar et al. “Anillin promotes cell contractility by cyclic resetting of RhoA residence kinetics”. In: *Developmental Cell* 49.6 (2019), pp. 894–906.

[116] SB Yuste, E Abad, and Katja Lindenberg. “Reaction-subdiffusion model of morphogen gradient formation”. In: *Physical Review E—Statistical, Nonlinear, and Soft Matter Physics* 82.6 (2010), p. 061123.

[117] Arnab Pal and V. V. Prasad. “First passage under stochastic resetting in an interval”. In: *Physical Review E* 99 (2019), p. 032123.

[118] Somrita Ray and Shlomi Reuveni. “Resetting transition is governed by an interplay between thermal and potential energy”. In: *The Journal of Chemical Physics* 154.17 (2021).

[119] Somrita Ray. “Space-dependent diffusion with stochastic resetting: A first-passage study”. In: *The Journal of Chemical Physics* 153.23 (2020).

[120] Syed Yunus Ali, Nabadip Choudhury, and Debasish Mondal. “Asymmetric restart in a stochastic climate model: A theoretical perspective to prevent the abnormal precipitation accumulation caused by global warming”. In: *Journal of Physics A: Mathematical and Theoretical* 55.30 (2022), p. 301001.

[121] Somrita Ray. “Expediting Feller process with stochastic resetting”. In: *Physical Review E* 106.3 (2022), p. 034133.

[122] Ofek Lauber Bonomo and Arnab Pal. “First passage under restart for discrete space and time: Application to one-dimensional confined lattice random walks”. In: *Physical Review E* 103 (2021), p. 052129.

[123] Aanjaneya Kumar and Arnab Pal. “Universal framework for record ages under restart”. In: *Physical Review Letters* 130.15 (2023), p. 157101.

[124] Gabriel Mercado-Vásquez and Denis Boyer. “Search of stochastically gated targets with diffusive particles under resetting”. In: *Journal of Physics A: Mathematical and Theoretical* 54.44 (2021), p. 444002.

[125] Paul C Bressloff. “Diffusive search for a stochastically-gated target with resetting”. In: *Journal of Physics A: Mathematical and Theoretical* 53.42 (2020), p. 425001.

[126] Arnab Pal, Iddo Eliazar, and Shlomi Reuveni. “First passage under restart with branching”. In: *Physical Review Letters* 122.2 (2019), p. 020602.

[127] Siddharth Jain et al. “Fick–Jacobs description and first passage dynamics for diffusion in a channel under stochastic resetting”. In: *The Journal of Chemical Physics* 158.5 (2023).

[128] Arnab Pal et al. “Local time of diffusion with stochastic resetting”. In: *Journal of Physics A: Mathematical and Theoretical* 52.26 (2019), p. 264002.

[129] Arnab Pal, Sarah Kostinski, and Shlomi Reuveni. “The inspection paradox in stochastic resetting”. In: *Journal of Physics A: Mathematical and Theoretical* 55.2 (2022), p. 021001.

[130] Katherine Henzler-Wildman and Dorothee Kern. “Dynamic personalities of proteins”. In: *Nature* 450.7172 (2007), pp. 964–972.

[131] Jeffrey R Moffitt, Yann R Chemla, and Carlos Bustamante. “Methods in statistical kinetics”. In: *Methods in enzymology*. Vol. 475. Elsevier, 2010, pp. 221–257.

[132] Dmitrii E Makarov. *Single molecule science: physical principles and models*. CRC Press, 2015.

[133] Nicolaas Godfried Van Kampen. *Stochastic processes in physics and chemistry*. Vol. 1. Elsevier, 1992.

[134] Crispin W Gardiner et al. *Handbook of stochastic methods*. Vol. 3. springer Berlin, 2004.

[135] Ido Golding et al. “Real-time kinetics of gene activity in individual bacteria”. In: *Cell* 123.6 (2005), pp. 1025–1036.

[136] Justin Whitehouse, Martin R Evans, and Satya N Majumdar. “Effect of partial absorption on diffusion with resetting”. In: *Physical Review E—Statistical, Nonlinear, and Soft Matter Physics* 87.2 (2013), p. 022118.

[137] Arup Biswas. *Rate enhancement of gated drift-diffusion process by optimal resetting*. https://github.com/arupb1998/Rate-enhancement-of-gated-drift-diffusion-process-by-optimal-resetting. Mathematica notebook with detailed calculations for confined geometry. 2025.

[138] Stephan Eule and Jakob J Metzger. “Non-equilibrium steady states of stochastic processes with intermittent resetting”. In: *New Journal of Physics* 18.3 (2016), p. 033006.

[139] Xiaowei Zhuang et al. “Fluorescence quenching: A tool for single-molecule protein-folding study”. In: *Proceedings of the National Academy of Sciences* 97.26 (2000), pp. 14241–14244.

[140] B Somogyi, JA Norman, and A Rosenberg. “Gated quenching of intrinsic fluorescence and phosphorescence of globular proteins. An extended model”. In: *Biophysical journal* 50.1 (1986), pp. 55–61.

[141] Jacob Willem Cohen. *The single server queue*. Vol. 8. Elsevier, 2012.

[142] Moshe Haviv. *Queues*. Springer, 2013.

[143] Noah Gans, Ger Koole, and Avishai Mandelbaum. “Telephone call centers: Tutorial, review, and research prospects”. In: *Manufacturing & Service Operations Management* 5.2 (2003), pp. 79–141.

[144] Ger Koole and Avishai Mandelbaum. “Queueing models of call centers: An introduction”. In: *Annals of Operations Research* 113.1 (2002), pp. 41–59.

[145] John N Daigle. *Queueing theory with applications to packet telecommunication*. Springer Science & Business Media, 2005.

[146] Laszlo Lakatos, Laszlo Szeidl, and Miklos Telek. *Introduction to queueing systems with telecommunication applications*. Vol. 388. Springer, 2013.

[147] Eitan Bachmat et al. "Analysis of airplane boarding times". In: *Operations Research* 57.2 (2009), pp. 499–513. DOI: 10.1287/opre.1080.0621.

[148] Eitan Bachmat. "Airplane boarding meets express line queues". In: *European Journal of Operational Research* 275.3 (2019), pp. 1165–1177. DOI: 10.1016/j.ejor.2018.12.036.

[149] Sveinung Erland et al. "Lorentzian-geometry-based analysis of airplane boarding policies highlights "slow passengers first" as better". In: *Physical Review E* 100.6 (2019), p. 062313. DOI: 10.1103/PhysRevE.100.062313.

[150] Robert B. Cooper. "Queueing Theory". In: *Proceedings of the ACM '81 Conference*. ACM, Jan. 1981, pp. 119–122.

[151] Mor Harchol-Balter. *Performance Modeling and Design of Computer Systems: Queueing Theory in Action*. Cambridge University Press, 2013. ISBN: 9781107027503.

[152] Dirk Helbing. "Traffic and related self-driven many-particle systems". In: *Reviews of Modern Physics* 73.4 (2001), pp. 1067–1141. DOI: 10.1103/RevModPhys.73.1067.

[153] D. V. Averin. "Electrons held in a queue". In: *Nature* 434.7031 (2005), pp. 285–287. DOI: 10.1038/434285a.

[154] M. Carmen Romano et al. "Queueing phase transition: theory of translation". In: *Physical Review Letters* 102.19 (2009), p. 198104. DOI: 10.1103/PhysRevLett.102.198104.

[155] A. Arazi, Eshel Ben-Jacob, and Uri Yechiali. "Bridging genetic networks and queueing theory". In: *Physica A: Statistical Mechanics and its Applications* 332 (2004), pp. 585–616. DOI: 10.1016/j.physa.2003.10.019.

[156] Erol Gelenbe. "Steady-state solution of probabilistic gene regulatory networks". In: *Physical Review E* 76.3 (2007), p. 031903. DOI: 10.1103/PhysRevE.76.031903.

[157] Tao Jia and Rahul V. Kulkarni. "Intrinsic noise in stochastic models of gene expression with molecular memory and bursting". In: *Physical Review Letters* 106.5 (2011), p. 058102. DOI: 10.1103/PhysRevLett.106.058102.

[158] Niraj Kumar, Abhyudai Singh, and Rahul V. Kulkarni. "Transcriptional bursting in gene expression: analytical results for general stochastic models". In: *PLoS Computational Biology* 11.10 (2015), e1004292. DOI: 10.1371/journal.pcbi.1004292.

[159] Suckjoon Jun et al. "Fundamental principles in bacterial physiology—history, recent progress, and the future with focus on cell size control: a review". In: *Reports on Progress in Physics* 81.5 (2018), p. 056601. DOI: 10.1088/1361-6633/aaa628.

[160] William H. Mather et al. "Correlation resonance generated by coupled enzymatic processing". In: *Biophysical Journal* 99.10 (2010), pp. 3172–3181. DOI: 10.1016/j.bpj.2010.08.030.

[161] Natalie A. Cookson et al. "Queueing up for enzymatic processing: correlated signaling through coupled degradation". In: *Molecular Systems Biology* 7.1 (2011), p. 561. DOI: 10.1038/msb.2011.94.

[162] William H. Mather et al. “Factorized time-dependent distributions for certain multiclass queueing networks and an application to enzymatic processing networks”. In: *Queueing Systems* 69.3 (2011), pp. 313–328. DOI: 10.1007/s11134-011-9226-1.

[163] V. P. Evstigneev et al. “Theoretical description of metabolism using queueing theory”. In: *Bulletin of Mathematical Biology* 76.9 (2014), pp. 2238–2248. DOI: 10.1007/s11538-014-9985-6.

[164] S. Kloska et al. “Queueing theory model of Krebs cycle”. In: *Bioinformatics* (2021). DOI: 10.1093/bioinformatics/btab613.

[165] Samuel C. Kou et al. “Single-Molecule Michaelis–Menten Equations”. In: *The Journal of Physical Chemistry B* 109.41 (2005), pp. 19068–19081. DOI: 10.1021/jp051490q.

[166] Jeffrey R. Moffitt and Carlos Bustamante. “Extracting signal from noise: kinetic mechanisms from a Michaelis–Menten-like expression for enzymatic fluctuations”. In: *The FEBS Journal* 281.2 (2014), pp. 498–517. DOI: 10.1111/febs.12601.

[167] Jeffrey R. Moffitt, Yann R. Chemla, and Carlos Bustamante. “Methods in statistical kinetics”. In: *Methods in Enzymology* 475 (2010), pp. 221–257. DOI: 10.1016/S0076-6879(10)75009-7.

[168] Kelly Velonia et al. “Single-enzyme kinetics of CALB-catalyzed hydrolysis”. In: *Angewandte Chemie* 117.4 (2005), pp. 566–570. DOI: 10.1002/ange.200461890.

[169] Ward Whitt. “The impact of a heavy-tailed service-time distribution upon the M/GI/s waiting-time distribution”. In: *Queueing Systems* 36.1 (2000), pp. 71–87. DOI: 10.1023/A:1019131516230.

[170] James C. Spall. *Introduction to Stochastic Search and Optimization: Estimation, Simulation, and Control*. Vol. 65. John Wiley & Sons, 2005. ISBN: 9780471330523.

[171] Brian P. English et al. “Ever-fluctuating single enzyme molecules: Michaelis–Menten equation revisited”. In: *Nature Chemical Biology* 2.2 (2006), pp. 87–94. DOI: 10.1038/nchembio759.

[172] Ophir Flomenbom et al. “Stretched exponential decay and correlations in the catalytic activity of fluctuating single lipase molecules”. In: *Proceedings of the National Academy of Sciences* 102.7 (2005), pp. 2368–2372. DOI: 10.1073/pnas.0409115102.

[173] Ofek Lauber Bonomo, Arnab Pal, and Shlomi Reuveni. “Mitigating long queues and waiting times with service resetting”. In: *PNAS Nexus* 1.3 (2022).

[174] Andrea Montanari and Riccardo Zecchina. “Optimizing searches via rare events”. In: *Physical Review Letters* 88.17 (2002), p. 178701.

[175] Arnab Pal, Viktor Stojkoski, and Trifce Sandev. “Random resetting in search problems”. In: *Target Search Problems*. Springer, 2024, pp. 323–355.

[176] Gourab Kumar Sar et al. “Resetting mediated navigation of active Brownian searcher in a homogeneous topography”. In: *Soft Matter* (2023).

[177] Arnob Ray et al. “Mitigating long transient time in deterministic systems by resetting”. In: *Chaos: An Interdisciplinary Journal of Nonlinear Science* 31.1 (2021), p. 011103.

[178] Trifce Sandev et al. “Heterogeneous diffusion with stochastic resetting”. In: *Journal of Physics A: Mathematical and Theoretical* 55.7 (2022), p. 074003.

[179] W John Thrasher and Michael Mascagni. “Examining sharp restart in a Monte Carlo method for the linearized Poisson–Boltzmann equation”. In: *Monte Carlo Methods and Applications* 26.3 (2020), pp. 223–244.

[180] Daniel Campos and Vicenç Méndez. “Phase transitions in optimal search times: how random walkers should combine resetting and flight scales”. In: *Physical Review E* 92.6 (2015), p. 062115.

[181] Viktor Stojkoski et al. “Income inequality and mobility in geometric Brownian motion with stochastic resetting: theoretical results and empirical evidence of non-ergodicity”. In: *Philosophical Transactions of the Royal Society A* 380.2224 (2022), p. 20210157.

[182] Shlomi Reuveni. “Optimal Stochastic Restart Renders Fluctuations in First Passage Times Universal”. In: *Physical Review Letters* 116 (2016), p. 170601.

[183] Łukasz Kuśmierz and Ewa Gudowska-Nowak. “Optimal first-arrival times in Lévy flights with resetting”. In: *Physical Review E* 92.5 (2015), p. 052127.

[184] Randolph Nelson. *Probability, stochastic processes, and queueing theory: the mathematics of computer performance modeling*. Springer Science & Business Media, 2013.

[185] Lawrence Brown et al. “Statistical analysis of a telephone call center: A queueing-science perspective”. In: *Journal of the American Statistical Association* 100.469 (2005), pp. 36–50.

[186] Stefano Gualandi and Giuseppe Toscani. “Call center service times are lognormal: A Fokker–Planck description”. In: *Mathematical Models and Methods in Applied Sciences* 28.08 (2018), pp. 1513–1527.

[187] Mor Harchol-Balter. “Task assignment with unknown duration”. In: *Proceedings 20th IEEE International Conference on Distributed Computing Systems*. IEEE, 2000, pp. 214–224.

[188] Ofek Lauber Bonomo, Uri Yechiali, and Shlomi Reuveni. “Queues with service resetting”. In: *European Journal of Operational Research* 322.3 (2025), pp. 908–919.

[189] Paul C Bressloff. “Queueing theory of search processes with stochastic resetting”. In: *Physical Review E* 102.3 (2020), p. 032109.

[190] Uttam Bhat, Caterina De Bacco, and S Redner. “Stochastic search with Poisson and deterministic resetting”. In: *Journal of Statistical Mechanics: Theory and Experiment* 2016.8 (2016), p. 083401.

[191] Arup Biswas et al. “A resetting particle embedded in a viscoelastic bath”. In: *Chaos: An Interdisciplinary Journal of Nonlinear Science* 35.3 (2025).

[192] Paul Langevin. “Sur la théorie du mouvement brownien”. In: *CR Acad. Sci. Paris* 146.530-533 (1908), p. 530.

[193] P5145211978ZPhyB Hänggi. “Correlation functions and masterequations of generalized (non-Markovian) Langevin equations”. In: *Zeitschrift für Physik B Condensed Matter* 31.4 (1978), pp. 407–416.

[194] Peter Häunggi and Peter Jung. “Colored noise in dynamical systems”. In: *Advances in chemical physics* 89 (1994), pp. 239–326.

[195] Eric Lutz. “Fractional Langevin equation”. In: *Physical Review E* 64.5 (2001), p. 051106.

[196] Angel Daniel Viñales and Marcelo Arnaldo Desposito. “Anomalous diffusion: Exact solution of the generalized Langevin equation for harmonically bounded particle”. In: *Physical Review E* 73.1 (2006), p. 016111.

[197] Marcelo Arnaldo Desposito and Angel Daniel Viñales. “Memory effects in the asymptotic diffusive behavior of a classical oscillator described by a generalized Langevin equation”. In: *Physical Review E* 77.3 (2008), p. 031123.

[198] Stanislav Burov and Eli Barkai. “Fractional Langevin equation: Overdamped, underdamped, and critical behaviors”. In: *Physical Review E* 78.3 (2008), p. 031112.

[199] Marcelo Arnaldo Desposito and Angel Daniel Viñales. “Subdiffusive behavior in a trapping potential: Mean square displacement and velocity autocorrelation function”. In: *Physical Review E* 80.2 (2009), p. 021111.

[200] Trifce Sandev, Živorad Tomovski, and Johan L A Dubbeldam. “Generalized Langevin equation with a three parameter Mittag-Leffler noise”. In: *Physica A: Statistical Mechanics and its Applications* 390.21-22 (2011), pp. 3627–3636.

[201] Haw Yang et al. “Protein conformational dynamics probed by single-molecule electron transfer”. In: *Science* 302.5643 (2003), pp. 262–266.

[202] Samuel C Kou and X Sunney Xie. “Generalized Langevin equation with fractional Gaussian noise: subdiffusion within a single protein molecule”. In: *Physical Review Letters* 93.18 (2004), p. 180603.

[203] Gerald R Kneller. “Communication: A scaling approach to anomalous diffusion”. In: *The Journal of Chemical Physics* 141.4 (2014).

[204] Igor Goychuk. “Viscoelastic subdiffusion: generalized Langevin equation approach”. In: *Advances in Chemical Physics* 150 (2012), pp. 187–253.

[205] Oliver F Lange and Helmut Grubmüller. “Collective Langevin dynamics of conformational motions in proteins”. In: *The Journal of Chemical Physics* 124.21 (2006).

[206] Hee Sun Lee, Surl-Hee Ahn, and Eric F Darve. “The multi-dimensional generalized Langevin equation for conformational motion of proteins”. In: *The Journal of Chemical Physics* 150.17 (2019).

[207] Ludvig Lizana et al. “Foundation of fractional Langevin equation: harmonization of a many-body problem”. In: *Physical Review E* 81.5 (2010), p. 051118.

[208] Alessandro Taloni, Aleksei Chechkin, and Joseph Klafter. “Generalized elastic model yields a fractional Langevin equation description”. In: *Physical Review Letters* 104.16 (2010), p. 160602.

[209] J L A Dubbeldam et al. “Polymer translocation through a nanopore: a showcase of anomalous diffusion”. Undefined/Unknown. In: *Physical Review E* 76 (2007), 010801(R). ISSN: 1539-3755.

[210] Robert Zwanzig. *Nonequilibrium Statistical Mechanics*. Oxford university press, 2001.

[211] Ke-Gang Wang and Jaume Masoliver. “Linear oscillators driven by Gaussian colored noise: crossovers and probability distributions”. In: *Physica A: Statistical Mechanics and its Applications* 231.4 (1996), pp. 615–630.

[212] Steven A Adelman. “Fokker–Planck equations for simple non-Markovian systems”. In: *The Journal of Chemical Physics* 64.1 (1976), pp. 124–130.

[213] Biswajit Das et al. “Enhanced directionality of active processes in a viscoelastic bath”. In: *New Journal of Physics* 25.9 (2023), p. 093051.

[214] Shuvojit Paul et al. “Bayesian inference of the viscoelastic properties of a Jeffrey’s fluid using optical tweezers”. In: *Scientific Reports* 11.1 (2021), p. 2023.

[215] Juan Ruben Gomez-Solano, Alex Blokhuis, and Clemens Bechinger. “Dynamics of self-propelled Janus particles in viscoelastic fluids”. In: *Physical Review Letters* 116.13 (2016), p. 138301.

[216] Juan Ruben Gomez-Solano. “Work extraction and performance of colloidal heat engines in viscoelastic baths”. In: *Frontiers in Physics* 9 (2021), p. 643333.

[217] Farshad Darabi, Brandon R Ferrer, and Juan Ruben Gomez-Solano. “Stochastic energetics of a colloidal particle trapped in a viscoelastic bath”. In: *New Journal of Physics* 25.10 (2023), p. 103021.

[218] Shuvojit Paul, Basudev Roy, and Ayan Banerjee. “Free and confined Brownian motion in viscoelastic Stokes–Oldroyd B fluids”. In: *Journal of Physics: Condensed Matter* 30.34 (2018), p. 345101.

[219] Arthur V Straube and Felix Höfling. “Memory effects in colloidal motion under confinement and driving”. In: *Journal of Physics A: Mathematical and Theoretical* 57.29 (2024), p. 295003.

[220] Wei Wang et al. “Time averaging and emerging nonergodicity upon resetting of fractional Brownian motion and heterogeneous diffusion processes”. In: *Physical Review E* 104.2 (2021), p. 024105.

[221] Trifce Sandev et al. “Stochastic dynamics with multiplicative dichotomic noise: Heterogeneous telegrapher’s equation, anomalous crossovers and resetting”. In: *Chaos, Solitons & Fractals* 165 (2022), p. 112878.

[222] MK Lenzi et al. “Transient anomalous diffusion in heterogeneous media with stochastic resetting”. In: *Physica A: Statistical Mechanics and its Applications* 588 (2022), p. 126560.

[223] Łukasz Kuśmierz and Ewa Gudowska-Nowak. “Subdiffusive continuous-time random walks with stochastic resetting”. In: *Physical Review E* 99.5 (2019), p. 052116.

[224] Vicenç Méndez, Axel Masó-Puigdellosas, and Daniel Campos. “Nonstandard diffusion under Markovian resetting in bounded domains”. In: *Physical Review E* 105.5 (2022), p. 054118.

[225] Viktor Stojkoski et al. “Geometric Brownian motion under stochastic resetting: a stationary yet nonergodic process”. In: *Physical Review E* 104.1 (2021), p. 014121.

[226] Ofir Tal-Friedman, Yael Roichman, and Shlomi Reuveni. “Diffusion with partial resetting”. In: *Physical Review E* 106.5 (2022), p. 054116.

[227] Nicolaas Godfried Van Kampen. *Stochastic Processes in Physics and Chemistry*. Vol. 1. Elsevier, 1992.

[228] S. C. Kou. “Stochastic modeling in nanoscale biophysics: Subdiffusion within proteins”. In: *The Annals of Applied Statistics* 2.2 (2008), pp. 501–535.

[229] Wei Min et al. “Observation of a Power-Law Memory Kernel for Fluctuations<? format?> within a Single Protein Molecule”. In: *Physical Review Letters* 94.19 (2005), p. 198302.

[230] Noëlle Pottier. “Aging properties of an anomalously diffusing particule”. In: *Physica A: Statistical Mechanics and its Applications* 317.3-4 (2003), pp. 371–382.

[231] Martin R Evans and Satya N Majumdar. “Diffusion with resetting in arbitrary spatial dimension”. In: *Journal of Physics A: Mathematical and Theoretical* 47.28 (2014), p. 285001.

[232] Axel Masó-Puigdellosas, Daniel Campos, and Vicenç Méndez. “Transport properties of random walks under stochastic noninstantaneous resetting”. In: *Physical Review E* 100.4 (2019), p. 042104.

[233] Viktor Stojkoski et al. “Autocorrelation functions and ergodicity in diffusion with stochastic resetting”. In: *Journal of Physics A: Mathematical and Theoretical* 55.10 (2022), p. 104003.

[234] Satya N Majumdar and Gleb Oshanin. “Spectral content of fractional Brownian motion with stochastic reset”. In: *Journal of Physics A: Mathematical and Theoretical* 51.43 (2018), p. 435001.

[235] Deepak Vinod et al. “Time-averaging and nonergodicity of reset geometric Brownian motion with drift”. In: *Physical Review E* 106.3 (2022), p. 034137.

[236] Yuriy L Raikher, Victor V Rusakov, and Régine Perzynski. “Brownian motion in a viscoelastic medium modelled by a Jeffreys fluid”. In: *Soft Matter* 9.45 (2013), pp. 10857–10865.

[237] Manh Hong Duong and Xiaocheng Shang. “Accurate and robust splitting methods for the generalized Langevin equation with a positive Prony series memory kernel”. In: *Journal of Computational Physics* 464 (2022), p. 111332.

[238] M Wiśniewski, J Łuczka, and J Spiechowicz. “Effective mass approach to memory in non-Markovian systems”. In: *Physical Review E* 109.4 (2024), p. 044116.

[239] Niklas Bockius et al. “Model reduction techniques for the computation of extended Markov parameterizations for generalized Langevin equations”. In: *Journal of Physics: Condensed Matter* 33.21 (2021), p. 214003.

[240] Andrew D Baczewski and Stephen D Bond. “Numerical integration of the extended variable generalized Langevin equation with a positive Prony representable memory kernel”. In: *The Journal of Chemical Physics* 139.4 (2013).

[241] Peter Siegle et al. “Markovian embedding of non-Markovian superdiffusion”. In: *Physical Review E* 81.1 (2010), p. 011136.

[242] Peter Siegle, Igor Goychuk, and Peter Hänggi. “Markovian embedding of fractional superdiffusion”. In: *Europhysics Letters* 93.2 (2011), p. 20002.

[243] Shamik Gupta, Satya N Majumdar, and Grégory Schehr. “Fluctuating interfaces subject to stochastic resetting”. In: *Physical Review Letters* 112.22 (2014), p. 220601.

[244] Igor M Sokolov. “Linear Response and Fluctuation-Dissipation Relations for Brownian Motion Under Resetting”. In: *Physical Review Letters* 130.6 (2023), p. 067101.

[245] Shamik Gupta and Arun M Jayannavar. “Stochastic Resetting: A (Very) Brief Review”. In: *Frontiers in Physics* (2022), p. 130.

[246] Wei Min and X Sunney Xie. “Kramers model with a power-law friction kernel: Dispersed kinetics and dynamic disorder of biochemical reactions”. In: *Physical Review E—Statistical, Nonlinear, and Soft Matter Physics* 73.1 (2006), p. 010902.

[247] Trifce Sandev et al. “Diffusion and Fokker-Planck-Smoluchowski equations with generalized memory kernel”. In: *Fractional Calculus and Applied Analysis* 18 (2015), pp. 1006–1038.

[248] Jakub Ślęzak, Ralf Metzler, and Marcin Magdziarz. “Superstatistical generalised Langevin equation: non-Gaussian viscoelastic anomalous diffusion”. In: *New Journal of Physics* 20.2 (2018), p. 023026.

[249] Anna S Bodrova and Igor M Sokolov. “Resetting processes with noninstantaneous return”. In: *Physical Review E* 101.5 (2020), p. 052130.

[250] Gennaro Tucci et al. “First-passage time of run-and-tumble particles with noninstantaneous resetting”. In: *Physical Review E* 106.4 (2022), p. 044127.

[251] Arup Biswas, Anupam Kundu, and Arnab Pal. “Search with stochastic home returns can expedite classical first passage under resetting”. In: *Physical Review E* 110.4 (2024), p. L042101.

[252] Deepak Gupta et al. “Stochastic resetting with stochastic returns using external trap”. In: *Journal of Physics A: Mathematical and Theoretical* 54.2 (2020), p. 025003.

[253] Arup Biswas et al. “Drift-diffusive resetting search process with stochastic returns: Speedup beyond optimal instantaneous return”. In: *Physical Review E* 111.1 (2025), p. 014142.

[254] Arnab Pal, Łukasz Kuśmierz, and Shlomi Reuveni. “Time-dependent density of diffusion with stochastic resetting is invariant to return speed”. In: *Physical Review E* 100.4 (2019), p. 040101.

[255] Mattia Radice. “One-dimensional telegraphic process with noninstantaneous stochastic resetting”. In: *Physical Review E* 104.4 (2021), p. 044126.

[256] Aleksander A Stanislavsky and Aleksander Weron. “Subdiffusive search with home returns via stochastic resetting: a subordination scheme approach”. In: *Journal of Physics A: Mathematical and Theoretical* 55.7 (2022), p. 074004.

[257] Paul C Bressloff. “Target competition for resources under multiple search-and-capture events with stochastic resetting”. In: *Proceedings of the Royal Society A* 476.2242 (2020), p. 20200475.

[258] Gabriel Mercado-Vásquez et al. “Intermittent resetting potentials”. In: *Journal of Statistical Mechanics: Theory and Experiment* 2020.11 (2020), p. 113203.

[259] Deepak Gupta, Arnab Pal, and Anupam Kundu. “Resetting with stochastic return through linear confining potential”. In: *Journal of Statistical Mechanics: Theory and Experiment* 2021.4 (2021), p. 043202.

[260] Deepak Gupta and Carlos A Plata. “Work fluctuations for diffusion dynamics submitted to stochastic return”. In: *New Journal of Physics* 24.11 (2022), p. 113034.

[261] Andre C Barato and Udo Seifert. “Thermodynamic uncertainty relation for biomolecular processes”. In: *Physical Review Letters* 114.15 (2015), p. 158101.

[262] Jordan M Horowitz and Todd R Gingrich. “Thermodynamic uncertainty relations constrain non-equilibrium fluctuations”. In: *Nature Physics* 16.1 (2020), pp. 15–20.

[263] Arnab Pal, Shlomi Reuveni, and Saar Rahav. “Thermodynamic uncertainty relation for first-passage times on Markov chains”. In: *Physical Review Research* 3.3 (2021), p. L032034.

[264] Priyo Shankar Pal et al. “Thermodynamic Trade-off Relation for First Passage Time in Resetting Process”. In: *Physical Review E* 108.4 (2023), p. 044117.

[265] Felix Faisant et al. “Optimal mean first-passage time of a Brownian searcher with resetting in one and two dimensions: experiments, theory and numerical tests”. In: *Journal of Statistical Mechanics: Theory and Experiment* 2021.11 (2021), p. 113203.

[266] William Feller. *An introduction to probability theory and its applications, Volume 2*. Vol. 81. John Wiley & Sons, 1991.

[267] *GitHub link for the Mathematica file containing the exact expressions*. URL: https://github.com/arupb1998/Drift-diffusive_search_process_under_resetting_and_stochastic_returns-Mathematica_file (visited on 10/02/2011).

[268] Srividya Iyer-Biswas and Anton Zilman. “First-passage processes in cellular biology”. In: *Advances in Chemical Physics* 160 (2016), pp. 261–306.

[269] Ralf Metzler, Sidney Redner, and Gleb Oshanin. *First-passage phenomena and their applications*. Vol. 35. World Scientific, 2014.

[270] Arup Biswas, Satya N. Majumdar, and Arnab Pal. “Target Search Optimization by Threshold Resetting”. In: *Phys. Rev. Lett.* 135 (22 Nov. 2025), p. 227101. DOI: 10.1103/752c-wqly.

[271] Mostafa Bachar, Jerry J Batzel, and Susanne Ditlevsen. *Stochastic biomathematical models: with applications to neuronal modeling*. Vol. 2058. Springer, 2012.

[272] George L Gerstein and Benoit Mandelbrot. “Random walk models for the spike activity of a single neuron”. In: *Biophysical journal* 4.1 (1964), pp. 41–68.

[273] Thibaud Taillefumier and Marcelo O Magnasco. “A phase transition in the first passage of a Brownian process through a fluctuating boundary with implications for neural coding”. In: *Proceedings of the National Academy of Sciences* 110.16 (2013), E1438–E1443.

[274] Albert N Shiryaev. *Optimal stopping rules*. Vol. 8. Springer Science & Business Media, 2007.

[275] Qing Zhang. “Stock trading: An optimal selling rule”. In: *SIAM Journal on Control and Optimization* 40.1 (2001), pp. 64–87.

[276] Merton H Miller and Daniel Orr. “A model of the demand for money by firms”. In: *The Quarterly journal of economics* 80.3 (1966), pp. 413–435.

[277] Michael Nygard. *Release it!: design and deploy production-ready software*. The Pragmatic Bookshelf, 2018.

[278] Kridanto Surendro, Wikan Danar Sunindyo, et al. “Circuit breaker in microservices: State of the art and future prospects”. In: *IOP Conference Series: Materials Science and Engineering*. Vol. 1077. 1. IOP Publishing. 2021, p. 012065.

[279] Fabrizio Montesi and Janine Weber. “From the decorator pattern to circuit breakers in microservices”. In: *Proceedings of the 33rd annual ACM symposium on applied computing*. 2018, pp. 1733–1735.

[280] Srutarshi Pradhan, Alex Hansen, and Bikas K Chakrabarti. “Failure processes in elastic fiber bundles”. In: *Reviews of modern physics* 82.1 (2010), pp. 499–555.

[281] Alex Hansen, Per Christian Hemmer, and Srutarshi Pradhan. *The fiber bundle model: modeling failure in materials*. John Wiley & Sons, 2015.

[282] Sudeshna Sinha. “Using thresholding at varying intervals to obtain different temporal patterns”. In: *Physical Review E* 63.3 (2001), p. 036212.

[283] Sudeshna Sinha and William L Ditto. “Dynamics based computation”. In: *physical review Letters* 81.10 (1998), p. 2156.

[284] Sudeshna Sinha and William L Ditto. “Computing with distributed chaos”. In: *Physical Review E* 60.1 (1999), p. 363.

[285] Sourav K Bhowmick et al. “Targeting temporal patterns in time-delay chaotic systems”. In: *International Journal of Bifurcation and Chaos* 24.02 (2014), p. 1450014.

[286] B De Bruyne and S Redner. “Optimization and growth in first-passage resetting”. In: *Journal of Statistical Mechanics: Theory and Experiment* 2021.1 (2021), p. 013203.

[287] Ralf Metzler, Gleb Oshanin, and Sidney Redner. *First-passage Phenomena and Their Applications*. World Scientific, 2014. ISBN: 978-981-4590-28-0.

[288] Ricardo Martínez-García et al. “Optimizing the Search for Resources by Sharing Information: Mongolian Gazelles as a Case Study”. In: *Physical Review Letters* 110.24 (2013), p. 248106.

[289] Kunal Bhattacharya and Tamás Vicsek. “Collective foraging in heterogeneous landscapes”. In: *Journal of the Royal Society Interface* 11.100 (2014), p. 20140674.

[290] Andrea Falcón-Cortés, Denis Boyer, and Gabriel Ramos-Fernández. “Collective learning from individual experiences and information transfer during group foraging”. In: *Journal of the Royal Society Interface* 16.151 (2019), p. 20180803.

[291] Marco Biroli et al. “Extreme Statistics and Spacing Distribution in a Brownian Gas Correlated by Resetting”. In: *Physical Review Letters* 130.20 (2023), p. 207101.

[292] Marco Biroli, Satya N Majumdar, and Grégory Schehr. “Critical number of walkers for diffusive search processes with resetting”. In: *Physical Review E* 107.6 (2023), p. 064141.

[293] Marco Biroli et al. “Exact extreme, order, and sum statistics in a class of strongly correlated systems”. In: *Physical Review E* 109.1 (2024), p. 014101.

[294] Iain D Couzin et al. “Effective leadership and decision-making in animal groups on the move”. In: *Nature* 433.7025 (2005), pp. 513–516.

[295] Iain D Couzin et al. “Uninformed individuals promote democratic consensus in animal groups”. In: *science* 334.6062 (2011), pp. 1578–1580.

[296] Larissa Conradt and Timothy J Roper. “Consensus decision making in animals”. In: *Trends in ecology & evolution* 20.8 (2005), pp. 449–456.

[297] Manuele Brambilla et al. “Swarm robotics: a review from the swarm engineering perspective”. In: *Swarm Intelligence* 7 (2013), pp. 1–41.

[298] Kristina Lerman, Alcherio Martinoli, and Aram Galstyan. “A review of probabilistic macroscopic models for swarm robotic systems”. In: *International workshop on swarm robotics*. Springer. 2004, pp. 143–152.

[299] Danielle L Chase and Orit Peleg. “The Physics of Sensing and Decision-Making by Animal Groups”. In: *Annual Review of Biophysics* 54.1 (2025), pp. 329–351.

[300] Satya N Majumdar, Arnab Pal, and Grégory Schehr. "Extreme value statistics of correlated random variables: a pedagogical review". In: *Physics Reports* 840 (2020), pp. 1–32.

[301] AM Reynolds and F Bartumeus. "Optimising the success of random destructive searches: Lévy walks can outperform ballistic motions". In: *Journal of Theoretical Biology* 260.1 (2009), pp. 98–103.

[302] David W Sims et al. "Scaling laws of marine predator search behaviour". In: *Nature* 451.7182 (2008), pp. 1098–1102.

[303] MC Santos et al. "Optimal random searches of revisitable targets: crossover from superdiffusive to ballistic random walks". In: *Europhysics Letters* 67.5 (2004), p. 734.

[304] A James, MJ Plank, and R Brown. "Optimizing the encounter rate in biological interactions: ballistic versus Lévy versus Brownian strategies". In: *Physical Review E—Statistical, Nonlinear, and Soft Matter Physics* 78.5 (2008), p. 051128.

[305] Javier Villarroel and Miquel Montero. "Continuous-time ballistic process with random resets". In: *Journal of Statistical Mechanics: Theory and Experiment* 2018.12 (2018), p. 123204.

[306] K Martens et al. "Probability distributions for the run-and-tumble bacterial dynamics: An analogy to the Lorentz model". In: *The European Physical Journal E* 35 (2012), pp. 1–6.

[307] Alexander R Sprenger et al. "Dynamics of active particles with translational and rotational inertia". In: *Journal of Physics: Condensed Matter* 35.30 (2023), p. 305101.

[308] Clemens Bechinger et al. "Active particles in complex and crowded environments". In: *Reviews of modern physics* 88.4 (2016), p. 045006.

[309] John C Sunil et al. "The cost of stochastic resetting". In: *Journal of Physics A: Mathematical and Theoretical* 56.39 (2023), p. 395001.

[310] John C Sunil et al. "Minimizing the profligacy of searches with reset". In: *Physical Review E* 110.5 (2024), p. 054122.

[311] Ofir Tal-Friedman et al. "Smart resetting: An energy-efficient strategy for stochastic search processes". In: *Physical Review Research* 7.1 (2025), p. 013033.

[312] Kristian Stølevik Olsen et al. "Thermodynamic cost of finite-time stochastic resetting". In: *Physical Review Research* 6.3 (2024), p. 033343.

[313] Venkataramana Ajjarapu, Ping Lin Lau, and Srinivasu Battula. "An optimal reactive power planning strategy against voltage collapse". In: *IEEE transactions on Power Systems* 9.2 (1994), pp. 906–917.

[314] Zhihong Feng, Venkataramana Ajjarapu, and Dominic J Maratukulam. "A comprehensive approach for preventive and corrective control to mitigate voltage collapse". In: *IEEE Transactions on Power Systems* 15.2 (2000), pp. 791–797.

This page intentionally left blank.

Appendices

This page intentionally left blank.

A

Appendices for Chapter 1

A.1 Derivation of $\langle min(T,R)\rangle$

Let Z represent the random variable

$$Z = min(T,R), \tag{A.1}$$

with the associated density $f_Z(t)$. We thus have

$$\langle min(T,R)\rangle = \int_0^\infty t f_Z(t) dt. \tag{A.2}$$

The density $f_Z(t)$ can be found from the cumulative distribution of Z as

$$f_Z(t) = -\frac{d}{dt} Pr(Z > t). \tag{A.3}$$

Now the cumulative distribution $Pr(Z > t)$ can easily be found by noting that the condition $Z = min(T,R) > t$ holds only when both of T and R are simultaneously greater than t. That in turn implies

$$P(Z > t) = Pr(T > t) Pr(R > t). \tag{A.4}$$

One can now do an integration by parts of the integral in Eq. (A.2) to have

$$\begin{aligned}\langle min(T,R)\rangle &= \int_0^\infty t f_Z(t) dt \\ &= \left[t \int f_Z(t) dt \right]_0^\infty - \int_0^\infty dt \left(\int dt f_Z(t) \right).\end{aligned} \tag{A.5}$$

Upon inserting Eq. (A.3) in the above equation and performing the integrations, we arrive at

$$\langle min(T,R)\rangle = \lim_{t\to\infty} tPr(Z>t) + \int_0^\infty dtPr(Z>t). \tag{A.6}$$

Assuming $Pr(Z>t)$ to decay faster than $1/t$ as $t\to\infty$, we finally have

$$\langle min(T,R)\rangle = \int_0^\infty dtPr(Z>t), \tag{A.7}$$

which upon substituting result form Eq. (A.4) yields

$$\langle min(T,R)\rangle = \int_0^\infty dtPr(T>t)Pr(R>t). \tag{A.8}$$

Now from the generic distribution of T and Poissonian resetting times R we have

$$Pr(T>t) = \int_t^\infty f_T(t')dt', \tag{A.9}$$

$$Pr(R>t) = \int_t^\infty f_R(t')dt' = \int_t^\infty re^{-rt'}dt' = e^{-rt}. \tag{A.10}$$

Plugging these results in Eq. (A.8) we have

$$\langle min(T,R)\rangle = \int_0^\infty dte^{-rt}\int_t^\infty dt' f_T(t') = \frac{1-\widetilde{T}(r)}{r}, \tag{A.11}$$

where $\widetilde{T}(r) = \int_0^\infty dt' e^{-rt'} f_T(t')$ is the Laplace transform of the FP density $f_T(t)$.

B

Appendices for Chapter 2

B.1 Calculation of the average MFPT by solving Eq. (2.1) in the Laplace space

Here, we provide the solution of Eq. (2.1) in the Laplace space. Following that, we calculate the mean first passage time for a diffusing particle with drift, starting from an initial position x_0, to reach the gated target. We start by Laplace transforming Eq. (2.1)

$$\begin{aligned} D\frac{\partial^2\tilde{Q}_0(s|x_0)}{\partial x_0^2} - \lambda\frac{\partial\tilde{Q}_0(s|x_0)}{\partial x_0} - (s+\alpha+r)\tilde{Q}_0(s|x_0) + \alpha\tilde{Q}_1(s|x_0) \\ = -1 - r\tilde{Q}_0(s|x_r) \\ D\frac{\partial^2\tilde{Q}_1(s|x_0)}{\partial x_0^2} - \lambda\frac{\partial\tilde{Q}_1(s|x_0)}{\partial x_0} - (s+\beta+r)\tilde{Q}_1(s|x_0) + \beta\tilde{Q}_0(s|x_0) \\ = -1 - r\tilde{Q}_1(s|x_r), \end{aligned} \tag{B.1}$$

where $\tilde{Q}_\sigma(s|y) \coloneqq \int_0^\infty dt\ e^{-st}Q_\sigma(t|y)$ denote the Laplace transform of $Q_\sigma(t|y)$. Eq. (B.1) is a second order, linear and non-homogeneous differential equation. Considering

$$\tilde{Q}_\sigma(s|x_0) = \tilde{Q}_\sigma^h(s|x_0) + \tilde{Q}_\sigma^{inh}(s|x_0), \tag{B.2}$$

where $\tilde{Q}_\sigma^h(s|x_0)$ and $\tilde{Q}_\sigma^{inh}(s|x_0)$ denote the homogeneous and inhomogeneous parts of $\tilde{Q}_\sigma(s|x_0)$, respectively, we can rewrite Eq. (B.1) in two separate parts. The homogeneous part reads

$$\begin{aligned} D\frac{\partial^2\tilde{Q}_0^h(s|x_0)}{\partial x_0^2} - \lambda\frac{\partial\tilde{Q}_0^h(s|x_0)}{\partial x_0} - (s+\alpha+r)\tilde{Q}_0^h(s|x_0) + \alpha\tilde{Q}_1^h(s|x_0) = 0, \\ D\frac{\partial^2\tilde{Q}_1^h(s|x_0)}{\partial x_0^2} - \lambda\frac{\partial\tilde{Q}_1^h(s|x_0)}{\partial x_0} - (s+\beta+r)\tilde{Q}_1^h(s|x_0) + \beta\tilde{Q}_0^h(s|x_0) = 0. \end{aligned} \tag{B.3}$$

Similarly, the inhomogeneous part reads

$$\begin{aligned} -(s+\alpha+r)\tilde{Q}_0^{inh}(s|x_0) + \alpha\tilde{Q}_1^{inh}(s|x_0) &= -1 - r\tilde{Q}_0(s|x_r), \\ -(s+\beta+r)\tilde{Q}_1^{inh}(s|x_0) + \beta\tilde{Q}_0^{inh}(s|x_0) &= -1 - r\tilde{Q}_1(s|x_r), \end{aligned} \tag{B.4}$$

which is a set of algebraic equations. Solving Eq. (B.4) we obtain

$$\begin{aligned} \tilde{Q}_0^{inh}(s) &= \frac{1}{s+r}\left(1 + \frac{r}{s+r+\alpha+\beta}[\alpha\tilde{Q}_1(s|x_r) + (s+r+\beta)\tilde{Q}_0(s|x_r)]\right), \\ \tilde{Q}_1^{inh}(s) &= \frac{1}{s+r}\left(1 + \frac{r}{s+r+\alpha+\beta}[\beta\tilde{Q}_0(s|x_r) + (s+r+\alpha)\tilde{Q}_1(s|x_r)]\right). \end{aligned} \tag{B.5}$$

We note that $\tilde{Q}_\sigma^{inh}(s)$ depends on x_r and not on x_0. Next, we proceed to solve Eq. (B.3). Noting that x_r does not appear in Eq. (B.3), we simply write $\tilde{Q}_\sigma^h(s|x_0) \equiv \tilde{Q}_\sigma^h$ for notational convenience. Writing Eq. (B.3) in a matrix form, we find

$$D\frac{\partial^2}{\partial x_0^2}\begin{pmatrix}\tilde{Q}_0^h \\ \tilde{Q}_1^h\end{pmatrix} - \lambda\frac{\partial}{\partial x_0}\begin{pmatrix}\tilde{Q}_0^h \\ \tilde{Q}_1^h\end{pmatrix} + \begin{pmatrix}-(s+\alpha+r) & \alpha \\ \beta & -(s+\beta+r)\end{pmatrix}\begin{pmatrix}\tilde{Q}_0^h \\ \tilde{Q}_1^h\end{pmatrix} = 0. \tag{B.6}$$

Taking $\Psi = \begin{pmatrix}\tilde{Q}_0^h & \tilde{Q}_1^h\end{pmatrix}^T$, we rewrite Eq. (B.6)

$$D\frac{\partial^2}{\partial x_0^2}\Psi - \lambda\frac{\partial}{\partial x_0}\Psi + \mathbf{A}\Psi = \mathbf{0}, \quad \text{where} \quad \mathbf{A} = \begin{pmatrix}-(s+\alpha+r) & \alpha \\ \beta & -(s+\beta+r)\end{pmatrix}. \tag{B.7}$$

We now choose $\Psi = \Phi e^{mx_0}$ as the trial solution of Eq. (B.7), that generates the characteristic equation $Dm^2\Phi - \lambda m\Phi + \mathbf{A}\Phi = \mathbf{0}$, which gives

$$\begin{pmatrix}Dm^2 - \lambda m - (s+\alpha+r) & \alpha \\ \beta & Dm^2 - \lambda m - (s+\beta+r)\end{pmatrix}\Phi = \mathbf{0}. \tag{B.8}$$

The roots of Eq. (B.8) can be found as

$$\begin{aligned} m_1 &= \frac{\lambda - \sqrt{\lambda^2 + 4D(s+r)}}{2D}, \\ m_2 &= \frac{\lambda - \sqrt{\lambda^2 + 4D(\alpha+\beta+s+r)}}{2D}, \\ m_3 &= \frac{\lambda + \sqrt{\lambda^2 + 4D(s+r)}}{2D}, \\ m_4 &= \frac{\lambda + \sqrt{\lambda^2 + 4D(\alpha+\beta+s+r)}}{2D}. \end{aligned} \tag{B.9}$$

A close inspection of the above roots reveals that m_1 and m_2 are negative, while m_3 and m_4 are positive (since $D, s, r > 0$). Since $\tilde{Q}_\sigma^h \sim e^{mx_0}$, and $\tilde{Q}_\sigma(s|x_0) = 1/s$ for $x_0 \to \infty$ (because the survival probability $Q_\sigma(t|x_0)|_{x_0\to\infty} = 1$ and its Laplace transform is $1/s$), we select only m_1 and m_2 as the plausible roots.

Letting Φ_1 denote the eigenvector corresponding to m_1 and utilizing Eq. (B.8), we get $\Phi_1 = \binom{1}{1}$. In a similar manner, the eigenvector corresponding to m_2 is given by $\Phi_2 = \begin{pmatrix} -\alpha/\beta \\ 1 \end{pmatrix}$. The general solution of Eq. (B.7) thus reads $\Psi = c_1\Phi_1 e^{m_1 x_0} + c_2\Phi_2 e^{m_2 x_0}$, and subsequently

$$\tilde{Q}_0^h = c_1 e^{m_1 x_0} - \frac{\alpha}{\beta} c_2 e^{m_2 x_0}, \tag{B.10}$$

$$\tilde{Q}_1^h = c_1 e^{m_1 x_0} + c_2 e^{m_2 x_0} \tag{B.11}$$

where c_1 and c_2 are constants to be determined in the following. To this end, we use the boundary condition $\frac{\partial Q_0(t|x_0)}{\partial x_0}|_{x_0=0} = 0$ (equivalently, $\frac{\partial \tilde{Q}_0(s|x_0)}{\partial x_0}|_{x_0=0} = 0$) which results in $\frac{\partial \tilde{Q}_0^h(s|x_0)}{\partial x_0}|_{x_0=0} = 0$, since $\tilde{Q}_\sigma^{inh}(s)$ does not depend on x_0. Applying this in Eq. (B.10) results in

$$c_2 = \left(\frac{\beta}{\alpha}\right)\frac{c_1 m_1}{m_2}. \tag{B.12}$$

To compute c_1, we recall the other boundary condition (absorbing) $Q_1(t|0) = 0$ (equivalently, $\tilde{Q}_1(s|0) = 0$). Combining Eq. (B.5) and Eq. (B.11) along with the boundary condition at $x_0 = 0$, we can write

$$\begin{aligned} \tilde{Q}_1(s|0) = c_1 + \left(\frac{\beta}{\alpha}\right)\frac{m_1}{m_2}c_1 + \frac{1}{s+r}\Bigg(\frac{r}{s+r+\alpha+\beta}[\beta\tilde{Q}_0(s|x_r) \\ + (s+r+\alpha)\tilde{Q}_1(s|x_r)] + 1\Bigg) = 0. \end{aligned} \tag{B.13}$$

Incorporating Eq. (B.12) in Eq. (B.13) and solving for c_1 and hence c_2 finally gives

$$c_1 = -\left[\frac{\alpha m_2}{(\alpha m_2+\beta m_1)(s+r)}\right]\left(1+\frac{r}{s+r+\alpha+\beta}[\beta\tilde{Q}_0(s|x_r)+(s+r+\alpha)\tilde{Q}_1(s|x_r)]\right),$$
$$c_2 = -\left[\frac{\beta m_1}{(\alpha m_2+\beta m_1)(s+r)}\right]\left(1+\frac{r}{s+r+\alpha+\beta}[\beta\tilde{Q}_0(s|x_r)+(s+r+\alpha)\tilde{Q}_1(s|x_r)]\right). \tag{B.14}$$

Plugging in everything together into Eq. (B.2), we find

$$\begin{aligned}\tilde{Q}_0(s|x_0) =& c_1 e^{m_1 x_0} - \frac{m_1}{m_2}c_1\, e^{m_2 x_0} + \frac{1}{s+r}\Bigg(1+\\ &\frac{r}{s+r+\alpha+\beta}\left[\alpha\tilde{Q}_1(s|x_r)+(s+r+\beta)\tilde{Q}_0(s|x_r)\right]\Bigg),\\ \tilde{Q}_1(s|x_0) =& c_1\, e^{m_1 x_0} + \left(\frac{\beta}{\alpha}\right)\frac{m_1}{m_2}c_1\, e^{m_2 x_0} + \frac{1}{s+r}\Bigg(1+\\ &\frac{r}{s+r+\alpha+\beta}\left[\beta\tilde{Q}_0(s|x_r)+(s+r+\alpha)\tilde{Q}_1(s|x_r)\right]\Bigg),\end{aligned} \tag{B.15}$$

which are written in terms of $\tilde{Q}_\sigma(s|x_r)$. Setting $x_r = x_0$ in Eq. (B.15) in a self-consistent manner, we find the exact expressions for the survival functions

$$\begin{aligned}\tilde{Q}_0(s|x_0) &= \frac{(\beta m_1+\alpha m_2)+m_1 e^{m_2 x_0}\left(\alpha+\frac{r(\alpha+\beta)}{\alpha+\beta+s}\right)-\alpha m_2 e^{m_1 x_0}}{\frac{\beta m_1 r s e^{m_2 x_0}}{\alpha+\beta+s}+(\alpha m_2 r e^{m_1 x_0}+\beta m_1 s+\alpha m_2 s)},\\ \tilde{Q}_1(s|x_0) &= -\frac{(\alpha+\beta+s)\left(\alpha m_2\left(e^{m_1 x_0}-1\right)+\beta m_1\left(e^{m_2 x_0}-1\right)\right)}{(\alpha+\beta+s)\left(\alpha m_2 r e^{m_1 x_0}+\beta m_1 s+\alpha m_2 s\right)+\beta m_1 r s e^{m_2 x_0}}.\end{aligned} \tag{B.16}$$

The averaged survival probability can be found by substituting Eq. (B.16) into Eq. (2.4). This results in

$$\tilde{Q}_r^G(s|x_0) = \frac{\beta m_1\left(\frac{r e^{m_2 x_0}}{\alpha+\beta+s}+1\right)+\alpha m_2\left(1-e^{m_1 x_0}\right)}{\frac{\beta m_1 r s e^{m_2 x_0}}{\alpha+\beta+s}+(\alpha m_2 r e^{m_1 x_0}+\beta m_1 s+\alpha m_2 s)}. \tag{B.17}$$

Generically, Eq. (B.17) can be used to derive all the first passage time moments. The observable of our interest in this problem, for example, the averaged MFPT reads $\langle T_r^G\rangle = \tilde{Q}_r^G(s|x_0)|_{s=0}$ [134]. This results in Eq. (2.7) in the main text.

Alternatively, we can get Eq. (2.7) from Eq. (B.15) by calculating individual mean first passage times conditioned on the initial state of the target state. To this end, let us denote $T_\sigma^G(x_0)$ as the first-passage time to reach the target at the origin starting from the position x_0 with initial target state being at σ. Using $\langle T_\sigma^G(x_0)\rangle = \tilde{Q}_\sigma(s|x_0)|_{s=0}$ and

setting $s \longrightarrow 0$ in Eq. (B.15), we get

$$\begin{aligned}\langle T_1^G(x_0)\rangle &= \frac{1}{r}\left(e^{\mu_1 x_0}-1\right)+\frac{1}{r}\left[\frac{\beta\mu_1}{\alpha\mu_2}e^{\mu_1 x_0}\left(1-e^{-\mu_2 x_0}\right)\right],\\ \langle T_0^G(x_0)\rangle &= \frac{1}{r}\left(e^{\mu_1 x_0}-1\right)+\frac{1}{r}\left[\frac{\mu_1}{\mu_2}e^{\mu_1 x_0}\left(e^{-\mu_2 x_0}\left(1+\frac{r}{\alpha}\right)+\frac{\beta}{\alpha}\right)\right],\end{aligned} \tag{B.18}$$

where $\mu_1 := -m_1|_{s=0} > 0$ and $\mu_2 := -m_2|_{s=0} > 0$. Finally, plugging in Eq. (B.18) into Eq. (2.5) in the main text, we obtain Eq. (2.7).

B.2 The average MFPT for gated drift-diffusion without resetting

In the absence of resetting, the backward master equations in terms of the survival probability read

$$\begin{aligned}\frac{\partial Q_0^{r=0}(t|x_0)}{\partial t} &= -\lambda\frac{\partial Q_0^{r=0}(t|x_0)}{\partial x_0}+D\frac{\partial^2 Q_0^{r=0}(t|x_0)}{\partial x_0^2}+ \quad \alpha\left[Q_1^{r=0}(t|x_0)-Q_0^{r=0}(t|x_0)\right]\\ \frac{\partial Q_1^{r=0}(t|x_0)}{\partial t} &= -\lambda\frac{\partial Q_1^{r=0}(t|x_0)}{\partial x_0}+D\frac{\partial^2 Q_1^{r=0}(t|x_0)}{\partial x_0^2}+ \quad \beta\left[Q_0^{r=0}(t|x_0)-Q_1^{r=0}(t|x_0)\right].\end{aligned} \tag{B.19}$$

Solving Eq. (B.19), we obtain the following expressions for the survival functions in the Laplace space

$$\begin{aligned}\tilde{Q_0}^{r=0}(s|x_0) &= \frac{1}{s}-\frac{1}{s}\frac{\alpha n_2}{\beta n_1+\alpha n_2}\left(e^{-n_1 x_0}-\frac{n_1 e^{-n_2 x_0}}{n_2}\right),\\ \tilde{Q_1}^{r=0}(s|x_0) &= \frac{1}{s}-\frac{1}{s}\frac{\alpha n_2}{\beta n_1+\alpha n_2}\left(e^{-n_1 x_0}+\frac{\beta n_1 e^{-n_2 x_0}}{\alpha n_2}\right),\end{aligned} \tag{B.20}$$

where $n_1 = \frac{-\lambda+\sqrt{4Ds+\lambda^2}}{2D}$ and $n_2 = \frac{-\lambda+\sqrt{4D(\alpha+\beta+s)+\lambda^2}}{2D}$. Setting $s \longrightarrow 0$, the underlying MFPTs can be computed as before. Eventually, one finds

$$\langle T_0^{r=0}\rangle = \frac{x_0}{\lambda}+\frac{2D\left(\beta+\alpha e^{-\frac{x_0\left(\sqrt{4D(\alpha+\beta)+\lambda^2}-\lambda\right)}{2D}}\right)}{\alpha\lambda\left(-\lambda+\sqrt{4D(\alpha+\beta)+\lambda^2}\right)}, \tag{B.21}$$

$$\langle T_1^{r=0}\rangle = \frac{x_0}{\lambda}+\frac{2\beta D\left(-e^{-\frac{x_0\left(\sqrt{4D(\alpha+\beta)+\lambda^2}-\lambda\right)}{2D}}+1\right)}{\alpha\lambda\left(-\lambda+\sqrt{4D(\alpha+\beta)+\lambda^2}\right)}. \tag{B.22}$$

The averaged MFPT is then given by

$$\begin{aligned}\langle T^G\rangle &= p_r\langle T_1^{r=0}\rangle + (1-p_r)\langle T_0^{r=0}\rangle \\ &= \frac{x_0}{\lambda} + \frac{2\beta D}{\alpha\lambda\left(\sqrt{4D(\alpha+\beta)+\lambda^2}-\lambda\right)}.\end{aligned} \tag{B.23}$$

Note that for $p_r \to 1$ ($\beta \to 0$), Eq. (B.23) reduces to $\langle T\rangle = x_0/\lambda$, as expected. Moreover, since $D, \alpha, \beta > 0$, the second term of the expression of $\langle T^G\rangle$ in Eq. (B.23) is always positive, which clearly shows $\langle T^G\rangle > \langle T\rangle$.

C

Appendices for Chapter 3

C.1 Moment generating function of S_R

In this section, we try to find the general expression for the mean and second moment as written in Eq. (3.6) and Eq. (3.7). For that we first find the general Laplace transform or the moment generating function of S_R. Using that one can find all the moments in systematic fashion as we show below. We start by recalling Eq. (3.4) from the main text

$$S_R = S_{on} + \begin{cases} S & \text{if } S < R\,, \\ \\ R + S'_R & \text{if } R \leq S\,. \end{cases} \tag{C.1}$$

The above equation can also be written in a more compact way as

$$S_R = S_{on} + I(S < R)S + I(R \leq S))R + I(R \leq S)S'_R, \tag{C.2}$$

where $I(R \leq S)$ is the indicator function which takes the value 1 when $R \leq S$ and zero otherwise. Thus,

$$\langle I(R \leq S)\rangle = Pr(R \leq S). \tag{C.3}$$

Let us now define $\widetilde{Z}(p) = \langle e^{-pZ}\rangle = \int f_Z(z)e^{-pz}dz$ as the moment generating function of the random variable Z, from which all its moments can be easily found. The Laplace transform of Eq. (C.2) can be given as

$$\begin{aligned} \widetilde{S}_R(p) &= \langle e^{-pS_R}\rangle \\ &= \langle e^{-p[S_{on}+I(S<R)S+I(R\leq S))R+I(R\leq S)S'_R]}\rangle \\ &= \langle e^{-pS_{on}}\rangle \left[\langle I(R \leq S)e^{-pS_{min}}\rangle + \langle I(S < R)e^{-pR_{min}-pS'_R}\rangle\right], \end{aligned} \tag{C.4}$$

where $S_{min} \equiv \{S|S < R\} =$ and $R_{min} \equiv \{R|R < R\}$. We have also used the fact that S'_R is an independent and identically distributed copy of S_R and thus independent of R & S. Performing the expectations over the indicator functions, we find

$$\begin{aligned}\widetilde{S}_R(p) &= \langle e^{-pS_{on}} \rangle \left[Pr(S < R) \langle e^{-pS_{min}} \rangle + Pr(R \leq S) \langle e^{-pR_{min}} \rangle \langle e^{-pS'_R} \rangle \right] \\ &= \widetilde{S}_{on}(p) \left[Pr(S < R) \widetilde{S}_{min}(p) + Pr(R \leq S) \widetilde{R}_{min}(p) \langle e^{-pS_R} \rangle \right] \\ &= \widetilde{S}_{on}(p) \left[Pr(S < R) \widetilde{S}_{min}(p) + Pr(R \leq S) \widetilde{R}_{min}(p) \widetilde{S}_R(p) \right], \end{aligned} \tag{C.5}$$

from where one finds

$$\widetilde{S}_R(p) = \frac{Pr(S < R) \widetilde{S}_{min}(p) \widetilde{S}_{on}(p)}{1 - Pr(R \leq S) \widetilde{R}_{min}(p) \widetilde{S}_{on}(p)}. \tag{C.6}$$

This is an exact expression for the distribution of S_R in Laplace space. This is also the moment generating function from which n^{th} moment of S_R can be computed directly via

$$\langle S_R^n \rangle = (-1)^n \left. \frac{d^n \widetilde{S}_R(p)}{dp^n} \right|_{p=0}. \tag{C.7}$$

For instance, the first moment reads

$$\begin{aligned}\langle S_R \rangle &= - \left. \frac{d\widetilde{S}_R(p)}{dp} \right|_{p=0} \\ &= \frac{Pr(S < R) \left[(1 - Pr(R \leq S)) (\langle S_{on} \rangle + \langle S_{min} \rangle) + Pr(R \leq S) \langle S_{on} \rangle + Pr(R \leq S) \langle R_{min} \rangle \right]}{(1 - Pr(R \leq S))^2} \\ &= \frac{Pr(S < R) \left[Pr(S < R) \langle S_{min} \rangle + Pr(R \leq S) \langle R_{min} \rangle + \langle S_{on} \rangle \right]}{(Pr(S < R))^2} \\ &= \frac{\langle \min(S, R) \rangle + \langle S_{on} \rangle}{Pr(S < R)}, \end{aligned} \tag{C.8}$$

which is Eq. (3.6) with the identification $\langle \min(S, R) \rangle = Pr(S < R) \langle S_{min} \rangle + Pr(R \leq S) \langle R_{min} \rangle$. A similar exercise for the second moment gives

$$\begin{aligned}\langle S_R^2 \rangle &= \left. \frac{d^2 \widetilde{S}_R(p)}{dp^2} \right|_{p=0} \\ &= \frac{\langle (\min(S, R) + S_{on})^2 \rangle}{Pr(S < R)} + \frac{2 Pr(R \leq S) (\langle R_{min} \rangle + \langle S_{on} \rangle) (\langle \min(S, R) \rangle + \langle S_{on} \rangle)}{Pr(S < R)^2}. \end{aligned} \tag{C.9}$$

which is identified as the Eq. (3.7) in the main text. Eq. (C.7) thus encodes all the information about the higher moments.

C.2 Moments of the service time for Poissonian resetting

In this section we take the representative case when the resetting times are drawn from an exponential distribution given by

$$f_R(t) = re^{-rt}. \tag{C.10}$$

where r is the resetting rate. The cumulative function is given by

$$Pr(R \leq t) = 1 - e^{-rt}. \tag{C.11}$$

The distribution of the random variable $\min(S, R)$ can be computed by noting

$$\begin{aligned} Pr(\min(S,R) \leq t) &= 1 - Pr(\min(S,R) > t) \\ &= 1 - Pr(S > t)Pr(R > t) \\ &= 1 - Pr(S > t)e^{-rt}, \end{aligned} \tag{C.12}$$

from which one can gets

$$f_{min(S,R)}(t) = e^{-rt} f_S(t) + re^{-rt} Pr(S > t), \tag{C.13}$$

which can be used to compute all the moments for the random variable $\min(S, R)$.

Mean service time with overheads: To compute the mean, we note that the first term on the numerator in Eq. (3.6)) can be written as

$$\langle \min(S,R) \rangle = \frac{1 - \widetilde{S}(r)}{r}, \tag{C.14}$$

where $\widetilde{S}(r) = \int_0^\infty dt\ e^{-st}\ f_S(t)$. The denominator can be written as

$$Pr(S < R) = \int_0^\infty dt\ f_S(t) Pr(R > t). \tag{C.15}$$

For exponential resetting times $Pr(R > t) = e^{-rt}$ and we have

$$Pr(S < R) = \int_0^\infty dt\ f_S(t) e^{-rt} = \widetilde{S}(r). \tag{C.16}$$

Combining together, we find

$$\langle S_r \rangle = \frac{1 - \widetilde{S}(r) + r\langle S_{on} \rangle}{r\widetilde{S}(r)}, \tag{C.17}$$

which is Eq. (3.8) in main text.

Second moment of the service time with overheads: To find the second moment for

Poisson resetting, we now use Eq. (3.7). The expectation $\langle \min(S,R)^2 \rangle$ in the numerator can be computed directly using Eq. (C.13)

$$\begin{aligned}
\langle \min(S,R)^2 \rangle &= \int_0^\infty dt\ t^2 \left(f_S(t) Pr(R > t) + f_R(t) Pr(S > t) \right) \\
&= \int_0^\infty dt\ t^2 \left(f_S(t)\, e^{-rt} + r\ Pr(S > t)\, e^{-rt} \right) \\
&= \int_0^\infty dt\ t^2 f_S(t)\, e^{-rt} + r \int_0^\infty dt\ t^2\ Pr(S > t)\, e^{-rt} \\
&= \frac{d^2\tilde{S}(r)}{dr^2} + r \int_0^\infty dt\ t^2 \left(1 - Pr(S < t)\right) e^{-rt} \\
&= \frac{d^2\tilde{S}(r)}{dr^2} + \frac{2}{r^2} - r \int_0^\infty dt\ t^2 Pr(S < t) e^{-rt} \\
&= \frac{d^2\tilde{S}(r)}{dr^2} + \frac{2}{r^2} - r \frac{d^2\left(\frac{\tilde{S}(r)}{r}\right)}{dr^2} \\
&= \frac{2r\ \frac{d\tilde{S}(r)}{dr} - 2\tilde{S}(r) + 2}{r^2}.
\end{aligned} \tag{C.18}$$

In the above derivation we have used the following property $\int_0^\infty dt\ t^n f(t) e^{-rt} = (-1)^n \frac{d^n \tilde{f}(r)}{dr^n}$. Next, to calculate $\langle R_{\min} \rangle$ we need to use the density of the conditional time R_{min} which is given by

$$f_{R_{\min}}(t) = \frac{f_R(t) \int_t^\infty dt'\ f_S(t')}{Pr(R \le S)} = \frac{f_R(t) Pr(S > t)}{Pr(R \le S)}. \tag{C.19}$$

Then, $\langle R_{\min} \rangle$ can be expressed as

$$\begin{aligned}
\langle R_{\min} \rangle &= \int_0^\infty dt\ t f_{R_{min}}(t) \\
&= \frac{1}{Pr(R \le S)} \int_0^\infty dt\ t\ r e^{-rt} Pr(S > t) \\
&= \frac{r}{1 - Pr(S < R)} \int_0^\infty dt\ t\ e^{-rt} \left(1 - Pr(S < t)\right) \\
&= \frac{r\left(\int_0^\infty dt\ t\ e^{-rt} - \int_0^\infty dt\ t\ e^{-rt} Pr(S < t) \right)}{1 - \tilde{S}(r)} \\
&= \frac{r\left(\frac{1}{r^2} + \frac{d\left(\frac{\tilde{S}(r)}{r}\right)}{dr} \right)}{1 - \tilde{S}(r)} \\
&= \frac{r\ \frac{d\tilde{S}(r)}{dr} - \tilde{S}(r) + 1}{r\left(1 - \tilde{S}(r)\right)}.
\end{aligned} \tag{C.20}$$

Substituting Eqs. (C.18) and (C.20) into Eq. (3.7), one obtains

$$\langle S_r^2 \rangle = \frac{2r\frac{d\widetilde{S}(r)}{dr}(1 + r\langle S_{on}\rangle) + 2(1 - \widetilde{S}(r))(1 + r\langle S_{on}\rangle)^2 + r^2\widetilde{S}(r)\langle S_{on}^2\rangle}{r^2\widetilde{S}(r)^2}, \tag{C.21}$$

which was announced in Eq. (3.9) in the main text.

C.3 General discussion on the "resetting induced efficiency criterion" for the mean queue length with different variability CV_{on}

In this section, we elaborate more on the general conditions that were obtained in Sec. (3.5) to underpin the effect of resetting. We start by deriving the most general criterion that ensures the existence of an optimal r^*. To see this, we introduce an infinitesimal resetting rate δr and ask under what condition the following inequality $\langle S_{\delta r \to 0}\rangle < \langle S_u\rangle$ holds. Expanding Eq. (3.8) in the power of δr and imposing the above condition, we derive a universal relation

$$CV^2 > 1 + 2\frac{\langle S_{on}\rangle}{\langle S\rangle}, \tag{C.22}$$

that guarantees the existence for an optimal resetting rate [129]. In terms of CV_u with the help of Eq. (3.14) this criterion takes the form

$$CV_u^2 > 1 + \frac{\langle S_{on}\rangle^2}{\langle S_u\rangle^2}(CV_{on}^2 - 1). \tag{C.23}$$

The above equation will be central to our remaining discussion where we study various cases for CV_{on}.

C.3.1 Case I: $CV_{on} < 1$

In Eq. (3.22) in the main text we argued that for $CV_u > 1$ the mean queue length can be reduced by introducing resetting when $CV_{on} < 1$. However, we emphasize that this is not a necessary (albeit sufficient) condition. From Eq. (C.23) we notice that the RHS is less than one for $CV_{on} < 1$. This in turn implies a finite optimal value of r^* also can be found under the same condition. This implies that ρ_{r^*} becomes less than ρ for $CV_u < 1$. As a result, for a sufficiently small ρ_{r^*}, one can still have $\langle N_{r^*}^I\rangle < \langle N\rangle$ from Eq. (3.21). In Fig. (3.3) we indeed find that the deviation occurs at value of CV_u which is less than unity.

C.3.2 Case II: $CV_{on} = 1$

In this case the RHS of Eq. (C.23) becomes exactly unity and hence, a finite optimal r^* shows up only when $CV_u > 1$. It is thus evident from Eq. (3.24) that $CV_u > 1$ is both a

necessary and sufficient condition for the reduction in the mean queue length. As shown in Fig. (3.3), the transition point (where $\langle N_{r^*}^{II}\rangle < \langle N\rangle$) is exactly found at $CV_u = 1$.

C.3.3 Case III: $CV_{on} > 1$

In this case the RHS of Eq. (C.23) is strictly greater than one. One can thus expect to find an optimal r^* for values of $CV_u > 1$. Thus the condition $\langle N_{r^*}^{II}\rangle < \langle N\rangle$ will be satisfied only when $CV_u > 1$. This is also evident from Fig. (3.3) where we see that the transition point occurs at $CV_u > 1$.

To derive the criterion (Eq. (3.26)) as mentioned in the main text we recall the PK formula from Eq. (3.25) for the optimally restarted process and the same without resetting from Eq. (3.1)

$$\langle N_{r^*}^{III}\rangle = \frac{\rho_{r^*}}{1-\rho_{r^*}} + \frac{\lambda^2}{2(1-\rho_{r^*})}\frac{\langle S_{on}\rangle^2}{\tilde{S}(r^*)}\left(CV_{on}^2 - 1\right) \tag{C.24}$$

$$\langle N\rangle = \frac{\rho}{1-\rho} + \frac{\rho^2}{2(1-\rho)}\left(CV_u^2 - 1\right), \tag{C.25}$$

and impose the condition $\langle N_{r^*}^{III}\rangle < \langle N\rangle$. For a finite r^*, this would yield

$$\begin{aligned}\lambda^2\frac{\langle S_{on}\rangle^2}{\tilde{S}(r^*)}\left(CV_{on}^2 - 1\right) &< \rho^2\left(CV_u^2 - 1\right)\\ CV_u^2 &> 1 + \left(\frac{\langle S_{on}\rangle}{\langle S_u\rangle}\right)^2\frac{1}{\tilde{S}(r^*)}(CV_{on}^2 - 1),\end{aligned} \tag{C.26}$$

which gives the criterion obtained in Eq. (3.26) where we have substituted $\rho = \lambda\langle S_u\rangle$. Finally, we remark that this is a sufficient condition (but not necessary). In other words, one can still find a CV_u where this condition is not satisfied but the inequality $\langle N_{r^*}^{III}\rangle < \langle N\rangle$ holds.

C.4 Moments for sharp resetting times

This section is dedicated to compute the first two moments of the service time under sharp resetting. Here, resetting occurs always after a fixed time interval τ such that

$$f_R(t) = \delta(t-\tau), \tag{C.27}$$

from which one can see

$$Pr(R > t) = \theta(\tau - t), \tag{C.28}$$

where $\theta(z)$ is the Heaviside theta function which takes value unity only when $z > 0$ and zero otherwise.

Mean service time with overheads: The numerator in Eq. (3.6) can be computed in the following way

$$\begin{aligned}\langle \min(S,R)\rangle &= \int_0^\infty Pr(S>t)Pr(R>t)dt \\ &= \int_0^\infty Pr(S>t)\theta(\tau-t)dt \\ &= \int_0^\tau dt\ q_S(t), \end{aligned} \tag{C.29}$$

where $q_S(t) = Pr(S > t)$ is the survival probability of the process S up to time t, which indicates the probability that the service has not yet been completed up to time t. The denominator in Eq. (3.6) is found to be

$$\begin{aligned} Pr(S<R) &= \int_0^\infty dt\ f_R(t)Pr(S<t) \\ &= \int_0^\infty dt\ \delta(t-\tau)Pr(S<t) \\ &= \int_0^\infty dt\ \delta(t-\tau)(1-q_S(t)) \\ &= 1-q_S(\tau). \end{aligned} \tag{C.30}$$

Substituting Eq. (C.29) and Eq. (C.30) in Eq. (3.6) we obtain the first moment for sharp resetting as

$$\langle S_\tau\rangle = \frac{\int_0^\tau q_S(t)dt + \langle S_{on}\rangle}{1-q_S(\tau)}, \tag{C.31}$$

which was announced in Eq. (3.39).

Second moment of service time with overheads: Following the same procedure as the previous section, we find

$$\begin{aligned}\langle \min(S,R)^2\rangle &= \int_0^\infty dt\ t^2\left(f_S(t)Pr(R>t) + f_R(t)Pr(S>t)\right) \\ &= \int_0^\infty dt\ t^2\left[-\frac{\partial q_S(t)}{\partial t}\theta(\tau-t) + q_S(t)\delta(\tau-t)\right] \\ &= \tau^2 q_S(\tau) - \int_0^\tau dt\ t^2\frac{\partial q_S(t)}{\partial t} \\ &= \tau^2 q_S(\tau) - \tau^2 q_S(\tau) + 2\int_0^\tau dt\ t\ q_S(t) \\ &= 2\int_0^\tau dt\ t\ q_S(t). \end{aligned} \tag{C.32}$$

The quantity $\langle R_{min} \rangle$ can also be obtained from Eq. (C.19) directly

$$\begin{aligned}\langle R_{\min} \rangle &= \int_0^\infty dt\ t f_{R_{min}}(t) \\ &= \frac{1}{Pr(\tau \leq S)} \int_0^\infty dt\ t\delta(t-\tau) Pr(S > t) \\ &= \frac{\tau q_S(\tau)}{q_S(\tau)} \\ &= \tau. \end{aligned} \tag{C.33}$$

Using Eqs. (C.32) and (C.33) in Eq. (3.7), we arrive at the following expression for the second moment of service time with overheads

$$\langle S_\tau^2 \rangle = \frac{2\int_0^\tau t q_S(t)dt + 2\langle S_{on} \rangle \int_0^\tau q_S(t)dt + \langle S_{on}^2 \rangle}{1 - q_S(\tau)} + \frac{2q_S(\tau)(\tau + \langle S_{on} \rangle)\left(\int_0^\tau q_S(t)dt + \langle S_{on} \rangle\right)}{(1 - q_S(\tau))^2}, \tag{C.34}$$

which is Eq. (3.40) in the main text.

D

Appendices for Chapter 4

D.1 Exact expressions for the MSD and correlation function

In this section, we provide the exact analytical expression for the MSD with resetting, *i.e.*, $\langle x^2(t)\rangle_r$ (plotted in Fig. (3.3)) and the correlation function both with and without resetting, *i.e.*, $C_r(t,t')$ (plotted in Fig. (3.4)) respectively, for Jeffreys fluid model. In both the expressions we assume $k_BT/m = 1$. With α, β defined as in Eq. (4.29), the MSD with resetting is given by

$$\begin{aligned}
&\langle x^2(t)\rangle_r \\
&= \frac{\beta^2}{\omega^2(\alpha^2-\beta^2)\left[4\beta^2 + r\tau_s(4\alpha + r\tau_s)\right]}\Bigg\{e^{-t\left(r+\frac{2\alpha}{\tau_s}\right)}\Bigg[\sqrt{\alpha^2-\beta^2}\left(-4\alpha+4\beta^2+(\beta^2-1)r\tau_s\right) \\
&\quad\times\sinh\left(\frac{2t\sqrt{\alpha^2-\beta^2}}{\tau_s}\right) - \left(4\alpha^2 - 2(2\alpha+1)\beta^2 + 2\beta^4 + r\left[(\alpha-2)\beta^2+\alpha\right]\tau_s\right) \\
&\quad\times\cosh\left(\frac{2t\sqrt{\alpha^2-\beta^2}}{\tau_s}\right)\Bigg] + \frac{2(\alpha^2-\beta^2)\left[4\alpha + r\tau_s(4\alpha-\beta^2+r\tau_s+1)\right]}{2\alpha+r\tau_s} \\
&\quad - \frac{\alpha(2\alpha-\beta^2-1)\left[4\beta^2+r\tau_s(4\alpha+r\tau_s)\right]e^{-t\left(r+\frac{2\alpha}{\tau_s}\right)}}{2\alpha+r\tau_s}\Bigg\}. \qquad \text{(D.1)}
\end{aligned}$$

The correlation function of the underlying process *i.e.* $C(t,t')$ for $t > t'$ is given by

$$C(t,t') = \frac{e^{-\frac{\alpha(t'+t)}{\tau_s}}}{2\omega^2(\alpha^2-\beta^2)}\Bigg\{\left[\beta^2(-2\alpha+\beta^2+1)+2\alpha^2-\beta^2 e^{\frac{2\alpha t'}{\tau_s}}\right]\cosh\left(\frac{\sqrt{\alpha^2-\beta^2}\,(t-t')}{\tau_s}\right)$$
$$+\left(-2\alpha^2+2\alpha\beta^2-\beta^4+\beta^2\right)\cosh\left(\frac{\sqrt{\alpha^2-\beta^2}\,(t'+t)}{\tau_s}\right)$$
$$-2\sqrt{\alpha^2-\beta^2}\,(\alpha-\beta^2)\left[\sinh\left(\frac{\sqrt{\alpha^2-\beta^2}\,(t'+t)}{\tau_s}\right)-e^{\frac{2\alpha t'}{\tau_s}}\sinh\left(\frac{\sqrt{\alpha^2-\beta^2}\,(t-t')}{\tau_s}\right)\right]\Bigg\}. \tag{D.2}$$

The correlation function under resetting, after utilizing Eq. (4.17) and Eq. (4.25), is given by

$$C_r(t,t') = \frac{e^{-r(t-t')}}{2\omega^2(\beta^2-\alpha^2)(4\beta^2+r\tau_s(4\alpha+r\tau_s))}\Bigg(\frac{r\tau_s\, e^{-rt'-\alpha(t'+t)/\tau_s}}{2\alpha+r\tau_s}\cosh\frac{-\sqrt{\alpha^2-\beta^2}(t-t')}{\tau_s}$$
$$\times\left[\beta^2(-2\alpha+\beta^2+1)(4\beta^2+r\tau_s(4\alpha+r\tau_s))+2(\alpha^2-\beta^2)\left(2((\beta^2-2\alpha)^2+\beta^2)+r\tau_s(6\alpha-2\beta^2+r\tau_s)\right)e^{t'(r+2\alpha/\tau_s)}\right]$$
$$+e^{-3rt'-\alpha(3t'+t)/\tau_s}\Bigg[-e^{2t'(r+\alpha/\tau_s)}(\beta^2(-2\alpha+\beta^2+1)+2(\alpha^2-\beta^2)e^{t'(r+2\alpha/\tau_s)})\cosh\frac{\sqrt{\alpha^2-\beta^2}(t-t')}{\tau_s}(4\beta^2+r\tau_s(4\alpha+r\tau_s))$$
$$+2\beta^2\Big(e^{2t'(r+\alpha/\tau_s)}\cosh\frac{\sqrt{\alpha^2-\beta^2}(t'+t)}{\tau_s}(4\alpha^2-2(2\alpha+1)\beta^2+2\beta^4+r((\alpha-2)\beta^2+\alpha)\tau_s)$$
$$-\sqrt{\alpha^2-\beta^2}(4\alpha-(\beta^2(r\tau_s+4))+r\tau_s)(e^{3rt'+4\alpha t'/\tau_s}\sinh\frac{\sqrt{\alpha^2-\beta^2}(t-t')}{\tau_s}-e^{2t'(r+\alpha/\tau_s)}\sinh\frac{\sqrt{\alpha^2-\beta^2}(t'+t)}{\tau_s})\Big)\Bigg]\Bigg) \tag{D.3}$$

Asymptotic behaviour of the correlation function

Let us now provide the exact asymptotic forms of the correlation function which was discussed briefly in section 4.4.2. The exact asymptotic form of the correlation function of the underlying reset-free process is given by

$$C(t,t';\ t\gg t')$$
$$\sim\frac{\exp\left[-\frac{t'(\sqrt{\alpha^2-\beta^2}+\alpha)+t(\alpha-\sqrt{\alpha^2-\beta^2})}{\tau_s}\right]}{4\omega^2(\alpha^2-\beta^2)}\Big(2(\alpha^2-\beta^2(\sqrt{\alpha^2-\beta^2}+1)+\alpha\sqrt{\alpha^2-\beta^2})e^{2\alpha t'/\tau_s}$$
$$+\beta^2(-2\alpha+\beta^2+1)+e^{2t'\sqrt{\alpha^2-\beta^2}/\tau_s}\left(-2\alpha^2+2\alpha(\beta^2-\sqrt{\alpha^2-\beta^2})+\beta^2(2\sqrt{\alpha^2-\beta^2}-\beta^2+1)\right)\Big) \tag{D.4}$$

Keeping t' fixed, in the limit $t\to\infty$ note that the term under the parenthesis is just a constant prefactor with the only t dependence coming through the exponential term outside which is $e^{-\frac{\left(\alpha-\sqrt{\alpha^2-\beta^2}\right)t}{\tau_s}}$, the result provided in Eq. (4.49).

On the other hand, the asymptotic behavior of the correlation function under resetting is given by

$$
\begin{aligned}
C_r(t,t';\ t \gg t') \sim{}& \frac{\beta^2 \exp\left[-\frac{t(-\sqrt{\alpha^2-\beta^2}+\alpha+r\tau_s)+t'(\sqrt{\alpha^2-\beta^2}+\alpha)}{\tau_s}\right]}{2\omega^2(\alpha^2-\beta^2)(2\alpha+r\tau_s)(4\beta^2+r\tau_s(4\alpha+r\tau_s))} \\
&\times\Bigg(\alpha(-2\alpha+\beta^2+1)(4\beta^2+r\tau_s(4\alpha+r\tau_s))(2\alpha+r\tau_s)e^{2t'\sqrt{\alpha^2-\beta^2}/\tau_s}\times \\
&\Big[4\alpha^2+2\beta^4+r\tau_s\sqrt{\alpha^2-\beta^2}-\beta^2(4\sqrt{\alpha^2-\beta^2}+r\tau_s(\sqrt{\alpha^2-\beta^2}+2)+2) \\
&\qquad +\alpha(4\sqrt{\alpha^2-\beta^2}+\beta^2(r\tau_s-4)+r\tau_s)\Big] \\
&+e^{t'(2\alpha/\tau_s+r)}\Big[8\alpha^3(r\tau_s+1)+2\alpha^2(r\tau_s(-\beta^2+r\tau_s+1)-4\sqrt{\alpha^2-\beta^2}) \\
&\quad +2\alpha\big(\beta^2(4(\sqrt{\alpha^2-\beta^2}-1)+r\tau_s(\sqrt{\alpha^2-\beta^2}-4))-3r\tau_s\sqrt{\alpha^2-\beta^2}\big) \\
&+r\tau_s\big(2\beta^4+\beta^2(4\sqrt{\alpha^2-\beta^2}+r\tau_s(\sqrt{\alpha^2-\beta^2}-2)-2)-r\tau_s\sqrt{\alpha^2-\beta^2}\big)\Big]\Bigg)
\end{aligned}
\tag{D.5}
$$

For fixed t' one can again see that the only t dependent term lies outside the parenthesis and is given by $e^{-rt-\frac{\left(\alpha-\sqrt{\alpha^2-\beta^2}\right)t}{\tau_s}}$, which is Eq. (4.50) from the main text.

E

Appendices for Chapter 5

E.1 Exact expression for the MFPT for the drift-diffusive process under stochastic return

In this section, we provide the exact expression for the MFPT the drift-diffusive system with resetting treated in the main text. This is given by

$$
\begin{aligned}
\langle \tau(\overline{r},\overline{\lambda},\overline{v})\rangle = \Bigg[& \Big((e^{\overline{v}}-e^{\overline{\lambda}})e^{\sqrt{\overline{v}^2+4\overline{r}}}\sqrt{\overline{v}^2+4\overline{r}}\,\Big(\overline{v}\big(\sqrt{\overline{v}^2+4\overline{r}}+\overline{v}\big)+4\overline{r}\Big) \\
& \times \Big(\overline{\lambda}\big(\sqrt{\overline{v}^2+4\overline{r}}-\overline{v}\big)-2\overline{r}\Big)\,\big(\overline{\lambda}(\sqrt{\overline{v}^2+4\overline{r}}+\overline{v})+2\overline{r}\big)\Big) \\
& + \frac{8\overline{r}^2 e^{-\sqrt{\overline{v}^2+4\overline{r}}}(e^{\sqrt{\overline{v}^2+4\overline{r}}}-1)}{(\overline{\lambda}+\overline{v})\sqrt{\overline{v}^2+4\overline{r}}(\sqrt{\overline{v}^2+4\overline{r}}+\overline{v})^2} - 2e^{\frac{1}{2}(\overline{v}-\sqrt{\overline{v}^2+4\overline{r}})}+2 \\
& + \frac{e^{-\sqrt{\overline{v}^2+4\overline{r}}-\overline{v}}}{(e^{\overline{\lambda}-\overline{v}}-1)(\overline{\lambda}-\overline{v})\sqrt{\overline{v}^2+4\overline{r}}}\Bigg(-(e^{\overline{\lambda}}-e^{\overline{v}})\Big[\overline{v}^2\big(e^{\sqrt{\overline{v}^2+4\overline{r}}}-1\big) \\
& + 2\overline{r}\big(e^{\sqrt{\overline{v}^2+4\overline{r}}}-1\big)+\overline{v}\big(e^{\sqrt{\overline{v}^2+4\overline{r}}}-2e^{\frac{1}{2}(\sqrt{\overline{v}^2+4\overline{r}}+\overline{v})}+1\big)\sqrt{\overline{v}^2+4\overline{r}}\Big]\Bigg) \\
& \times (\overline{\lambda}(\overline{v}-\overline{\lambda})+\overline{r})^{-1}\Big[e^{\overline{v}/2}\overline{r}(\overline{\lambda}-\overline{v})\Big(e^{\overline{v}/2}\big(\overline{\lambda}(\sqrt{\overline{v}^2+4\overline{r}}-\overline{v})-2\overline{r}\big) \\
& - 2\overline{\lambda}\sqrt{\overline{v}^2+4\overline{r}}e^{\overline{\lambda}+\frac{1}{2}\sqrt{\overline{v}^2+4\overline{r}}}+e^{\sqrt{\overline{v}^2+4\overline{r}}+\frac{\overline{v}}{2}}\big(\overline{\lambda}(\sqrt{\overline{v}^2+4\overline{r}}+\overline{v})+2\overline{r}\big)\Big)\Big]\Bigg] \\
\Bigg/ \Bigg[& 4\overline{r}^2(\overline{\lambda}-\overline{v})\Bigg(-2\overline{\lambda}(\overline{v}^2+4\overline{r})(\sqrt{\overline{v}^2+4\overline{r}}+\overline{v})e^{\frac{1}{2}(2\overline{\lambda}+\sqrt{\overline{v}^2+4\overline{r}}+\overline{v})} \\
& - 2e^{\overline{v}}\overline{r}\big(-2\overline{\lambda}\sqrt{\overline{v}^2+4\overline{r}}+\overline{v}(\sqrt{\overline{v}^2+4\overline{r}}+\overline{v})+4\overline{r}\big) \\
& + 2e^{\sqrt{\overline{v}^2+4\overline{r}}+\overline{v}}\big(\overline{\lambda}(\overline{v}^3+\overline{v}^2\sqrt{\overline{v}^2+4\overline{r}}+2\overline{r}\sqrt{\overline{v}^2+4\overline{r}}+4\overline{v}\overline{r}) \\
& + \overline{r}\big(\overline{v}(\sqrt{\overline{v}^2+4\overline{r}}+\overline{v})+4\overline{r}\big)\big)\Bigg]\Bigg]
\end{aligned}
$$

E.2 Derivation of the *CV* criterion for resetting with stochastic return

In this section, we shall derive the CV criterion as in Eq. (5.44). We start by considering a small resetting rate $\delta r \to 0$ limit of Eq. (5.8). The reason for doing so is that whenever the first order term $O(\delta r)$ is negative, the MFPT of the reset process is guaranteed to be smaller than that of the underlying process. For reader's convenience, we rewrite Eq. (5.8) here

$$
\langle T_R(r,\lambda,v)\rangle = \frac{\frac{1-\widetilde{T}(r)}{r} + r\int_{-\infty}^{L} dx\,\widetilde{G}(x,r)\langle t^{ret}(x)\rangle}{1 - r\int_{-\infty}^{L} dx\;\widetilde{G}(x,r)\epsilon_O^{ret}(x)}. \tag{E.1}
$$

For this let us first expand Eq. (E.1) with respect to $\delta r \to 0$. Note that in this limit we have

$$\widetilde{T}(\delta r \to 0) = 1 - \delta r \langle T \rangle + \frac{\delta r^2}{2}\langle T^2 \rangle + \mathcal{O}(\delta r^3). \tag{E.2}$$

Substituting this in Eq. (E.1) we obtain

$$\begin{aligned}\langle T_R(\delta r, \lambda, v)\rangle = &\left(\langle T\rangle - \frac{\delta r}{2}\langle T^2\rangle + \delta r \int_{-\infty}^{L} dx \widetilde{G}(x,0)\langle t^{ret}(x)\rangle\right) \\ &\times \left(1 + \delta r \int_{-\infty}^{L} dx\ \widetilde{G}(x,0)\epsilon_O^{ret}(x)\right).\end{aligned} \tag{E.3}$$

With slight rearrangement, we obtain

$$\begin{aligned}&\langle T_R(\delta r, \lambda, v)\rangle \\ &= \langle T\rangle + \delta r\left(-\frac{\langle T^2\rangle}{2} + \int_{-\infty}^{L} dx \widetilde{G}(x,0)\langle t^{ret}(x)\rangle + \langle T\rangle \int_{-\infty}^{L} dx\ \widetilde{G}(x,0)\epsilon_O^{ret}(x)\right) + \mathcal{O}(\delta r^2).\end{aligned}$$

The first term is the MFPT of the underlying reset-free process. Thus any infinitesimal δr is supposed to decrease the MFPT beyond that only when the term under the parentheses is less than zero. In that case, we obtain

$$\begin{aligned}&\left(-\frac{\langle T^2\rangle}{2} + \int_{-\infty}^{L} dx \widetilde{G}(x,0)\langle t^{ret}(x)\rangle + \langle T\rangle \int_{-\infty}^{L} dx\ \widetilde{G}(x,0)\epsilon_O^{ret}(x)\right) < 0 \\ &\implies \langle T^2\rangle > 2\int_{-\infty}^{L} dx \widetilde{G}(x,0)\langle t^{ret}(x)\rangle + 2\langle T\rangle \int_{-\infty}^{L} dx\ \widetilde{G}(x,0)\epsilon_O^{ret}(x) \\ &\implies \langle T^2\rangle - \langle T\rangle^2 > 2\int_{-\infty}^{L} dx \widetilde{G}(x,0)\langle t^{ret}(x)\rangle + 2\langle T\rangle \int_{-\infty}^{L} dx\ \widetilde{G}(x,0)\epsilon_O^{ret}(x) - \langle T\rangle^2 \\ &\implies \frac{\langle T^2\rangle - \langle T\rangle^2}{\langle T\rangle^2} > \frac{2}{\langle T\rangle^2}\int_{-\infty}^{L} dx \widetilde{G}(x,0)\langle t^{ret}(x)\rangle + \frac{2}{\langle T\rangle}\int_{-\infty}^{L} dx\ \widetilde{G}(x,0)\epsilon_O^{ret}(x) - 1.\end{aligned} \tag{E.4}$$

Noting that that $\widetilde{G}(x,r) = \int_0^\infty dt\ e^{-rt} G(x,t) \implies \widetilde{G}(x,0) = \int_0^\infty dt\ G(x,t)$ we have

$$\begin{aligned}
\frac{\langle T^2\rangle - \langle T\rangle^2}{\langle T\rangle^2} &> \frac{2}{\langle T\rangle^2}\int_{-\infty}^{L} dx \int_0^\infty dt\ G(x,t)\langle t^{ret}(x)\rangle \\
&\quad + \frac{2}{\langle T\rangle}\int_{-\infty}^{L} dx \int_0^\infty dt\ G(x,t)\epsilon_O^{ret}(x) - 1 \\
\implies \frac{\langle T^2\rangle - \langle T\rangle^2}{\langle T\rangle^2} &> \frac{2}{\langle T\rangle}\int_{-\infty}^{L} dx \left(\frac{1}{\langle T\rangle}\int_0^\infty dt\ G(x,t)\right)\langle t^{ret}(x)\rangle \\
&\quad + 2\int_{-\infty}^{L} dx \left(\frac{1}{\langle T\rangle}\int_0^\infty dt\ G(x,t)\right)\epsilon_O^{ret}(x) - 1. \qquad \text{(E.5)}
\end{aligned}$$

Finally identifying the coefficient of variation (CV) as $CV = \frac{\sqrt{\langle T^2\rangle - \langle T\rangle^2}}{\langle T\rangle}$ we have the following the CV criterion

$$CV^2 > \frac{2}{\langle T\rangle}\overline{\langle t^{ret}(x)\rangle} + 2\overline{\epsilon_O^{ret}(x)} - 1, \qquad \text{(E.6)}$$

as written in Eq. (5.44) of the main text. Recall that we use the notation $\overline{f(x)} = \int_0^\infty dx f(x) G_0(x)$ with $G_0(x)$ being defined as

$$G_0(x) = \frac{1}{\langle T\rangle}\int_0^\infty dt G(x,t). \qquad \text{(E.7)}$$

F

Appendices for Chapter 6

F.1 Survival probability and probability current of a single ballistic searcher

In this section, we compute the survival probability $Q(L, x_0, t)$ and the current through the resetting threshold $j_{L,1}(L, x_0, t)$ for a single ballistic searcher. If v_i denotes the random initial velocity of the i^{th} searcher then it can survive up to time t without hitting either target or resetting threshold in two ways: First, if $v_i t < L - x_0$ when $v_i > 0$ so that the walker starts moving towards the resetting threshold but failing to reach the same in the given time and second, when $|v_i|t < x_0$ if the initial velocity $v_i < 0$ so that the walker starts moving towards the target yet fails to hit it by time t. Summing over these two possibilities, we can write the survival probability as

$$Q(L, x_0, t) = \int_0^\infty dv\ \phi(v)\ \theta(L - x_0 - vt) + \int_{-\infty}^0 dv\ \phi(v)\ \theta(x_0 - |v|t), \tag{F.1}$$

where $\theta(z)$ is the Heaviside theta function which takes values unity only when $z > 0$, and 0 otherwise. Assuming $\phi(v)$ to be symmetric so that $\phi(-v) = \phi(v)$, one can rewrite the above equation as

$$Q(L, x_0, t) = \int_0^{\frac{L-x_0}{t}} dv\ \phi(v) + \int_0^{\frac{x_0}{t}} dv\ \phi(v). \tag{F.2}$$

Denoting the function $\Phi(v)$ as

$$\Phi(v) = \int_0^v dv' \phi(v'), \tag{F.3}$$

we finally arrive at

$$Q(L, x_0, t) = \Phi\left(\frac{L - x_0}{t}\right) + \Phi\left(\frac{x_0}{t}\right). \tag{F.4}$$

The probability current through the resetting threshold at $x = L$ is essentially the total number of accumulated particles there at time t so that

$$\begin{aligned} j_{L,1}(L, x_0, t) &= \int_0^\infty dv\ \phi(v)\ \delta\left(t - \frac{L - x_0}{v}\right) \\ &= \frac{L - x_0}{t^2}\ \phi\left(\frac{L - x_0}{t}\right). \end{aligned} \tag{F.5}$$

Here, $\delta(x)$ is the Dirac-delta function. Note that only the positive velocities contribute to the current through the threshold while the negative velocities contribute to the current through the target at the origin given by

$$\begin{aligned} j_{0,1}(L, x_0, t) &= \int_{-\infty}^0 dv\ \phi(v)\ \delta\left(t - \frac{x_0}{v}\right) \\ &= \frac{x_0}{t^2}\ \phi\left(\frac{x_0}{t}\right). \end{aligned} \tag{F.6}$$

F.2 Derivation of exact form of the scaling function for $N = 2$

Here we derive the scaling function (or the scaled MFPT) for $N = 2$ ballistic searchers i.e. $\mathcal{F}(u, 2)$. It is convenient to make the change of variable $t = 1/x$ and re-write the scaling function (Eq. (6.20)) as

$$\mathcal{F}(u, N) = \frac{2}{N\, u^2}\, \frac{I_N(u)}{J_N(u)}, \tag{F.7}$$

where $I_N(u)$ and $J_N(u)$ are given by

$$I_N(u) = \int_0^\infty \frac{dx}{x^2} \left[1 - \frac{1}{2}\, e^{-u\, x} - \frac{1}{2}\, e^{-(1-u)x}\right]^N \tag{F.8}$$

$$J_N(u) = \int_0^\infty dx\, e^{-u\, x} \left[1 - \frac{1}{2}\, e^{-u\, x} - \frac{1}{2}\, e^{-(1-u)x}\right]^{N-1}. \tag{F.9}$$

For general $N \geq 2$, it is not easy to compute the two integrals $I_N(u)$ and $J_N(u)$, and hence $\mathcal{F}(u, N)$ in Eq. (F.7). However for $N = 2$, as we show below, one can compute $\mathcal{F}(u, 2)$ exactly for all $u \in [0, 1]$. This will serve also as a benchmark to compare to the asymptotic behaviors of $\mathcal{F}(u, N)$ for general N in the two asymptotic limits $u \to 0$ and $u \to 1$.

For $N = 2$, let us start with the integral $J_2(u)$ in Eq. (F.9) which is relatively simpler

to evaluate. Setting $N = 2$ in Eq. (F.9) we get

$$J_2(u) = \int_0^\infty dx\, e^{-ux} \left[1 - \frac{1}{2}\, e^{-u\,x} - \frac{1}{2}\, e^{-(1-u)x}\right] = \frac{3}{4u} - \frac{1}{2}\,. \tag{F.10}$$

The computation of $I_2(u)$ in Eq. (F.8) turns out to be tricky as we show in below. Following Eq. (F.8), we write

$$I_2(u) = \int_0^\infty \frac{dx}{x^2} \left[1 - \frac{1}{2}\, e^{-u\,x} - \frac{1}{2}\, e^{-(1-u)\,x}\right]^2 . \tag{F.11}$$

To get rid of the singularity x^{-2} in the integrand, it is convenient to first take a derivative with respect to u. This gives

$$I_2'(u) = \frac{dI_2(u)}{du} = \int_0^\infty \frac{dx}{x} \left[1 - \frac{1}{2}\, e^{-u\,x} - \frac{1}{2}\, e^{-(1-u)\,x}\right] \left[e^{-u\,x} - e^{-(1-u)\,x}\right] . \tag{F.12}$$

We note one important fact from this equation that will be useful later, namely

$$I_2'\left(u = \frac{1}{2}\right) = 0\,. \tag{F.13}$$

The integrand in Eq. (F.12) still has an singularity $1/x$. To get rid of this term, let us take one more derivative with respect to u. Further simplification leads to the following integral that can be trivially computed to yield

$$I_2''(u) = \frac{d^2 I_2(u)}{du^2} = \int_0^\infty dx \left[e^{-2ux} - e^{-2(1-u)x} - e^{-ux} - e^{-(1-u)x}\right] = -\frac{1}{2u} - \frac{1}{2(1-u)}\,. \tag{F.14}$$

Now, integrating it back with respect to u gives

$$I_2'(u) = -\frac{1}{2}\ln u + \frac{1}{2}\ln(1-u) + C_1\,, \tag{F.15}$$

where the unknown constant $C_1 = 0$ is fixed from the condition in Eq. (F.13). Thus we get

$$I_2'(u) = -\frac{1}{2}\ln u + \frac{1}{2}\ln(1-u)\,. \tag{F.16}$$

Integrating once more we get

$$I_2(u) = -\frac{1}{2}\left[u\ln u - u\right] + \frac{1}{2}\left[1 - u - (1-u)\ln(1-u)\right] + C_0\,, \tag{F.17}$$

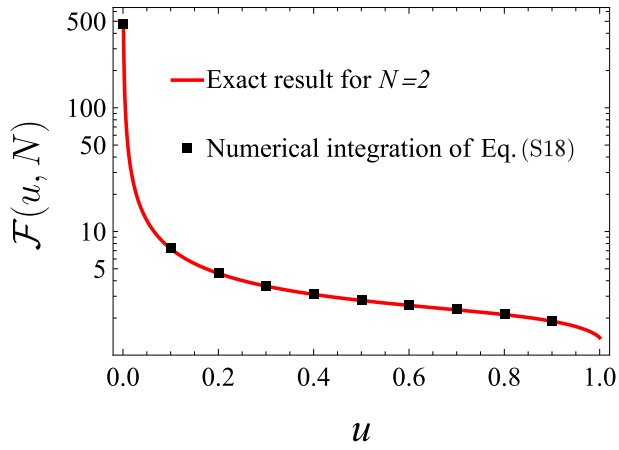

Figure F.1: *Comparison of the scaling function for $N = 2$ as in Eq. (F.27) with that obtained via numerical integration of Eq. (6.20) .*

where the constant C_0 is fixed from the value $I_2(0)$ in Eq. (F.11). Thus we finally get

$$I_2(u) = I_2(0) - \frac{1}{2}\, u\, \ln u - \frac{1}{2}\,(1-u)\, \ln(1-u)\,, \tag{F.18}$$

where, using Eq. (F.11),

$$I_2(0) = \frac{1}{4}\, a_2 \quad \text{with} \quad a_2 = \int_0^\infty \frac{dx}{x^2}\, [1 - e^{-ux}]^2\ . \tag{F.19}$$

To evaluate the integral a_2, we do one integration by part that gives

$$a_2 = 2 \int_0^\infty \frac{dx}{x}\, e^{-x}\, (1 - e^{-x})\ . \tag{F.20}$$

To do the remaining integral in Eq. (F.20), let us introduce an auxiliary parameter b and define

$$a_2(b) = 2 \int_0^\infty \frac{dx}{x}\, e^{-x} \left(1 - e^{-b\,x}\right)\,, \tag{F.21}$$

such that $a_2(b = 1) = a_2$. Differentiating Eq. (F.21) with respect to b we get

$$a_2'(b) = \frac{da_2(b)}{db} = 2 \int_0^\infty dx\, e^{-(b+1)\,x} = \frac{2}{b+1}\,. \tag{F.22}$$

Integrating it back with respect to b and using $a_2(b = 0) = 0$, we get

$$a_2(b) = 2\, \ln(b+1)\,. \tag{F.23}$$

Consequently,

$$a_2 = a_2(b = 1) = 2\, \ln 2\,. \tag{F.24}$$

Using this result in Eq. (F.19) gives

$$I_2(0) = \frac{a_2}{4} = \frac{1}{2}\,\ln 2\,. \tag{F.25}$$

Following Eq. (F.18), we get the complete expression for $I_2(u)$ as

$$I_2(u) = \frac{1}{2}\,\left[\ln 2 - u\,\ln u - (1-u)\,\ln(1-u)\right]\,. \tag{F.26}$$

Substituting $J_2(u)$ from Eq. (F.10) and $I_2(u)$ from Eq. (F.26) into Eq. (F.7) with $N = 2$ gives the exact scaling function $\mathcal{F}(u,2)$ as

$$\mathcal{F}(u,2) = \frac{2}{u\,(3-2u)}\,\left[\ln 2 - u\,\ln u - (1-u)\,\ln(1-u)\right]\,. \tag{F.27}$$

In Fig. (F.1) we show that the exact result as in Eq. (F.27) matches exactly with the numerical integration of Eq. (6.20) for $N = 2$. The limiting behaviors of $\mathcal{F}(u,2)$ are given by

$$\mathcal{F}(u,2) \approx \begin{cases} \frac{2\ln 2}{3\,u} & \text{as} \quad u \to 0 \\ \\ 2\,\ln 2 - 2\,(1-u)\,\ln(1-u) & \text{as} \quad u \to 1\,. \end{cases} \tag{F.28}$$

Derivation of the scaling function for general N is subject matter of the next section.

F.3 Asymptotic behaviors of scaling funtion for general $N \geq 2$

We now consider the scaling function $\mathcal{F}(u,N)$ in Eq. (F.7) for general $N \geq 2$. Unlike the $N = 2$ case, it turns out to be much harder to compute the scaling function explicitly for general $N > 2$. However, as mentioned earlier, one can extract the asymptotic behaviors of $\mathcal{F}(u,N)$, for arbitrary $N \geq 2$, in the two limits $u \to 0$ and $u \to 1$ as shown below.

F.3.1 The limit $u \to 0$

We will show that for general $N \geq 2$, the scaling function $\mathcal{F}(u,N)$ diverges as $u \to 0$, and this leading divergence originates from the denominator $J_N(u)$ in Eq. (F.7) as $u \to 0$. Hence, for the numerator $I_N(u)$ in Eq. (F.7), it is enough only the leading $u = 0$ behavior where it turns out to be finite for all $N \geq 1$. This becomes evident by setting $u = 0$ in Eq. (F.8), and it gives

$$I_N(0) = \frac{a_N}{2^N} \quad \text{where} \quad a_N = \int_0^\infty \frac{dx}{x^2}\,(1-e^{-x})^N\,. \tag{F.29}$$

We then need to evaluate $J_N(u)$ in Eq. (F.9) in the limit $u \to 0$. By naively putting $u = 0$ in Eq. (F.9) one finds that the resulting integral diverges. To extract the leading divergence of $J_N(u)$ as $u \to 0$, we first make a change of variable $u\, x = y$ in the integral in Eq. (F.9). This gives

$$J_N(u) = \frac{1}{u} \int_0^\infty dy\, e^{-y} \left[1 - \frac{1}{2}\, e^{-y} - \frac{1}{2}\, e^{-\frac{(1-u)}{u}\, y}\right]^{N-1} . \tag{F.30}$$

Now, in the limit $u \to 0$, we can safely neglect the third term inside the parenthesis $[\ldots]$ since the resulting integral is convergent. This gives the leading order behavior as $u \to 0$

$$J_N(u) \approx \frac{1}{u} \int_0^\infty dy\, e^{-y} \left[1 - \frac{1}{2}\, e^{-y}\right]^{N-1} . \tag{F.31}$$

Making the change of variable $z = 1 - \frac{1}{2}\, e^{-y}$, the integral can be done exactly leading to

$$J_N(u) \approx \left[\frac{2}{N}\left(1 - 2^{-N}\right)\right] \frac{1}{u} \quad \text{as} \quad u \to 0\,. \tag{F.32}$$

Substituting Eq. (F.32) and Eq. (F.29) into the exact expression for $\mathcal{F}(u, N)$ in Eq. (F.7) then gives the leading small u behavior

$$\mathcal{F}(u, N) \approx \frac{a_N}{2^N - 1}\, \frac{1}{u} \quad \text{as} \quad u \to 0\,, \tag{F.33}$$

where a_N is defined in Eq. (F.29). Note that this result is valid for any $N \geq 2$. For $N = 2$, using $a_2 = 2 \ln 2$ from Eq. (F.24), we see that the general result in Eq. (F.33) for $N = 2$ matches perfectly with the leading asymptotic behavior as $u \to 0$ derived in Eq. (F.28) from the exact scaling function for $N = 2$.

F.3.2 The limit $u \to 1$

We now consider the $u \to 1$ limit of the scaling function $\mathcal{F}(u, N)$ in Eq. (F.7). It is easier to first consider the denominator $J_N(u)$ defined in Eq. (F.9). Setting $u = 1$, we find

$$J_N(1) = \frac{1}{2^{N-1}} \int_0^\infty dx\, e^{-x}\, (1 - e^{-x})^{N-1} = \frac{1}{N\, 2^{N-1}}\,. \tag{F.34}$$

The last integral is trivially performed upon the change of variable $z = 1 - e^{-x}$. In fact, setting $u = 1 - \epsilon$, it is easy to compute the next order term for small ϵ. One finds that

$$J_N(1 - \epsilon) = \frac{1}{N\, 2^{N-1}} + b_N\, \epsilon + O\left(\epsilon^2\right) , \quad \text{where } b_N = -\frac{1}{2^{N-1}} \int_0^1 dz\, z^{N-1} \ln(1 - z)\,. \tag{F.35}$$

We will see later that the $O(\epsilon)$ term in $J_N(1-\epsilon)$ does not contribute to the first two leading behaviors of $\mathcal{F}(u,N)$ as $u \to 1$. We now turn to the integral $I_N(u)$ defined in Eq (F.8). Setting $u = 1-\epsilon$ we get

$$I_N(1-\epsilon) = W_N(\epsilon) = \int_0^\infty \frac{dx}{x^2} \left[1 - \frac{1}{2}e^{-(1-\epsilon)x} - \frac{1}{2}\,e^{-\epsilon x}\right]^N . \tag{F.36}$$

Now, exactly at $u = 1$, i.e., at $\epsilon = 0$, the integral is convergent and we get

$$I_N(1) = W_N(0) = \frac{a_N}{2^N}\,, \quad \text{where} \quad a_N = \int_0^\infty \frac{dx}{x^2}\,(1-e^{-x})^N\,. \tag{F.37}$$

Note that the same a_N also appeared in Eq. (F.29) near the limit $u \to 0$ which is not surprising given the fact that the function $I_N(u)$ defined in Eq. (F.8) is symmetric around $u = 1/2$.

Our goal is to evaluate the next order correction to $I_N(1-\epsilon) = W_N(\epsilon)$ as $\epsilon \to 0$. To do this, we first differentiate $W_N(\epsilon)$ in Eq. (F.37) once with respect to ϵ. This gives

$$W_N'(\epsilon) = \frac{N}{2}\int_0^\infty \frac{dx}{x}\left[1 - \frac{1}{2}\,e^{-(1-\epsilon)x} - \frac{1}{2}\,e^{-\epsilon x}\right]^{N-1}\left[e^{-\epsilon x} - e^{-(1-\epsilon)x}\right]. \tag{F.38}$$

We note that as $\epsilon \to 0$, the first derivative $W_N'(\epsilon)$ also diverges. To extract this divergence, we take one more derivative of $W_N'(\epsilon)$ in Eq. (F.38) with respect to ϵ. This gives

$$\begin{aligned} W_N''(\epsilon) = {} & \frac{N(N-1)}{4}\int_0^\infty dx\left[1 - \frac{1}{2}\,e^{-(1-\epsilon)x} - \frac{1}{2}\,e^{-\epsilon x}\right]^{N-2}\left[e^{-\epsilon x} - e^{-(1-\epsilon)x}\right]^2 \\ & - \frac{N}{2}\int_0^\infty dx\left[1 - \frac{1}{2}\,e^{-(1-\epsilon)x} - \frac{1}{2}\,e^{-\epsilon x}\right]^{N-1}\left[e^{-\epsilon x} + e^{-(1-\epsilon)x}\right]. \end{aligned} \tag{F.39}$$

Next we make a change of variable $\epsilon\, x = y$. This gives

$$\begin{aligned} W_N''(\epsilon) = {} & \frac{N(N-1)}{4\,\epsilon}\int_0^\infty dy\left[1 - \frac{1}{2}\,e^{-y} - \frac{1}{2}\,e^{-\frac{(1-\epsilon)}{\epsilon}y}\right]^{N-2}\left[e^{-y} - e^{-\frac{(1-\epsilon)}{\epsilon}y}\right]^2 \\ & - \frac{N}{2\,\epsilon}\int_0^\infty dy\left[1 - \frac{1}{2}\,e^{-y} - \frac{1}{2}\,e^{-\frac{(1-\epsilon)}{\epsilon}y}\right]^{N-1}\left[e^{-y} + e^{-\frac{(1-\epsilon)}{\epsilon}y}\right]. \end{aligned} \tag{F.40}$$

At this stage, we can now take the $\epsilon \to 0$ limit inside the integral and neglect the term $e^{-\frac{1-\epsilon}{\epsilon}y}$ everywhere, since the resulting integrals remain convergent. This leads to the leading $\epsilon \to 0$ behavior of the second derivative

$$W_N''(\epsilon) \approx \frac{N(N-1)}{4\,\epsilon}\int_0^\infty dy\, e^{-2y}\left[1 - \frac{1}{2}\,e^{-y}\right]^{N-2} - \frac{N}{2\,\epsilon}\int_0^\infty dy\, e^{-y}\left[1 - \frac{1}{2}\,e^{-y}\right]^{N-1}. \tag{F.41}$$

These two integrals can now be easily performed by making the change of variable

$1-\frac{1}{2}e^{-y}=z$. This gives a very simple expression for the leading behavior as $\epsilon \to 0$

$$W_N''(\epsilon) \approx -\frac{N}{2^N \epsilon}\,. \tag{F.42}$$

Integrating back once with respect to ϵ gives

$$W_N'(\epsilon) \approx -\frac{N}{2^N}\,\ln(\epsilon) + C_3\,, \tag{F.43}$$

where C_3 is an integration constant whose value is not relevant for us. Integrating further with respect to ϵ we get the two leading order terms as $\epsilon \to 0$

$$I_N(1-\epsilon) = W_N(\epsilon) = W_N(0) - \frac{N}{2^N}\,\epsilon\,\ln(\epsilon) + O(\epsilon)\,. \tag{F.44}$$

Using $W_N(0)$ from Eq. (F.37), we then obtain, as $u \to 1$,

$$I_N(u) = \frac{a_N}{2^N} - \frac{N}{2^N}\,(1-u)\,\ln(1-u) + O(1-u)\,, \tag{F.45}$$

where a_N is given in Eq. (F.37).

Finally, substituting the leading behaviors of $I_N(u)$ from Eq. (F.45) and of $J_N(u)$ from Eq. (F.35) as $u \to 1$ into our main formula (F.7), we obtain the following asymptotic behavior of $\mathcal{F}(u,N)$ as $u \to 1$ for arbitrary $N \geq 2$

$$\mathcal{F}(u,N) = a_N - N\,(1-u)\,\ln(1-u) + O(1-u)\,. \tag{F.46}$$

Hence, summarizing, the two limiting asymptotic behaviors of the scaling function $\mathcal{F}(u,N)$, for arbitrary $N \geq 2$, are given by

$$\mathcal{F}(u,N) \approx \begin{cases} \frac{a_N}{2^N-1}\,\frac{1}{u} & \text{as} \quad u \to 0 \\ \\ a_N - N\,(1-u)\,\ln(1-u) + O(1-u) & \text{as} \quad u \to 1\,, \end{cases} \tag{F.47}$$

where we recall that the constant a_N is defined in Eq. (F.37). Note that for $N=2$, using $a_2 = 2\ln 2$ from Eq. (F.24), the general result in Eq. (6.22) does coincide with the leading asymptotic behaviors of $\mathcal{F}(u,2)$ in Eq. (F.28) obtained from the exact scaling function for $N=2$.

F.4 Derivations of $\langle \mathcal{N}_{\mathbf{TR}}(u,N)\rangle$, $\langle \overline{\mathbb{T}}_N^{\mathbf{TR}}(u)\rangle$ and $\langle \overline{\mathbb{T}}_N^{\mathbf{FP}}(u)\rangle$

The MFPT under TR mechanism can be interpreted as a sum over stochastic timescales emanating from all possible events eventually leading to a completion of the process.

We recall

$$\langle \overline{\mathcal{T}}_N^{\rm TR}(u)\rangle = \langle \mathcal{N}_{\rm TR}(u,N)\rangle \times \langle \overline{\mathbb{T}}_N^{\rm TR}(u)\rangle + \langle \overline{\mathbb{T}}_N^{\rm FP}(u)\rangle, \tag{F.48}$$

where individual quantities were defined in the main text. In this section, we explicitly derive these quantities and elaborate further.

F.4.1 Derivation of $\langle \mathcal{N}_{\rm TR}\rangle$

A stochastic trajectory under TR mechanism can experience multiple resetting events before the first passage to the target. The number of these TR events fluctuates between the realizations and our aim is to compute the mean number of resetting events till the first passage. Since, the system can undergo only two possible events: TR events (which can be called as a *unsuccessful* event) and a first passage event (a *successful* event), clearly the number of TR events is distributed according to a geometric distribution. Here, the *success probability* is nothing but the splitting probability to the threshold $\epsilon_L(u,N)$ so that the *unsuccess probability* is given by $\epsilon_0(u,N)$ which is the splitting probability to the target. Thus, the mean number of TR events can be obtained as the mean of the geometric distribution

$$\langle \mathcal{N}_{\rm TR}(u,N)\rangle = \sum_{k=0}^{\infty} k(\epsilon_L(u,N))^k \times \epsilon_0(u,N)) = \frac{1-\epsilon_0(u,N)}{\epsilon_0(u,N)}, \tag{F.49}$$

where $\epsilon_0(u,N)$ can be found using Eq. (6.17) as follows

$$\epsilon_0(u,N) = 1-\epsilon_L(u,N) = Nu\int_0^\infty d\tau\, \frac{e^{-\frac{u}{\tau}}}{2\tau^2}\left(1-\frac{1}{2}e^{-\frac{1-u}{\tau}}-\frac{e^{-\frac{u}{\tau}}}{2}\right)^{N-1}. \tag{F.50}$$

In Fig. (F.2) we show the variation of the splitting probabilities with u for $N=7$. Note that for $u<1/2$ we have $\epsilon_0>1/2$. In Fig. (F.3)(a), we plot $\langle \mathcal{N}_{\rm TR}(u,N)\rangle$ as a function of u for several values of N.

F.4.2 Derivation of $\langle \overline{\mathbb{T}}_N^{\rm TR}(u)\rangle$

Recall that the random variable $\mathbb{T}_N^{\rm TR}$ denotes the waiting time between two consecutive TR events conditioned on survival. The normalized density of this conditional time can then be written as

$$\begin{aligned} f_{\mathbb{T}_N^{\rm TR}}(t) &= \frac{j_{L,N}(L,x_0,t)}{\epsilon_L(L,x_0,N)} \\ &= \frac{j_{L,1}(L,x_0,t)[Q(L,x_0,t)]^{N-1}}{\int_0^\infty dt\; j_{L,1}(L,x_0,t)[Q(L,x_0,t)]^{N-1}}, \end{aligned} \tag{F.51}$$

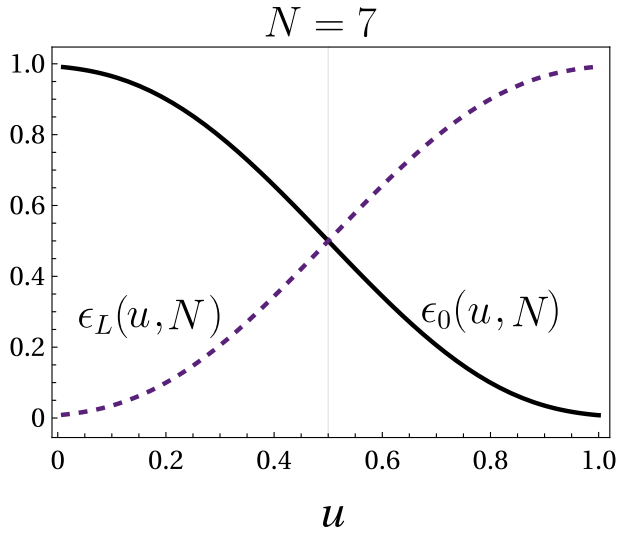

Figure F.2: *Variation of the splitting probabilities with u for $N = 7$ as found from Eq. (F.50). Note that when $u < 1/2$ we have $\epsilon_0 > \epsilon_L$.*

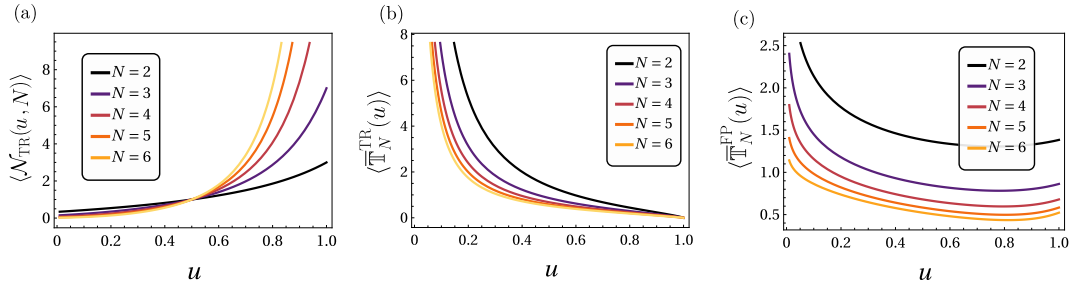

Figure F.3: *Variation of $\langle \mathcal{N}_{TR}(u,N)$ as in Eq. (F.49), $\langle \overline{\mathbb{T}}_N^{TR}(u)\rangle$ as in Eq. (F.53) and $\langle \overline{\mathbb{T}}_N^{FP}(u)\rangle$ as in Eq. (F.55) with respect to u for distinct values of N.*

where the common factor N has been canceled out from the numerator and denominator. From the distribution, one can find the mean time between two consecutive resetting events as

$$\langle \mathbb{T}_N^{\rm TR}(L,x_0)\rangle = \int_0^\infty dt\; t f_{\mathbb{T}_N^{\rm TR}}(t). \tag{F.52}$$

Plugging the values of the survival probability as in Eq. (6.14) and the probability current to the threshold as in Eq. (6.15) in the above equation one arrives at $\langle \mathbb{T}_N^{\rm TR}\rangle$ (in a dimensionless form)

$$\begin{aligned}\langle \overline{\mathbb{T}}_N^{\rm TR}(u)\rangle &= \frac{v_0}{x_0}\langle \mathbb{T}_N^{\rm TR}(L,x_0)\rangle \\ &= \frac{\int_0^\infty dt\; \frac{1}{2t}\exp\left(-\frac{1-u}{t}\right)\left[1-\frac{1}{2}\exp\left(-\frac{1-u}{t}\right)-\frac{1}{2}\exp\left(-\frac{u}{t}\right)\right]^{N-1}}{u\int_0^\infty dt\; \frac{1}{2t^2}\exp\left(-\frac{1-u}{t}\right)\left[1-\frac{1}{2}\exp\left(-\frac{1-u}{t}\right)-\frac{1}{2}\exp\left(-\frac{u}{t}\right)\right]^{N-1}}.\end{aligned} \tag{F.53}$$

In Fig. (F.3)(b), we plot $\langle \overline{\mathbb{T}}_N^{\rm TR}(u)\rangle$ as a function of u for different N.

F.4.3 Derivation of $\langle \overline{\mathbb{T}}_N^{\mathbf{FP}}(u) \rangle$

Finally, we turn our attention to the random variable $\mathbb{T}_N^{\mathrm{FP}}$ that denotes the random time for the first passage since the last TR event. This is simply the conditional time that the target is found before the threshold by any of the N searchers. Following these arguments, we can write the normalized density of $\mathbb{T}_N^{\mathrm{FP}}$ as

$$\begin{aligned} f_{\mathbb{T}_N^{\mathrm{FP}}}(t) &= \frac{j_{0,N}(L, x_0, t)}{\epsilon_0(L, x_0, N)} \\ &= \frac{j_{0,1}(L, x_0, t)[Q(L, x_0, t)]^{N-1}}{\int_0^\infty dt\ j_{0,1}(L, x_0, t)[Q(L, x_0, t)]^{N-1}}. \end{aligned} \tag{F.54}$$

Finally plugging the survival probability Eq. (6.14) and the probability current to the target as in Eq. (6.16) we find the mean of $\mathbb{T}_N^{\mathrm{FP}}$ (in the dimensionless form) as

$$\begin{aligned} \langle \overline{\mathbb{T}}_N^{\mathrm{FP}}(u) \rangle &= \frac{v_0}{x_0} \int_0^\infty dt\ t f_{\mathbb{T}_N^{\mathrm{FP}}}(t) \\ &= \frac{\int_0^\infty dt\ \frac{1}{2t} \exp\left(-\frac{u}{t}\right) \left[1 - \frac{1}{2}\exp\left(-\frac{1-u}{t}\right) - \frac{1}{2}\exp\left(-\frac{u}{t}\right)\right]^{N-1}}{u \int_0^\infty dt\ \frac{1}{2t^2} \exp\left(-\frac{u}{t}\right) \left[1 - \frac{1}{2}\exp\left(-\frac{1-u}{t}\right) - \frac{1}{2}\exp\left(-\frac{u}{t}\right)\right]^{N-1}}. \end{aligned} \tag{F.55}$$

In Fig. (F.3)(c), we plot $\langle \overline{\mathbb{T}}_N^{\mathrm{FP}}(u) \rangle$ as a function of u for different values of N.